Institute of Ageing and Chronic Disease

Redox regulation of mitochondrial responses in denervated and ageing skeletal muscle

Mattia Scalabrin

Thesis submitted in accordance with the requirements of the

University of Liverpool for the degree of

Doctor of Philosophy

Liverpool, March 2020

Publications

- *Redox responses in skeletal muscle following denervation.* Mattia Scalabrin, Natalie Pollock, Caroline A Staunton, Susan V Brooks, Anne McArdle, Malcolm J Jackson1and Aphrodite Vasilaki. Redox Biology, Vol. 26, September 2019, 101294. DOI: 10.1016/j.redox.2019.101294

Conferences

- September 2018 - BIRAX Ageing Conference, London, United Kingdom - Poster Presentation: *Redox regulation of mitochondrial responses to denervation in skeletal muscle.* Scalabrin M, Pollock N, Jackson M.J., Vasilaki A.

- June 2018 - 19th Biennial Meeting of the Society for Free Radical Research International. Lisbon, Portugal - Oral Presentation: *Redox responses to denervation in skeletal muscle*. Scalabrin M., Pollock N., McArdle A., Jackson M.J. and Vasilaki A.

- April 2018 - Experimental Biology, San Diego, Cal, US - Poster presentation: *Effect of denervation on redox-regulation in skeletal muscle.* Scalabrin M, Pollock N, McArdle A, Jackson MJ and Vasilaki A. Faseb Journal Vol. 32, No. 1_supplement, April 2018, Abstract ID: 907.1.

Abstract

Sarcopenia is a characteristic of ageing where a substantial reduction of muscle tissue, strength and function are seen (Baumann et al, 2016). Previous reports have suggested that an age-related loss of stability of the neuromuscular junction can result in muscle fibre denervation, which in turn impacts on the capacity to activate muscles as well as altering muscle fibre architecture, composition, cross sectional area and number. Hence, muscle fibre denervation may play a fundamental role in sarcopenia.

Previous studies (Muller et al, 2007; Bhattacharya et al, 2009; Pollock et al, 2017) have highlighted a significant increase in mitochondrial peroxide release in denervated muscle fibres but the physiological role of this increase is still unclear. Therefore, the main aim of this study was to determine the sources of peroxide in denervated muscle fibres and the physiological effect that this peroxide release has on skeletal muscle. A specific focus was given to the adaptive responses induced by the increased peroxide release and its effects on the metabolism and mitochondria of denervated muscle fibres.

The main findings of this thesis are:

- In response to surgically induced denervation of the Tibialis Anterior and Extensor Digitorum Longus muscles, a significant increase in peroxide release from mitochondria occurred from enzymes not involved in the electron transport chain. During prolonged denervation, muscles underwent significant atrophy accompanied by increased content of cytosolic enzymes such as phospholipase A2 and NADPH Oxidase 2 which may be responsible for the initiation of proteolysis.
- In the experimental model of denervation, there was a significant increased content of mitochondrial fission markers with no apparent changes in fusion together with a progressive accumulation of p62 indicating mitophagy impairment. There was also a reduction of mitochondria content at 21 days post-denervation with the activation of pro-apoptotic pathways involving the Bcl-2 family.
- Nuclear magnetic resonance metabolomics showed that prolonged denervation was associated with metabolic changes in pathways related to insulin resistance, increase of protein breakdown and activation of purine metabolism.
- Given the extensive cellular alterations observed with prolonged, surgically induced denervation, similar measurements were performed in skeletal muscle from old mice to identify whether these changes were also evident during ageing. From 18 months, mice exhibited an instability of the neuromuscular junction with progressive fragmentation and nerve sprouting. However, not all of the biochemical changes observed in skeletal muscle following surgically induced denervation were also seen in skeletal muscle during ageing.

In conclusion, the results of the present work suggest that the increase in peroxide release in fully denervated muscle fibres triggers multiple responses resulting in impairment of mitophagy, insulin resistance, increased proteolysis and fibre atrophy.

Table of Contents

List of Figures

List of Tables

Abbreviations

µg	Micro grams
µl	Micro liters
µM	Micro moles
ν	Frequency (expressed in Hertz)
^{1}H	Proton as referred to in NMR Metabolomics
1D	One dimensional
$^{2}H_2O$	Deuterated water
4-HNE	4-hydroxynonenal
AACOCF3	Arachidonyl trifluoromethyl ketone
ACh	Acetylcholine
AChR	Acetylcholine Receptors
ADP	Adenosine Diphosphate
AGEs	Advanced Glycation End Products
Akt	Protein Kinase B
AMP	Adenosine Monophosphate
Apaf-1	Apoptotic protease activating factor 1
APS	Ammonium Persulfate
ATP	Adenosine Triphosphate
AU	Arbitrary Unit
BAX	Bcl-2-associated X protein
BCA	Bicinchoninic Acid Assay
Bcl-2	B-cell lymphoma 2
BSU	Biomedical Service Unit
Ca^{2+}	Calcium ions

CMA	Chaperone-Mediated Autophagy
CO_2	Carbon Dioxide
Complex-I	NADH-coenzyme Q oxidoreductase
Complex-II	Succinate-Q oxidoreductase
Complex-III	Q-cytochrome c oxidoreductase
Complex-IV	Cytochrome c oxidase
COX	Cyclooxygenases
cPLA2	Calcium-dependent phospholipase A2
CSA	Cross Sectional Area
CuZnSOD	Copper-zinc Superoxide Dismutase
Cyto	Cytosolic extract
DAPI	4′,6-diamidino-2-phenylindole
ddH_2O	Double distilled water
DOK7	Downstream of tyrosine kinase 7
Drp1	Dynamin-1-like protein
DTNB	Elleman’s solution or 5,5-dithio-bis-(2-nitrobenzoic acid)
DUOX	gp91phosphorylated homologues distinguishing DUAL Oxidase isoforms
E	Energy (expressed in Joules)
ECL	Enhanced Chemiluminescence
EcSOD	Extracellular Superoxide dismutase
EDL	Extensor Digitorum Longus muscle
EDTA	Ethylenediaminetetraacetic acid
EGTA	Ethylene glycol-bis(β-aminoethyl ether)-N,N,N′,N′-tetraacetic acid
EWGSOP	European Working Group on Sarcopenia
EPR	Electron Paramagnetic Resonance

FAD	Flavin adenine dinucleotide
FADH2	Flavin Adenine Dinucleotide
FCCP	Carbonyl cyanide 4-(trifluoromethoxy)phenylhydrazone
FMN	Flavin mononucleotide
FMNH2	Reduced Flavin mononucleotide
g	Grams
GADPH	Glyceraldehyde 3-phosphate dehydrogenase
GC	Gastrocnemius muscle
gp91phox	gp91 phosphorylated
G Proteins	Guanine nucleotide-binding proteins
GPx	Glutathione Peroxidase
GSH	Reduced Glutathione
GSSG	Oxidised Glutathione
GTP	Guanosine Triphosphate
h	Planck's constant
H&E	Haemotoxylin and Eosin staining
H_2O_2	Hydrogen Peroxide
Hepes buffer	4-(2-hydroxyethyl)-1-piperazineethanesulfonic acid
HO•	Hydroxyl radical
Hsp	Heat Shock Proteins
IMP	Inosine-5'-Monophosphate
iPLA2	Calcium-independent phospholipase A2 isoform
IRS1	Insulin receptor substrate 1
K_2HPO_4	Dipotassium hydrogen phosphate trihydrate
KCl	Potassium Chloride

kDa	KiloDaltons
Keap-1	Kelch-like ECH-associated protein 1
K-MES	MES Potassium salt
LAMP-2A	Lysosome-Associated Membrane Protein 2
LC3	Microtubule-associated proteins 1A/1B light chain 3B
LOX	Lipoxygenases
M	Molar
M.O.M	Mouse On Mouse
MAPK	Mitogenactivated protein kinases
MCAT	Mouse strain overxepressing the catalase enzyme
Mff	Mitochondrial fission factor
Mfn-2	Mitofusin 2
mg	Milligrams
Mg_2ATP	Adenosine 5′-triphosphate magnesium salt
$MgCl_2$	Magnesium Chloride
$MgCl_2 \cdot 6H_2O$	Magnesium Chloride, Hexahydrate
Mito	Mitochondrial extract
ml	Millilitre
MnSOD	Manganese-dependent Superoxide Dismutase
M.O.M	Mouse On Mouse blocking
MOPS	3-(N-Morpholino)propane sulfonic acid
MSEA	Metabolite Set Enrichment Analysis
MuSK	Muscle-Specific Kinase
MyHC	Myosin Heavy Chain isoform
Na_2HPO_4	Disodium hydrogen phosphate trihydrate

NAD+	Nicotinamide Adenine Dinucleotide oxidised
NADH	Nicotinamide Adenine Dinucleotide + Hydrogen - reduced
NF-κB	Nuclear factor kappa-light-chain-enhancer of activated B cells
NMJ	Neuromuscular junction
NMJs	Neuromuscular junctions
NMR	Nuclear Magnetic Resonance
NO	Nitric Oxide
NOS	Nitric Oxide Synthase
NOX	gp91phosphorylated homologues distinguishing NADPH Oxidase isoforms
NOX1	NADPH Oxidase 1
NOX2	NADPH Oxidase 2
NOX4	NADPH Oxidase 4
NF-κB	nuclear factor kappa-light-chain-enhancer of activated B cells
Nrf2	Nuclear factor erythroid 2-related factor 2
$O_2^{\bullet-}$	Superoxide anion
O_2	Oxygen
OCT	Optimal cutting temperature compound
$ONOO^-$	Peroxynitrite
OPA1	Optic Atrophy 1
p22phox	p22 phosphorylated
p40phox	p40 phosphorylated
p47phox	p47 phosphorylated
p67phox	p67 phosphorylated
PBS	Phosphate Buffer Saline
pDRP1	Phosphorylated Dynamin-1-Like Protein

Pi	Inorganic Phosphate
ppm	Parts Per Million
Prx	Peroxiredoxin
Prx6	Peroxiredoxin 6
PVDF	Polyvinylidene difluoride
QH_2	Reduced Ubiquinone
Qi	Coenzyme Q oxidised
Qo	Centre of complex III
Rac	Ras-related C3 botulinum toxin substrate
RLRs	RIG-1-like receptors
ROMO1	Reactive Oxygen Species Modulator 1
ROS	Reactive Oxygen Species
rpm	Round per Minute
SDS	Sodium dodecyl sulphate
SO_2H	Sulfinic acid
SO_3H	Sulfonic acid
SOH	Sulfenic acid
SOL	Soleus muscle
sPLA2	Secretory phospholipase A2 isoform
SSA	5-Sulfasalicylic
TA	Tibialis Anterior muscle
TBS	Tris Buffer Saline
TBS-T20	Tris Buffer Saline - Tween 20
TEA	Triethanolamine
Temed	NNN'N'-tetramethylethylene-diamine

TMRM	Tetramethylrhodamine, methyl ester
TSP	Selectively deuterated TrimethylSilyl Propionate
TNF-α	Tumour necrosis factor alpha
Trx	Thioredoxin Reductase
TrxR	Thioredoxin
Vi	Initial volume
XMP	Xanthosine Monophosphate
YFP	Yellow Fluorescent Protein
δ	Chemical shift
Δψm	Mitochondrial membrane potential

Acknowledgements

The past 3 years have been among the most exciting and demanding of my life so far. I sincerely express my gratitude to my supervisory team: Dr Aphrodite Vasilaki, Prof Malcolm Jackson and Dr Natalie Pollock. They were always there to support and motivate me doing everything they could to allow me to reach my full potential encouraging me to elaborate my own thoughts and interpret every result independently.

A special mention goes also to all the other members of the group: Anne, Caroline, Clare, Jamie, Sam, Kay but in particular to Euan, Shah, Lorenzo and Wasu for having been such a help, support and distraction in the past 3 years. It is also impossible not to mention Dr Marie Phelan for having been so helpful and patient during the NMR metabolomics experiments and my advisors Dr Kasia Whysall and Professor John Wilding having been an important additional support and guidance. Furthermore, I would like to thank the Institute of Ageing and Chronic Disease and the U.S. National Institutes of Health for the financial support and The University of Liverpool and the Biomedical Service Unit for providing all the necessary support in order to complete this project.

Outside my PhD, a special thank goes to Melissa who, since she became part of my life, always made me feel loved, appreciated and proud of who I am. Thank you also to my best friend Andrea who has always been there to support me although living in another country and to Stan and Natasha for welcoming in their family with open arms and for making me feel at home since the very beginning.

And last (but not least) thank you to my family, in particular my parents and two brothers, whom by setting the right example and making a lot of sacrifices allowed me to become the person that I am today.

Dedicato a mamma e papá
(Dedicated to my mother and father)

Chapter 1. Introduction

1.1 Skeletal muscle

In mammals 3 major types of muscles can be identified: smooth, cardiac and skeletal. Smooth muscle is an involuntary, non-striated muscle found in many organs such as stomach, intestines, urinary bladder, uterus and that can also be found in arteries and veins. Cardiac muscle, as the name suggests, constitutes the main tissue of the heart walls. It is an involuntary, striated muscle, whose activity is regulated by special pacemaker cells. Skeletal muscle is a voluntary, striated muscle whose contraction is tightly regulated by the somatic nervous system. This very dynamic and plastic tissue accounts for 30-40% of total body mass (Janseen et al, 2000) and contains 50-75% of the proteins of our body (Frontera and Ochala, 2015).

The majority of skeletal muscle (75%) is composed of water, 20% proteins (which 80% is represented by contractile, regulatory and cytoskeletal proteins), salts, minerals, carbohydrates and lipids that all together represent the remaining 5% (Frontera and Ochala, 2015). Skeletal muscle has multiple important functions including the conversion of chemical energy into mechanical energy in order to generate force and power necessary for posture maintenance and movement. In addition, skeletal muscle exerts important metabolic roles including: storage of amino acids and carbohydrates, production of heat and it is accountable for consumption of the majority of oxygen (O_2) and fuel used during physical activity and exercise (Frontera and Ochala, 2015). *Figure 1.1* demonstrates the multilevel structure of skeletal muscle which is composed of different tissues including: muscle tissue, nerves, blood vessels and connective tissue (Powers and Howley, 1994).

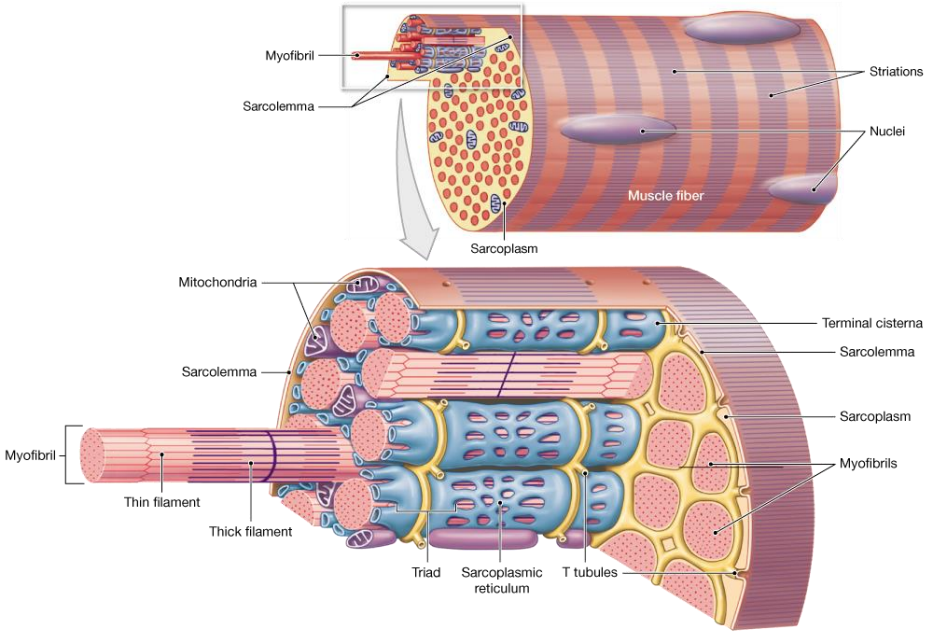

***Figure 1.1**. Schematic representation of the skeletal muscle composition. Image from Pearson Education, Inc.*

Muscle fibres are long multinucleated cells whose plasma membrane is known as the sarcolemma and is developed from the fusion of single nucleated cells known as myoblasts. Each muscle fibre is formed by around 1,000 small structures (1 to 2 µm in diameter) that represent the main contractile elements and are known as myofibrils. Myofibrils are composed mainly of two proteins called myosin and actin. Actin, together with troponin and tropomyosin, forms the thin filament which functions as anchorage for myosin. Myosin is formed of 6 polypeptides: 2 heavy chains and 4 light chains (2 regulatory and 2 alkali) with the heavy chain that contains the heads capable to interact with the actin binding site and possess an adenosine triphosphate (ATP) binding site responsible for hydrolysing ATP into ADP and Pi releasing the energy necessary for contraction (Lodish, 2000). Myosin is responsible for binding the anchorage site and pull the thick filament with it (Saladin and Kenneth, 2012). Following a stimulus capable of releasing calcium ions (Ca^{2+}) from the endoplasmic reticulum, Ca^{2+} binds to troponin C exposing specific sites present on the actin filaments. At this stage, actin

and myosin are almost ready to interact but another step is necessary to initiate the contraction (Saladin and Kenneth, 2012). Actin and myosin can be found in two different structural states, strong and weak, coupled with ATP (Baumann et al, 2016). The link between ATP and myosin is a weak structural state and ATP hydrolysis is necessary to induce a change of the myosin structural status allowing cross bridging between actin and myosin. The ATP binding and hydrolysis cycle allows the interaction of actin and myosin that result in the sliding of the actin filaments toward the M-Line (*Figure 1.2*) (Baumann et al, 2016).

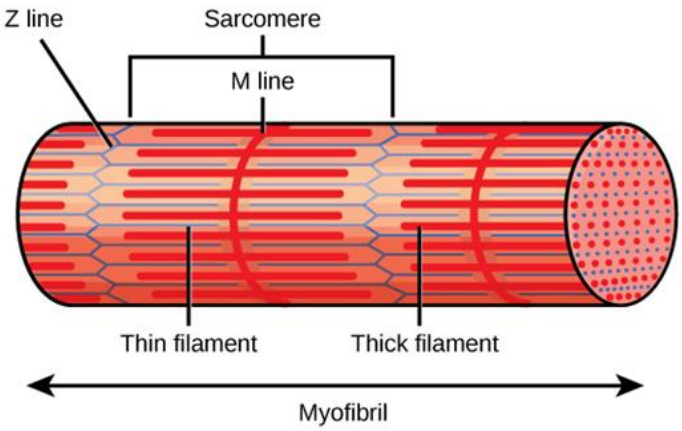

Figure 1.2. *Schematic representation of a myofibril and its contractile components. Image from https://courses.lumenlearning.com*

Four different Myosin Heavy Chains (MyHC) isoforms have been discovered in skeletal muscle: MyHC-I, MyHC-IIa, MyHC-IIb and MyHC-IIx. These isoforms have significant differences (in metabolism, characteristics and functioning) but they also share a lot of similarities. They all encode between 1935-1942 amino acids and have a molecular weight between 200-220 kDa (Sawano et al, 2016). In addition, these isoforms share a very high level of similarity in amino acid sequence; however, one of the main differences among these is that in the 19th position of the N-Terminus,

MyHC-I contains the amino acid leucine, MyHC-IIa methionine, MyHC-IIb valine and MyHC-IIx isoleucine (Sawano et al, 2016).

Differences in muscle fibres contractile and metabolic properties are due to their Myosin Heavy Chain isoform composition (Harridge et al, 1996) and are presented in *Table 1.1*.

***Table 1.1**. Classification of fibre types in skeletal muscles. Adapted from Powers and Howley, 1994.*

	Twitch speed	ATPase activity	Glycolytic activity	Resistance to fatigue	Energy system
Type Ix	Slow	Low	Moderate	High	Aerobic
Type IIa	Fast	High	Moderate to high	Moderate	Mixed
Type IIb	Fast	High	High	Low	Anaerobic
Type IIx	Fast	High	High	Low	Anaerobic

Skeletal muscle has a high plasticity and it is able to modify its fibre size and fibre composition according to need (Scott et al, 2001). In addition, some age-related structural and physiological “abnormalities” are commonly seen including variations in size, shape and organization of muscle fibres (Lexell and Taylor, 1991) that will be further discussed later in this chapter.

1.2 The Neuromuscular System

The neuromuscular system is composed of motor units and every motor unit comprises a motor neuron and all the muscle fibres innervated by it. The core system of every motor unit is the neuromuscular junction which represents one of the major subclass of synapses and that plays a central role in the network that connects the brain with the skeletal muscles (Jones et al, 2017).

1.2.1 Neuromuscular system anatomy and physiology

The neuromuscular system is a complex network of different types of cells: motor neurons, Schwann cells, muscle fibres and kranocytes (Sugiura and Lin, 2011). The core structure of this system, the neuromuscular junction (NMJ), is a chemical synapse that connects a motor neuron and a muscle fibre (Rygiel et al, 2016). Due to the activity of docking protein downstream-of-tyrosine-kinase 7 (DOK7), NMJs show a characteristic "*pretzel*" conformation that is shared among mammals and allows the link of the axon terminal to the post-synaptic receptors (Hepple and Rice, 2016).

The main role played by the NMJ is the conversion of the action potential from the nerve into muscle contraction (Tintignac et al, 2015). This task requires control, coordination and the signal must be transmitted quickly and reliably. To generate a contraction, a neurotransmitter, acetylcholine (ACh), is released by the presynaptic terminal of the motor neurons. Once released, ACh binds to nicotinic acetylcholine receptors present on the post-synaptic receptors on the muscle fibre surface. The link between ACh and nicotinic receptors generates an action potential that is distributed across the surface of the sarcolemma penetrating within the muscle fibre through the transverse tubules. This depolarization stimulates the voltage-sensitive dihydropyridine receptors present in the transverse tubules that in turn activate the ryanodine receptors (calcium channels composed of four monomers embedded in the sarcolemma membrane). The activation of ryanodine receptors leads to an increase in cytoplasmic levels of calcium initiating the contraction process described above (Baumann et al, 2016).

Several proteins cooperate to maintain the stability of the NMJ, activating a cascade of signals that involves the entire neuromuscular system (Hepple and Rice, 2016). An important role in this signalling event is played by agrin, a large heparin sulphate proteoglycan generated in the cell bodies of motor neurons and transported alongside

the axons to the motor neuron terminal. Agrin is then released in the post-synaptic cleft and sequestered by the agrin receptors present on the myotube surface (McMahan, 1990). Once incorporated in the muscle this large heparin sulphate proteoglycan of 220kDa is able to link and activate an important muscle-specific tyrosine kinase known as Muscle-Specific Kinase (MuSK) (McMahan, 1990; Tsen et al, 1995). Once activated, MuSK interacts with DOK7 leading to clustering of the acetylcholine receptors in the classic pretzel configuration (Koneczny et al, 2014).

1.3 Mitochondria

Mitochondria are small structures of 1-2 micron in length and ~0.2-0.7 micron in diameter that play a primary role in most eukaryote systems. Mitochondria occupy approximately 25% of a normal eukaryote cell (Lodish et al, 2004) and approximately 10-15% of the total muscle volume (Eisenberg, 1983). These structures were firstly observed in 1890 by Richard Altmann who named them "*bioblasts*". Subsequently, Carl Brenda renamed them "*mitochondria*" but it was only in 1954 that the important role played by mitochondria was recognized by Philip Siekevitz who defined these structures as "*the powerhouse of the cell*" (McBride et al, 2006). Since 1954, mitochondria have been well known for their primary role in energy production generating ATP utilizing nutrient substrates and O_2 (Porter and Wall, 2012). Nevertheless, this is not the only role played by these structures as they also play a role in cellular signalling, cell growth, differentiation and death (McBride et al, 2006).

Mitochondria are formed by an inner and an outer membrane of phospholipids and proteins with different characteristics and functions. These membranes create 4 different compartments:

- Outer mitochondrial membrane;
- Intermembrane space (the space between the outer and inner membranes);

- Inner mitochondrial membrane (in which the complexes of the ETC and ATP synthase are found);
- Matrix (space within the inner membrane) (Alberts et al, 2002; McBride et al, 2006).

Cells are able to produce ATP through different pathways such as: glycolysis, citric acid cycle/oxidative phosphorylation (the combination is known as cellular respiration) and β-oxidation (Alberts et al, 2002).

Glycolysis, a ten enzyme-catalysed reaction, is an oxygen-independent pathway that occurs in the cytosol and that yields pyruvate as its main product (Voet et al, 2006). Once pyruvate molecules are generated by glycolysis, these are actively transported into the mitochondrial matrix where they are oxidised and combined with coenzyme A producing CO_2, acetyl-CoA, and Nicotinamide Adenine Dinucleotide + Hydrogen (NADH) (Voet et al, 2006).

Once Acetyl-CoA is formed within the mitochondria, the second step of cellular respiration begins. The citric acid cycle, also known as the Krebs cycle, is a series of chemical reactions that requires 8 enzymes involved in the conversion of Acetyl-CoA in 2 molecules of water and carbon dioxide and the production of guanosine triphosphate, 3 NADH molecules, 1 $FADH_2$ and 1 ATP (Wagner, 2014).

The third stage of cellular respiration is known as oxidative phosphorylation, a metabolic pathway where several enzymes are used to oxidise nutrients releasing energy that is then used to generate ATP. To release the energy necessary to generate ATP, a series of redox reactions take place where electrons are transferred from donors to acceptors. In eukaryotic cells, this series of reactions takes place within the mitochondria and is carried out by a set of proteins that together form the Electron Transport Chain (ETC). Four main protein complexes are involved in this process and the energy generated is

used to transport protons through the mitochondrial membrane. The potential energy produced in the form of pH gradient and electrical potential across the membrane induces a rotational movement of a part of the ATP synthase enzyme which converts the adenosine diphosphate (ADP) into ATP.

The 4 protein complexes are (*Figure 1.3*):

- NADH-coenzyme Q oxidoreductase (complex I);
- Succinate-Q oxidoreductase (complex II);
- Q-cytochrome c oxidoreductase (complex III);
- Cytochrome c oxidase (complex IV) (Guo et al, 2018).

Following all the reactions of the ETC, for each NADH molecule that enters the transport chain, a total of 10 protons are pumped into the mitochondrial inter-membrane space:

- Complex I pumps 4 protons;
- Complex II reduces 2 protons but none of them is pumped outside the matrix;
- Complex III pumps 4 protons (two of them obtained from complex II);
- Complex IV pumps 2 protons (Guo et al, 2018).

The pumping of protons across the mitochondrial matrix into the intermembrane space generates an accumulation of positive charge in the intermembrane space and an accumulation of negative charges within the matrix (Li et al, 2013). This charge misbalance between the matrix and the inner membrane generates a mitochondrial membrane potential ($\Delta\psi m$) necessary to activate the final step of oxidative phosphorylation (Li et al, 2013).

The final step of cellular respiration is carried out by ATP synthase, a protein complex composed of sixteen subunits (Rubinstein et al, 2003). The increased mitochondrial membrane potential induces a flux of protons through the channel at the base of ATP

synthase activating this complex inducing conformational changes and generating the energy necessary to couple ADP with inorganic phosphate (Pi) forming ATP. Three to four protons are required to synthesise one ATP molecule; this ratio can vary according to different conditions (Schemidt et al, 1998).

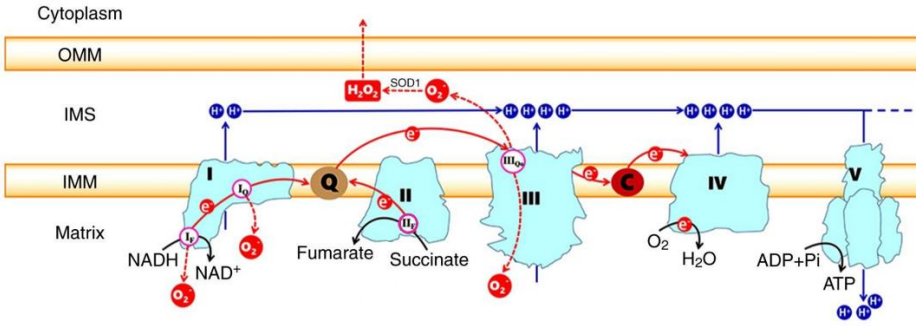

Figure 1.3. *Graphical representation of the ETC and its reactions resulting in the production of ATP and Reactive Oxygen Species. Image adapted from Zhao et al, 2019.*

The process described above involving glycolysis, citric acid cycle and oxidative phosphorylation is able to form 38 molecules of ATP (2 from glycolysis, 2 from citric acid cycle and 34 from ETC) from a single molecule of glucose (Bonora et al, 2012). Although mitochondria play fundamental roles within the cell, they are also major contributors to intracellular oxidant production (Holmstron and Finkel, 2010). Mitochondrial oxidants, also known as mitochondrial reactive oxygen species, are mainly generated during oxidative phosphorylation.

1.4 Reactive Oxygen Species

Reactive Oxygen Species (ROS) is a general term used to refer to reactive molecules generated as by-product of normal aerobic metabolism and are commonly produced in the mitochondrion (Rahal et al, 2014). Nevertheless, ROS can also be formed during

reactions involving cytochrome P-450 enzymes, peroxisomal oxidase, NADPH Oxidase and xanthine oxidase (Rahal et al, 2014).

In the mitochondrion the leakage of electrons from complex I and III induces a one-electron reductions of an O_2 molecule generating superoxide anion (Sakellariou et al, 2014a; Rahal et al, 2014). Recent data indicate that a maximum of approximately 0.15% of the total electron flow in the mitochondria gives origin to ROS (Jackson et al, 2016a). Among the complexes of the ETC, complex I and complex III are mainly involved in the production and release of superoxide (Figure 1.3) with complex I being the main producer of superoxide both *in vivo* and *in vitro* (Sakellariou et al, 2014a). Two mechanisms are involved in the superoxide production within complex I:

- **NADH-FMN interaction and NADH/NAD+ ratio**

  Complex I can produce superoxide through the reaction of O_2 with reduced Flavin mononucleotide produced during the process that transfer electrons from NADH to ubiquinone. The reduced state of Flavin mononucleotide is determined by the NADH/NAD+ ratio which increase can be induced by several factors such as mitochondrial damages, ischemia, low ATP request or various mutations. The increase of NADH/NAD+ ratio has been linked with increased superoxide production by complex I in the ETC (Kussmaul and Hirst, 2006; Murphy, 2009).

- **Reverse electron transport**

  It is also possible that along the ETC, electrons are driven backwards from reduced coenzyme Q (CoQH2) into complex I with subsequent reduction of NAD+ into NADH. This pathway occurs when the electrons supply is elevated and there is a reduction in the concentration of coenzyme Q available.

Although the role played by complex III in superoxide production during normal conditions is small compared to complex I, it is important to not underestimate the role of this complex in the production of ROS (Murphy, 2009). Complex III ROS production can be triggered by two events:

- Increased supplementation of reduced coenzyme Q;
- Inhibition of oxidised coenzyme Q (Qi - one of the two centres of the complex III) by antimycin (a secondary metabolite produced by Streptomyces bacteria) enhancing the reaction between O_2 with an ubisemiquinone bound to the other centre of the complex III (Qo) (Neft and Farley, 1972; Cadenas et al, 1977; Bleier and Drose, 2013).

Another important factor associated with mitochondrial ROS production and release is the O_2 concentration. The increase of O_2 flux within mitochondria is associated with increased mitochondrial ROS production (Stowe and Camara, 2009). Paradoxically, this increase is registered also during hypoxia where the complex III ROS production is increased (Bell et al, 2007). The theories proposed to explain this increased mitochondrial ROS production in both hyperoxia and hypoxia still remain controversial. A state of hyperoxia could induce an increase of mitochondrial ROS production given the increased O_2 concentration within the mitochondria with more chances of interaction of an electron and an O_2 molecule. On the other hand, the increase of mitochondrial ROS production during hypoxia is still not fully understood. Nevertheless, as proposed by Aon and colleagues (2010), a hypoxic state seems to increase mitochondrial membrane potential explaining the increase in ROS production.

ROS can be divided into free radicals (atom/molecules presenting one or more unpaired electrons such as superoxide) or non-radical derivate of O_2 (such as hydrogen peroxide) (Powers et al, 2011). Both free radical and non-radical ROS have the ability to interact

with other molecules altering their structure and inducing damage to nucleic acids, proteins and lipids (Duan and Kasper, 2011). The uncontrolled accumulation of ROS, a condition known as "*oxidative stress*" has been associated with carcinogenesis, neurodegeneration, atherosclerosis, diabetes and ageing (Ray et al, 2012). Nevertheless, several studies have also highlighted the capacity of the cells to restrict and control ROS utilising these molecules for the activation of important signalling pathways (Li et al, 2013).

ROS production in skeletal muscle holds a particular relevance as during contraction a high ROS flow has been reported (Barbieri and Sestili, 2012). Furthermore, in muscles, ROS may trigger different signalling pathways able to induce different responses from adaptation to cell death (Barbieri and Sestili, 2012).

1.5 Reactive Oxygen Species production in skeletal muscle

Different ROS can be found in skeletal muscle including the free radical superoxide and the non-radical hydrogen peroxide (H_2O_2) (Powers and Jackson, 2008). As shown in *Figure 1.4*, within the skeletal muscle different enzymes and metabolic processes can induce the production of ROS (Powers and Jackson, 2008).

1.5.1 Superoxide anion

Superoxide is the product of the incomplete reduction of an O_2 molecule by a single electron that results in the formation of a reactive molecule with a relatively long half-life and limited radical character (Sakellariou et al, 2014a). Given the negative charge, superoxide cannot easily diffuse across the cell membranes (it can only do this by exploiting voltage-dependent anion channels), therefore the production site of superoxide is of major relevance (Han et al, 2003). Increasing evidence suggests that superoxide produced by complex I is released into the matrix while superoxide produced by complex III is released both in the matrix and in the intermembrane space (Szeto,

2008). In addition, in skeletal muscles, superoxide can be generated also by NADPH oxidase (present in the mitochondrion, sarcoplasmic reticulum and transverse tubules) and by xanthine oxidase in the endothelium (Powers et al, 2011). As mentioned previously, superoxide possess a limited radical character as it does not directly react with polypeptides, sugars, or nucleic acids but can be quickly converted onto secondary ROS such as H_2O_2 or peroxynitrite. It has been calculated that in aqueous solution, superoxide is dismutated to H_2O_2 at a rate of approximately 2 x 10^9 $M^{-1}s^{-1}$ (Beckman and Koppenol, 1996) mainly by the activity of two enzymes: Copper-zinc superoxide dismutase and Manganese-dependent superoxide dismutase (Li et al, 2013).

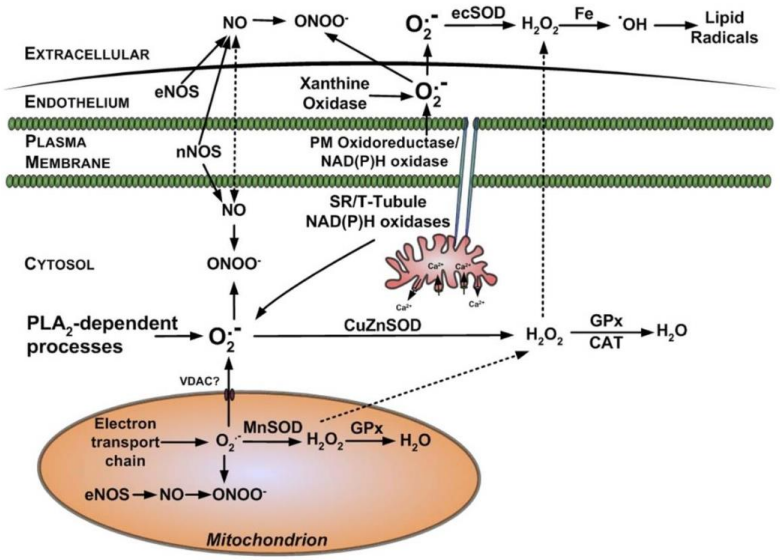

Figure 1.4. *Schematic representation of ROS production in eukaryotic cells. Superoxide ($O_2^{\cdot -}$) mainly generated in mitochondria during the electron transport chain is quickly converted into a more stable compound known as Hydrogen peroxide (H_2O_2) by enzymes belonging to the superoxide dismutase family (MnSOD and CuZnSOD). Alternatively, superoxide can also be converted into peroxynitrite ($ONOO^-$) following the interaction with nitric oxide (NO) a reactive nitrogen species generated by the activity of the Nitric Oxide Synthase (NOS) family. Generation of $ONOO^-$ is harmful for the cell since this free radical can damage a wide array of molecules including DNA and proteins. Image from Powers and Jackson, 2008.*

1.5.2 Hydrogen peroxide

Hydrogen peroxide is a non-radical ROS mainly generated through the dismutation of superoxide by the superoxide dismutase enzymes (Fukai and Fukai, 2011). As explained by Go and colleagues (2015), H_2O_2 can also be generated as a consequence of several one- or two-electron reduction reactions by 31 different enzymes. Among these 31 enzymes, a primary role in skeletal muscle is played by NADPH Oxidase, Phospholipase A2, Monoamine Oxidase A and Monoamine oxidase B (Sies, 2017, Go et al, 2015).

H_2O_2 is involved in a large series of signalling pathways such as cell shape changes, inflammatory response, immune cell proliferation and recruitment. Together with calcium ions and ATP, H_2O_2 is recognised as one of the main transcription-independent signalling molecule within the cell (Sies, 2017; Flohe et al, 2011). Hydrogen peroxide's main role in redox regulation is played through thiol peroxidases and the involvement of the reversible oxidation of cysteine residues and the formation of disulphide bonds (Sies, 2017; Flohe et al, 2011). Once generated, H_2O_2 is quite stable with a long half-life (1ms) compared to superoxide (1μs) (Bienert et al, 2006) and in skeletal muscle, during resting conditions, its levels have been estimated to be around 10-100 nM (Jackson et al, 2016a). Furthermore, H_2O_2 can also move through the different muscle cell compartments exploiting specific aquaporin channels, also identified as peroxiporins for their specificity for H_2O_2 (Bienert et al, 2006; Sies, 2017).

H_2O_2 is rapidly produced within the cell but despite its weak reactivity its accumulation can by cytotoxic (Lennicke et al, 2015). Therefore, within the cell, antioxidant enzymes such as glutathione peroxidase, catalase and peroxiredoxins are present and capable of catalysing the reduction of H_2O_2 (Lubos et al, 2011).

1.5.3 Hydroxyl radical

Hydroxyl radical ($HO^{\bullet}$) is a highly reactive and short-lived molecule generated by the reaction of H_2O_2 and active copper or iron atoms (Vatansever et al, 2013). The generation of H_2O_2 in close proximity of these metals creates the conditions for the initiation of a Fenton reaction that leads to the production of hydroxyl radical (Halliwell, 1989).

Hydroxyl radical plays a role in DNA damage. Indeed, this molecule is a strong mutagen that targets DNA, in particular the 5-methyl group on the thymine base forming a 5-formyluracil base that can induce pyrimidine transitions like G:C to A:T (and *vice versa*) seriously affecting DNA replication (Tsunoda et al, 2010). Furthermore, hydroxyl radical compared to other ROS such as H_2O_2 is more prone to inactivate most of mitochondrial enzyme proteins seriously affecting mitochondrial survival (Zhang et al, 1990).

1.5.4 Alternative sources of H_2O_2

1.5.4.1 Monoamine Oxidase

Monoamine Oxidases is a family of enzymes that in mammals is composed by 2 isoforms: Monoamine Oxidase A and Monoamine Oxidase B. The two Flavin isoforms found in mammals share approximately 70% of sequence homology and present some overlap in functions despite using different substrates and being inhibited by different inhibitors (Duicu et al, 2016). During normal physiological conditions Monoamine Oxidase A shows a particular preference for serotonin and norepinephrine while Monoamine Oxidase B appears to be more active in processing phenethylamine. In addition both isoforms oxidise (at a similar rate) tyramine and dopamine (Edmondson, 2014). These enzymes are present in the mitochondrial outer membrane and their primary functions are the regulation of neurotransmitter levels and the degradation of amines produced from important neurotransmitters such as serotonin, dopamine and

norepinephrine that could function as false neurotransmitters (Edmondson, 2014; Duicu et al, 2016). Both Monoamine Oxidase A and B play an important role in H_2O_2 production being capable of producing a large amount of this ROS, increasing its steady state concentration both in the mitochondrial matrix and the cytosol through the following reaction (Cadenas and Davies, 2000; Duicu et al, 2016):

$$R\text{-}\ CH_2\text{-}NH_2 + O_2 + H_2O \rightarrow R\text{-}CHO + NH_3 + H_2O_2$$

1.5.4.2 Phospholipase A2

The phospholipase A2 family of enzymes is involved in the hydrolysis of sn-2 fatty acyl chains of phospholipids generating fatty acid such as arachidonic acid (Sakellariou et al, 2014a). This family of enzymes is found in mammalian tissues, in arachnid, insects and snake venom (Nicolas et al, 1997). Arachidonic acid is an important substrate for cyclooxygenases (COX) and lipoxygenases (LOX) both involved in the generation of ROS playing a role in different physiological processes such as inflammation, apoptosis or cell injury (Sun et al, 2010).

Three different major isoforms of PLA2 have been identified:

- The secretory PLA2 located prevalently in the sarcolemma and mitochondria;
- The calcium-dependent PLA2 (cPLA2) mainly found in the cytosol but with the capacity to translocate within the mitochondria during stress conditions;
- The calcium-independent PLA2 (iPLA2) found in mitochondria even during non-stress conditions (Sun et al, 2010).

Particularly involved in the production of arachidonic acid is the cPLA2 isoform that plays a role in the modulation of several processes (Sun et al, 2010). It also plays an important physiological role during skeletal muscle contraction influencing contracting properties and fatigue characteristics of the muscle (Sakellariou et al, 2014a). Calcium-

dependent PLA2 activity is influenced by different factors such as the intracellular levels of calcium, the phosphorylation state and the exposure to ROS such as H_2O_2 (Sakellariou et al, 2014a). For instance, an increase of calcium flux induces the activation and movement of cPLA2 to the endoplasmic reticulum and perinuclear membrane allowing it to release arachidonic acid using the membrane phospholipids as substrate (Sun et al, 2010).

Arachidonic acid produced by cPLA2 is involved in enhancing ETC ROS production (Sakellariou et al, 2014a) and an increase in cPLA2 expression and content is indicative of an increased production of fatty acid hydroperoxides concentration in skeletal muscle (Abruzzo et al, 2010). Additionally, arachidonic acid produced by cPLA2 can be used by Mitogen-activated protein kinase (MAPK) as substrate to induce the phosphorylation and translocation of p40 phosphorylated, p47 phosphorylated and p67 phosphorylated to the membrane, allowing the assembling of NADPH Oxidase 2 (Zhao et al, 2002).

1.5.4.3 NADPH Oxidase

NADPH Oxidase is a family of multi-subunit enzymes mainly localized on the cell membrane (Sun et al, 2010). NADPH Oxidase, which was firstly described in phagocytes, plays an important role in the immune system being responsible of the initiation of the respiratory burst (Nguyen et al, 2017), a very quick release of ROS from different cells (in particular from immune system cells following exposure to infections) (Inoguchi et al, 2003).

As shown in table 1.2, NADPH Oxidase isoforms are expressed in different tissues where they play several different functions.

In skeletal muscle 2 main NADPH Oxidases are expressed (Figure 1.5):

- NADPH Oxidase 2 (NOX2) found in the sarcolemma, transverse tubules and sarcoplasmic reticulum;

- NADPH Oxidase 4 (NOX4) expressed in the sarcolemma, sarcoplasmic reticulum, transverse tubules but also in the inner mitochondrial membrane (Ferreira and Laitano, 2016; Loureiro et al, 2016).

Table 1.2. *Overview of the main NADPH Oxidase isoforms, their expression in different tissues, cell localisation, functions and regulatory components. Table was adapted from Panday et al, 2014; Breitenbach et al, 2018.*

Isoform	Expression	Cell localisation	Biochemical function	Regulatory factors
NOX1	Colon, Prostate, Placenta, Rectum, Smooth muscle, Uterus.	Cytoplasm	Signalling	p22, NOXO1, NOXA1
NOX2	Cardiomyocytes, Central Nervous System, Endothelian cells, Fibrobalsts, Skeletal Muscle Paghocytes/granulocytes.	Plasma membrane	Immune defense, Signalling	p22, p47, p67, p40, Rac
NOX3	Fetal kidney, Inner ear.	Plasma membrane	Synthesis of otolith	p22, NOXO1, NOXA1
NOX4	Eye, Kidney, Liver, Ovary, Skeletal muscle.	Nucleus, Endoplasmic Reticulum, Mitochondria	Cell division signalling	p22
NOX5	Cerebrum, Mammary glands, Lymphatic tissue, Protstate, Spleen, Testis.	Plasma membrane	Signalling	Ca2+
DUOX1	Cerebellum, Lungs, Respiratory tract epithelium, Thyroid.	Plasma membrane	Cell cycle regulation, Peroxidase domain, Synthesis of Thyroxine.	DUOXA1, DUOXA2, Ca2+
DUOX2	Colon pancreatic islets, Pancreas, Prostate, Stomach, Thyroid.	Plasma membrane	Cell cycle regulation, Peroxidase domain, Synthesis of Thyroxine.	DUOXA1, DUOXA2, Ca2+

NOX4 is associated with the regulatory subunit p22 and its activity is normally regulated by its own level of expression (Loureiro et al, 2016). In contrast, NOX2 needs specific agonists for its activation (e.g. cytokines, growth factors or mechanical

stress) able to induce the association of all the regulatory subunits that compose this enzyme (Konior et al, 2014).

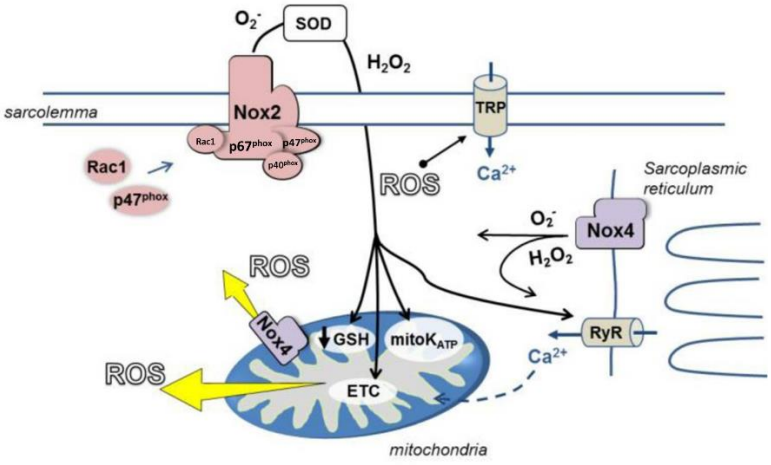

Figure 1.5. *Schematic representation of NOX2 and NOX4 localisation and ROS release sites in skeletal muscle. Image adapted from Ferreira and Laitano, 2016.*

NOX2 is composed of different proteins whose content, location and function are required for the correct functioning of this enzyme. The NOX2 components shown in Figure 1.6 are:

- gp91 phosphorylated (gp91phox) - several homologues of gp91phox have been identified (NOX 1-5, DUOX 1-2);
- p22 phosphorylated (p22phox);
- p40 phosphorylated (p40phox);
- p47 phosphorylated (p47phox);
- p67 phosphorylated (p67phox).

The large glycosylated protein gp91phox and the smaller adapter protein p22phox compose the membrane-bound part of this protein (Panday et al, 2015). p22phox contains a SRC Homology 3 Domain site which is fundamental for the link of the triumvirate of

soluble oxidase component p40phox, p47phox and p67phox linked together by the interaction of SRC Homology 3 Domain and SH3 binding sites (Panday et al, 2015).

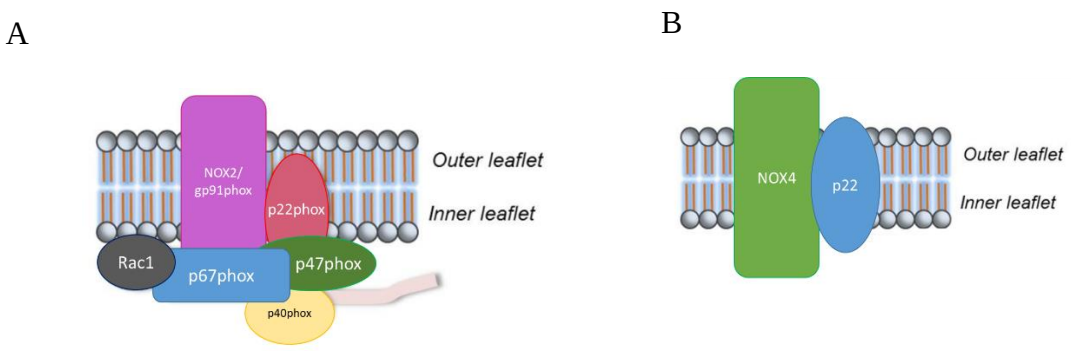

Figure 1.6. *Schematic representation of the NOX2 (A) and NOX4 (B) structures and subunits. Image adapted from Ferreira and Laitano, 2016.*

p40phox plays an important role in the recruitment of p47phox and p67phox and it appears to have an important regulatory effect on this complex assembly (Holmstron and Finkel, 2010). The phosphorylation of p47 results in protein shape modification, translocation to the membrane and binding to p22phox (Holmstron and Finkel, 2010). The phosphorylation of p67 is another important step in the correct functioning of NOX2. Indeed, p67phox is involved in the transfer of electrons from NADPH to FAD. Lastly, a small protein called Ras-related C3 botulinum toxin substrate (Rac) is necessary for activation of this complex (Holmstron and Finkel, 2010). This protein switches between inactive (when it is bound to Guanosine Diphosphate) and active forms (when it binds Guanosine Triphosphate) (Holmstron and Finkel, 2010). Once Rac is activated and linked with p67phox, the electron flow from NADPH to FAD begins resulting in the formation of superoxide and the release of NADH-dissociated protons that become available to interact with superoxide and generate H_2O_2 (Nisimoto et al, 2014).

NOX2 activation results in a significant increase of H_2O_2 that can have important physiological implications, playing an important role in signalling (Sun et al, 2010). For instance, H_2O_2 generated by NOX2 appears to play an important role during contraction (Ward et al, 2014) alongside a lot of other fundamental functions such as insulin resistance or activation of atrophy pathways (Ferreira and Laitano 2016).

NOX4 is an O_2 sensor able to regulate the KCNK3/TASK-1 potassium channel and the activity of Hypoxia Inducible Factor 1 Alpha (Lee et al, 2006). In addition, recent evidences suggests that NOX4 may also play a role in angiotensin II-induced muscle wasting regulating the activity of Nuclear factor erythroid 2-related factor 2 (Nrf2) protein (Kadoguchi et al, 2018).

1.5.5 Redox homeostasis and oxidative stress

Redox homeostasis is: "*the capacity of the cells to continuously deal with challenges that generate electrophiles. Challenges brought by different stressors are the result of metabolic or environmentally non-injurious temporary movement toward the edge of the normal physiological range. Maintenance of redox homeostasis is achieved through feedback mechanisms operating at different level of complexity such as relief of the inhibition of an enzyme or transcriptional up-regulation*" (Ursini et al, 2016). In simpler terms, redox homeostasis can be described as a balance between ROS production and the ability of the body to detoxify these reactive compounds. Both an increase in ROS production and an alteration in the functionality of the detoxifying systems can lead to an alteration of redox homeostasis and to an increased accumulation of ROS-related damage (Gaschler and Stockwell, 2017). The accumulation of ROS and ROS-related damage result in a condition known as "*oxidative stress*", a potential trigger of ageing and other different pathologies such as diabetes (Paravicini and Touyz, 2006), neurodegeneration (Andersen, 2004; Shukla et al, 2011) and is also able

to promote tumour metastasis through the direct interaction with specific genes (Ishikawa et al, 2008; Trachootham et al, 2009). Oxidative stress can be defined as a physiological chronic misbalance between pro-oxidant/antioxidant concentrations that leads to alterations of homeostasis and accumulation of high levels of ROS (Uttara et al, 2009).

The accumulation of ROS that has been registered during ageing has been reported to trigger an increase of proteolysis that can explain the correlation between oxidative stress and sarcopenia (Baumann et al, 2016). The mechanisms that connect the accumulation of ROS during ageing and muscle wasting are still not completely clear. As suggested by Powers and colleagues (2011), the mechanism behind ROS-related muscle wasting can be compared to the one observed during prolonged periods of physical inactivity. Indeed, during ageing as well as during immobilisation, ROS accumulation stimulate protein breakdown enhancing the activity of protease systems such as ubiquitin-proteasome, caspase or calpains (Baumann et al, 2016).

Recent evidence suggests that ROS might play a crucial role also in regulating lifespan. To understand this, it is necessary to introduce a concept that dates back to the end of XIX century and that was proposed by the German pharmacologist Hugo Schulz. The concept of "*hormesis*" suggests that a little stress at cell level is able to protect the cells from a larger stress (Mattson and Calabrese, 2010). Bearing this in mind, the mitochondrial release of oxidants can trigger the activation of a series of protective pathways able to extend the lifespan of the cells reinforcing the idea that ROS, under certain circumstances, might play a beneficial role in the organism (Holmstrom and Finkel, 2014).

1.5.6 Redox signalling

For many years ROS production was seen as an unregulated process where the target of these molecules were completely random. Through the years, several studies have

revealed that some oxidant species (in particular H_2O_2) might play an important signalling role (Holmstrom and Finkel, 2014).

The reduction-oxidation signalling mechanism (also known as redox-dependent signalling mechanism) it is a highly conserved mechanism that triggers different responses (including increased expression of repair and protective enzymes) following changes in redox of homeostasis (Holmstrom and Finkel, 2014). This process mainly alters structures through the interaction with different amino acids, in particular the amino acid cysteine (Ray et al, 2012). Cysteine is a semi-essential amino acid with formula $C_3H_7NO_2S$, it is one of the least abundant and one of the most conserved amino acids in nature (Poole, 2015). This amino acid contains a low pKa sulfhydryl group (-SH) in his side chain that is very susceptible to oxidation and is able to form a disulphide bonds with another sulfhydryl group making it the main target of oxidants (Janssen-Heininger et al, 2008; Miki and Funato, 2012). Its characteristics and the tendency to be clustered make this amino acid the perfect mediator of ROS-induced post-translations modifications (Poole, 2015; Wood et al, 2016). However, other amino acids such as methionine, tryptophan, and tyrosine can also be targeted by ROS (Janssen-Heininger et al, 2008). The pKa of an amino acid is fundamental for its susceptibility to oxidation and depends on the charge of the neighbouring amino acid. Therefore, the 3-dimensional arrangement of a protein is fundamental for determining ROS-derived modifications (Janssen-Heininger et al, 2008).

Once oxidised, an amino acid can experience a series of different modifications some of which are reversible such as: S-nitrosylation, S-glutathionylation, S-sulfhydration, formation of sulfenic acid and of inter-/intra-molecular disulphide bonds (Murray and Van Eyk, 2012). In addition, amino acids targeted by ROS can also undergo irreversible modifications such as the formation of sulfinic or sulfonic acids (Murray and Van Eyk,

2012). Sulfenic acid (-SOH) is a short-lived species that can form disulphide bonds with nearby cysteines. When sulfenic acid oxidises further, it can form sulfinic acid ($-SO_2H$) or sulfonic acid ($-SO_3H$) (Nagy and Winterbourn, 2010). Both sulfinic and sulfonic acid are less reactive than sulfenic acid and therefore their capacity to form disulphide bonds is much lower (Nagy and Winterbourn, 2010). The formation of disulphide bonds induced by ROS is a fundamental step in redox signalling as it is able to alter the protein structure producing stable dimers, polymers, or complexes with the potential to induce different functional outcomes in the targeted proteins (Janssen-Heininger et al, 2008; Trivedi et al, 2009).

ROS can induce several other modifications at protein level such as carbonylation and glycation that are currently used as markers of oxidative change. Carbonylation is the most common type of alteration during oxidative stress and during this process carbonyl groups are introduced into proteins by a metal-catalysed oxidation of specific amino acids or indirectly by the reaction with species derived from lipid peroxidation (Lyons et al, 1997). Another marker of oxidative stress generally used is 4-hydroxynonenal (4-HNE), one of the aldehydic products of lipid peroxidation that is a key mediator of oxidative stress-induced cell death (Lyons et al, 1997). Furthermore, the addition of a sugar molecule to a protein (known as glycation) results in the formation of Advanced Glycation End Products (AGEs). The levels of AGEs significantly increase during exposure to ROS and, therefore, it has been used as a marker of oxidative stress (Lyons et al, 1997).

1.6 Adaptive responses in skeletal muscle

As already mentioned, antioxidants are the primary mechanism of defence against ROS stress. These molecules are involved in the termination of radical propagation

donating electrons to ROS without becoming a radical themselves (Gaschler et al, 2017).

The accumulation of ROS induces changes in the redox-status of the cell triggering a series of post-translational signals that allow the cell to develop an appropriate cellular response. Important transcription factors activated by changes of the muscle redox-status are nuclear factor kappa-light-chain-enhancer of activated B cells (NF-κB) and Nuclear factor erythroid 2-related factor 2 (Nrf2) (Kurutas et al, 2014).

NF-κB is a dimeric transcription factor composed of p50 and p65 subunits mainly located in the cytoplasm of the cell where it is associated with a transcriptional repressor IκB (Sadi and Sadi, 2010). Activating factors such as cytokines, radiation and exposure to oxidative stress induce activation of the IκB kinase (IKK) complex inducing phosphorylation and subsequent degradation of IκBs (Wan and Lenardo, 2010). The now liberated NF-κB is free to translocate to the nucleus where binding to regulatory DNA sequences known as κB sites is able to regulate gene expression.

Similarly to NF-κB, during normal conditions, Nrf2 is located in the cytosol where it is associated with Kelch-like ECH-associated protein 1 (Keap1), a cytoskeletal protein responsible for the ubiquitination and proteolysis of Nrf2. Keap1 is rich in cysteine residues making it a very sensitive detector of redox-balance changes. Once oxidised Keap1 goes through some conformational changes that result in Nrf2 accumulation and translocation to the nucleus (Sadi and Sadi, 2010). Once in the nucleus, Nrf2 plays an important role as master regulator of cytoprotective genes through the coordination of antioxidant response elements, cis-regulatory elements able to regulate genes transcription following alteration of the redox balance of the cell (Raghunath et al, 2018; Kasai et al, 2020).

Previous studies have shown that in skeletal muscle, in response to changes of redox homeostasis, the contents of several antioxidants enzymes are increased including: superoxide dismutase, catalase, thioredoxins, glutathione peroxidase and Peroxiredoxins (Kurutas et al, 2014).

1.6.1 Superoxide Dismutase

Superoxide dismutase (SOD) is a family of metalloenzymes that plays a fundamental role within the cell generating H_2O_2 through the dismutation of superoxide according the following reaction:

$$2O_2^{\bullet-} + 2H^+ \rightarrow H_2O_2 + O_2$$

In skeletal muscle, three different isoform of superoxide dismutase have been identified:

- Copper-zinc SOD (CuZnSOD) a homodimer primarily located in the cytosol (but a small portion is also found in the mitochondrial intermembrane space and in the nucleus) with a molecular weight of 32 kDa (Fukai and Fukai, 2011).
- Manganese SOD (MnSOD) a homotetramer with a molecular weight of 88 kDa that is expressed in the mitochondria (Fukai and Fukai, 2011; Becuwe et al, 2015).
- Extracellular SOD (EcSOD) a homotetramer located outside the muscle cell with a molecular weight of 135 kDa (Fukai and Fukai, 2011).

In skeletal muscle the majority of SOD is located in the cytosol (65-85%) while the remaining 15-35% is found in the mitochondria (Powers et al, 2011).

1.6.2 Catalase

Catalase is a highly efficient tetramer of four polypeptide chains containing heme and is ubiquitously expressed in different compartments of the muscle cell (Powers et al,

2011). Catalase is involved in the reduction of 2 H_2O_2 molecules into water and O_2 following a two-step reaction (Heck et al, 2010):

$$2\ H_2O_2 \rightarrow 2\ H_2O + O_2$$

Once the catalase active site interacts with H_2O_2, it induces proton transfer between the O_2 atom of H_2O_2 and the amino acids asparagine 148 and histidine 75. At this stage a H_2O molecule and $Fe^{(IV)}$=O are released and the iron can interact with the second molecule of H_2O_2 to form $Fe^{(III)}$, H_2O and O_2 (Zamocky et al, 2008). Catalase has been reported to have a lower affinity for H_2O_2 at low concentrations compared to glutathione peroxidase. Its steady concentration in muscle cells is relatively low but it is significantly increased in response to a rise in H_2O_2 levels (Lubos et al, 2018).

1.6.3 Glutathione Peroxidase

The Glutathione Peroxidase (GPx) family is a selenium-containing enzyme family composed of five different isoforms expressed in mammalian cells (GPx 1-5) (Lubos et al, 2011). These five isoforms differ in localization and substrate specificity. GPx1 and GPx4 are mainly expressed in the mitochondria, GPx3 is mainly found in the extracellular space, GPx2 in the gastrointestinal system and GPx5 is mainly expressed in the male reproductive tract (Jiao et al, 2017).

GPx is responsible for the reduction of H_2O_2 with the assistance of reduced glutathione (GSH - a tripeptide with glutamate, cysteine and glycine residues) used as electron donor (Li et al, 2003):

$$2GSH + H_2O_2 \rightarrow GSSG + 2H_2O$$

The inactivation of H_2O_2 by GPx causes oxidation of reduced glutathione generating oxidised glutathione (GSSG) which is then recycled back to GSH by Glutathione

Reductase that uses NADPH as substrate for this reaction. The bioavailability of NADPH guarantees the correct maintenance of reduced glutathione and the correct functionality of this antioxidant system (Li et al, 2003).

Compared to Catalase, GPx shows a great affinity for H_2O_2 when the levels of this ROS are low (Lubos et al, 2018).

1.6.4 Peroxiredoxins

Peroxiredoxins (Prxs), also known as thiol-specific antioxidants, are a family of cysteine- dependent enzymes involved in the reduction of H_2O_2 using electrons from the thioredoxin enzymes (Rhee et al, 2005). In skeletal muscle, six different isoforms are found distributed in different compartments (Rhee et al, 2005). Prxs I, II and VI are found mainly in the cytosol, III is mainly expressed within the mitochondria and IV can be found both in the endoplasmic reticulum and the extracellular space (Sakellariou et al, 2014a).

Peroxiredoxins can be divided in three different main categories:

- Typical 2-Cys Prxs (Prxs 1-4);
- Atypical 2-Cys Prxs (Prxs 5);
- 1-Cys Prx (Prx6).

As described by Chae and colleagues (1994), all Prxs conserve a cysteine residue known as "*required peroxidatic cysteine*". Nevertheless, in the case of 2-Cys Prxs (the largest class of Prxs) another semi-conserved cysteine is present and it is known as "*resolving cysteine"* placed near residue 170 and being able to form a disulphide bond with the required peroxidatic cysteine (Wood et al, 2003). Among all the Prxs, those mainly involved in the reduction of H_2O_2 are the 2-Cys Prxs that are also involved in the reduction of peroxynitrite and in the regulation of peroxide-mediated signalling pathways (Wood et al, 2003). Among all the Prxs, the 1-Cys Prx6, found in all

mammals, presents unique characteristics. This Prx shows bi-functional capacities due to two different active sites:

- Cys47, Arg132 and His39 allow this protein to perform its normal peroxidatic activity;
- Ser32, His26 and Asp140 allow this protein to exert PLA2 activity (Fisher, 2011).

The switching of Prx6 activity between peroxidatic and PLA2 can be determined both by pH and hyperoxidation (Fisher, 2011). If the pH is neutral (around 7-8), peroxidatic activity is acquired. In contrast, if the pH is more acidic (between 3 and 5 with a peak at 4) PLA2 activity appears to be activated (Chen et al, 2000). Conversely, when hyperoxidation of Prx6 occurs, phospholipase activity is enhanced and the 3 amino acids play a pivotal role in the functionality of this enzyme. His26 only has binding functions, Ser32 both binds and hydrolyses the liposome while Asp140 is involved in the catalytic processes that generates arachidonic acid and lipid peroxides (Kim et al, 2016). As described by Wu and colleagues (2009), His26 and Asp140 are significantly more distant in Prx6 compared to cPLA2 and a structural rearrangement is required for the correct functioning of Prx6 as PLA2. The phosphorylation of Thr177 (located in the C-terminal domain) induces the conformational changes necessary to allow Prx6 to execute the hydrolysis of sn-2 fatty acyl chains of phospholipids (Wu et al, 2009).

1.6.5 Thioredoxin

Thioredoxins (Trx) are proteins encoded by the genes TXN and TXN2 and are expressed in the majority of the organisms (Wollman et al, 1988). They play an important role as antioxidants but also play an important role in redox signalling. These small proteins of 12kD contain two vicinal cysteines in their amino acid sequence that allow these proteins to reduce the disulphide bonds present in other proteins using the

electrons released by NADPH Oxidase (Cheng et al, 2010). Thioredoxins are maintained in their reduced state by the activity of thioredoxin reductase (TrxR) (Nordberg and Arnér, 2001). Among the three isoforms of TrxR discovered in mammalians cells, two are expressed in skeletal muscle:

- Thioredoxin Reductase 1 (TrxR1) found both in the cytosol and in the extracellular space;
- Thioredoxin Reductase 2 (TrxR2) expressed in mitochondria.

1.6.6 Heat Shock Proteins

Heat Shock Proteins (Hsp) are a family of proteins that plays a primary role in response to various stress conditions and are named according to their molecular weight. Some of them are also known as chaperonin proteins because they are involved in stabilising the newly formed and refolding proteins that have been damaged by cellular stress (Jee, 2016).

Hsps are found in different compartments within the cell and their location is important considering that the cytosol is a reducing environment while the endoplasmic reticulum is more oxidising (Jee, 2016). These compartmental differences mean that each environment requires a specific chaperone network (Janssen-Heininger et al, 2008). Hsp10, Hsp60, Hsp75 are found in the mitochondria and are mainly involved in ensuring correct protein folding. Hsp40 and Hsp110 are mainly found in the cytosol, Hsp70, Hsp90, Hsp100 are found in the cytoplasm and Hsp47 and GRP78 are found in the endoplasmic reticulum (Jee, 2016).

Hsps also play an important role in redox-signalling (Shigeoka and Maruta, 2014). For example, mammalian Hsp25, 60, 70 and 90 present a redox-active cysteine in their structure which, following an increase in oxidative stress, is oxidised generating the formation of a disulphide bond (Janssen-Heininger et al, 2008). This oxidative stress-

related modification of the Hsps induces modifications in the functionality of these proteins. However, not only disulphide formation is able to induce modifications in the Hsp activity; nitrosylation and glutathionylation are also able to induce alteration of Hsp activity (Janssen-Heininger et al, 2008).

1.7 Ageing

Ageing is a natural process that occurs in all the living organisms and is influenced by different intrinsic and extrinsic factors such as:

- Genetic;
- Lifestyle;
- Diseases;
- Environmental factors (Bulla and Shafwe, 2011).

Ageing can be defined as a complex pattern of physiological and pathophysiological modifications that occur during lifetime and that lead to deterioration of the entire organism and its functions (Bulla and Shafwe, 2011). Given the complexity of the ageing process, an interdisciplinary approach is required by scientists for its study (Dillin et al, 2014) and several theories have tried to explain how the interaction of environmental, genetic and epigenetic variables lead ageing of an organism.

Ageing theories can be divided in two main categories:

- Programmed theories;
- Damage-related theories.

While programmed theories suggest that the same factors able to influence our development are able to direct our senescence, damage-related theories identify the accumulation of damage at different levels as the main cause of ageing.

Among the damage-related theories of ageing, the oxidative stress theory stands out. Indeed, during ageing and several other conditions, the levels of oxidative stress tend

to increase with the potential of causing disturbance of homeostasis with severe impact on health inducing tissue degeneration and system dysfunctions (Bouzid et al, 2014; Fulco et al, 2003).

1.7.1 Skeletal muscle and Ageing

Skeletal muscle is seriously affected by the ageing process showing different variations in size, shape and organisation (Cruz-Jentoft et al, 2019). Several studies have highlighted that the peak in muscle mass is reached around the age of 24 followed by a decrease of approximately 10% in the next 25 years (Keller et al, 2013; Kalyani et al, 2014). After the age of 50, muscle wasting accelerates with a loss of 10% per decade (Lexell et al, 1988). The age-related loss of muscle mass, together with the decline of muscle function is defined as "*sarcopenia*".

1.7.1.1 Sarcopenia

Sarcopenia is a disease (Diagnosis Code ICD-10-MC) where a substantial reduction of muscle tissue (substituted by intramuscular fat and connective tissue) and muscle strength occurs (Baumann et al, 2016). Several internal and external components are involved in the development of this disease and, according to the European Working Group on Sarcopenia (EWGSOP), in order to diagnose it, different factors must be taken into consideration (Vellas et al, 2018; Cruz-Jentoft et al, 2019). In the recently released guidelines, the attention is focused more on muscle strength rather than muscle mass (in particular lower limb muscle strength). As explained by Cruz-Jentoft and colleagues (2019), the diagnosis of sarcopenia is confirmed by the simultaneous presence of low muscle quantity and poor muscle quality. In addition, when low muscle quantity and strength are present together resulting in low physical performance, sarcopenia can be considered severe (Cruz-Jentoft et al, 2019).

1.7.1.2 Age-related structural changes in skeletal muscle

Sarcopenia is characterised by significant changes in muscle structure that results in the loss of muscle mass with two main factors contributing to it:

- Loss of muscle fibres;
- Muscle fibres atrophy.

While the loss of muscle fibres appears to be non-specific and can only partially explain the age-related loss of muscle mass, muscle fibre atrophy appears to be driven by more specific factors playing an important role in sarcopenia (Deschenes, 2004). Previous reports have suggested that fast-twitch glycolytic fibres appear more vulnerable to age-related atrophy compared to slow-twitch fibres (Wang and Pessin, 2013). Indeed, type I fibre cross sectional area does not differ from young and old adults while type IIa, type IIb and type IIx fibres of older adults show, respectively, a 13%, 22% and 26% reduction of cross sectional area (Lexell et al, 1988; Deschenes, 2004). These fibre-specific differences can be attributed to how different signalling pathways are able to trigger protein degradation regulating the activity of a series of genes identified as "*atrogins*" in the different fibre types (Wang and Pessin, 2013; Lang et al, 2017).

Researchers have also demonstrated that, in addition to the decrease in skeletal muscle cross sectional area, older adults' fibers present myopathic modifications including necrotic or hyalinised myofibres, split or fragmented myofibers and accumulation in degenerative inclusion bodies, lipofuscin, and lipid droplets that significantly impair the contractility of these fibers (Williams et al, 2002; Dumitru et al, 2018, McCormick and Vasilaki, 2018). Furthermore, previous studies showed that in older adults' muscles there is an increase in MURF1 activity. This protein can regulate the proteasomal degradation of sarcomeric related proteins resulting in the breakdown of myosin filaments, significantly impacting the muscle fibre contractile properties (Coehn et al, 2009).

1.7.1.3 Age-related functional changes in skeletal muscle

The loss of muscle mass has a tremendous impact on muscle strength (the maximal force that a muscle or a muscle group can exert during a contraction) (Cheatham, 2013). During ageing, the force per unit area, the velocity of contraction and the motor neuron firing rate appear to be reduced with a major impact on absolute strength and power (Powers et al, 2013, Connelly et al, 1999). Longitudinal studies have reported that the loss of muscle function is not linear with the loss of muscle mass (Baumann et al, 2016). As mentioned earlier, after the age of 50 the loss of muscle mass in the lower limbs is around 1-2% per year while the loss of muscle strength is more prominent with a 1.5-5% loss per year (Cruz-Jentoft et al, 2019).

A characteristic of ageing and some chronic diseases associated with muscle wasting is the reduction of neurological properties, including changes at the nervous system level that have a direct impact on the voluntary capacity to activate muscles. This has also a direct impact on fibre architecture/composition, the excitation-contraction coupling processes and cross bridge mechanics (Baumann et al, 2016). These results open the possibility that denervation may play a primary role in the characteristic age-related loss of muscle mass and strength.

1.7.2 Neuromuscular junction during ageing

The efficacy and mass of the neuromuscular system tends to deteriorate during ageing and early reports described this phenomenon in rats (Gutman and Hanzlikova, 1966) and few years later also in humans (Oda, 1984). Previous reports have also shown that between the age of 25 and the age of 65, the number of motor units declines approximately 40% (McNeil et al, 2005). Nevertheless, from the age of 65 to the age of 80, there is an acceleration that results in the loss of a further 33% of motor units (McNeil et al, 2005). The reasons behind this age-related loss of motor units are still

unclear but several studies have suggested that during ageing there is a progressive degeneration at different levels of the spinal cord (starting from the ventral horn) that are able to trigger different consequences at peripheral level (Deschenes, 2004).

Impairments at the spinal cord level seem to be able to induce loss of motoneurons and reduced axonal transport that might affect the availability of important trophic factors and the movement of organelles (e.g. Mitochondria) necessary for the survival of the NMJ (Jang and Van Remmen, 2011; McDonagh et al, 2016). A study performed by Balice-Gordon (1997) demonstrates that in mice, the NMJs are very stable until they reach 12-18 months when some loss of motor terminal branches begins. These modifications have been seen in experimental denervation models suggesting that, most likely, this progressive instability is the result of the loss of efficacy of the denervation-reinnervation cycles (McDonagh et al, 2016). The process of denervation-reinnervation, induces a transient disconnection between the muscle and the motor neuron followed by the subsequent reinnervation from the same motor neuron or the sprouting of a nearby axon (Hepple and Rice, 2016). This process is cyclically repeated in adult life (Jang and Van Remmen, 2011; Aare et al, 2016). Nevertheless, with ageing its efficacy tends to decrease leading to loss of terminal branches and nerve sprouting able to induce motor unit remodelling, progressive reduction of the motor units number spatial domain (Larsson et al, 1999) and loss of NMJs (Aare et al, 2016; Jang and Van Remmen, 2011). Impairment and failure of the denervation-reinnervation process can impact muscle health triggering a series of consequences (shown in *Figure 1.5*) that culminate in the loss of muscle mass, loss of muscle strength and loss of muscle functions characteristic of sarcopenia (Jang and Van Remmen, 2011).

Following the loss of terminal branches, in the attempt to compensate, axonal sprouting occurs where a healthy motoneuron sprouts to form additional synapses with non-

overlapped acetylcholine receptors (Son and Thompson, 1995; Jang and Van Remmen, 2011). Several studies through the years have tried to determine the stimuli able to drive a healthy motoneuron to a non-overlapped acetylcholine receptor. Early evidence suggests that the lack of contractile activity may be responsible for this phenomenon (Son and Thompson, 1995). More recent evidence suggests that the increased peroxide release from denervated muscle fibres may be aimed at stimulating re-innervation through sprouting (Pollock et al, 2017).

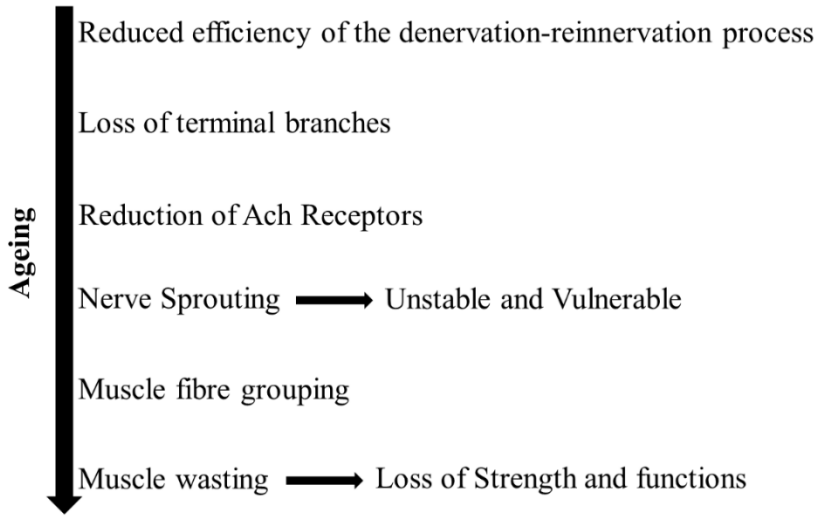

Figure 1.7. *Age-associated modifications at the neuromuscular level that culminate with sarcopenia. Adapted from Hepple and Rice, 2016.*

As a consequence of nerve sprouting, surviving muscle fibres tend to organise themselves in a way that a single motor neuron can innervate a higher number of fibres at the same time. The formation of bigger clusters is seen following denervation and is aimed to increase the chances of clustered muscle fibres to remain innervated for their remaining lifespan (Aare et al, 2016). Fibre grouping is also widely observed during sarcopenia reinforcing the idea that denervation plays a primary role in age-related muscle wasting (Hepple and Rice, 2016). Nevertheless, with ageing even the efficiency of this process is dramatically reduced and the newly formed branches are

more vulnerable to neurodegenerative processes and usually they disappear within weeks (Jang and Van Remmen, 2011).

A study performed by Aare and colleagues (2016) on rats, showed that in old animals, denervated fibres are on average 35-50% smaller than innervated fibres while this difference is less marked in young animals (approximately 7%). This denervation-related reduction in fibre size seems to confirm the role played by denervation in muscle wasting. Indeed, impairments of the NMJs are able to activate atrophy pathways in denervated fibres resulting in fibre atrophy and increase number of angular fibres, two main characteristics of skeletal muscle ageing (Baloh et al, 2007; Hepple and Rice, 2016).

Several studies also demonstrated that the age-related changes in the morphology of the NMJ differ between muscle fibre types suggesting that these changes can be related to the fibre metabolism. For instance, further studies conducted both in old rats and humans demonstrated that with ageing there is a preferential loss of fast motor units compared to slow motor units (Jang and Van Remmen, 2011).

1.7.3 Reactive oxygen species and ageing in skeletal muscle

An increase in skeletal muscle contractile activity induces an increase in O_2 consumption and an increase in intracellular generation of superoxide and nitric oxide (Jackson and McArdle, 2016; Gomes et al, 2017). As discussed previously, physiological concentrations of ROS play an essential role in redox signalling and cell survival, playing a central role also in muscle contraction (Jackson and McArdle, 2016; Gomes et al, 2017).

During ageing a significant accumulation of ROS is seen in skeletal muscle and, although their role remain controversial, evidence suggests that their accumulation can result in mitochondrial DNA damage, together with oxidative damage to lipids and proteins, playing a central role in sarcopenia (Jang and Van Remmen, 2011; Jackson

and McArdle, 2016). In addition, other reports suggest that during ageing, the accumulation of ROS in skeletal muscle can also be associated with contractile dysfunction and fatigue (Powers et al, 2011).

During ageing most tissues also show a progressive decrease in antioxidant defences, but in skeletal muscle the activity of superoxide dismutase isoforms, catalase and glutathione peroxidase isoforms increases (Vasilaki et al, 2006a; Steinbacher and Eckl, 2015). This increase in antioxidant defences seems to be muscle type-specific with type I fibres showing the most prominent increase (Steinbacher and Eckl, 2015) while type II showing a lower increase in antioxidant enzymes and a higher rate of oxidative injury, making them more prone to denervation and muscle fibre atrophy (Jang and Van Remmen, 2011; Gomes et al, 2017). In addition, ageing skeletal muscle shows a significantly higher mitochondrial iron content that exposes the muscle to the generation of the highly reactive $HO^{\bullet}$ from H_2O_2 (Szentesi et al, 2019).

1.8 Mitochondrial dysfunction, reactive oxygen species and denervation

As previously mentioned, mitochondria play several important roles within the muscle cell from energy production to cell signalling. At pre-synaptic level, mitochondria can be found in the nerve terminals (they usually travel along the microtubules using the axonal transport system) while in the post synaptic region of the muscle fibre can be found in the sub sarcolemma region (Jang and Van Remmen, 2011). The role that these mitochondria play are different: energy support, regulation of calcium, support of synaptic transmission, and apoptosis. Several studies have highlighted that mitochondria located in proximity of the NMJ can be responsible of the transportation of calcium ions in the endoplasmic reticulum, nucleus and plasma membrane of cells (including skeletal muscle cells) (Karam et al, 2017). Following denervation, the loss of overlap between the motoneuron and the acetylcholine receptor present in the post-synaptic

receptors induces alterations in calcium metabolism (Baumann et al, 2016). Calcium levels significantly increase in the cytosol, overloading mitochondria and, consequently, inducing increased ROS production. Mitochondrial dysfunction and increased levels of cytosolic calcium seem to have an impact not only in the activation of atrophy patterns, they also appear to be associated with lower levels of neurotransmitters released by the presynaptic terminal of surrounding fibres, with reduced capability of the motor unit to generate an action potential (Baumann et al, 2016). In addition as Jang and Van Remmen (2011) suggested, it is reasonable to believe that dysfunction of the mitochondria present in the NMJ region can have a negative impact on the motor unit survival inducing alterations of key proteins involved in the maintenance of the NMJ. Indeed, an increase in calcium ion flux can polarize the mitochondria in proximity of the Ach receptors inducing the activation of proteases such as calpain, whose physiological role is still controversial but interacting with rapsyn (involved in the stabilization of the acetylcholine receptors) can induce the disruption of the acetylcholine receptors complex (Jang and Van Remmen, 2011).

As initially demonstrated by Muller and colleagues (2007a), following surgically induced denervation there is a significant increase in mitochondrial ROS production. In the following years, other studies (Bhattacharya et al, 2009; Abruzzo et al, 2010; Pollock et al, 2017) demonstrated that ROS production is significantly increased following denervation and that mitochondria appear to be the main source of peroxide production. The increase in peroxides release from mitochondria of denervated muscle fibres is induced only marginally by the ETC while other enzymes such as NADPH Oxidase, PLA2, Monoamine Oxidase A and Monoamine oxidase B seem playing a predominant role (Pollock et al, 2017). Nevertheless, the causes and the physiological

meanings and consequences of this increased peroxide release are still poorly understood.

A study from Giniatullin and collagues (2006) has also highlighted how the increase in H_2O_2 released from mitochondria can significantly inhibit the release of the acetylcholine from the pre-synaptic terminals as well as the activity of Synaptosomal associated protein 25 which plays an important role in the NMJ regulating the neurotransmitter release (Ramakrishnan et al, 2012). Furthermore, the increased peroxide release following denervation appears to also induce the activation of NF-κB and/or Tumor Necrosis Factor alpha (TNF-α) inflammatory pathways which could lead to the upregulation of atrophy patterns such as Atrogin-1/MAFbx and 26S protease system (Abruzzo et al, 2010). These alterations result in disruption of the balance between protein synthesis and protein degradation with muscle fibre atrophy and loss of muscle mass (Sun et al, 2006). Evidence suggests that denervation-induced atrophy can be highly attributable to mitochondrial dysfunctions (Karam et al, 2017).

1.9 Aims of the work reported in this thesis

Recent studies have highlighted significant age-related changes in the innervation of skeletal muscle with loss of integrity of the NMJ accompanied by a significant loss of muscle mass. Recent evidence from our group (Pollock et al, 2017) also highlighted that one of the main consequences of the loss of integrity of the NMJ is the significant increase in peroxide release in denervated muscle fibres. Nevertheless, the physiological meaning and impact of this increase in peroxide release is still poorly understood.

The aims of the present thesis are:

- Examine the effects of skeletal muscle denervation on redox homeostasis in skeletal muscle focusing on the content of proteins that may contribute to peroxide generation and other adaptive and regulatory proteins.

- Examine the effects of skeletal muscle denervation on mitochondria with a specific focus on: mitophagy, activation of apoptosis and mitochondrial number.
- Determine the metabolic changes induced by denervation in skeletal muscle.
- Investigate whether the redox-related changes observed in our denervation model also occur during skeletal muscle ageing since muscle denervation appears to be a key characteristic of sarcopenia.
- Evaluate the age-related changes occurring between the nerve-muscle interactions and to examine whether the age-related loss in the stability of the NMJs results in skeletal muscle loss or *vice versa*.

Chapter 2. Materials and Methods

2.1 Mouse models

All mice were kept in the Biomedical Service Unit (BSU) facilities fed on a standard laboratory diet and subjected to a 12-h light/dark cycle. All the experiments were performed in accordance with UK Home Office guidelines under the UK Animals (Scientific Procedures) Act 1986 and received ethical approval from the University of Liverpool Animal Welfare Ethical Review Body. Two main strains were used in the present thesis C57BL/6J and B6.Cg-Tg(Thy1-YFP)16Jrs/J mice. For experiment 4 mice in each experimental group were used.

2.1.1 C57BL/6J mice

Also known as Black 6, C57BL/6J mice present a high resistance to tumours and are often used in the production of transgenic models as this strain allows researchers to induce specific mutations. They present a relatively low bone density and during ageing can develop hair loss (https://www.jax.org). They can also develop diet-related obesity, type II diabetes and atherosclerosis.

2.1.2 B6.Cg-Tg(Thy1-YFP)16Jrs/J

These mice, also known as Thy-1 YFP (Yellow Fluorescent Protein), express high levels of a yellow fluorescent protein in their motor and sensory neurons only. YFP expression is present since gestation and allows detailed visualisation of the nervous system and skeletal muscle innervation using fluorescent microscopy. The mutation was generated by injecting into fertilized B6CBAF1 mouse eggs a transgenic construct containing YFP gene derived from a mouse Thy1gene. Subsequently, mice were backcrossed with wild type C57BL/6J mice for at least five generations. Previous unpublished data from our group and our collaborators failed to detect differences in the muscle phenotype of C57BL/6J and B6.Cg-Tg(Thy1-YFP)16Jrs/J mice.

2.2 Surgical transection of the peroneal and sciatic nerve to induce muscle denervation

To induce denervation in different muscles of the lower hind limb, mice underwent two different types of surgical procedure:

- The complete removal of a small section of the peroneal nerve in the right lower limb (peroneal nerve transection) to induce denervation in the Tibialis Anterior (TA) and Extensor Digitorum Longus (EDL) muscles;
- The complete removal of a small section of the sciatic nerve in the right lower limb (sciatic nerve transection) to induce complete denervation of all the muscles in the lower hind limb.

Both surgical procedures were performed in a sterile environment using specific instruments for microsurgical procedures adequately sterilised before use and between surgeries of different mice. Before surgery, each mouse was put into an induction chamber where a mix of O_2 and isofluorane (97:3 ratio) was used to initially anesthetise the mouse. The mouse was then moved on the pre-surgery station where it was weighted, placed in a nose cone connected to a vaporiser supplying a mix of O_2 and isofluorane 0.2% and ophthalmic lubricant was applied to the eyes in order to prevent cornea drying during surgery. Following the removal of hair from the surgical area, Buprenorphine (an analgesic; 1mg/kg, SC 0.1ml) and Baytril (an antibiotic; 2.5% 1 in 10 dilution, SC 0.07ml) were injected and the mouse moved to the surgery theatre where, still connected to the vaporizer supplying gas anaesthetic, the surgical procedure was carried out.

A small incision was performed at the level of the sciatic notch which was identified through palpation of the knee. At this level the sciatic nerve splits in three different branches: the tibialis, the peroneal and the sural nerves.

For the sciatic nerve transection, a section of the sciatic nerve was removed before the trifurcation described above, whereas for the peroneal nerve transection, once the peroneal nerve was identified a tiny section was removed. The wound was then sutured using CliniSorb Q 6/0, Super Glide (Reverse Cutting), Undyed, 13mm needle (International Medical Supplies, Stockport, UK).

After surgery, mice were maintained in isolation cages until the complete recovery of movement and then placed back in their original cages. Mice were checked regularly to identify any post-surgical pain, discomfort or stress conditions.

2.3 Sample collection and preparation

For each project, mice were sacrificed by cervical dislocation and muscles were dissected and treated differently according to the analysis performed (see *Figures 2.1*, *2.2* and *2.3*).

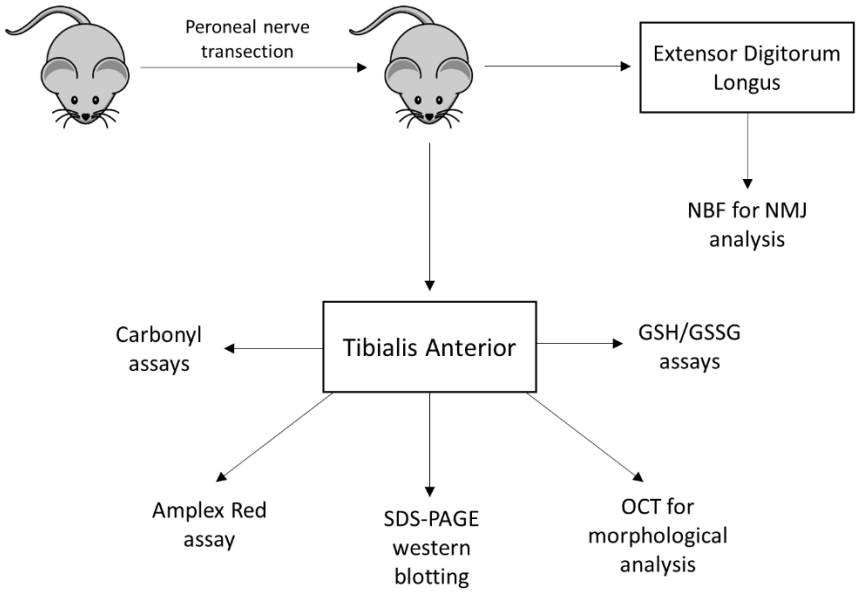

***Figure 2.1**. Schematic overview of tissue utilisation for the experiments presented in Chapter 3 focused on determining the redox response following skeletal muscle denervation.*

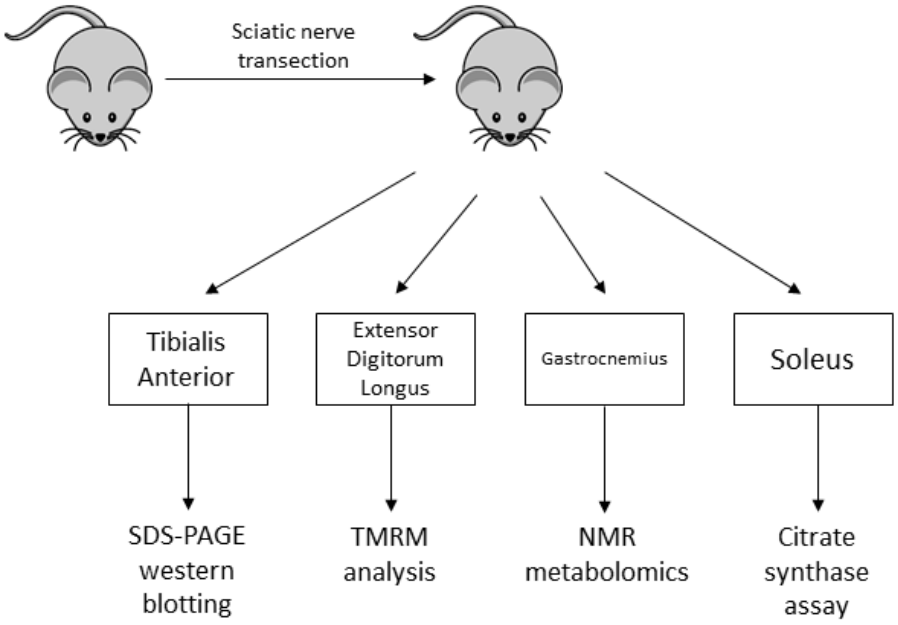

Figure 2.2. *Schematic overview of tissue utilisation for the experiments presented in Chapter 4 and 5 focused on determining the mitochondrial status and metabolic changes following skeletal muscle denervation.*

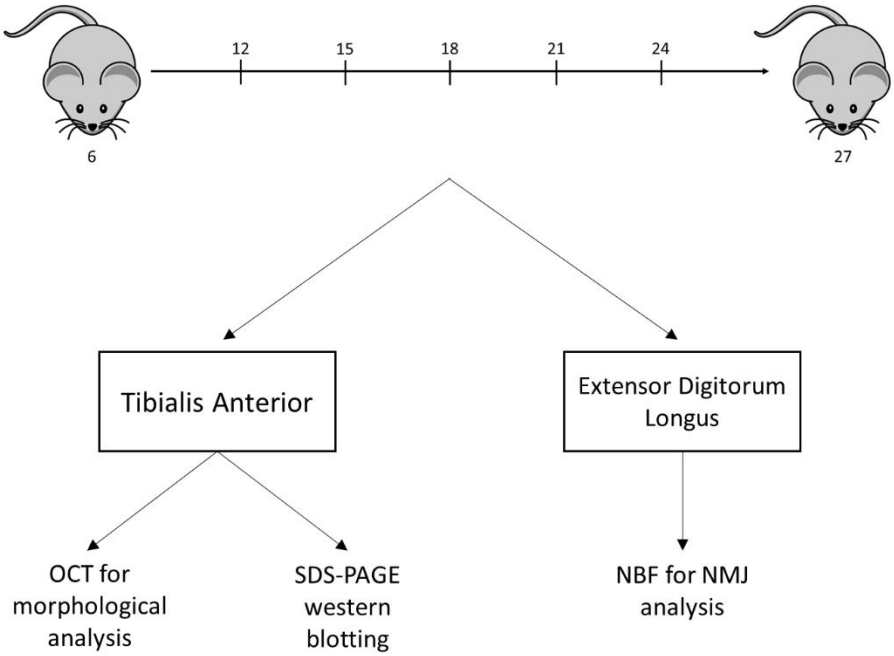

Figure 2.3. *Schematic overview of tissue utilisation for the experiments presented in Chapter 6 focused on determining the age-related changes of the NMJ, muscle morphology and the antioxidant enzymatic response.*

2.3.1 Sample preparation for SDS-PAGE western blot analysis

Frozen muscles were cryopulverised in liquid nitrogen using a mortar and pestle. The resulting powder was added to 1% Sodium Dodecyl Sulphate (SDS) containing Pierce™ Protease and Phosphatase Inhibitor Mini Tablets, Ethylenediaminetetraacetic acid (EDTA) Free. Samples were then homogenised for 30-60 seconds maintaining the tube on ice to avoid overheating. Following homogenisation, samples were collected in 1.5ml polypropylene Eppendorf tubes (Thermo Fisher Scientific, Waltham, MA, USA) and centrifuged for 10 minutes at 14,000g at a constant temperature of 4ºC. Following centrifugation, the supernatant was collected and stored at -20ºC for further analysis while the pellet containing insoluble proteins and cell debris was discarded.

2.3.2 Sample preparation for Oxyblot analysis

For the analysis of protein carbonylation, the powder collected after cryopulverisation was added to 180µl of Hepes Buffer (20mM of 4-(2-hydroxyethyl)-1-piperazineethanesulfonic acid pH7.4, 150mM NaCl, 1mM EDTA and protease and phosphatase inhibitors). Samples were homogenised for 30-60 seconds while kept on ice during the entire process, the homogenate was collected in 1.5ml polypropylene Eppendorf tubes and centrifuged for 10 minutes at 14,000rpm at a constant temperature of 4ºC.

After centrifugation, the supernatant solution containing proteins was collected and stored at -20ºC for further analysis while the pellet containing insoluble proteins and cell debris discarded.

2.3.3 Sample preparation for GSH and GSSG assays

Following cryopulverisation, 1% 5-Sulfasalicylic acid (SSA) was added to the samples. Samples were homogenised for 30-60 seconds on ice, transferred to 1.5ml polypropylene Eppendorf tubes, centrifuged for 10 minutes at 14,000rpm at a constant temperature of 4ºC. After centrifugation, the supernatant containing reduced and oxidised glutathione

was collected, placed in a different Eppendorf tubes and stored at -20ºC until further analysis.

2.3.4 Sample preparation for morphological analysis

Samples for histoimmunochemical analysis were placed perpendicularly on a cork for cryosectionning, embedded in Optimal Cutting Temperature (OCT – Sigma-Aldrich Ltd, Gillingham, Dorset, United Kingdom) and submerged in isopentane cooled in liquid nitrogen. Once the OCT was set, samples were covered with aluminium foil and kept in liquid nitrogen until used or stored at -80ºC for further analysis.

For immunohistochemical analysis, 12µm thick sections were obtained by cryosectionning performed on a Leica 1900 (Leica, Wetzlar, Germany). Samples were collected on Superfrost Plus glass slides (Thermo Fisher Scientific, Waltham, MA, USA) and stored at -20ºC until analysis.

2.3.5 Sample preparation for the analysis of the neuromuscular junction

Muscles were dissected and fixed in 10% Neutral Buffer Formalin (Genta Medical, York, United Kingdom) for 1 hour at room temperature. Following incubation in formalin, samples were kept in 1% PBS-Sodium Azide at 4ºC until usage.

2.3.6 Sample preparation for analysis of mitochondrial peroxide generation

Immediately following dissection, muscles were submerged in ice-cold relaxing solution (4.5µM Mg2ATP, 10mM Imidazole, 2mM EGTA, 100mM KCl, 1mM $MgCl_2$) containing saponin from quillaja bark (200µM - Sigma-Aldrich Ltd, Gillingham, Dorset, United Kingdom) and dissected into small bundles for analysis.

2.3.7 Sample preparation for TMRM analysis

Following dissection, muscles were pinned on a sylgard dish and submerged in ice-cold relaxing solution (Section 2.3.6) while fibres were manually teased out of the

muscle under a dissecting microscope. Isolated fibres were incubated for 30 minutes at room temperature in relaxing solution containing Saponin (0.164mM - Sigma-Aldrich Ltd, Gillingham, Dorset, United Kingdom). Following permeabilisation fibres were used for analysis.

2.3.8 Sample preparation for NMR Metabolomics

Following dissection, samples were stored at -80ºC until utilisation. Samples were ground in liquid nitrogen and the powder accurately weighted to determine the amount of tissue available.

2.3.9 Sample preparation for Citrate synthase assay

Following dissection, muscles were immediately frozen in liquid nitrogen and stored at -80ºC until further analysis. Samples were cryopulverised in liquid nitrogen and the resulting powder was added to 120µl of extraction buffer (250mM Sucrose, 10mM Trizma Base, 1mM ethylene glycol-bis(β-aminoethyl ether)-N,N,N′,N′-tetraacetic acid - EGTA). Samples were sonicated for 15 seconds in ice and centrifuged at 12,000g for 10 minutes at 4ºC. Supernatants were collected for the analysis.

2.4 Biochemical assays

For most of the experiments performed, protein quantification was necessary and 2 specific protocols were chosen for their compatibility with the chemicals used to extract proteins.

2.4.1 Bicinchoninic Acid assay

The bicinchoninic acid assay (BCA assay), is a copper-based protein assay used to measure the amount of proteins present in a solution. It provides a good range of detection from 0.5µg/ml to 1.5µg/ml. This method analyses the colour change, from

light green to purple through which is possible to estimate the amount of proteins present (Smith et al, 1985).

2.4.1.1 Reagents

For this analysis a kit purchased from Thermo Fisher Scientific was used (Waltham, MA, USA) containing:

- BCA Reagent A
    - Sodium carbonate,
    - Sodium Bicarbonate,
    - Bicinchoninic Acid,
    - Sodium tartrate;
- BCA Reagent B
    - 4% Copper(II);
- 2mg/ml Bovine Serum Albumin (Thermo Fisher Scientific, Waltham, MA, USA).

2.4.1.2 Protocol

Samples were removed from the -20ºC freezer and slowly defrosted on ice. A standard curve was prepared following the protocol recommended by Thermo Fisher as presented in *Table 2.1*. The protein standard was left on ice while a fraction of the sample was diluted 1:60 and 1:120. Twenty microlitres of both samples and protein standards were added to a 96 well plate (Costar, Corning Incorporated, New York, USA).

Immediately before use, 1 part of BCA Reagent B was mixed with 49 parts of BCA Reagent A and 180µl added to the each well. The plate was then incubated for 30 minutes at 36ºC in a dark environment and, following incubation, it was read on the plate reader Spectro Star Nano (BMG LabTech, Offenburg, Germany) set at 562nm wavelength. The mean absorbance was recorded and used for protein quantification.

Table 2.1 *Protocol recommended by Thermo Fisher for the preparation of protein standards using Bovine Serum Albumin stock with concentration of 2mg/ml.*

Vial	Volume of Diluent (µl)	Volume and Source of BSA (µl)	Final BSA Concentration (µg/µl)
A	700	100 of Stock	250
B	400	400 of vial A dilution	125
C	450	300 of vial B dilution	50
D	400	400 of vial C dilution	25
E	400	100 of vial D dilution	5
F	400	0	0

2.4.2 Bradford Assay

This is a slightly different method for the quantification of proteins compared with the BCA assay. The proteins, present in an acidic environment, link with Coomassie Dye to induce a change of colour from the green-anthracite to blue which is recorded at a wavelength of 595nm. This method is able to detect peptides or proteins over 3kDa (Bradford, 1976) with no risk of interference from protein fragments, free amino acids and dye.

2.4.2.1 Reagents

- Bradford Ultra (Expedeon, San Diego, Ca, USA);
- 2mg/ml Bovine Serum Albumin (Thermo Fisher Scientific, Waltham, MA, USA).

2.4.2.2 Protocol

Samples were removed from the -20ºC freezer and slowly defrosted on ice. A standard curve was prepared following the protocol described for the BCA assay. The protein standard was left on ice while a small fraction of the sample was diluted 1:60 and 1:120. Twenty microliters of both samples and protein standard were added to a 96 well plate (Costar, Corning Incorporated, New York, USA) and 180µl of Bradford Ultra was added to each well.

The plate was left at room temperature for 5 minutes in a dark environment and then analysed on the Spectro Star Nano plate reader (BMG LabTech, Offenburg, Germany) set at 595nm wavelength. The mean absorbance was recorded and used for protein quantification.

2.5 SDS-PAGE western blot analysis

SDS-PAGE western blot analysis, also known as protein blotting, immunoblot or simply western blot, is a technique which uses synthetic or animal-derived antibodies for the detection of specific proteins.

This method allows a semi-quantitative analysis of the content of specific proteins in a sample through the analysis of the colour intensity of a signal generated on a blotting membrane by the interaction between a protein and its specific antibody.

2.5.1 Reagents

- 1% SDS (Sigma-Aldrich Ltd, Gillingham, Dorset, United Kingdom);
- Pierce™ Protease and Phosphatase Inhibitor Mini Tablets, EDTA Free (Thermo Fisher Scientific, Waltham, MA, USA);
- BLU 4x
    - 1M Tris/Hcl (Sigma-Aldrich Ltd, Gillingham, Dorset, United Kingdom),
    - Glycerol (Sigma-Aldrich Ltd, Gillingham, Dorset, United Kingdom),
    - 20% SDS (Sigma-Aldrich Ltd, Gillingham, Dorset, United Kingdom),
    - Beta-Mercaptolethanol (Sigma-Aldrich Ltd, Gillingham, Dorset, United Kingdom),

    - Distilled water (ddH_2O);
- ddH_2O;
- Acrylagel (30% w/v Acrylamide Stock Solution) (Geneflow Ltd., Staffordshire, UK);
- ProtoGel Resolving Buffer (Tris/SDS) (Geneflow Ltd., Staffordshire, UK);
- ProtoGel Stacking Buffer (Tris/SDS) (Geneflow Ltd., Staffordshire, UK);
- 10% Ammonium Persulphate (APS) (Sigma-Aldrich Ltd, Gillingham, Dorset, United Kingdom);
- NNN'N'-tetramethylethylene-diamine (Temed);
- Ethanol 99.9% chemical gradient (Sigma-Aldrich Ltd, Gillingham, Dorset, United Kingdom);
- Running Buffer
    - 100mL Tris-Glycine (Sigma-Aldrich Ltd, Gillingham, Dorset, United Kingdom),
    - 10mL SDS 10% (Sigma-Aldrich Ltd, Gillingham, Dorset, United Kingdom),
    - 890mL ddH_2O;
- PageRuler™ Plus Prestained Protein Ladder, 10 to 250 kDa (Thermo Fisher Scientific, Waltham, MA, USA);
- Anode 1 (pH 10.4)
    - 36.34g Trizma Base (Sigma-Aldrich Ltd, Gillingham, Dorset, United Kingdom),
    - 200ml Methanol HPLC (Thermo Fisher Scientific, Waltham, MA, USA),
    - 800mL ddH_2O;

- Anode 2 (pH 10.4)
    - 3.02g Trizma Base (Sigma-Aldrich Ltd, Gillingham, Dorset, United Kingdom),
    - 200ml Methanol HPLC (Thermo Fisher Scientific, Waltham, MA, USA),
    - 800mL ddH_2O;
- Cathode (pH 7.6)
    - 5.24g 6-amino n hexanoic acid (Sigma-Aldrich Ltd, Gillingham, Dorset, United Kingdom),
    - 200ml Methanol HPLC (Thermo Fisher Scientific, Waltham, MA, USA),
    - 800mL ddH_2O;
- Ponceau S solution (Sigma-Aldrich Ltd, Gillingham, Dorset, United Kingdom);
- Tris Buffer Saline - Tween 20 (TBS-T20)
    - Tris Buffer Saline (TBS 1x - Sigma-Aldrich Ltd, Gillingham, Dorset, United Kingdom),
    - Tween 20 (Sigma-Aldrich Ltd, Gillingham, Dorset, United Kingdom);
- 5% non-fatty milk
    - Milk powder (Sigma-Aldrich Ltd, Gillingham, Dorset, United Kingdom),
    - TBS-T20;
- Primary antibody (see *table 2.5* for further information);
- Secondary antibody (see *table 2.6* for further information);

- SuperSignal™ West Dura Extended Duration Substrate (Thermo Fisher Scientific, Waltham, MA, USA).

2.5.2 Sample preparation and gel electrophoresis

After protein quantification using either the BCA or Bradford assays, 30µg of protein (unless differently stated) for each sample was added to ddH_2O and 4µL of BLU 4x (diluted 1:4) to achieve an equal final volume for each sample.

Samples were boiled at 95ºC for 5 minutes on a thermo-block (Falc, Bergamo, Italy) to allow proteins to acquire the random-coil aspect required for the separation of the proteins, exclusively, according their molecular weight. Following boiling, samples were left at room temperature for 2 minutes before being centrifuged at 4ºC for another 2 minutes at 13,000rpm. For most of the experiments, gels were prepared using Mini-PROTEAN® Tetra Handcast Systems (Bio-Rad, Hercules, CA, USA). Poly-acrylamide gels with different poly-acrylamide percentages were prepared following the recipe presented in *Table 2.2*. Once the gels had set, samples were loaded on gels together with a protein ladder. In the last well of the gel, a control sample was also added to verify the specificity of the secondary antibody excluding any risk of non-specific binding.

Table 2.2. *Recipes used for the preparation of the poly-acrylamide gels. The units presented in the table are millilitres (ml).*

	Stacking	6%	8%	10%	12%	15%
Protogel Acrylamide (30%)	1.3	2	2.67	3.33	4	5
4x Resolving buffer	2.5	2.5	2.5	2.5	2.5	2.5
ddH_2O	6.1	5.39	4.72	4	3.33	2.39
APS 10%	0.05	0.1	0.1	0.1	0.1	0.1
Temed	0.01	0.01	0.01	0.01	0.01	0.01

One dimensional electrophoresis was carried out to separate the proteins contained in each sample according their molecular weight. The process was carried in a wet environment submerging the slides and the cassette in a running buffer containing glycine and 10% SDS. The initial voltage was set at 60V and maintained constant until the samples had run through the stacking gel. The voltage was then increased to 80V until the bromophenol dye had reached the bottom of the gel (approximately 1.5-2 hr).

2.5.3 Western blotting of separated proteins

During this stage, samples are transferred from the gel to a membrane following the same principles described above. As proteins migrate through a gel in an electrical field, proteins can also be transferred, by an electrical field, from the gel onto a membrane that "*blots*" the proteins from the gel onto the membrane.

Two different types of membrane are commercially available: nitrocellulose and Polyvinylidene difluoride (PVDF). Unless differently specified, Amersham™ Protran® western blotting nitrocellulose membrane (GE Healthcare Bio-Sciences, Pittsburgh, USA) was used. The semi-dry transfer was chosen and a "*sandwich*" was created using 6 chromatography papers 1.5mm thick (Sigma-Aldrich Ltd, Gillingham, Dorset, United Kingdom), nitrocellulose and gel as shown in *Figure 2.5*.

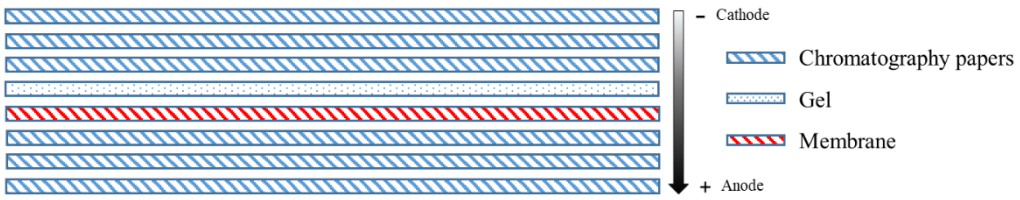

Figure 2.4. *Graphical representation of the sandwich preparation for the transfer of proteins from a gel to a nitrocellulose or PVDF membrane.*

A constant current of 45mA per gel was applied for 90 minutes and following transfer, the membrane was kept and stained using Ponceau S (Sigma-Aldrich Ltd, Gillingham, Dorset, United Kingdom). Ponceau S solution binds to the proteins present on the membrane generating a red signal that was detected with the use of ChemidocTM imaging system (Bio-Rad, Hercules, CA, USA). Ponceau was used to verify the effectiveness of the transfer and to normalise the results of the western blot as suggested by Romero-Calvo and colleagues (2010) and Thacker and colleagues (2015). These independent studies found that total protein membrane staining methods such as Ponceau and Comassie Blu optimally balance accuracy and precision and represent a more accurate alternative to GADPH and β-actin. These high-abundance proteins not only can be affected by the experimental conditions but also their signal gets quickly saturated possibly leading to mistake in the normalisation process (Romero-Calvo et al, 2010; Thacker et al, 2015).

Ponceau S solution was washed away from the membrane using TBS-T20 and the membrane was blocked in 5% non-fatty milk at room temperature for 1 hour with gentle shacking. At this point the "*secondary only*" lane was cut from the membrane and incubated overnight at 4ºC in TBS-T20 while the rest of the membrane was incubated overnight at 4ºC in the primary antibody diluted in 5% non-fatty milk according to the manufacturer's recommendation (see *Table 2.4* for further details) while the "*secondary only*" membranes were kept in TBS-T20.

After incubation, the membranes (including the "*secondary only*" membranes) were repeatedly washed in TBST-T20 and incubated for 1 hour at room temperature with a secondary antibody diluted in 5% non-fatty milk according to the manufacturer's recommendation (see *Table 2.4* for further details). After incubation with the

secondary antibody the membrane was repeatedly washed to eliminate any trace of secondary antibody not linked to the primary antibody.

Where a ChemidocTM imaging system (Bio-Rad, Hercules, CA, USA) was used, enhanced chemiluminescence (ECL) solution was prepared by mixing an equal amount of SuperSignal™ West Dura Extended Duration Substrate solution A with SuperSignal™ West Dura Extended Duration Substrate solution B.

Table 2.3. *List of the antibodies used for SDS-PAGE western blot analysis*

	Company	Code	Host Species	Molecular Weight (kDa)	Dilution
3-NT	ABCAM	ab61392	Mouse	N/A	1:1300
4-HNE	ABCAM	ab46545	Rabbit	N/A	1:2000
Agrin	Thermo Fisher	MA1-20378	Mouse	200	1:1000
Catalase	ABCAM	ab16731	Rabbit	60	1:1000
Caspase-3	Cell Signalling	9662S	Rabbit	30, 19, 17	1:1000
COX-IV	ABCAM	ab16056	Rabbit	14	1:750
Drp1	Cell Signalling	8570S	Rabbit	78-82	1:1000
GAPDH	Cell Signalling	5174S	Rabbit	36	1:1000
GPX1	ABCAM	ab22604	Rabbit	22	1:1000
HSP-10	ENZO	ADI-SPA-110-F	Rabbit	10	1:500
HSP-25	ENZO	ADI-SPA-801d	Rabbit	25	1:1000
HSP-60	Cell Signalling	4869S	Rabbit	60	1:1000
HSP-70	ABCAM	ab31010	Rabbit	70	1:1000
HSC-70	Stress Gen	SPA815	Rat	72	1:1000
Mitofusin-2	Cell Signalling	9482S	Rabbit	80	1:1000
Monoamine Ox. A	ABCAM	ab126751	Rabbit	59	1:1000
MuSK	ABCAM	ab92950	Rabbit	105	1:750
NADPH Oxidase 4	ABCAM	ab133303	Rabbit	67	1:1000
NOX2/gp91phox	ABCAM	ab43801	Mouse	65	1:1000
OPA1	Cell Signalling	80471S	Rabbit	82-100	1:1000
p22 phox	Santa-Cruz	sc-271968	Mouse	22	1:1000
p40 phox	Santa-Cruz	sc-48388	Mouse	40	1:1000
p47 phox	Santa-Cruz	sc-17845	Mouse	47	1:1000
p62	ABCAM	ab56416	Mouse	62	1:1000
p67 phox	BD Bioscience	610913	Mouse	67	1:1000
pDrp1 (Ser616)	Cell Signalling	3455S	Rabbit	78-82	1:1000
Phospholipase A2	Cell Signalling	2832S	Rabbit	95	1:1000
PRX-6	ABCAM	ab133348	Rabbit	25	1:1000
Rac-1	ABCAM	ab33186	Mouse	21	1:1000
S100	ABCAM	ab183979	Rabbit	11	1:1000
SOD 1	ENZO	ADI-SOD-100	Rabbit	21	1:1000
SOD 2	Cell Signalling	13194S	Rabbit	25	1:1000
Trx2	Cell Signalling	12029S	Mouse	56	1:1000

Table 2.4. *List of secondary antibodies used for SDS-PAGE western blot analysis.*

	Company	Code	Diluition
Anti-mouse IgG, HRP-linked Antibody	Cell Signalling	7076S	1:6000
Anti-rabbit IgG, HRP-linked Antibody	Cell Signalling	7074S	1:5000
Anti-rat IgG, HRP-linked Antibody	Cell Signalling	7077S	1:3000/5000
IRDye® 800CW Goat anti-Mouse IgG	LI-Cor	925-32210	1:10000
IRDye® 800CW Goat anti-Rabbit IgG	LI-Cor	925-32211	1:10000

The ECL solution was added to the membranes that were then analysed using the ChemiDocTX. If LICOR Cx (Licor, Bad Homburg, Germany) was chosen for the analysis, a fluorescent conjugated secondary antibody was used and the membrane was analysed without the addition of other chemicals. The images obtained from ChemidocTM imaging system and LICOR Cx were analysed using the ImageJ software following the protocol by McLean (2011) and the results normalised using Ponceau as presented in Appendix 1.

2.6 Oxyblot analysis

Oxyblot analysis is a procedure to analyse the levels of carbonylation formed in proteins by interaction with ROS. The MERK Millipore kit (S7150 - Merk, Darmstadt, Germany) was used for this analysis.

2.6.1 Reagents

- 1x DNPH solution (Kit component);
- 1x Derivitalization solution (Kit component);
- Neutralization solution (Kit component);
- 12% SDS (Sigma-Aldrich Ltd, Gillingham, Dorset, United Kingdom);

- Phosphate Buffer Saline (PBS 1x, Sigma-Aldrich Ltd, Gillingham, Dorset, United Kingdom);
- Tween 20 (Sigma-Aldrich Ltd, Gillingham, Dorset, United Kingdom);
- Blocking dilution buffer 0.01%
    - PBS-T20,
    - BSA;
- BLU 1x
    - 1M Tris/Hcl (Sigma-Aldrich Ltd, Gillingham, Dorset, United Kingdom),
    - Glycerol (Sigma-Aldrich Ltd, Gillingham, Dorset, United Kingdom),
    - 20% SDS (Sigma-Aldrich Ltd, Gillingham, Dorset, United Kingdom),
    - β-Mercaptolethanol (Sigma-Aldrich Ltd, Gillingham, Dorset, United Kingdom),
    - Distilled water.

2.6.2 Protocol

Following protein quantification using the Bradford assay, 30µg of proteins (V_i) were added to an equivalent volume of 12% SDS to ensure protein denaturation. Samples were then vortexed for few seconds and derivatised by adding 2 times V_i of DNPH 1x solution (the same volume of 1x Derivitisation-control was also added to a positive control). Samples were incubated for 15 minutes at room temperature and 1.5 times V_i Neutraliser solution was added to stop the derivitisation. Samples were then added to a polyacrylamide gel and run as described for the SDS-PAGE western blot analysis (section 2.5.2) using the same transfer method described in section 2.5.3. The only

difference was the use of PVDF Membrane (GE Healthcare Bio-Sciences, Pittsburgh, USA) which was activated in 95% ethanol for 15 seconds prior to adding it to the transfer apparatus. Following transfer, the membrane was blocked with the blocking buffer provided with the kit for 1 hour at room temperature. After blocking, the primary antibody was diluted 1:150 in the blocking buffer and the membrane incubated at room temperature for 1 hour. The membrane was then washed with PBS-T20 and incubated in the secondary antibody (diluted 1:300) at room temperature for 1 hour before washing with PBS-T20. At this point the ECL solution was prepared by mixing an equal amount of SuperSignal™ West Dura Extended Duration Substrate solution A with SuperSignal™ West Dura Extended Duration Substrate solution B. The ECL solution was then added to the membranes and they were immediately exposed in the ChemiDocTX (Bio-Rad, Hercules, CA, USA) set with the chemiluminescence protocol. The images recorded were collected for densitometry analysis that was performed using the ImageJ software as previously described (section 2.5.3).

2.7 Glutathione assay

The levels of total glutathione in samples was measured using glutathione reductase to induce the formation of sulfhydryl groups. The interaction between the sulfhydryl groups with the Elleman's reagent generates a yellow change of colour in the samples which is recorded by a spectroscopic plate reader set at 37ºC and 415nm wavelength. The plate reader provides information about the rate at which each sample change colour (slope) and the average slope is used to indirectly measure the levels of glutathione contained in the sample (Baker et al, 1990).

2.7.1 Reagents

- 1% 5-Sulfasalicylic acid (SSA) (Sigma-Aldrich Ltd, Gillingham, Dorset, United Kingdom);

- Glutathione reductase (1346 units/ml Sigma-Aldrich Ltd, Gillingham, Dorset, United Kingdom);
- Oxidised glutathione (Sigma-Aldrich Ltd, Gillingham, Dorset, United Kingdom);
- Reduced glutathione (Sigma-Aldrich Ltd, Gillingham, Dorset, United Kingdom);
- Stock Buffer (pH 7.5)
    - 143mM of sodium phosphate (Na_2HPO_4 - Sigma-Aldrich Ltd, Gillingham, Dorset, United Kingdom),
    - 6.3mM of Tetrasodium EDTA (Na_4EDTA - Sigma-Aldrich Ltd, Gillingham, Dorset, United Kingdom);
- NADPH (Sigma-Aldrich Ltd, Gillingham, Dorset, United Kingdom);
- Elleman's solution or 5,5-dithio-bis-(2-nitrobenzoic acid) (DTNB - Sigma-Aldrich Ltd, Gillingham, Dor-set, United Kingdom).

2.7.2 Protocol

Samples were taken from the -20ºC freezer and slowly defrosted on ice. Reagent solutions were prepared as follow: the daily buffer was prepared adding 3.5mg of NADPH in 14ml of stock buffer and placed immediately on ice. In addition, 6mM of DTNB were dissolved in stock buffer and placed in ice.

A standard curve was prepared dissolving 16mg of reduced glutathione and 16mg of oxidised glutathione in 10ml of 1%SSA and a range of dilutions was prepared to obtain different concentrations ranging from 10.4µM to 0.081 µM plus a blank (1%SSA only).

Once defrosted, samples were diluted 1:20 in 1%SSA and 20µl of diluted sample or standard added to a 96-well plate (Costar, Corning Incorporated, New York, USA). A

"*cocktail*" solution was then prepared as presented in *Table 2.5.* Glutathione reductase was added immediately before analysis.

Table 2.5. *Cocktail recipe based on the analysis of different number of samples.*

	10	20	30	40
Daily Buffer	1.75ml	3.5ml	5.25ml	7ml
Elleman's solution (DTNB)	250µl	500µl	75µl	1ml
ddH_2O	250µl	500µl	750µl	1ml
Glutathione Reductase	25µl	50µl	750µl	100µl

200µl of cocktail solution were added to each well while the plate reader Spectro Star Nano (BMG LabTech, Offenburg, Germany) was set at 37ºC and 415nm wavelength with readings taken every 20 seconds for a total duration of 10 minutes (300 cycles). The average slope of the absorbance change was collected for data analysis.

2.8 Oxidised glutathione assay

2.8.1 Reagents

- 1% SSA (Sigma-Aldrich Ltd, Gillingham, Dorset, United Kingdom);
- Glutathione reductase (1346 units/ml Sigma-Aldrich Ltd, Gillingham, Dorset, United Kingdom);
- Oxidised glutathione (Sigma-Aldrich Ltd, Gillingham, Dorset, United Kingdom);
- Reduced glutathione (Sigma-Aldrich Ltd, Gillingham, Dorset, United Kingdom);
- Stock Buffer (pH 7.5)
    - 143mM of Sodium Phosphate dibasic (Na_2HPO_4 - Sigma-Aldrich Ltd, Gillingham, Dorset, United Kingdom),

    - 6.3mM of Na_2EDTA (Sigma-Aldrich Ltd, Gillingham, Dorset, United Kingdom);
- 2-Vynylpyridine (Sigma-Aldrich Ltd, Gillingham, Dorset, United Kingdom);
- Triethanolamine (TEA - Sigma-Aldrich Ltd, Gillingham, Dorset, United Kingdom).

2.8.2 Protocol

Samples were taken from the -20ºC freezer and slowly defrosted in ice. Once defrosted, samples were diluted 1:20 in 1% SSA reaching a final volume of 200µl. The standard curve was prepared as for the glutathione assay (section 2.7.2). Two microlitres of 2-vynilpyridine were added to the samples and the standards and each was vortexed immediately for one minute. To verify if the sample pH was between 6 and 7, 1µl of sample was removed and applied to a pH strip (pH range 1-11, Thermo Fisher Scientific, Waltham, MA, USA). If the pH was higher than 7, 2µl of 2-vynilpyridine were added. In contrast, if the pH was lower than 6, 3µl of TEA (diluted 1:1 in distilled water) were added to the sample to neutralise the excess 2-vynilpyridine. Samples and standards were left at room temperature for 1 hour and subsequently loaded on a 96 well plate (Costar®, Corning Incorporated, New York, USA). Samples were then analysed as described for the glutathione assay (section 2.7.2).

2.9 Haemotoxylin and Eosin staining (H&E)

The Haemotoxylin and Eosin staining takes its name after the two different dyes used to perform this analysis: *haemotoxylin* (a basic dye able to stain acidic structures with a purple/blue staining) and *eosin* (an acidic dye, negatively charged able to stain basic structures within the cell giving them a pink colour).

2.9.1 Reagents

- PBS-T20
    - PBS 1x (Sigma-Aldrich Ltd, Gillingham, Dorset, United Kingdom),
    - Tween 20 (0.04% - Sigma-Aldrich Ltd, Gillingham, Dorset, United Kingdom);
- Harry's Haemotoxylin (Sigma-Aldrich Ltd, Gillingham, Dorset, United Kingdom);
- Acid Alcohol (Thermo Fisher Scientific, Waltham, MA, USA);
- Eosin (Sigma-Aldrich Ltd, Gillingham, Dorset, United Kingdom);
- Ethanol 70% (Sigma-Aldrich Ltd, Gillingham, Dorset, United Kingdom);
- Ethanol 90% (Sigma-Aldrich Ltd, Gillingham, Dorset, United Kingdom);
- Ethanol 100% (Sigma-Aldrich Ltd, Gillingham, Dorset, United Kingdom);
- DPX Mountant (Sigma-Aldrich Ltd, Gillingham, Dorset, United Kingdom).

2.9.2 Protocol

Prior to start the H&E staining, slides with samples sections were defrosted at room temperature for at least 30 minutes and submerged in PBS-T20 for 5 minutes to remove any excess OCT and any bubbles present between the sample and the slide.

Slides were then submerged in haemotoxylin for 6 minutes after which the slides were washed with water. At this point, slides were dipped into acid alcohol and immediately submerged in Eosin for 10 seconds. Slides were then washed with 70% ethanol for 1 minute, 90% ethanol for another minute and 100% ethanol for another 2 minutes.

The slides were left to air dry before 2 drops of DPX mounting media were added to a cover glass before placing it on the slide carefully avoiding bubble formation. Slides were visualised on the Nikon Ci (Nikon, Kingston, UK) using 4x and 20x magnifications.

2.10 Wheat Germ Agglutinin staining

2.10.1 Reagents

- PBS (Sigma-Aldrich Ltd, Gillingham, Dorset, United Kingdom);
- PBS-T20
    - PBS (Sigma-Aldrich Ltd, Gillingham, Dorset, United Kingdom),
    - Tween 20 (0.05% - Sigma-Aldrich Ltd, Gillingham, Dorset, United Kingdom);
- Methanol (Thermo Fisher Scientific, Waltham, MA, USA);
- Rhodamine, Wheat germ agglutinin (WGA - Vector Lab, Burlingame, California, USA);
- 4′,6-diamidino-2-phenylindole (DAPI - Vector Lab, Burlingame, California, USA);
- Mounting media (Leica, Wetzlar, Germany);
- Cover slips (Leica, Wetzlar, Germany).

2.10.2 Protocol

Following cryosectionning, slides were left to dry at room temperature for 15-20 minutes. Once dried, an area was drawn around the sections using a hydrophobic marker pen (Vector Lab, Burlingame, CA, USA) and the sections were left to dry for further 10 minutes. Sections were rehydrated with ice cold PBS for 5 minutes, fixed with ice cold methanol for 10 minutes at room temperature and washed 3 times with PBS-T20 for 5 minutes.

Wheat germ agglutinin was diluted 1:1000 in PBS and added to the slides for 10 minutes at room temperature. Slides where washed once in PBS-T20 for 5 minutes and 1 time in distilled water to remove any salt residue that could interfere with the analysis. Slides were then left to dry at room temperature in a dark environment before

adding the cover slips using a mounting media containing DAPI staining (Vector Lab, Burlingame, CA, USA). Slides were analysed on the Zeiss LSM 800 confocal microscope (Zeiss, Oberkochen, Germany).

2.11 Analysis of the neuromuscular junction

Alpha-Bungarotoxin is a 74 amino acid neurotoxin component of the venom of some snakes. It is able to bind in an irreversible manner with the nicotinic ACh receptors found at the NMJ level (Moise et al, 2002). When conjugated with Alexa Fluor™ 647, this neurotoxin can be used to stain the ACh receptors of the NMJ to visualise their structure.

2.11.1 Reagents

- Neutral Buffer Formalin (Genta Medical, York, United Kingdom);
- 1% PBS-Sodium Azide
    - PBS (Sigma-Aldrich Ltd, Gillingham, Dorset, United Kingdom),
    - Sodium Azide (Sigma-Aldrich Ltd, Gillingham, Dorset, United Kingdom);
- α-Bungarotoxin, Alexa Fluor™ 647 conjugate (Thermo Fisher Scientific, Waltham, MA, USA).

2.11.2 Protocol

Samples were removed from 1% PBS-Sodium Azide, washed in PBS for 5 minutes and then stained with α-Bungarotoxin, Alexa Fluor™ 647 conjugate (Invitrogen, Paisley, United Kingdom) diluted 1:500 in PBS for at least 30 minutes, in a dark environment at room temperature.

Samples were kept in a dark environment until analysed with a Nikon A1 confocal microscope (Nikon, Kingston, UK). A Z-stack analysis was performed and the

resulting images were analysed in ImageJ and the NMJ-morph Extension following the protocol published by Jones and colleagues (2016).

2.12 Immunofluorescence staining

Immunofluorescence is a light microscopy technique that uses fluorescence to visualise the distribution of a specific target within a cell or tissue. Similar to western blot analysis, the use of primary and fluorescent secondary antibodies is necessary to detect the target of interest. If the primary antibody is already conjugated with a fluorescent probe, the secondary antibody is not needed. When the fluorescent probe tagged to the antibody is excited (at a specific wavelength) it generates a fluorescent signal which allows a detailed qualitative analysis of the distribution of a specific protein or structure within the cell or a tissue.

2.12.1 Reagents

- PBS (Sigma-Aldrich Ltd, Gillingham, Dorset, United Kingdom);
- PBS-T20
    - PBS (Sigma-Aldrich Ltd, Gillingham, Dorset, United Kingdom),
    - Tween 20 (0.05 - Sigma-Aldrich Ltd, Gillingham, Dorset, United Kingdom);
- Goat serum (Sigma-Aldrich Ltd, Gillingham, Dorset, United Kingdom);
- Various antibodies;
- Rhodamine, WGA (Vector Lab, Burlingame, California, USA);
- DAPI (Vector Lab, Burlingame, California, USA);
- Mouse On Mouse (M.O.M) blocking (Vector Lab, Burlingame, California, USA);
- Mounting media (Leica, Wetzlar, Germany);

- Cover slips (Leica, Wetzlar, Germany).

2.12.2 Protocol

Following cryosectioning, the slides were left to dry at room temperature for 30 minutes. With a hydrophobic marker pen (Vector Lab, Burlingame, CA, USA) an area around the sections was drawn and the samples were left to dry for another 10 minutes. Samples were rehydrated with PBS for 5 minutes. Following rehydration, samples were blocked for 1 hour at room temperature using 5% goat serum in PBS containing Mouse On Mouse (M.O.M) blocking. The primary antibody was prepared by diluting it in PBS with 5% goat serum and slides were incubated overnight at 4°C. Following incubation, slides were washed 3 times for 5 minutes in PBS-T20. The secondary antibody was prepared in PBS with 12% goat serum and slides were incubated at room temperature for 1 hour before they were washed 3 times in PBS-T20 for 5 minutes. Slides were then stained using the Rhodamine wheat germ agglutinin protocol described before (section 2.11). Once dry, coverslips were mounted and the slides were visualised using the Zeiss LSM 800 confocal microscope (Zeiss, Oberkochen, Germany).

Table 2.6. *List of primary antibodies used for the immunofluorescence staining.*

	Company	Code	Host species	Dilution
MyHC-I	ABCAM	ab11083	Mouse	1:250
MyHC-IIa	DSHB	SC-71	Mouse	1:250
MyHC-Iib	DSHB	BF-F3	Mouse	1:250

Table 2.7. *List of secondary antibodies used for the immunofluorescence staining.*

	Company	Code	Host species	Dilution
Anti-mouse Alexa fluor IgG1 647	Invitrogen	A21240	Goat	1:500
Anti-mouse Alexa fluor IgM 448	Invitrogen	A21042	Goat	1:500

2.13 Tetramethylrhodamine, methyl ester (TMRM)

TMRM is a cell-permeant cationic dye that is quickly sequestered by mitochondria generating a fluorescent signal able to provide information regarding the mitochondrial membrane potential in isolated and permeabilised muscle fibres.

In physiological conditions, mitochondria show a membrane potential of -150mV (Perry et al, 2011). Being TMRM a cationic dye (with positive charge), it is able to accumulate within the negatively charged mitochondria in inverse proportion to the mitochondrial membrane following the principle described by the Nernst equation:

$$E = E° - \frac{RT}{nF} \ln Qc$$

Where E is the cell potential, E° the cell potential in standard condition, R the ideal gas constant (8.314 J/mol-K), T the temperature in Kelvins, n the number of moles of dye transferred, F the Faraday constant (95,484.56 C/mol) and lnQc the natural log of quotient content at the moment in time (Perry et al, 2011).

Separation of muscle fibres is usually carried out in a relaxing solution where single muscle fibres are teased out from the muscle using fine forceps (Fine Science Tools GmbH, Heidelberg, Germany). For this protocol, a relaxing solution consisting of EDTA and Magnesium was used to prevent rigor mortis and induce muscle relaxation following dissection (Bozler, 1954).

Permeabilisation of the muscle fibres allows the study of important functional parameters of the mitochondria that would not be possible in normal cells as some probes and effectors cannot reach the mitochondria in non-permeabilised cells (Brand and Nicholls, 2011).

2.13.1 Reagents

- Relaxing solution

    - 4.5µM Adenosine 5′-triphosphate magnesium salt (Mg_2ATP - Sigma-Aldrich Ltd, Gillingham, Dorset, United Kingdom),
    - 10mM Imidazole (Sigma-Aldrich Ltd, Gillingham, Dorset, United Kingdom),
    - 2mM EGTA (Sigma-Aldrich Ltd, Gillingham, Dorset, United Kingdom),
    - 100mM Potassium Chloride (KCl - Sigma-Aldrich Ltd, Gillingham, Dorset, United Kingdom),
    - 1mM Magnesium Chloride ($MgCl_2$ - Sigma-Aldrich Ltd, Gillingham, Dorset, United Kingdom);
- Saponin (0.025g/500µl) (Sigma-Aldrich Ltd, Gillingham, Dorset, United Kingdom);
- TMRM (Invitrogen, Paisley United Kingdom);
- Buffer Z
    - 110mM MES Potassium salt (K-MES - Sigma-Aldrich Ltd, Gillingham, Dorset, United Kingdom),
    - 35mM KCl (Sigma-Aldrich Ltd, Gillingham, Dorset, United Kingdom),
    - 1mM EGTA (Sigma-Aldrich Ltd, Gillingham, Dorset, United Kingdom),
    - 5.3mM Na_2ATP (Sigma-Aldrich Ltd, Gillingham, Dorset, United Kingdom),
    - 10mM Dipotassium hydrogen phosphate trihydrate (K_2HPO_4 - Sigma-Aldrich Ltd, Gillingham, Dorset, United Kingdom),

    - 3mM Magnesium Chloride, Hexahydrate ($MgCl_2 \cdot 6H_2O$ - Sigma-Aldrich Ltd, Gillingham, Dorset, United Kingdom);
- Oligomycin A (Sigma-Aldrich Ltd, Gillingham, Dorset, United Kingdom);
- Carbonyl cyanide 4-(trifluoromethoxy)phenylhydrazone (FCCP - Sigma-Aldrich Ltd, Gillingham, Dorset, United Kingdom).

2.13.2 Protocol

Saponin solution was prepared fresh by adding 0.025g of saponin to 500µl of relaxing solution. Eight microlitres of saponin were diluted in 1000µl of relaxing solution (Dilution A) and 500µl of Dilution A was added to 1000µl of relaxing solution (working dilution).

Immediately following dissection, muscles were added into ice-cold relaxing solution and muscle fibres were manually teased out from the muscle under a microscope (Nikon, Kensington, UK). Following isolation, fibres were incubated for 30 minutes in saponin and left at room temperature to induce permeabilisation of the sarcolemma. Following permeabilization, fibres were transferred in a glass bottom 35mm petri dish (MatTek, Ashland, MA, USA) and submerged with 30nM of TMRM solution prepared by diluting 1.5µl of TMRM stock solution in 5ml of Buffer Z. The dish was then placed on an inverted confocal microscope (Nikon, Kensington, UK) and a time course experiment was set using 60x magnification objective at an excitation/emission wavelength of 543/605. A single image was captured every 3 minutes for a total of 90 minutes. Following 45 minutes, oligomycin was added to the dish at a concentration of 2.5µM. Olygomycin interferes with ATP Synthase of the ETC inducing accumulation of protons in the mitochondrial intermembrane space consequently increasing mitochondrial membrane potential. As TMRM was used in a non-quenching way, this increase in mitochondrial potential corresponds to an increase in fluorescent signal that was

recorded every 3 minutes. After 72 minutes, FCCP was added to the solution to reach a final concentration of 4µM. FCCP is a photonophore able to induce depolarization of the mitochondrial inner-membrane inducing an increase proton flux into the mitochondrial matrix and therefore significantly depolarising the mitochondrial membrane inducing a significant reduction of the fluorescent signal. Following addition of FCCP, the signal was recorded every 3 minutes until the end of the protocol (90 minutes total).

2.14 Analysis of mitochondrial peroxide generation

The Amplex Red assay allows the detection of mitochondrial peroxide release. This technique is based on the activity of a reagent (Amplex Red) that, reacting with H_2O_2 in a 1:1 stoichiometry manner, generates a resorufin fluorescent signal with a maximal emission of 585nm.

This very straightforward assay is able to detect levels of H_2O_2 as low as 10 picomoles in 100µl of volume. Furthermore, this technique allows the analysis of the H_2O_2 production both under normal mitochondrial respiratory conditions and following the addition of specific inhibitors of ETC enzymes or other enzymes involved in the production of H_2O_2 in the mitochondria.

As for the TMRM analysis, muscle bundles were permeabilised using saponin. This compound allows the permeabilisation of muscle fibres by interacting with the cholesterol molecules forming pores on the cell membrane bilayers inducing the dispersion of all cytosolic components (Jacob et al, 1991). Previous studies (Casas et al, 2008; Kuznetson et al, 2009; Mathers and Staples, 2015) have demonstrated the efficacy of this permeabilisation protocol to study mitochondrial functions in skeletal muscles. Furthermore, previous studies in denervated muscles carried out independently by our collaborators (Muller et al, 2007) and our laboratory (Pollock et al, 2017) have shown

no major differences in the analysis of peroxides release using Amplex Red in isolated mitochondria and permeabilised muscle bundles.

2.14.1 Reagents

- ROS buffer
    - 125mM KCl (Sigma-Aldrich Ltd, Gillingham, Dorset, United Kingdom),
    - 10mM Hepes (Sigma-Aldrich Ltd, Gillingham, Dorset, United Kingdom),
    - 5mM $MgCl_2$ (Sigma-Aldrich Ltd, Gillingham, Dorset, United Kingdom),
    - 2mM K_2HPO_4 (Sigma-Aldrich Ltd, Gillingham, Dorset, United Kingdom),
- Amplex Red Solution (in 50ml of ROS buffer)
    - 50µl SOD from bovine erythrocytes (at 37.5U/mg, Sigma-Aldrich Ltd, Gillingham, Dorset, United Kingdom)
    - 19.44mM Amplex Red solution (Thermo Fisher Scientific, Waltham, MA, USA)
    - 10µl Horseradish peroxidase (5U/mg Sigma, Aldrich Ltd, Gillingham, Dorset, United Kingdom)
- Saponin (0.025g/500µl) (Sigma-Aldrich Ltd, Gillingham, Dorset, United Kingdom);
- Specific ETC substrates
    - Glutamate/Malate – Complex I substrate, 0.25M in dH_2O (Sigma-Aldrich Ltd, Gillingham, Dorset, United Kingdom),

    - Succinate – Complex II substrate, 0.5M in dH_2O (Sigma-Aldrich Ltd, Gillingham, Dorset, United Kingdom),
    - Rotenone – ETC inhibitor, 200µM in Ethanol (Sigma-Aldrich Ltd, Gillingham, Dorset, United Kingdom);
- Specific enzymes inhibitors
    - Arachidonyl trifluoromethyl ketone (AACOCF3), PLA2 inhibitor, 20µM;
    - Apocynin – NADPH Oxidase inhibitor, 0.5mM;
    - Chlorgyline - Monoamine Oxidase A inhibitor, 100µM;
    - Pargyline – Monoamine Oxidase B inhibitor, 100µM.

2.14.2 Protocol

Following permeabilisation of the muscle bundles using the same protocol as for the TMRM analysis (section 2.13), the fluostar plate reader (BMG labtech Ltd, Aylesbury, United Kingdom) was set a 37°C. Individual muscle bundles were placed in a black 96 well plate (Corning, Wiesbaden, Germany) and incubated with 100µl of Amplex Red solution with specific substrates or inhibitors. The plate was then placed in the plate reader set at 590nm and incubated at 37°C for 5 minutes before analysis that was performed using a kinetic protocol collecting readings every 2 seconds for 10 minutes. At the end of the protocol, the muscle bundles were removed from the wells and frozen at -80°C for cryopulverisation, homogenisation and protein quantification using the Bradford Assay (section 2.4.3) and the results used to normalise the results obtained during this analysis.

2.15 Citrate synthase assay

Citrate synthase is an enzyme localised within the mitochondrial matrix responsible of the condensation of dicarboxylate oxaloacetate and acetyl CoA to tricarboxylate. The

activity of this enzyme can be used to indirectly determine the mitochondria number within a tissue homogenate. A kit from Cayman Scientific (Cayman Scientific, Ann Arbor, MI, USA) was used and the samples were treated following the instructions provided with the kit.

2.15.1 Reagents

- Extraction buffer
    - 250mM Sucrose (Sigma-Aldrich, Gillingham, Dorset, UK),
    - 10mM Trizma Base (Sigma-Aldrich, Gillingham, Dorset, UK),
    - 1mM EGTA (Sigma-Aldrich, Gillingham, Dorset, UK);
- Buffer assay (Cayman Scientific, Ann Arbor, MI, USA);
- Acetyl-CoA (Cayman Scientific, Ann Arbor, MI, USA);
- Developer reagent (Cayman Scientific, Ann Arbor, MI, USA);
- Oxaloacetate (Cayman Scientific, Ann Arbor, MI, USA).

2.15.2 Protocol

Samples were ground in liquid nitrogen and the resulting powder was mixed with 120µl of extraction buffer. Samples were sonicated for 15 seconds on ice and centrifuged at 12,000g for 10 minutes at 4ºC. Supernatants were then collected and quantified using the Bradford assay.

An equal amount of protein from each sample was diluted 1:50 in the Buffer Assay provided with the kit and the samples stored on ice until use. A solution (Solution A) containing Acetyl-CoA and a developer reagent was prepared according to the kit guidelines and 50µl added to each well. Thirty microlitres of diluted sample and 20µl of a solution (Solution B) containing Oxaloacetate diluted in buffer assay were mixed according to the manufacturer instructions and added to the wells immediately before starting the reading. The plate was read using the Spectro Star Nano (BMG LabTech,

Offenburg, Germany) set at 412nm with readings every 30 seconds for a total of 20 minutes. Readings from the plate reader were plotted as absorbance (y-axis) versus time in minutes (x-axis). The slope of the linear portion of the curve was calculated and the final Reaction Rate was quantified using the equation below:

$$\frac{\text{Slope}}{5.712\text{nM}^{-1}} \text{ x} \frac{0.1\text{ml}}{0.03\text{ml}} \text{ x Sample dilution} = \mu\text{mols/min/ml}$$

2.16 Nuclear Magnetic Resonance-Based Metabolomics

Nuclear Magnetic Resonance (NMR) Metabolomics is a technique developed in 1974 by Wilson and Burlingame. NMR is a reliable and highly reproducible technique that allows the investigation of metabolites in different tissues.

2.16.1 Reagents

- Solvent solution
    - 50% HPLC grade acetonitrile (Thermo Fisher Scientific, Waltham, MA, USA),
    - 50 % ultra-pure water;
- Selectively deuterated TrimethylSilyl Propionate (TSP);
- Rehydration buffer
    - 100mM Sodium phosphate pH 7.4,
    - 100% deuterated water (^2H_2O).

2.16.2 Protocol

Following weighting, a variable volume (depending on sample amount) of solvent solution was added and samples were sonicated twice in an ice bath using an exponential micro probe for 30 seconds at 23kHz of frequency.

Following sonication, samples were vortexed for 60 seconds at maximum speed and centrifuged at 21,500g for 10 minutes at 4ºC. Supernatants were collected and centrifuged again using the same settings before being collected and lyophilised overnight at -80ºC.

The following day, lyophilised samples were rehydrated in 200µl of rehydration buffer, centrifuged at 21,500g for 10 minutes at 4ºC and the resulting supernatant added to NMR glass tubes that were then analysed on a 700MHz spectrometers (Bruker, Coventry, United Kingdom) fitted with Samplejet auto-samples and a proton-optimised triple resonance NMR "*inverse*" probe to simultaneously decouple multiple nuclei and optimise for ^{1}H observations (http://bruker.com). Samples were run overnight and the resulting spectra obtained were analysed with TopSpin 3.5 (Bruker, Coventry, United Kingdom) and ChenomX 8.2 (Edmonton, Alberta, Canada) for the correct "*annotation*" of the metabolites present in the tissue. The pattern file was verified using tameNMR on Galaxy.liv.ac.uk as suggested by Afgan and colleagues (2016) and formatted for the analysis and quantification of the metabolites using MetaboAnalyst 4.0 and R studio.

2.17 Statistical analysis

Statistical analysis was performed using IBM SPSS statistic version 22 software (IBM analytics, New York, USA). All tests were carried out with a 95% confidence interval and the level of significance was set at 0.05. Normal distribution was checked using the Shapiro-Wilk test and the data were expressed as the mean ± standard error mean. One-way ANOVA was chosen to analyse most of the variables that were showing a normal distribution using Bonferroni's correction in the *post-hoc* analysis to find eventual differences between the control group and the other time points. For those variables where the assumption of normality was violated, differences within and

between groups were determined by Kruskal-Wallis test followed by Mann-Witney U test for *post-hoc* analysis applying Bonferroni's correction.

Furthermore, when required, the Multivariate ANalysis Of VAriance (MANOVA) was performed using the Wilk's Lambda model and using Bonferroni's correction to find eventual crude differences between the experimental groups.

2.17.1 Statistical analysis for NMR metabolomics

For NMR metabolomics, an initial analysis was performed using the online software MetaboAnalyst and the analysis was implemented using R studio as recommended by Chong and Xia (2018). For the statistical analysis, spectra were normalised to total area and scaled using the Pareto method. This scaling method use the $\sqrt{SD}$ as scaling factor maintaining the data structure intact while allowing a close analysis of the original measurements (van den Berg et al, 2016). Following normalisation and scaling, a Principal Component Analysis was performed to verify the eventual presence of differences between groups. This statistical procedure uses an orthogonal transformation to convert a set of possibly correlated variables into a set of values of linearly uncorrelated variables (Principal Components) (Patel, 2016). One-way ANOVA was performed to verify any crude differences between the groups for each metabolite applying Tuckey's correction to avoid the risk of Type II errors.

A heatmap was also generated using all metabolites showing significant differences between groups to facilitate the interpretation of the results. Pathway analysis using the KEGG reference was performed using Metabolite Set Enrichment Analysis (MSEA) to identify eventual effects of denervation on specific metabolic pathways (Xia and Wishart, 2010).

Chapter 3. Redox responses following skeletal muscle denervation

3.1 Introduction

Loss of muscle mass and strength has a severe impact on the quality of life and survival of older adults and is referred as sarcopenia. One of the main factors responsible for driving the loss of muscle mass and strength during ageing is skeletal muscle denervation. As described by several authors (Aare et al, 2006; Jang and Van Remmen, 2011, McDonagh et al, 2016) denervated muscle fibres show a significant reduction in size of approximately 35-50% compared to innervated fibres. The main causes of denervation in ageing are still unclear, but evidence shows that failure of the denervation-reinnervation cycle may play a fundamental role. The denervation-reinnervation cycle is an important mechanism that occurs throughout life and that, when efficient, gives the neuromuscular system great plasticity and adaptability to external stimuli. When impaired, it initiates a cascade of events that result in denervation and loss of muscle mass, strength and power (Hepple and Rice, 2016).

Table 3.1. *List of the main transcription factors regulated by ROS in developed skeletal muscle. Adapted from Espinosa-Diez et al, 2015.*

Transcription factor	DNA binding domain	Cellular process regulated in skeletal muscle
AP-1	12-O-Tetradecanoylphorbol-13-acetate response element	Cell proliferation, apoptosis, differentiation
Nrf2	Antioxidant Response Elements	Cytoprotective responses to ROS
CREB	cAMP response element	Promotes myoblast proliferation
HSF-1	Heat shock elements	Regulates Heat Shock Proteins response
NF-kB	Response elements	Antioxidant response

Another notable characteristic of ageing is an increase in ROS levels that, if not adequately counteracted, can result in oxidative stress (McDonagh et al, 2016). As discussed earlier in this thesis, several studies have highlighted how ROS play an important role also in signalling. Oxidants can activate and inactivate transcription factors (Table 3.1 for further information), membrane channels, metabolic enzymes in

addition to modulating calcium-dependent and phosphorylation signalling pathways (Winterbourn et al, 2008).

Hydrogen peroxide, a non-radical ROS, plays a key role in cell signalling and is usually generated within the mitochondria by the dismutation of superoxide (section 1.5.3). Besides the mitochondrial ETC, 31 other enzymes have been implicated in the generation of H_2O_2 including NADPH oxidase, PLA2 and the Monoamine oxidase isoforms (Go et al, 2016).

Nerve transection models have been used to examine the mechanisms leading to reduction in muscle mass and function following the loss of innervation. Studies using these denervation models in rodents also highlighted a role of mitochondrial oxidative stress in the mechanisms of denervation-induced muscle atrophy. In 2007, a study by Dr. Van Remmen's group (Muller et al, 2007) highlighted a significant increase in mitochondrial ROS production (nearly 30 fold after 7 days) while a more recent study from our group (Pollock et al, 2017) highlighted that the increased release of mitochondrial peroxide is induced by the activity of several enzymes not involved in the ETC.

The goal of the present chapter was to examine the effects of prolonged skeletal muscle denervation on redox homeostasis of the muscle. Specifically, our aim was to determine the effect of prolonged denervation on the muscle content of proteins that may contribute to peroxide release and those that regulate redox responses.

3.2 Materials and Methods

3.2.1 Mouse model

Twenty-four wild type C57BL/6 and B6.Cg-Tg(Thy1-YFP)16Jrs/J adult male mice (8 to 10 months old) were purchased from The Charles Rivers Laboratory (Bar Harbor, ME, USA) and kept in the Biomedical Service Unit (BSU) facilities in accordance with the UK Home Office guidelines under the UK Animals (Scientific Procedures) Act 1986.

3.2.2 Surgical denervation of the Tibialis Anterior and Extensor Digitorum Longus muscles

To induce full denervation of the TA and EDL muscles, mice underwent a surgical procedure to remove a small section of the peroneal nerve in the right limb as previously described by Pollock et al (2017) and explained in section 2.2. Mice were sacrificed at different time points after denervation (1, 3, 7, 14, 21 days) through cervical dislocation and TA and EDL muscles collected and prepared for further analysis.

3.2.3 Haematoxylin and Eosin staining

TA muscles were prepared as presented in section 2.3.4, stained following the standard protocol for H&E staining (section 2.9) and each slide was examined using Nikon Ci microscope at 4x and 20x magnifications.

3.2.4 Imaging of neuromuscular junctions

Following dissection, muscles were fixed in 10% Neutral Buffer Formalin (Genta Medical, York, United Kingdom) as explained in section 2.3.5, stained with α-Bungarotoxin-Alexa Fluor™ 647 conjugate (Invitrogen, Paisley, United Kingdom) diluted 1:500 in PBS and analysed as stated in section 2.11.

3.2.5 Analysis of mitochondrial peroxide generation

Amplex-Red analysis was used to determine the mitochondrial release of H_2O_2 and other peroxides from the TA muscle. Immediately following dissection fibres were separated in small bundles and permeabilised as presented in section 2.3.6. Approximately 15-20 bundles per sample were placed in a black 96 well plate (Corning, Wiesbaden, Germany) with Amplex Red solution without added substrates to assess State 1 ROS production, or ROS production in the presence of specific enzymes inhibitors (see section 2.14.1 for further information) and the signal analysed as explained in section 2.14.2.

3.2.6 Total glutathione and oxidised glutathione assays

Tibialis Anterior muscles were ground in liquid nitrogen and the resulting powder was added to 1% SSA (Sigma-Aldrich Ltd, Gillingham, Dorset, United Kingdom) and treated as shown in section 2.3.3. Total glutathione was assessed using the recycling method described in section 2.7. To analyse GSSG content, before the analysis, samples prepared as for the GSH assay were derivatised by the addition of 2µl of 2-Vinylpyridine as presented in section 2.8.

3.2.7 SDS-PAGE and western blot analysis

For SDS-PAGE and western blot analysis TA muscles were ground in liquid nitrogen and treated as explained in section 2.3.1. For each SDS-PAGE analysis, 30µg of total protein were added to a polyacrylamide gel and electrophoresis performed as presented in section 2.5. Following transfer of the proteins onto a membrane, Ponceau red (Sigma-Aldrich, St. Louis, MI, USA) was used to to normalise the results as described by Romero-Calvo and colleagues (2010).

Chemiluminescence signal was detected using the ChemiDocTM imaging system (Bio-Rad, Hercules, CA, USA) after the addition of ECL to each membrane (Bio-Rad,

Hercules, CA, USA). Densitometric analysis was performed using the ImageJ software (McLean, 2011). Most of the subunits analysed in this chapter showed changes within the dynamic range of western blots that could be quantified by densitometry. However, some proteins were undetectable, or barely detectable in the baseline (non-denervated) and, therefore, in these cases only example blots are presented to show the changes observed.

3.2.8 Analysis of protein carbonylation

Tibialis Anterior muscles were homogenised in Hepes buffer and processed using the OxyBlot Protein Oxidation Detection Kit (Merk, Darmstadt, Germany) (sections 2.3.2 and 2.6). Samples were separated on 12% polyacrylamide using a protocol similar to the one used for the SDS-PAGE (section 2.6). Densitometry analysis of the bands at different molecular weights was performed using the ImageJ software.

3.3 Results

3.3.1 Anthropometric measurements

The statistical analysis identified no significant differences in total body weight between the control and denervation groups (*Figure 3.1a*). Analysis of the denervated TA mass showed a significant reduction in muscle weight starting at 7 and proceeding up to 21 days when compared with the control group $F(5,19)=33.204$ $p<0.01$ (*Figure 3.1b*). Statistical analysis also showed that there were no significant differences between the control and the other groups in total fibre numbers (*Figure 3.1c*) although there were significant differences in muscle fibres CSA. As shown in *Figure 3.1d*, 7 days following denervation there is a significant decrease of large muscle fibres (>2001μm) with a related increase of small/medium muscle fibres.

The H&E staining (*Figure 3.2a*) was undertaken to determine potential infiltration of the muscle with immune cells. No significant accumulation of immune cells was seen in skeletal muscle following denervation (*Figure 3.2a*).

3.3.2 Qualitative analysis of the neuromuscular junction following denervation

Analysis of the NMJ following denervation (representative images shown in *Figure 3.2b*) showed a progressive breakdown of the pre-synaptic terminal (in green) starting almost immediately (1 day) following surgery and resulting in full muscle denervation from 7 days post-surgery. Fourteen days following denervation progressive enlargement of the NMJ endplate (in red) was seen as a result of the disruption of the ACh receptors.

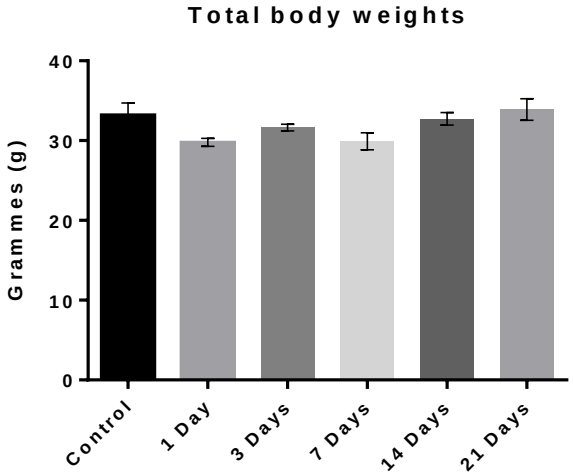

Figure 3.1a. *Total body weights from control mice (non-denervated) and mice at 1, 3, 7, 14 and 21 days post-denervation. Histograms represent the mean and the standard error of the mean for each experimental group (n=4).*

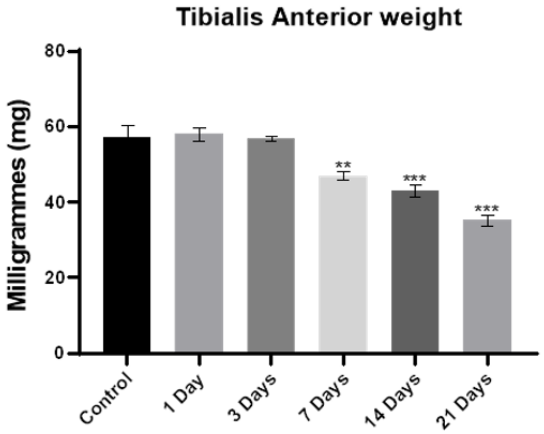

Figure 3.1b. *Tibialis Anterior muscle weights from control mice (non-denervated) and mice at 1, 3, 7, 14 and 21 days post-denervation. Histograms represent the mean and the standard error of the mean for each experimental group (n=4).*
*** p<0.01 - *** p<0.001 compared with the control group.*

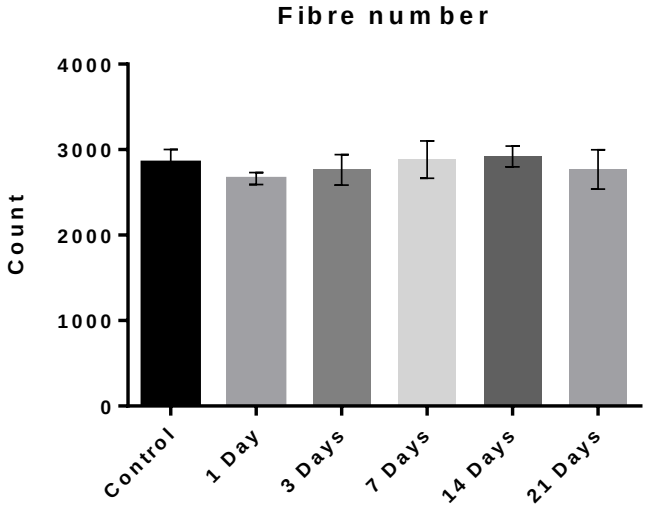

Figure 3.1c. *Fibre number in Tibialis Anterior muscle from control mice (non-denervated) and mice at 1, 3, 7, 14 and 21 days post-denervation. Histograms represent the mean and the standard error of the mean for each experimental group (n=4).*

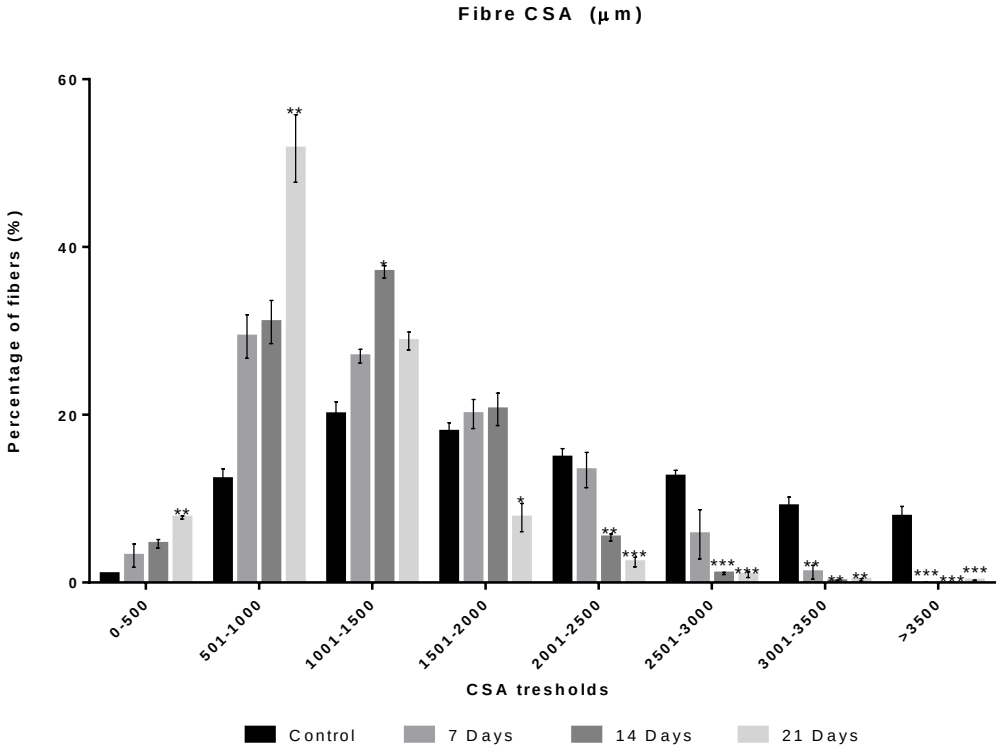

Figure 3.1d. *Analysis of fibre CSA from Tibialis Anterior muscle in control mice (non-denervated) and mice at 7, 14 and 21 days post-denervation.*
Histograms represent the mean fibre percentage in each threshold and the standard error of the mean for each experimental group (n=4).
** p<0.05 - ** p<0.01 - *** p<0.001 compared with the control group.*

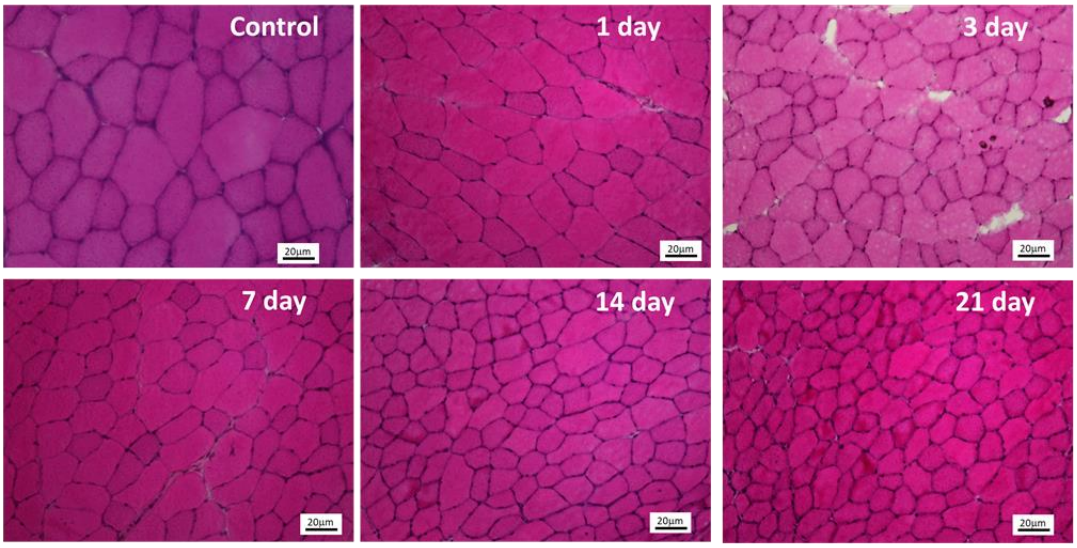

Figure 3.2a. *Transverse sections of Tibialis Anterior muscles visualized by H&E staining from control mice (non-denervated) and mice at 1, 3, 7, 14 and 21 days post-denervation.*

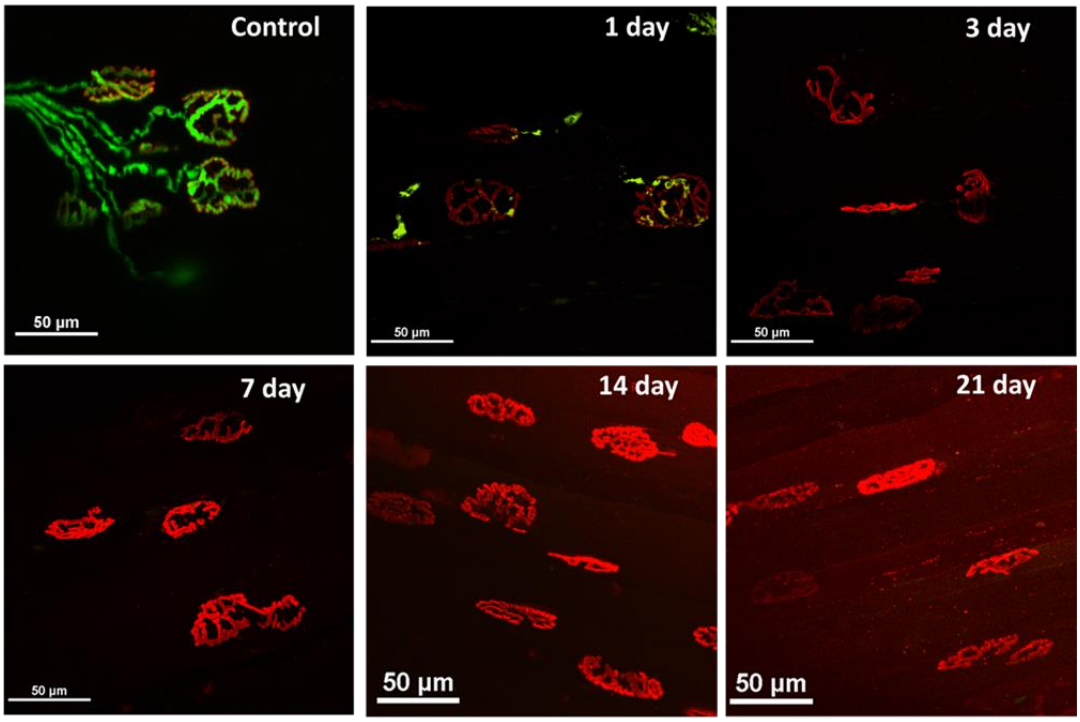

Figure 3.2b. *Represntative NMJs observed in whole EDL muscle from a control mice (non-denervated) and a mice at 1, 3, 7, 14 and 21 days post-denervation. Images show the peripheral nerves (green) and acetylcholine receptors (red).*

3.3.3 Peroxide release from bundles of muscle fibres

As shown in *Figure 3.3a*, data from the Amplex Red assay showed a statistically significant increase in peroxide production following denervation $F(4,11)=44.354$ $p<0.01$. Peak peroxide production was at 7 days although levels remained significantly elevated up to 21 days. The addition of specific inhibitors Chlorgyline $F(3,8)=4.902$ $p<0.05$, Pargyline $\chi^2(3)=9.667$ $p<0.05$, Apocynin $F(3,8)=4.349$ $p<0.05$ and AACOCF3 $F(3,8)=8.347$ $p<0.01$ reduced peroxide release to variable extents at 7, 14 and 21 days post-denervation (*Figure 3.3b*). This decrease suggests that these mitochondrial enzymes play a primary role in peroxides release following denervation.

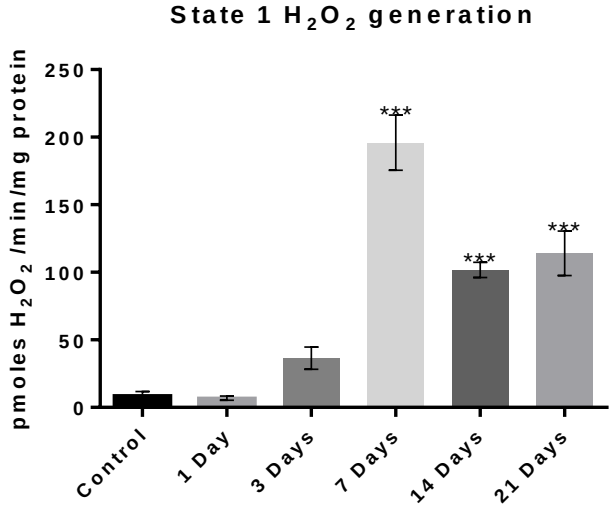

Figure 3.3a. *State 1 H_2O_2 production in mitochondria in permeablised Tibialis Anterior fibre determined by oxidation of amplex red from control (non-denervated) mice and mice at 1, 3, 7, 14 and 21 days post-denervation.*
*Histograms represent the mean and standard error of the mean for each experimental group (n=4). *** p<0.001 compared with the control group.*

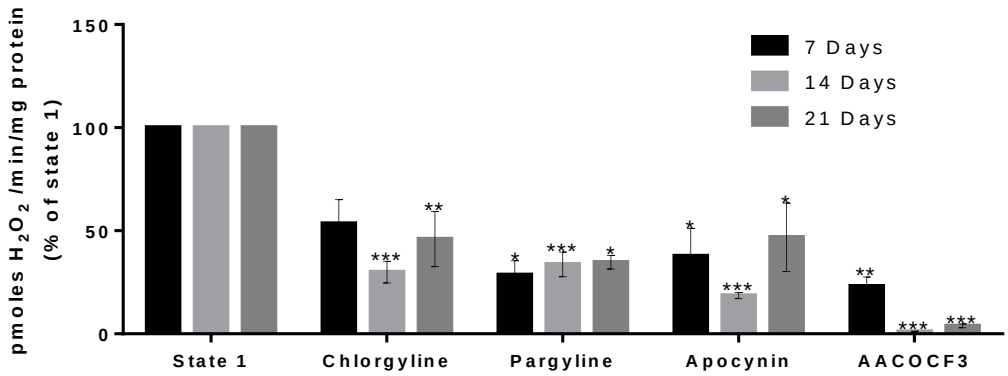

Figure 3.3b. *State 1 mitochondrial H_2O_2 generation from permeabilised fibres of the Tibialis Anterior muscle in the presence of different enzyme inhibitors. Chlorgyline (Monoamine Oxidase A -100µM), parglyline (Monoamine Oxidase B - 100µM), apocynin (NADPH oxidase - 0.5mM), AACOCF3 (PLA_2 - 20µM) resulted in significantly reduced H_2O_2 generation compared untreated fibre bundles at 14 and 21 days post-denervation. Histograms represent the mean percentage of State 1 and standard error of the mean for each experimental group (n=4). * p<0.05 - ** p<0.01 - *** p<0.001 compared with its state 1 (fibres not exposed to any inhibitor).*

3.3.4 Total glutathione and oxidised glutathione content

The glutathione (GSH) and oxidised glutathione (GSSG) contents of denervated muscles are shown in *Figure 3.4a* and *Figure 3.4b*. Data show no statistically significant differences with time post-denervation in GSH $F(5,16)=1.473$ $p>0.05$ and GSSG $F(5,15)=1.291$ $p>0.05$. There was also no significant change in the percentages of glutathione that was oxidised $F(5,15)=0.169$ $p>0.05$.

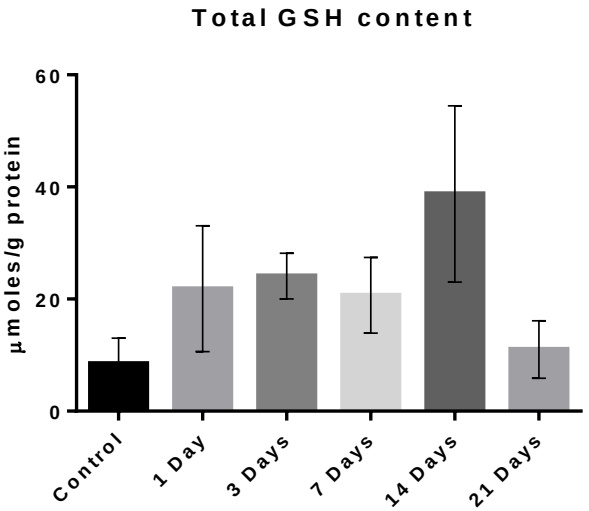

Figure 3.4a. *Total glutathione (GSH) contents in Tibialis Anterior muscles from control (non-denervated) mice and mice at 1, 3, 7, 14 and 21 days post-denervation.*
Histograms represent the mean and standard error of the mean for each experimental group (n=4).

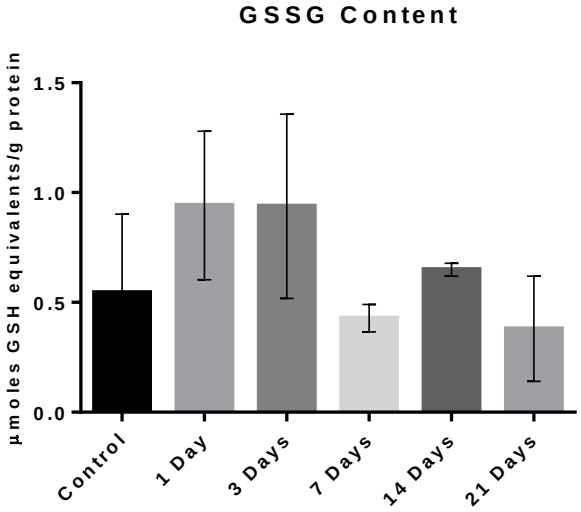

Figure 3.4b. *Oxidised glutathione (GSSG) contents in Tibialis Anterior muscles from control (non-denervated) mice and mice at 1, 3, 7, 14 and 21 days post-denervation.*
Histograms represent the mean and standard error of the mean for each experimental group (n=4).

3.3.5 Protein oxidation in TA muscles following denervation

Oxyblot analysis showed considerable variability within groups but no overall differences were seen with time. The Oxyblot (original blots presented in Appendix 2) revealed 6 major bands of approximate molecular weight 95, 75, 65, 55, 35 and 25 kDa (*Figure 3.5*). A comparison of the different time points with the control group demonstrated that only the band seen at approximately ~25 KDa, showed increased intensity at 7 days following denervation $F(5,17)=3.616$ $p<0.05$ (*Figure 3.5*).

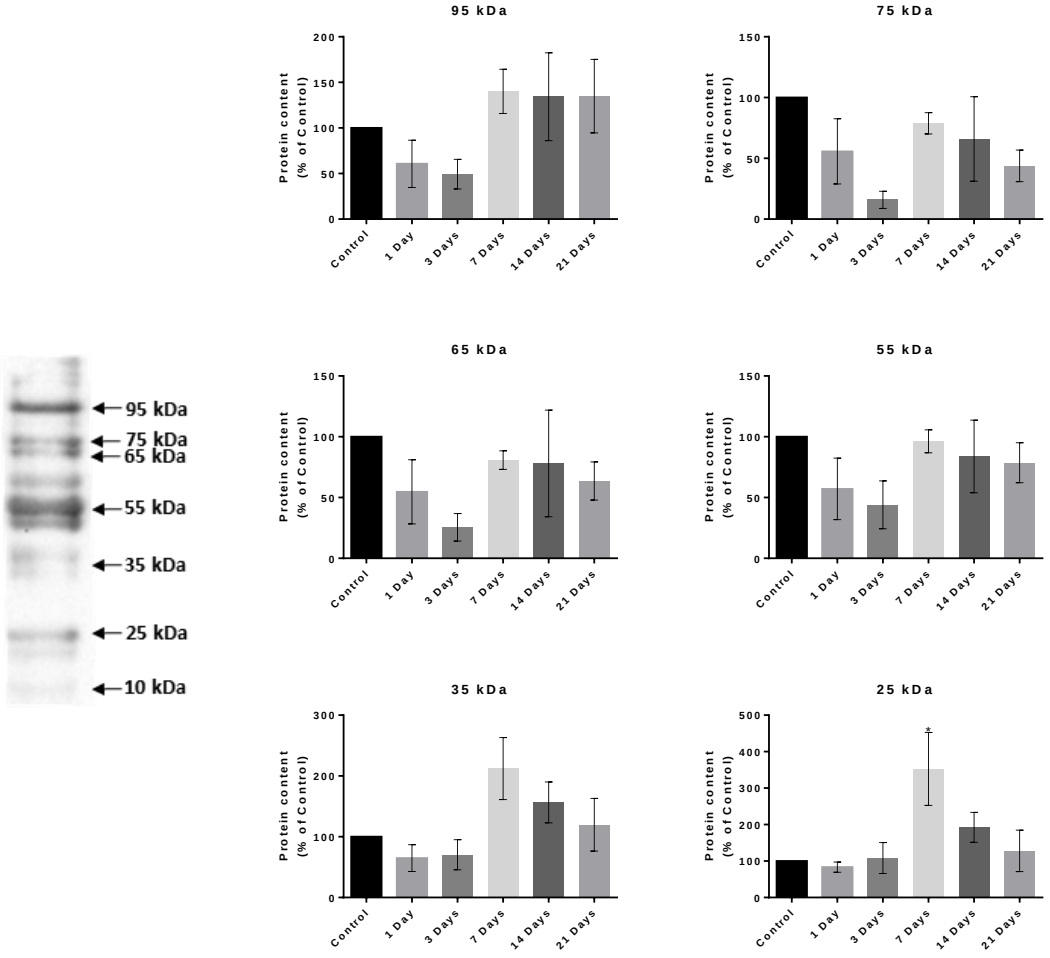

Figure 3.5. *Quantification of protein carbonyls by densitometric analysis of the protein bands at different molecular weights. A representative lane of an Oxyblot for control muscle showing the bands detected with approximate molecular weights indicated (kDa). Histograms represent the mean and standard error of the mean for each experimental group (n=4). * $p<0.05$ compared with the control group.*

3.3.6 Content of NADPH oxidase subunits in denervated muscle

The proteins analysed were: NOX2/gp91 phosphorylated (NOX2/gp91 phox - *Figure 3.6a*), p22 phosphorylated (p22phox - *Figure 3.6.b*), p40 phosphorylated (p40phox -, *Figure 3.6c*), p47 phosphorylated (p47phox - *Figure 3.6d*), p67 phosphorylated (p67phox - *Figure 3.6e*), Ras-related C3 botulinum toxin substrate 1 (Rac-1 - *Figure 3.6f*) and NADPH Oxidase 4 (NOX4 - *Figure 3.6g*). The protein content of all the NOX2 subunits was increased significantly after denervation. However, this increase differed in terms of timing and magnitude of change.

NOX2/gp91phox ($F(5,14)=10.309$, $p<0.01$), p22phox ($\chi^2(5)=17.486$ $p<0.001$) showed maximum protein content at 14 days post denervation. p47phox protein content reached a statistically significant value at 3 days post denervation ($F(5,15)=7.390$, $p<0.01$). p67phox protein content was increased at 14 days post denervation ($F(5,17)=15.595$, $p<0.01$) but changes were maintained significant up to 21 days after denervation. Rac-1 showed a statistically significant increase at 7 days ($F(5,16)=3.829$, $p<0.01$) post-denervation. Analysis of NOX4 protein content showed little change up to 14 days post-denervation, although a trend toward an increase was seen at 21 days that did not reach significance when compared with the control group.

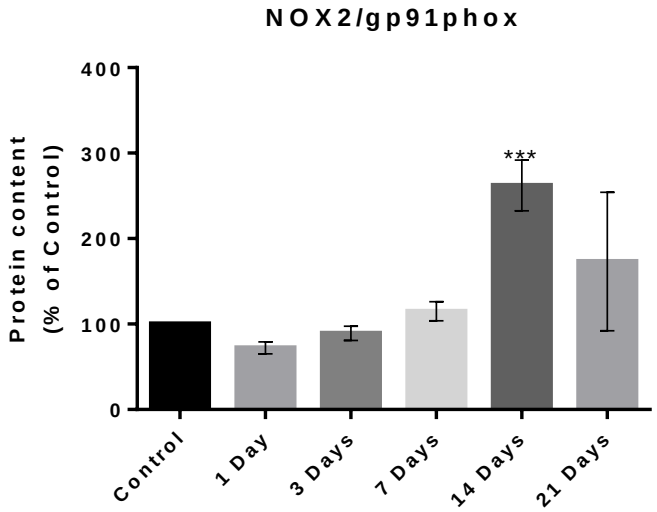

***Figure 3.6a**. Quantification of western blots of NOX2/gp91phox in Tibialis Anterior muscle from control mice (non-denervated) and mice at 1, 3, 7, 14 and 21 days post-denervation. Histograms represent the mean protein content and standard error of the mean for each experimental group (n=4).*
**** p<0.001 compared with the control group.*

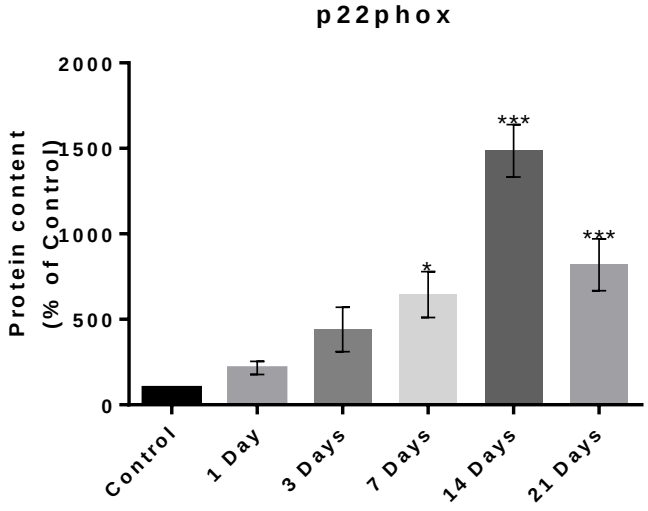

***Figure 3.6b**. Quantification of western blots of p22phox in Tibialis Anterior muscle from control mice (non-denervated) and mice at 1, 3, 7, 14 and 21 days post-denervation. Histograms represent the mean protein content and standard error of the mean for each experimental group (n=4).*
** p<0.05 - *** p<0.001 compared with the control group.*

***Figure 3.6c**. Representative western blots of p40phox in Tibialis Anterior muscle from control mice (non-denervated) and mice at 1, 3, 7, 14 and 21 days post-denervation. As shown in the figure the control group was not detectable when analysed together with the 14 and 21 days group making impossible to accurately quantify the relative content of this protein. Despite this it is clear the progressive increase in content of this protein observed from 7 days following denervation.*

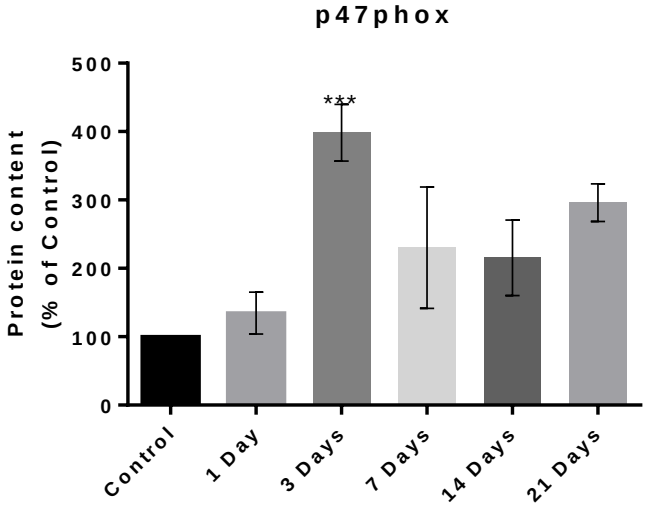

***Figure 3.6d**. Quantification of western blots of p47phox in Tibialis Anterior muscle from control mice (non-denervated) and mice at 1, 3, 7, 14 and 21 days post-denervation. Histograms represent the mean protein content and standard error of the mean for each experimental group (n=4).*
*** $p<0.001$ compared with the control group.

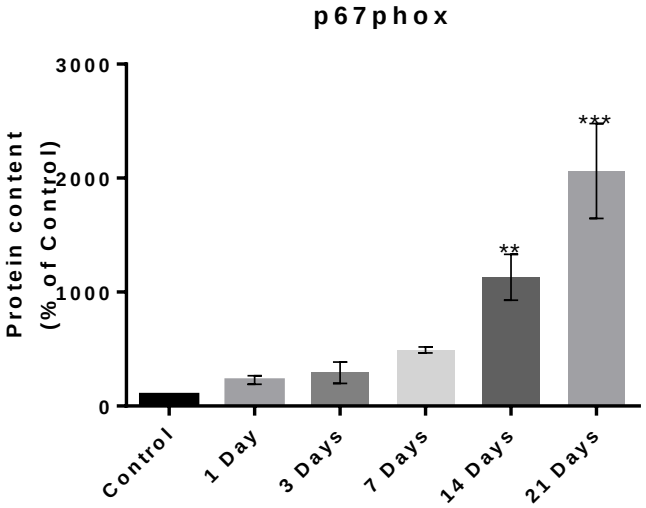

***Figure 3.6e**. Quantification of western blots of p67phox in Tibialis Anterior muscle from control mice (non-denervated) and mice at 1, 3, 7, 14 and 21 days post-denervation. Histograms represent the mean protein content and standard error of the mean for each experimental group (n=4).*
** p<0.01 - *** p<0.001 compared with the control group.

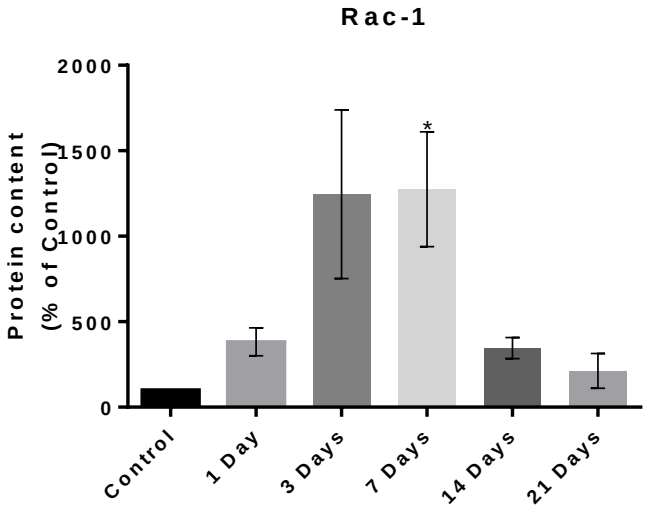

***Figure 3.6f**. Quantification of western blots of Rac-1 in Tibialis Anterior muscle from control mice (non-denervated) and mice at 1, 3, 7, 14 and 21 days post-denervation. Histograms represent the mean protein content and standard error of the mean for each experimental group (n=4).*
* p<0.05 compared with the control group.

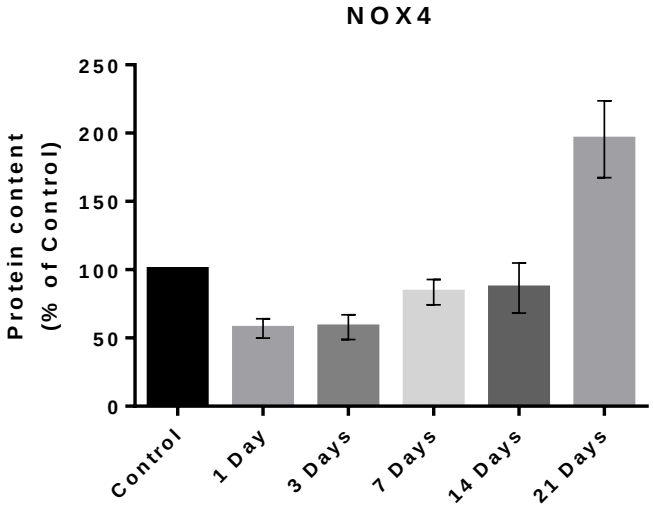

***Figure 3.6g**. Quantification of western blots of NOX4 in Tibialis Anterior muscle from control mice (non-denervated) and mice at 1, 3, 7, 14 and 21 days post-denervation. Histograms represent the mean protein content and standard error of the mean for each experimental group (n=4).*

3.3.7 Muscle protein content of Prx6, cPLA2 and Monoamine Oxidase A in denervated muscle

Prx6 was undetectable in the baseline (non-denervated) samples making impossible to accurately quantify the relative content of the protein at 14 and 21 days post-denervation. Therefore, example blots are presented (*Figure 3.7a*) where the significant increase of this protein is clear from 7 days following denervation.

Calcium-dependent PLA2 content is shown in *Figure 3.7b* and indicate a statistically significant increase at 14 days post-denervation ($F(5, 16)=98.569$, $p<0.01$) and a further increase up to 21 days compared with the control group.

Monoamine Oxidase A showed an increase in content in denervated muscle with a peak at 7 days post-denervation (*Figure 3.7c*) ($F(5, 16)=10.986$, $p<0.01$).

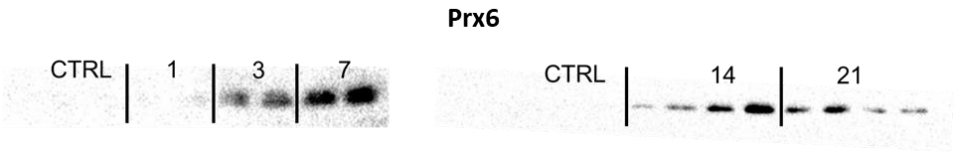

***Figure 3.7a**. Representative western blots of Prx6 in Tibialis Anterior muscle from control mice (non-denervated) and mice at 1, 3, 7, 14 and 21 days post-denervation.*

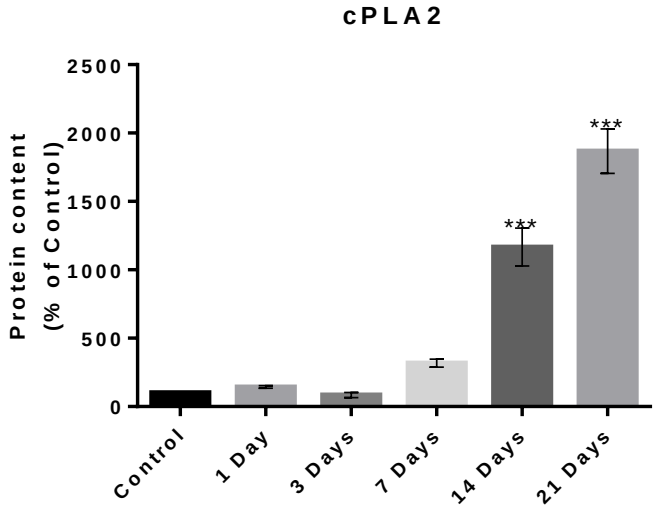

***Figure 3.7b**. Quantification of western blots of $cPLA_2$ in Tibialis Anterior muscle from control mice (non-denervated) and mice at 1, 3, 7, 14 and 21 days post-denervation. Histograms represent the mean protein content and standard error of the mean for each experimental group (n=4).*
**** $p<0.001$ compared with the control group.*

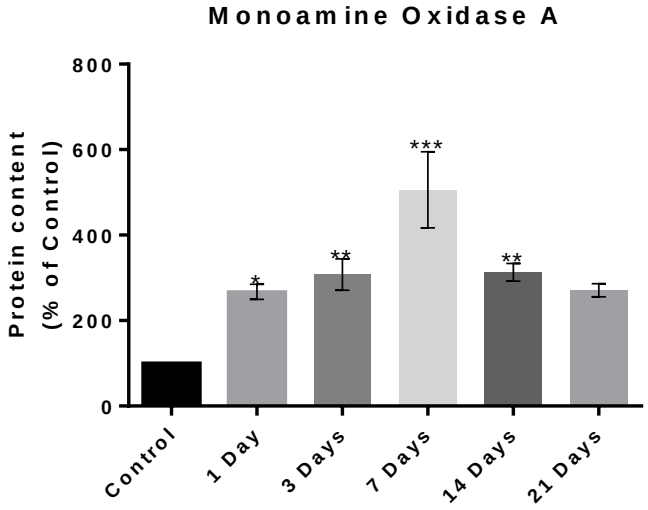

***Figure 3.7c**. Quantification of western blots of Monoamine Oxidase A in Tibialis Anterior muscle from control mice (non-denervated) and mice at 1, 3, 7, 14 and 21 days post-denervation. Histograms represent the mean protein content and standard error of the mean for each experimental group (n=4).*
* p<0.05 - ** p<0.01 - *** p<0.001 compared with the control group.

3.3.8 Muscle content of mitochondria-localised regulatory enzymes post-denervation

Three major mitochondrial antioxidants enzymes were analysed: Manganese Super-oxide Dismutase (MnSOD - *Figure 3.8a*), Thioredoxin Reductase 2 (TrxR2 - *Figure 3.8b*) and Glutathione Peroxidase 1 (GPx1 - *Figure 3.8c*).

MnSOD content in muscle did not change significantly following denervation ($F(5,15)=3.829$ $p>0.05$). In contrast, TrxR2 was statistically significantly increased at 3 and 7 days post denervation ($F(5,15)=10.899$ $p<0.01$). GPX1 content showed an increased protein content at 3, 7 and 21 days following denervation ($\chi^2(5)=17.210$ $p<0.01$).

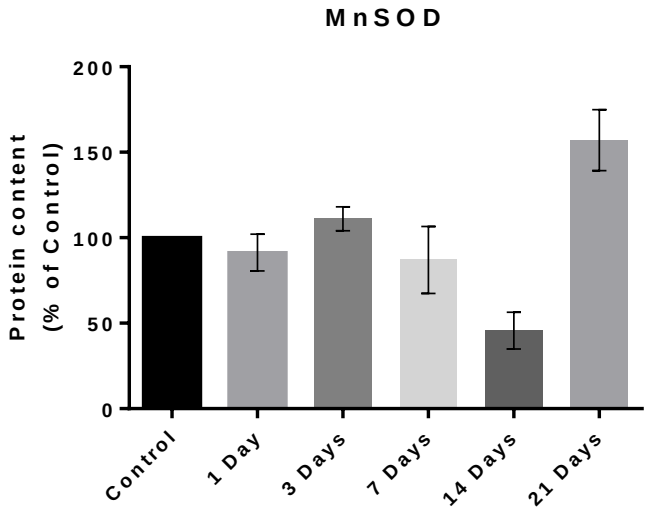

Figure 3.8a. *Quantification of western blots of MnSOD in Tibialis Anterior muscle from control mice (non-denervated) and mice at 1, 3, 7, 14 and 21 days post-denervation.*
Histograms represent the mean protein content and standard error of the mean for each experimental group (n=4).

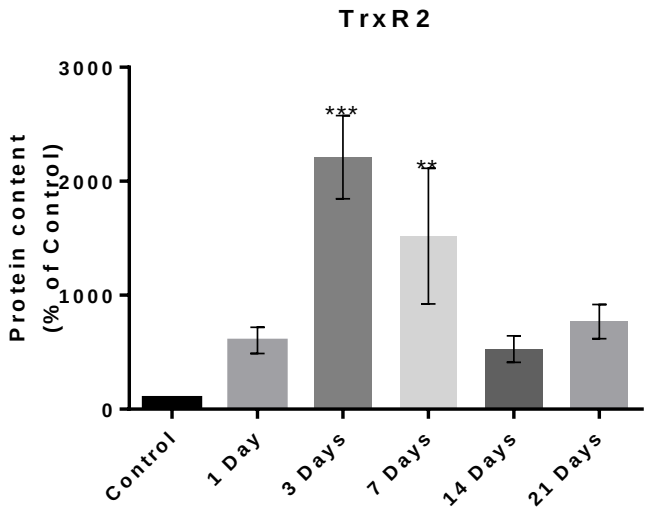

Figure 3.8b*. Quantification of western blots of TrxR2 in Tibialis Anterior muscle from control mice (non-denervated) and mice at 1, 3, 7, 14 and 21 days post-denervation. Histograms represent the mean protein content and standard error of the mean for each experimental group (n=4).*
*** p<0.01 - *** p<0.001 compared with the control group.*

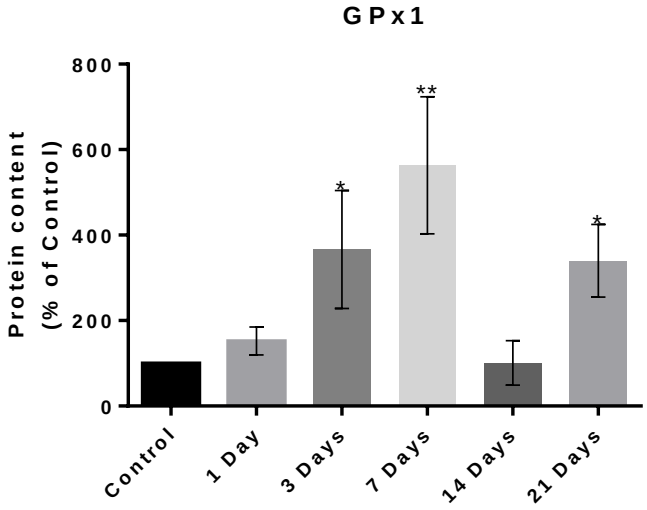

***Figure 3.8c**. Quantification of western blots of GPx1 in Tibialis Anterior muscle from control mice (non-denervated) and mice at 1, 3, 7, 14 and 21 days post-denervation.*
Histograms represent the mean protein content and standard error of the mean for each experimental group (n=4).
* $p<0.05$ - ** $p<0.01$ compared with the control group.

3.3.9 Heat Shock Proteins content of denervated muscle fibres

TA muscles from adult mice respond to denervation by a relatively slow increase in Hsp protein content. The Hsc70 content in denervated TA muscles was significantly increased at 14 and 21 days post-denervation ($F(5, 15)=16.073$ - *Figure 3.9a*). Hsp25 was significantly increased at 3, 7, 14 and 21 days following denervation ($F(5, 16)=147.142$, $p<0.01$ - *Figure 3.9b*). Hsp70 was barely detectable at basal levels (non-denervated) making impossible to perform relative quantification of the protein content at 14 and 21 days post-denervation. Therefore, only an example blot is presented (*Figure 3.9c*). However, in the representative blots presented in *Figure 3.9c*, it is clear that an increase of this protein occurs immediately following denervation which is maintained up to 21 days.

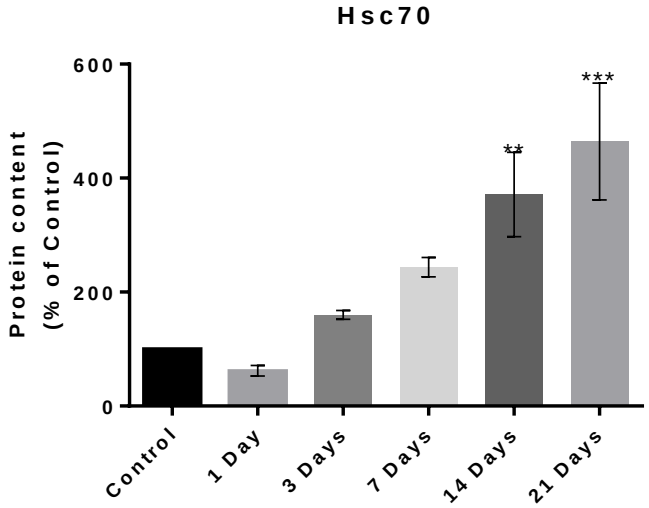

Figure 3.9a. *Quantification of western blots of Hsc70 in Tibialis Anterior muscle from control mice (non-denervated) and mice at 1, 3, 7, 14 and 21 days post-denervation.*
Histograms represent the mean protein content and standard error of the mean for each experimental group (n=4).
*** p<0.01 - *** p<0.001 compared with the control group.*

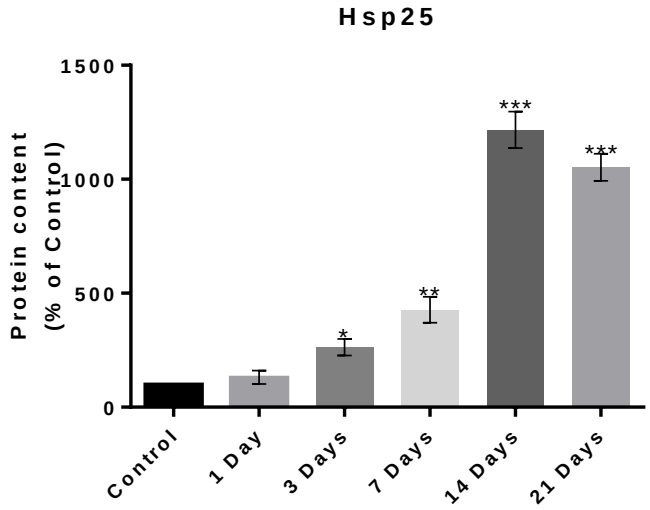

Figure 3.9b. *Quantification of western blots of Hsp25 in Tibialis Anterior muscle from control mice (non-denervated) and mice at 1, 3, 7, 14 and 21 days post-denervation.*
Histograms represent the mean protein content and standard error of the mean for each experimental group (n=4).
* p<0.05 - ** p<0.01 - *** p<0.001 compared with the control group.

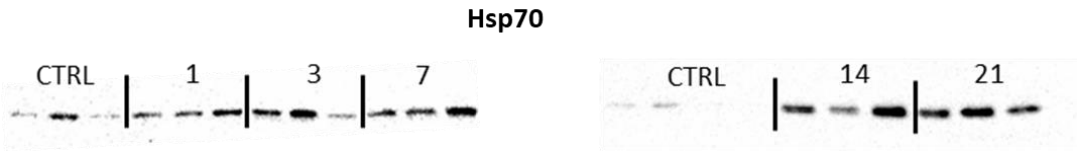

***Figure 3.9c**. Representative western blots of Hsp70 in Tibialis Anterior muscle from control mice (non-denervated) and mice at 1, 3, 7, 14 and 21 days post-denervation. As shown in the figure the control group was not detectable when analysed together with the 14 and 21 days group making relative quantification impossible.*

3.4 Discussion

It is well recognised that during ageing, alongside a significant loss of muscle mass, strength and power, there is a significant reduction of functional innervation of the skeletal muscles. Previous studies (Muller et al, 2007; Bhattacharya et al, 2009; Pollock et al, 2017) have investigated this phenomenon focusing their attention on the significant increase in peroxide release from mitochondria of denervated skeletal muscle fibres. During normal conditions, the ETC plays a central role in peroxide production and release; however other enzymes present within the mitochondria appear to play an important role in peroxide release in denervated muscle fibres (Pollock et al, 2017).

In the present study, compared with previous works, we extended the time course of denervation up to 21 days to examine the long-term effects of peroxide release on those proteins that regulate redox homeostasis in muscle. To investigate the changes in peroxide release from denervated skeletal muscle fibres, we used a surgical procedure aimed at inducing full denervation on the TA and EDL muscles. *Figure 3.2b* shows the effectiveness of this denervation protocol in inducing a progressive loss of innervation from day 1 and full denervation between 3 and 7 days when traces of the nerve are not visible anymore. Furthermore, between 7 and 21 days the ACh receptors in denervated muscle fibres started to progressively breakdown. This loss of pre-synaptic axonal input translates in a significant loss of muscle mass starting at 7 days following denervation which continues up to 21 days. Our results show that this loss of muscle mass was not due to a loss of muscle fibres but rather due to a significant muscle fibre atrophy. As shown in *Figure 3.2a*, a significant decrease in the number of large muscle fibres occurred following denervation accompanied by a significant increase of medium/small muscle fibres.

Previous work from our group (Pollock et al, 2017) demonstrated an increase in mitochondrial peroxide release at 7 days following denervation and addition of substrates and inhibitors of the ETC excluded the possibility that the increase in peroxide release resulted from the ETC activity (*result not shown in detail*). Our results showed that other enzymes such as the two isoforms of Monoamine oxidase (Monoamine oxidase A and Monoamine oxidase B), NADPH Oxidase and PLA2 may play a fundamental role in peroxide release (*Figure 3.3b*).

Monoamine oxidase A and B share 70% of their sequences but present different substrate specificity (Duicu et al, 2016). Both isoforms are expressed in skeletal muscle and are normally located on the mitochondrial outer membrane (Billet, 2004; Manoli et al, 2005) where they play an important function in regulating neurotransmitter levels and in degrading amines that could function as false neurotransmitters (Cadenas and Davies, 2000). The addition of Chlorgyline (inhibitor of monoamine oxidase A) and Pargyline (inhibitor of Monoamine oxidase B) reduced the oxidation of Amplex red at 7, 14 and 21 days following denervation. In addition, while we failed to detect significant changes in Monoamine oxidase B content (*result not shown in detail*), we saw a significant increase of Monoamine oxidase A content at 7 days following denervation.

In line with previous studies (Bhattacharya et al, 2009; Pollock et al, 2017), we showed a significant reduction of the Amplex Red signal following the addition of Apocynin (*Figure 3.3b*) suggesting a primary role played by NOX enzymes in the mitochondrial peroxide release following denervation. Given its subcellular localisation, NOX4 could likely be an important contributor to mitochondrial peroxide release following denervation but our analysis of NOX4 content showed no significant changes throughout the time course. However, as the focus of the present work was to analyse NOX4

protein content and not activity, we cannot exclude the possibility that NOX4 activity is altered in response to denervation.

Bhattacharya and colleagues (2009) suggested that mitochondria of denervated muscle fibres can also release lipid peroxide via PLA2 activity in addition to H_2O_2. Lipid peroxidation is a process that results in the deterioration of phospholipids via free-radical propagated chain reactions leading to the formation of lipid radicals, lipid peroxyl radicals and lipid peroxides (Ayala et al, 2014). PLA2 generates arachidonic acid that, interacting with different phospholipids that compose the mitochondrial membrane, is able to produce large amounts of lipid peroxides (Balsinde et al, 2002). Our results suggested that PLA2 is also responsible for the significant increase in peroxide release in denervated skeletal muscle. In the present study, the addition of AACOCF3 (PLA2 inhibitor used in the present work – Figure 3.3b) to the Amplex Red assay resulted in the most significant drop in peroxide release suggesting that this enzyme plays a fundamental role in mitochondria of denervated muscle fibres. Furthermore we also saw a significant increase in protein content of the cytosolic isoform of this enzyme (cPLA2) which is able to stimulate the assembly and activation of NOX2 in the cytosol. Indeed, the arachidonic acid produced by cPLA2 is used by MAPK to induce phosphorylation of p40, p47 and p67 (3 important components of NOX2) allowing their translocation to the membrane (Chatterjee et al, 2011).

NOX2 is a multimeric enzyme found mainly in the cytosol that catalyses the conversion of O_2 to superoxide (Groemping and Rittinger, 2005; Ferreira and Laitano, 2016). This enzyme requires that its isoforms translocate to the membrane where this complex is assembled. Five different subunits compose this enzyme: p22phox and NOX2/gp91phox are membrane-bound while p40phox, p47phox and p67phox translocate to the membrane following activation through phosphorylation. In the present study we demonstrated that

there is a significant increase in the content of NOX2/gp91phox and p22phox 14 days following denervation, together with p67phox and p40phox (Figures 3.6a-e). Our data also showed that the protein contents of p47phox and Rac1 are significantly increased between 3 to 7 days post-denervation. Phosphorylation of p47 and activation of Rac1 have previously been reported in skeletal muscle with these post-translational events leading to the activation of NOX2 (Ferreira and Laitano, 2016).

The activation of this enzyme results in a significant production of superoxide in the extracellular space that, once converted onto H_2O_2 is able to translocate back into the muscle fibre where it plays different fundamental physiological roles. For instance, H_2O_2 generated by NOX2 plays an important role during muscle contraction (Ward et al, 2014) but is also able to interact with the angiotensin II system inducing insulin resistance or activating atrophy pathways involving the Proteasome 26S (Ferreira and Laitano, 2016). Furthermore, it has been suggested that, following denervation, the H_2O_2 produced by NOX2 may function as a signal aimed at stimulating and directing nerve sprouting in the attempt of restoring the connection between the ACh receptors and a motor neuron (Pollock et al, 2017). Despite the fact that we can only speculate about the physiological role played by the H_2O_2 produced by NOX2 in denervated skeletal muscle, the significant muscle atrophy observed could be explained by the activation of the ubiquitin proteasome pathway by the activity of NOX2.

Another interest of this study was to determine the response of Prx6 following denervation as this atypical 1-Cys Prx can function either as antioxidant or as phospholipase (Fisher et al, 2011; Brandes et al, 2014). Prx6 is mainly a cytosolic enzyme but can translocate to the mitochondria where it binds and reduces phospholipid hydroperoxides (Eismann et al, 2009). Once in the mitochondrion, Prx6 can become over-oxidised and undergo

conformational changes that allow this protein to acquire PLA2 activity (Fisher et al, 2011) producing arachidonic acid and lipid peroxides itself (Chatterjee et al, 2011).

The protein content of Prx6 was undetectable in control samples but was increased from 3 days following denervation. Our data suggest that in response to denervation Prx6 translocates to the mitochondria where it may get over-oxidised starting to contribute to the peroxides release and the activation of NOX2 via the Prx6-PLA2-mediated signalling pathway (Chatterje et al, 2011).

A further objective of this study was to examine the response of the mitochondrial antioxidant system following the increase in peroxide release in denervated muscle fibres. The contents of 3 major mitochondrial antioxidant enzymes: MnSOD, TrxR2 and GPx1 were analysed. While the content of MnSOD did not change following denervation, both TrxR2 and GPx1 contents were significantly increased at 3 and 7 days (*Figure 3.8b* and *Figure 3.8c*). TrxR2, the mitochondrial isoform of thioredoxin reductase, catalyses the NADPH-dependent reduction of thioredoxin (Patenaude et al, 2004). As GPx1 acts to prevent the harmful accumulation of H_2O_2 (Lubos et al, 2011), the initial response observed may reflect an adaptive response following the disruption of the NMJ in an attempt to maintain redox homeostasis in the muscle. Nevertheless, the increase content of Hsp proteins over long term suggests a disturbance of the redox homeostasis with significant increase in oxidative stress and protein degradation.

It has previously been shown that exposure to elevated levels of H_2O_2 appears to promote protein degradation in skeletal muscle via the ubiquitin-proteasome pathway (Powers et al, 2011). An increase in H_2O_2 can induce activation of redox-sensitive genes that code for ubiquitin and regulatory E2 and E3 proteins; upregulation of these genes increases the rate of ubiquitin conjugation within skeletal muscle that accelerates the targeting of muscle proteins for degradation by the 26S proteasome (Li et al, 2003).

In this context Hsp70 is critical in maintaining terminally misfolded proteins in a soluble state for ubiquitin conjugation and proteasomal degradation (Shiber et al, 2013). In this denervation model, the Hsp70 content was increased following denervation and remained increased up to 21 days (*Figure 3.9c*) suggesting that Hsp70 may play a role in protein homeostasis in the denervated muscle fibres. Prolonged denervation also resulted in an increased content of Hsc70 (*Figure 3.9a*) which plays an important role during chaperone-mediated autophagy (CMA). Once Hsc70 recognises and binds a targeted protein, it makes the protein available to the lysosome-associated membrane protein 2 (LAMP-2A) that unfold and translocate the proteins into the lysosomal lumen for degradation (Cuervo and Wong, 2014; Zhou et al, 2017; Kaushik and Cuervo, 2015). CMA operates at basal conditions in most mammalian cells, but it is activated in response to stressors, such as oxidative stress (Xilouri and Stefanis, 2016). LAMP-2A was not measured in the current study but we speculate that the increased content of Hsc70 is linked to CMA although further studies are required to identify the precise mechanisms involved.

Finally, we observed that the muscle Hsp25 content was also significantly increased from 3 days following denervation and remained increased until 21 days (*Figure 3.9b*). Previously it has been demonstrated that overexpression of Hsp25 in skeletal muscle cells resulted in dose-dependent protection against H_2O_2-induced damage that was associated with increased GSH levels and GPx1 activity (Escobedo et al, 2004). In our analysis there was no change in GSH concentration following denervation but a significant increase in Gpx1 content that is maintained up to 21 days. These data suggest that following denervation Hsp25 and Gpx1 may play a synergetic role in response to the increase of peroxide release from mitochondria. To our knowledge, no other studies have investigated eventual changes of GSH or GSSG levels in denervated

muscles. However, a previous study from Agostini and colleagues (2010) analysed changes in GSH levels using Gas chromatography–mass spectrometry finding that during muscle atrophy GSH content increases in response to an increase of ROS accumulation.

In the present study, the lack of changes in GSH and GSSG levels may be related to a lack of sensitivity of the assay used. In future studies aimed to analyse the glutathione response in denervated fibres the use of relatively new and more reliable techniques such as Gas chromatography–mass spectrometry can potentially shed new light over the effects of denervation on GSH and GSSG levels.

The carbonyl content of muscle soluble proteins following denervation was examined to verify whether the increased peroxide release resulted in significant changes in protein oxidation (*Figure 3.5*). Despite the high variability recorded, analysis of the bands at different molecular weights showed significant changes in the proteins around 25 kDa, with a maximum increase around 7 days, which coincided with the maximal increase in peroxide release. Carbonylation is the most common type of alteration seen during oxidative stress where a carbonyl group is introduced into proteins by a metal-catalysed oxidation of specific amino acids or indirectly by the reaction with species derived from lipid peroxidation (Lyons and Jenkins, 1997). The increased carbonylation seen at 7 days reinforce the possibility that over long term the denervation-induced release in peroxide leads to oxidative stress.

Overall, our data suggest that following denervation, there is a significant increase in peroxide release that is maintained up to 21 days. This increase is associated with changes in content of Prx6 and the cytosolic isoform of PLA2 which, as suggested, play a primary role in NADPH oxidase 2 activation. The initial increase in the antioxidant enzymes TrxR2 and GPx1 content and the later increase in Hsps content suggests a

possible initial protection within the muscle bulk; however, long term exposure to peroxides together with the activation of cPLA2 and NOX2 is likely to activate degenerative processes and trigger muscle atrophy.

Chapter 4. Mitochondrial status following skeletal muscle denervation

4.1 Introduction

Mitochondria, known as "*the power generators of the cell*", are rod-shaped organelles that play a pivotal role in cellular metabolism as they host important respiratory steps such as the citric acid cycle, β-Oxidation, oxidative phosphorylation while are also involved in calcium handling and heme biosynthesis (Mishra and Chan, 2016).

Mitochondria perform these functions using nutrients such as glucose and through a series of chemical reactions in which components such as NADPH and O_2 are used to generate ATP. The number of mitochondria in a cell depends on the metabolic requirements of that cell; indeed, the higher the mitochondria number, the higher is the amount of energy that can be produced (Mishra and Chan, 2016). Muscle fibres present a significantly high mitochondria density that varies according to fibre type. For example, the mitochondrial density in heart muscle cells is approximately 40% of total cell volume whereas slow twitch skeletal muscle fibres (Type I) present a density of 8-12% (which can increase up to 19% in highly trained endurance athletes); the percentage decreases in Type IIa (Intermediate fibres) with a density that variates between 5 to 10% with a further decrease to 2% in Type IIx muscle fibres of highly trained strength athletes (Ortenblad et al, 2018).

Maintaining skeletal muscle mitochondrial functions as well as content is important for sustained health throughout the lifespan. During ageing there is a significant reduction in mitochondria number accompanied by changes in ultrastructure and localisation. For instance, mitochondria in muscle fibres from older individuals show a more rounded appearance with vacuoles within the matrix and a shorter cristae when compared with mitochondria from muscles of younger subjects (Seo et al, 2016). These modifications are associated with impaired mitochondria metabolism, ATP production rate, protein synthesis and increased ROS production (Seo et al, 2016). In addition, with

age there is a significantly lower rate of mitochondrial biogenesis with reduced transcriptional regulation that results in significant alterations of cell homeostasis (Baker and Haynes, 2011). The increased production of ROS by impaired mitochondria has a significant impact on the redox homeostasis of skeletal muscle resulting in a greater oxidative damage to DNA, lipids and proteins (Nabben et al, 2011) with all these modifications associated with muscle wasting (Seo et al, 2016).

Mitochondria are dynamic organelles as their turnover and morphology continually changes through the cell life cycle, changes that are driven by the combined action of fission, fusion and motility (Youle and van der Bliek, 2012). Cells are able to modify their number of mitochondria according to the physiological stimuli through a complex and well-coordinated process known as mitochondrial biogenesis. This process provides the cell with adequate mitochondrial turnover and adaptation to physiological stresses through growth and division of pre-existing mitochondria (Elguero et al, 2012).

Another important process that plays a major role in maintaining a healthy pool of mitochondria is mitophagy. This phenomenon was firstly observed in 1962 by Ashford and Porter and describes the fission of damaged and superfluous mitochondria that are recycled by fusion with healthy mitochondria providing constant quality control and recycle of the mitochondria population (Youle and van der Bliek, 2012). As suggested by Palikaras and colleagues (2015), healthy cells have a correct balance between mitophagy and mitochondrial biogenesis. Imbalance, in either direction, can have a significant impact on mitochondria number, health and efficiency.

Changes in the number and functionality of the mitochondria population has a severe impact on the survival of the cells and impairment of the mitochondria population is reported to be responsible of the initiation of sarcopenia (Alway et al, 2017).

In the previous chapter we described a significant increase in peroxide release from mitochondria of denervated skeletal muscle fibres that may trigger atrophy; however, the impact that this increase in peroxide release has on the functionality and stability of mitochondria is still unclear. In the current chapter the effects of skeletal muscle denervation on mitophagy, activation of apoptosis and mitochondrial number and quality were examined.

4.2 Materials and Methods

4.2.1 Mouse model

Twelve wild type male C57BL/6 adult mice (8 to 10 months old) were purchased from The Charles Rivers Laboratory (Bar Harbor, ME, USA) and kept in the Biomedical Service Unit (BSU) facilities in accordance with the UK Home Office guidelines under the UK Animals (Scientific Procedures) Act 1986.

4.2.2 Surgical denervation of the lower hind-limb

Eight mice underwent a surgical procedure to remove a small section of the sciatic nerve to induce denervation (section 2.2). Mice were sacrificed 7 and 21 days following denervation by cervical dislocation and muscles from both legs were collected and prepared for further analysis.

4.2.3 SDS-PAGE western Blot analysis

For each analysis, 30µg of total protein from the TA muscle were added to 4µl of Blu-mercaptoethanol (4x) and ddH_2O to a final volume of 16µL. SDS-PAGE/Western Blot analysis was performed as previously described in section 2.5. Different primary antibodies (*Table 2.3* for further details) were detected using near-infrared fluorescent IRDye secondary antibodies (Licor, Bad Homburg, Germany) and the membranes analysed on the Licory Odissey CLx (Licor, Bad Homburg, Germany).

4.2.7 Citrate synthase assay

This experiment was performed using the kit purchased from Cayman Scientific (Ann Arbor, MI, USA). An equal amount of proteins from the soleus muscle was diluted 1:50 in the Buffer Assay provided with the kit and treated as presented in section 2.15.

4.2.8 Mitochondria membrane potential analysis

Mitochondrial membrane potential was assessed in the EDL using TMRM as previously described in section 2.13. Images were collected using an inverted confocal microscope (Nikon, Kensington, UK) and changes in fluorescence overtime were analysed using the NIS-Elements imaging software (Nikon, Kensington, UK).

4.3 Results

4.3.1 Anthropometric measurements

No significant differences in total body weight were seen between the groups (*Figure 4.1a*). The Tibialis Anterior muscle showed a significant reduction in weight at 7 days following denervation progressing up to 21 days, $F(2,9)= 17.765$ $p<0.01$ (*Figure 4.1b*). The EDL showed a significant reduction in weight at 21 days following denervation $F(2,9)= 6.909$ $p<0.05$ (*Figure 4.1c*) while the soleus muscles $F(2,9)= 6.412$ $p<0.05$ show a significant reduction in muscle mass at 7 and 21 days following denervation (*Figure 4.1d*).

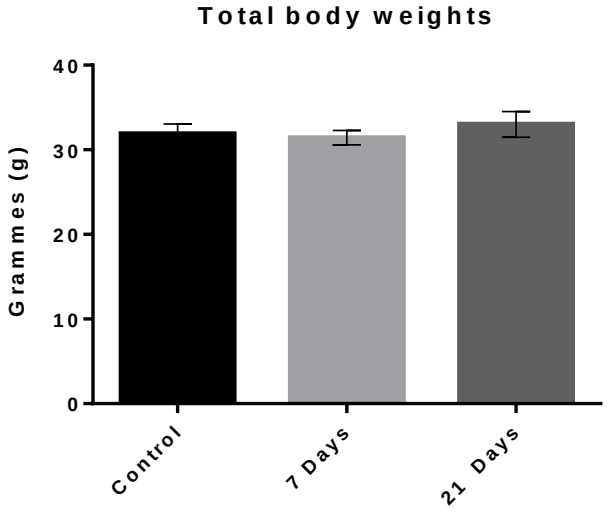

Figure 4.1a. *Total body weights from control mice (non-denervated) and mice at 7 and 21 days post-denervation. Histograms represent the mean and the standard error of the mean for each experimental group (n=4).*

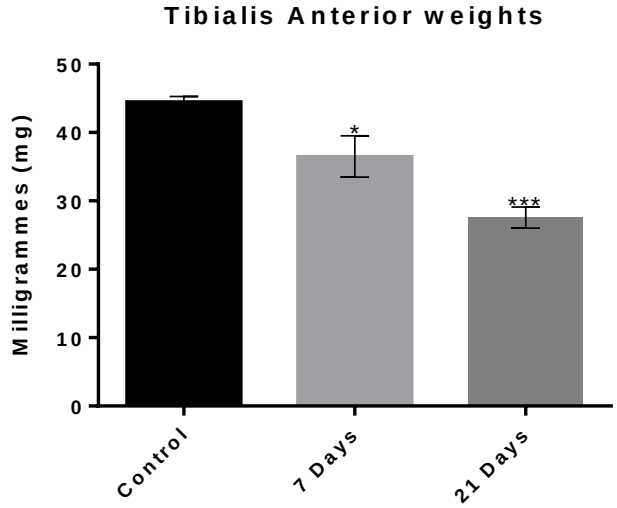

Figure 4.1b. *Tibialis Anterior muscle weights from control mice (non-denervated) and mice at 7 and 21 days post-denervation. Histograms represent the mean and the standard error of the mean for each experimental group (n=4).*
** p<0.05 -*** p<0.001 compared with the control group.*

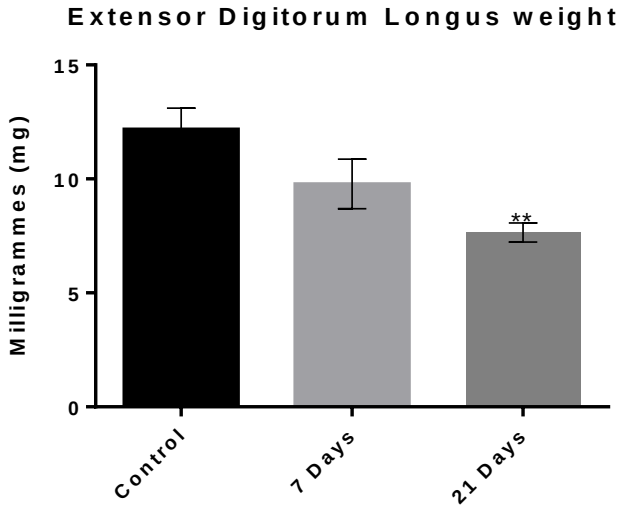

Figure 4.1c. *Extensor Digitorum Longus muscle weights from control mice (non-denervated) and mice at 7 and 21 days post-denervation. Histograms represent the mean and the standard error of the mean for each experimental group (n=4).*
*** p<0.01 compared with the control group.*

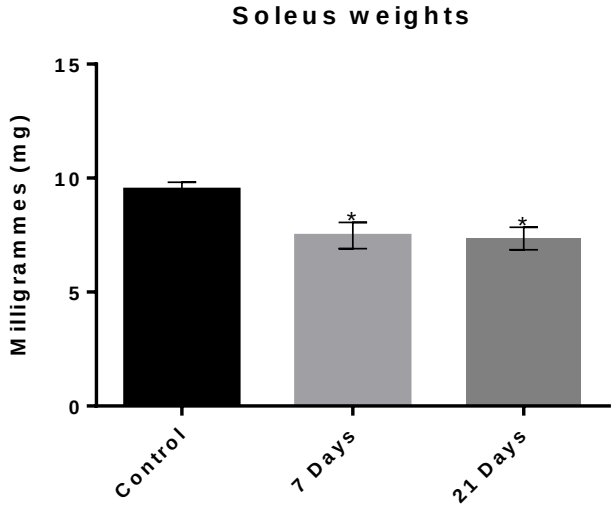

Figure 4.1d. *Soleus muscle weights from control mice (non-denervated) and mice at 7 and 21 days post-denervation. Histograms represent the mean and the standard error of the mean for each experimental group (n=4).*
** p<0.05 compared with the control group.*

4.3.2 Mitophagy markers

Specific proteins involved in the mitophagy process were analysed through SDS-PAGE western blot. The ratio of phosphorylated Dinamin-like Protein 1 (pDrp1)/Dinamin-like Protein 1 (Drp1) showed a significant increase at 7 and 21 days compared with the control group $F(2,9)=16.001$ $p<0.05$ (*Figure 4.2a*). Analysis of Optic Atrophy 1 (OPA1) showed no significant differences between the 3 groups (*Figure 4.2b*). Similarly, analysis of Mitofusin 2 (Mfn-2) showed no significant changes following denervation (*Figure 4.2c*). Analysis of p62 $F(2,9)=13.722$ $p<0.05$ instead revealed a significant increase in the content of this protein in skeletal muscle at 7 and 21 days following denervation (*Figure 4.2d*).

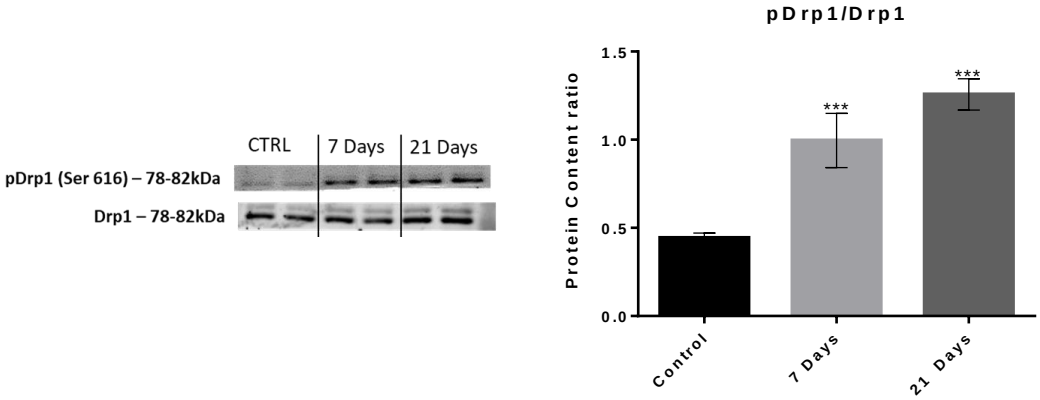

Figure 4.2a. *Representative western blot and quantification of the ratio between phosphorylated Drp1 and Drp1 protein content used as a marker of mitochondria fission in Tibialis Anterior muscle from Control (non-denervated) and mice at 7 and 21 days post-denervation. Histograms represent the mean protein content and standard error of the mean for each experimental group (n=4).*
**** p<0.001 compared with the control group.*

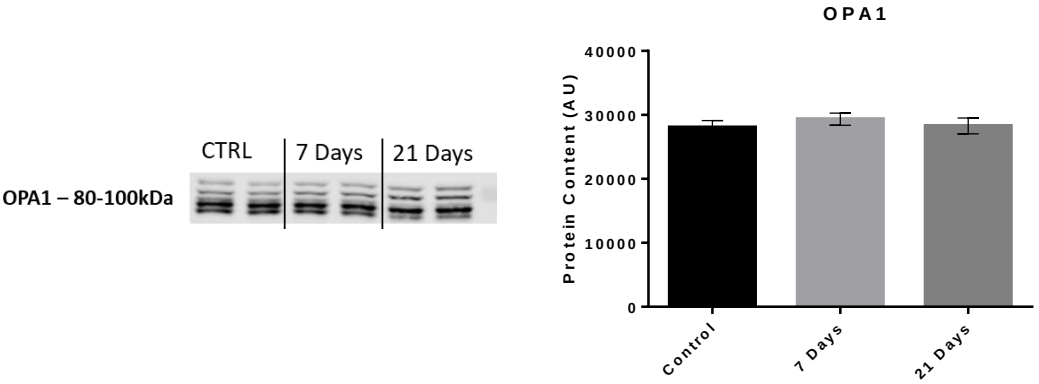

Figure 4.2b. *Representative western blot and quantification of OPA1 protein content used as a marker of mitochondria fusion in Tibialis Anterior muscle from Control (non-denervated) and mice 7 and 21 days post-denervation. Histograms represent the mean protein content and standard error of the mean for each experimental group (n=4).*

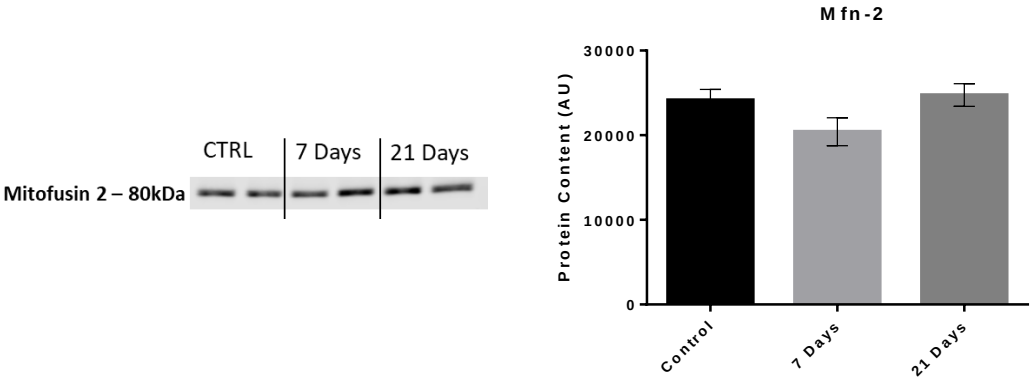

Figure 4.2c. *Representative western blot and quantification of Mfn-2 protein content used as a marker of mitochondria fusion in Tibialis Anterior muscle from Control (non-denervated) and mice 7 and 21 days post-denervation. Histograms represent the mean protein content and standard error of the mean for each experimental group (n=4).*

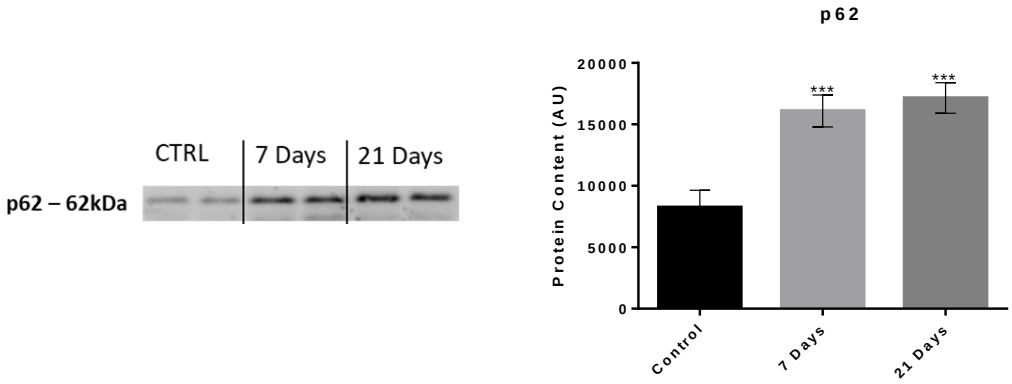

Figure 4.2d. *Representative western blot and quantification of p62 protein content used as a marker mitophagy in Tibialis Anterior muscle from Control (non-denervated) and mice 7 and 21 days post-denervation. Histograms represent the mean protein content and standard error of the mean for each experimental group (n=4). *** $p<0.001$ compared with the control group.*

4.3.3 Apoptosis pathway activation

The ratio between Bcl-2-associated X protein (BAX) and B-cell lymphoma 2 (Bcl-2) increased following denervation at both 7 and 21 days reaching significance only at 21 days $F(2,9)=11.210$ $p<0.05$ (*Figure 4.3a*). Caspase-3 content was significantly increased 7 and 21 days following denervation $F(2,9)=132.152$ $p<0.05$ (*Figure 4.3b*). Similarly, cleaved caspase-3 was also significantly increased 7 days and 21 days following denervation $F(2,9)=4.928$ $p<0.05$ (*Figure 4.3c*).

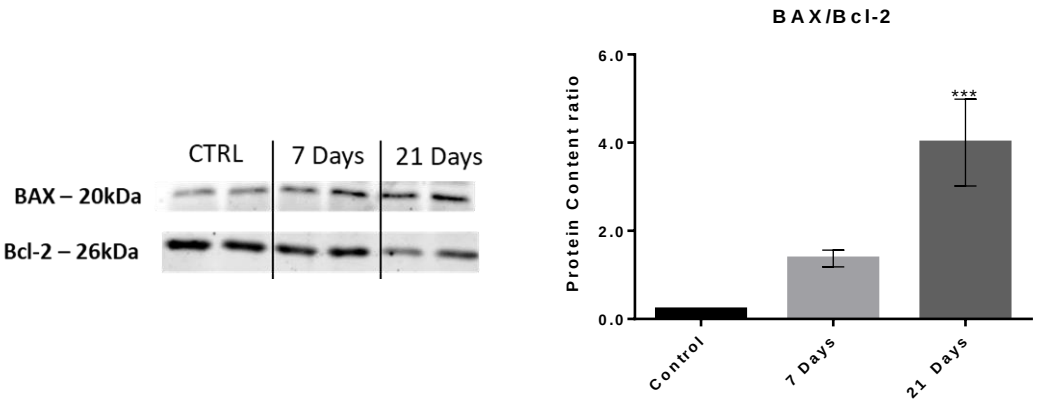

Figure 4.3a. *Representative western blot and quantification of the ratio between BAX and Bcl-2 proteins content used as a marker of activation of apoptosis in Tibialis Anterior muscle from Control (non-denervated) and mice 7 and 21 days post-denervation. Histograms represent the mean protein content and standard error of the mean for each experimental group (n=4).*
**** p<0.001 compared with the control group.*

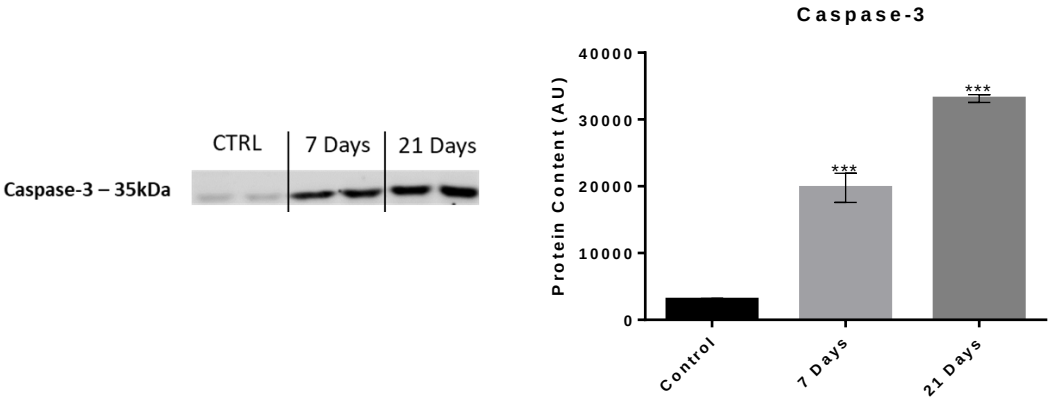

Figure 4.3b. *Representative western blot and quantification of caspase-3 protein content used as a marker of activation of apoptosis in Tibialis Anterior muscle from Control (non-denervated) and mice 7 and 21 days post-denervation. Histograms represent the mean protein content and standard error of the mean for each experimental group (n=4).*
**** p<0.001 compared with the control group.*

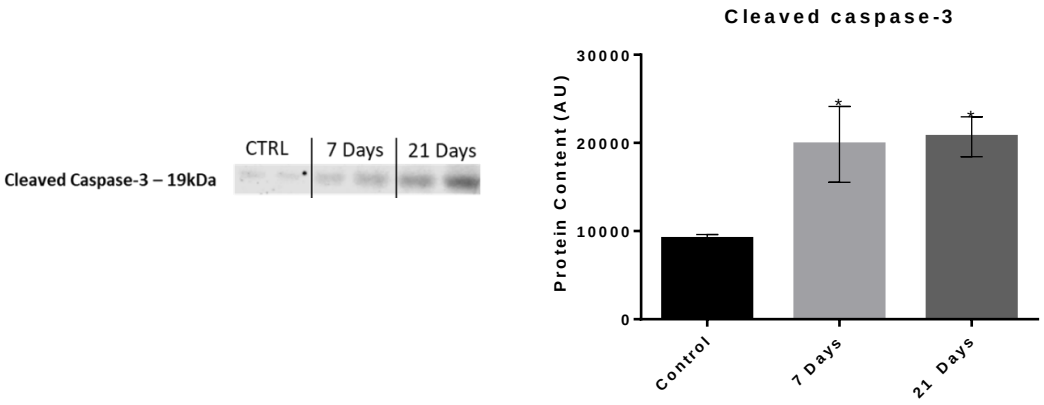

Figure 4.3c. *Representative western blot and quantification of cleaved caspase-3 protein content used as a marker of activation of caspase-3 and apoptosis in Tibialis Anterior muscle from Control (non-denervated) and mice 7 and 21 days post-denervation. Histograms represent the mean protein content and standard error of the mean for each experimental group (n=4).*
** p<0.05 compared with the control group.*

4.3.4 Mitochondria content

The citrate synthase assay showed a trend to a decrease activity reflecting a decrease in mitochondria content already at 7 days following denervation but the decrease in content became statistically significant at 21 days following denervation $F(2,9)=7.924$ $p<0.05$ (*Figure 4.4*).

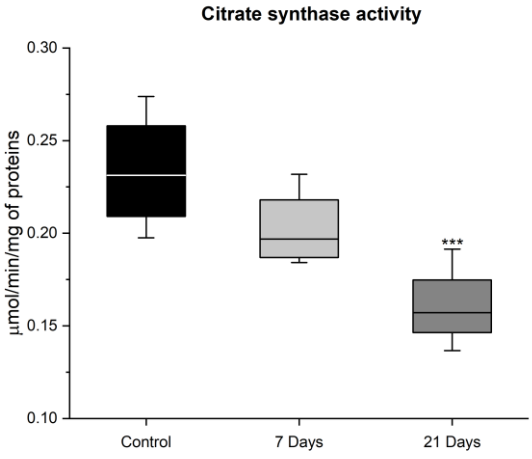

Figure 4.4. *Citrate synthase activity expressed as mean µM/min/proteins and standard error of the mean for each experimental group (n=4). The assays were performed in duplicate for each sample. Histograms represent the mean activity and standard error of the mean for each experimental group (n=4).*
**** p<0.001 compared with the control group.*

4.3.5 Mitochondrial membrane potential

The fluorescent signal generated by TMRM was recorded and plotted against time. Data are shown in *Figure 4.5a* together with 2 representative images showing an isolated muscle fibre in bright-field and the fluorescent image of the same fibre following loading of TMRM (*Figure 4.5b*). The analysis showed a very high variability and fluctuation of the fluorescent signal with no significant differences between groups (*Figure 4.5a*). Due to this variability it was decided to not proceed with further analysis.

A

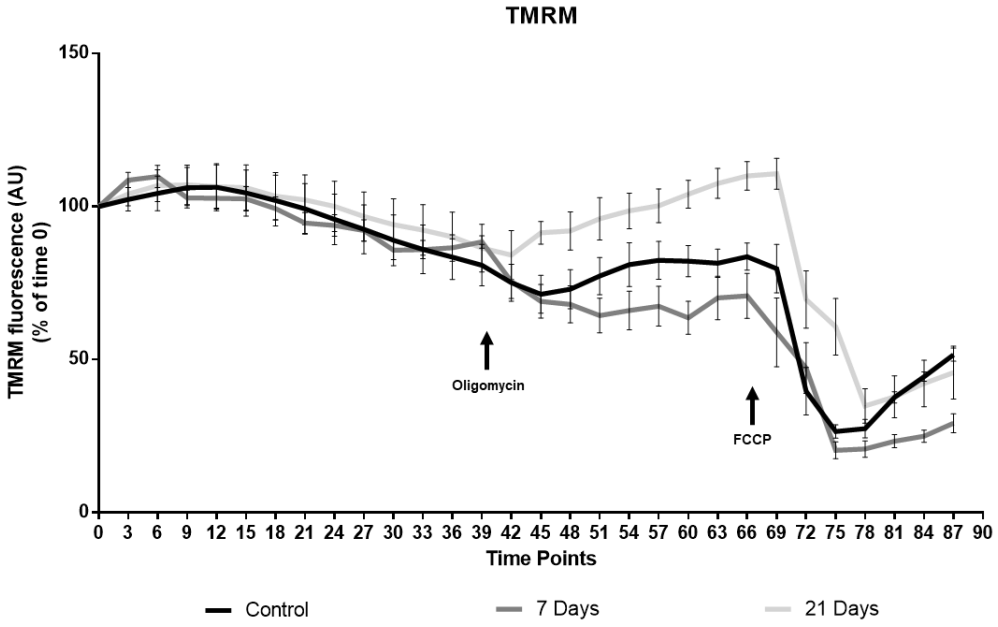

B

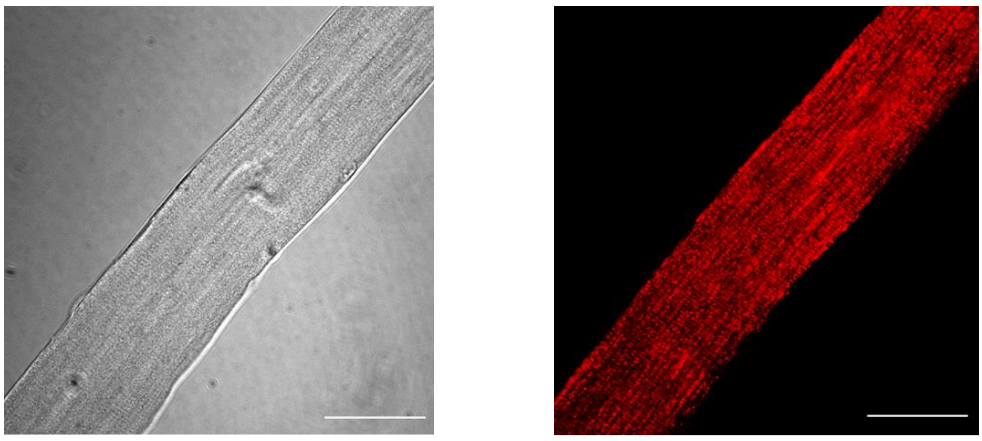

Figure 4.5. A) *Measurement of ΔΨm in intact mitochondria of isolated EDL muscle fibres from control (non-denervated) and mice at 7 and 21 post-denervation, assessed by changes in TMRM (30nM) fluorescence in response to oligomycin (Olm, 2.5 μM) and FCCP (4 μM), added at the indicated time points.* ***B)*** *Representative images of an isolated muscle fibres in bright-field and fluorescent image following loading with TMRM (scale bar 50μm).*

4.4 Discussion

Mitochondria play fundamental roles within eukaryotic cells including: production of ATP, calcium handling, regulation of cell growth, cell death and cell signalling through the generation of ROS in response to alterations in cell homeostasis (Brand et al, 2013). Given the important roles played, the maintenance of a healthy pool of mitochondria is fundamental to the survival of the cell and mitochondrial abnormalities have been associated with several muscle wasting conditions such as sarcopenia, cachexia and muscular dystrophies (Vainshtein et al, 2015). A correct mitochondrial turnover is vital in the process of maintaining a healthy pool of mitochondria and it is usually controlled by a dynamic and tightly regulated process known as mitophagy (Stotland and Gottilieb, 2015).

Previous studies (Spendiff et al, 2016; Sonjak et al, 2019) have reported that denervated skeletal muscle fibres show a significant decrease in mitochondria number and functionality that is also typical of ageing muscles. A study from Dr. Nishimune's group (Rogers et al, 2017) showed that the impairment of mitophagy plays a fundamental role in the disruption of the NMJ of mice affected by amyotrophic lateral sclerosis. In the previous chapter we observed a significant increase in peroxide release from mitochondria of denervated skeletal muscle. This significant increase was accompanied by an initial increase in GPx1 and TRxR2 content, proteins that play an important role in the reduction of H_2O_2. Over a longer term a significant increase in Hsp content at 14 and 21 days was also seen suggesting the presence of oxidative stress in mitochondria from denervated muscle fibres and the activation of proteolysis processes. No previous studies appear to have investigated how the loss of innervation affects mitophagy in the denervated muscle fibre and the impact that denervation-induced alteration of mitophagy can have on the mitochondria population. In the present study, markers of

mitophagy and apoptosis together with changes in mitochondria number and mitochondria membrane potential were analysed to determine the impact that the accumulation of peroxide has on mitochondria and their functionality.

Mitophagy is a fundamental process which involves the activity of several proteins. Two main steps are involved in mitophagy: fission and fusion. These processes are tightly regulated by proteolysis and post-translational modifications (Hoppins et al, 2007). Fission and fusion divides and fuses the two lipid bilayers that enclose the mitochondria (the inner membrane and the outer membrane) (Youle and van der Bliek, 2012). As the name suggest, fission is the process of mitochondrial breaking down which is able to generate new organelles (Youle and van der Bliek, 2012). This process is directed by a cytosolic protein belonging to the dynamin family, known as Drp1 (Mishra and Chan, 2016) a cytosolic protein usually recruited by Mid49, Mid51 and Mitochondrial fission factor (Mff) (Friedman et al, 2011; Elgass et al, 2013). Drp1 is a protein found mainly in the cytosol in proximity of the endoplasmic reticulum (Hu et al, 2017). The activity of Mid49, Mid51 recruits Dpr1 while Mff is responsible of its phosphorylation (pDrp1). Once phosphorylated, Drp1 is activated and forms spirals around the mitochondria membrane inducing transection of both the outer and inner membrane (Hu et al, 2017). Previous studies have used the pDrp1/Drp1 ratio to determine the activation of Drp1 and an increase of fission. In the present study, as shown in *Figure 4.2a* we observed a significant increase in this ratio at 7 and 21 days following denervation suggesting increased fission.

Fusion is the process where mitochondrial organelles are assembled together. Fusion is usually increased following several physiological stimuli such as increased oxidative phosphorylation and inhibition of protein synthesis (mainly through starvation and mTOR inhibition) (Youle and van der Bliek, 2012). In the mitochondria, 3 different

dynamin proteins (present at different levels) are involved in the fusion process where the inner and outer membrane get reunited (Youle and van der Bliek, 2012). Mfn1 and Mfn2 are membrane anchored proteins involved in the fusion of the mitochondrial outer membrane while OPA1 is involved in the fusion of the mitochondrial inner membrane (Youle and van der Bliek, 2012).

Mfn-1 is found in different tissues including: heart, liver, pancreas, adrenal glands and testis. Mfn-2 is more abundant in the heart, skeletal muscle, brain and brown adipose tissue while OPA1 is mostly expressed in the retina, brain, testis, liver, heart, and skeletal muscle (Zorzano et al, 2015). In the present study Mfn-2 and OPA-1 were examined as markers of mitochondrial fusion. As shown in *Figure 4.2b* and *Figure 4.2c* no changes were observed in denervated skeletal muscle which may indicate a possible impairment of mitophagy. Fission and fusion play a major role in maintaining healthy mitochondria as mitochondria with mutated DNA can fuse with intact mitochondria potentially overcoming the problems induced by mitochondrial DNA modifications and maintaining the level of mutated mitochondria under 80-90% (Nakada et al, 2001). Defective mitochondria that cannot be recycled are removed from the network, engulfed by autophagosomes, delivered to the lysosome for proteolytic degradation (Vainshtein et al, 2015). Our results suggest a possible impairment of the mitophagy process since there was a significant mitochondria breakdown unaccompanied by an adequate fusion response. Malfunctioning of the mitophagy process may lead to a vicious cycle that results in the accumulation of dysfunctional mitochondria and the incorrect disposal of damage proteins with accumulation of p62. For this reason, an increase in p62 content has been reported to be a reliable marker for autophagy and mitophagy impairments (Liu et al, 2017). The accumulation of p62 in denervated muscle fibres

observed here fits with the hypothesis that the increased peroxide release reported in the previous chapter may led to breakdown of damaged mitochondria.

Youle and van der Bliek (2012) suggested that following fission, uncoupled mitochondria accumulate debris within their structure and experience fluctuations of the membrane potential that they are unable to deal with. These authors also suggest that these fluctuations may function as a marker of mitochondrial damage and trigger their disposal (Youle and van der Bliek, 2012). Part of the aims of this study was to analyse the mitochondrial membrane potential using a fluorescent probe that is rapidly sequestered within the mitochondria and is capable of generating a signal which intensity is associated with mitochondria membrane potential (Perry et al, 2011). To quantify the mitochondria membrane potential we used a protocol previously used by our group (Sakellariou et al, 2016) employing a fluorescent probe (TMRM) and recording the fluorescent signal overtime following addition of Olygomicin and FCCP. Oligomycin is capable of blocking the ATP synthase complex at the level of the ETC inducing accumulation of protons in the mitochondrial intermembrane space (Perry et al, 2011). Its addition is associated with an increase in the mitochondria membrane potential. FCCP is a protonophore able to induce permeabilisation of the mitochondrial inner membrane inducing an increased proton flux and a drop of the mitochondrial potential associated with the disappearing of fluorescent signal. As suggested by Perry and colleagues (2011), this protocol allows a more accurate determination of mitochondrial membrane potential through the analysis of the area under the TMRM fluorescence trace. In the results reported here we observed great variability within the groups. Despite this variability, there was a suggestion of possible impairment of mitochondrial membrane potential (*Figure 4.5a*) but we did not proceed with the analysis of the results.

Another important focus of the present study was to assess mitochondria number as a reduction has been reported during ageing and disease (Sun et al, 2016). Analysis of citrate synthase activity suggested that, in accordance with previous findings, denervated muscle fibres experience a significant reduction in mitochondrial number. Our results therefore show that, following denervation, the significant increase in peroxide release reported in Chapter 3 has a tremendous impact on mitochondria, inducing a significant reduction in mitochondria number with impairment of mitophagy and increased fission. As previously discussed, mitochondria are involved in a series of different signalling functions that ensures the correct functioning and survival of the cell (McBride et al, 2006). In the present study, it was speculated that the increase in peroxide release together with the inhibition of mitophagy may trigger activation of apoptosis. Therefore, we investigated the Bax/Bcl-2 ratio and the caspase-3 activation. The Bcl-2 family plays a fundamental role in the regulation of the mitochondria-mediated apoptotic signal transduction (Siu and Alway, 2005). In particular, among the Bcl-2 family, the pro-apoptotic member BAX plays a central role in regulating the apoptotic machinery (Siu and Alway, 2005).

In the present study an increase in the BAX/Bcl-2 ratio was found following denervation that is in line with the previous work of Siu and Alway (2005). The significant increase of the BAX/Bcl-2 ratio is associated with mitochondria membrane permeabilisation and release of cytochrome c which, interacting with apoptotic protease activating factor 1, induces the formation of the apoptosome responsible of the activation of different caspases including caspase-3, -6 and -7 which are all known as "*executional*" caspases (Slee et al, 2001; Sandri et al, 2001). The activation of these caspase usually triggers apoptosis through the cleavage of specific proteins (Slee et al, 2001). Dupont-Versteegden (2006) suggests that a close correlation exists between activation of apoptosis and skeletal

muscle atrophy. In the previous chapter we highlighted how skeletal muscle fibres in denervated muscles showed significant muscle fibre atrophy and the current results shed new light on one of the possible pathways responsible for this. Caspase-3 activation has previously been associated with skeletal muscle atrophy (Sandri et al, 2001) inducing protein degradation and enhancing proteasomal activity through the cleavage of Rpt2 and Rpt6 two specific 19S proteasome subunits (Wang et al, 2010). Together with the 20S proteasome, the 19S proteasome compose the 26S and 30S proteasomes of which it is the regulatory component (Tanaka, 2009). The 19S proteasome plays a fundamental role in recognising ubiquitinated proteins and, after unfolding them, translocate them into the core component of the proteasome where degradation takes place (Tanaka, 2009). Previous studies have investigated the role of Caspase-3 and proteasome activation both in denervated (Siu and Alway, 2005) and in ageing muscles (Baumann et al, 2016) suggesting that mitochondria play a fundamental role in driving muscle atrophy. In the present study we collected evidence that suggest that the increased peroxide release from mitochondria of denervated muscle fibres triggers a cascade of events that culminate with the possible activation of the proteasome system. It has been speculated that an increase in ROS production may be responsible for damaging mitochondria triggering a subsequent increase of mitochondrial fission (Jezek et al, 2018), loss of mitochondria (Alway et al, 2017) and activation mitochondria-induced apoptosis (Siu and Always, 2005). Our results suggest that starting from 7 days following denervation, there is a significant impairment of mitophagy (determined through the analysis of p62) together with an increase in fission resulting in a significant reduction of the mitochondria population at 21 days following nerve transection. In addition, we investigated the hypothesis that mitochondria may play a pivotal role in muscle atrophy seen following denervation. Our results suggest that the increase in the

BAX/Bcl-2 ratio results in a significant increase in caspase-3 content and its cleavage. The significant increase in caspase-3 content may induce the activation of the 26S proteasome system which previous studies (Siu and Always, 2005; Bhattacharya et al, 2009; Romanello et al, 2010; Hepple, 2014; Baumann et al, 2016) have indicated as one of the possible causes of skeletal muscle atrophy in denervated muscles and during ageing.

Chapter 5. Metabolic changes induced by skeletal muscle denervation

5.1 Introduction

The use of Nuclear Magnetic Resonance spectroscopy for metabolic profiling is a developing and promising technique that allows scientists to obtain extensive quantitative information about a tissue, a fluid or an entire living organism (Emwans et al, 2019).

Initially developed by Wilson and Burlingame back in 1974, this technique allows the analysis of a large array of metabolites in a reliable and reproducible way.

NMR is based on the physics principle of the energy difference:

$$E = h\nu$$

Energy "*E*" (in Joules) is proportional to frequency "*ν*" (in Hertz) where "*h*" is Planck's constant ($6.62607004 \times 10^{-34}$ m^2kg/s). Every proton (^1H) has a certain magnetic moment; when a magnetic field is applied to a certain proton this generates changes in the magnetisation (the ^1H will be in resonance with the applied magnetic field). The differences between the original magnetic state and the applied magnetic state is defined as "*frequency*" and generates a radio wave in the electromagnetic spectrum (Tognarelli et al, 2015).

Since NMR metabolomics generates a spectrum of all the resonances, each signal in the spectrum can be defined as a ^1H resonance and the chemical shift can be then defined as the frequency of the resonance expressed with reference to a standard compound which is defined to be at 0 ppm (Tognarelli et al, 2015).

Metabolites with multiple ^1H environments will give rise to spectra with multiple signals creating a spectrum similar to the one presented in *Figure 5.1*.

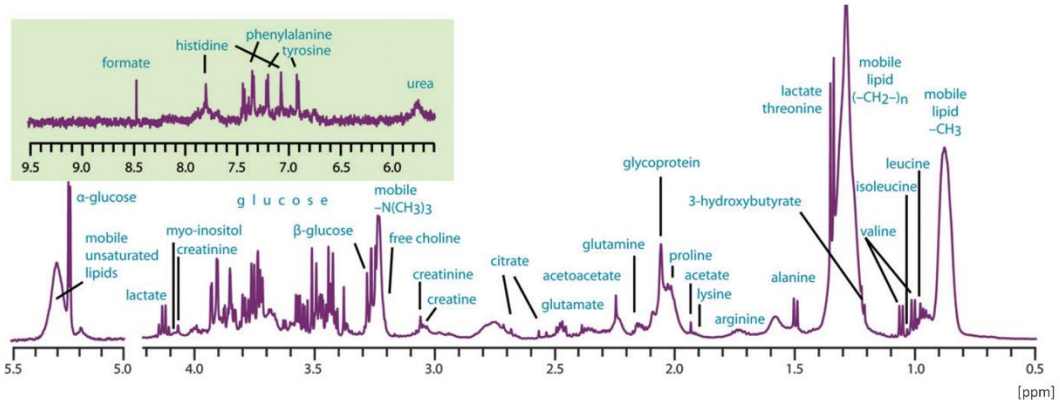

Figure 5.1. *Representative NMR metabolomics spectra and its component metabolites as presented by Soininen et al, (2009).*

One of the most key features of NMR metabolomics is that the results are highly reproducible and comparable independently of the magnetic field used during the experiment (Emwans et al, 2019). To allow this, every signal is reported as a fraction of the operating frequency of the spectrometer using a scale set in Parts Per Million (ppm) which is independent of the spectrometer frequency (Kemp, 1986). The chemical shift (the position in ppm where the signal generated by a specific metabolite is found compared to the reference chemical) is calculated by the following formula:

$$\delta = \frac{frequency\ of\ signal\ (Hz) - frequency\ of\ reference (Hz)}{\text{spectrometer frequency (mHz)}}$$

For the protocol chosen for this project, selectively deuterated trimethylsilyl propionate (TSP) was used as a reference. This compound is used in NMR metabolomics for two reasons: it is soluble in aqueous buffers and all the ^{1}H atoms in this molecule are equivalent and more shielded than almost all the organic compounds found in nature. This means that TSP generates a singlet with a chemical shift (δ) equal to 0. Therefore, this chemical can be used as a reference to identify other chemicals and to normalise the data generated (Dona et al, 2016).

The aim of the present study was to determine the metabolic changes induced in skeletal muscle following denervation.

5.2 Materials and Methods

5.2.1 Nuclear Magnetic Resonance Metabolomics of denervated gastrocnemius

The gastrocnemius muscle from the mice used in Chapter 4 was used for NMR metabolomics analysis and treated as presented in section 2.16. The Spectra obtained were analysed with TopSpin 3.5 (Bruker, Coventry, United Kingdom), ChenomX 8.2 (Edmonton, Alberta, Canada) and tameNMR on Galaxy.liv.ac.uk (github.com/PGB-Liv/tameNMR)

5.2.2 Metabolite identification

A pattern file containing all the peaks predicted in mouse skeletal muscle was obtained using TopSpin 3.5 software. Using previously published data (Sparling et al, 1990; Soinnien et al, 2009), we identified some of the peaks present in our spectra as lipids. However, due to the limited information available we were not able to determine which specific lipids they were; hence these were labelled simply as "*lipids*". In addition, for those peaks where annotation was not available in the ChenomX database, the label "*unknown*" was applied. For all those annotated peaks, the KEGG compound code was applied for pathways analysis. These annotations were then converted to peak boundaries (pattern file) that defines "*bins*" that every peak should be divided into. This procedure called "*binning*" was then verified by uploading the pattern file to Galaxy.liv.ac.uk as suggested by Afgan and colleagues (2016) to exclude any risk of bin overlapping which may interfere with the analysis. Statistical analysis of the "*bins*" was performed as explained in section 2.17.1.

5.3 Results

5.3.1 Anthropometric measurements

No significant differences in total body weight were seen between groups (*Figure 4.1a* - section 4.3.1). The Gastrocnemius muscle (*Figure 5.2*) showed a significant reduction in mass at 7 days following denervation and a further reduction at 21 days $F(2,9)=99.858$ $p<0.001$.

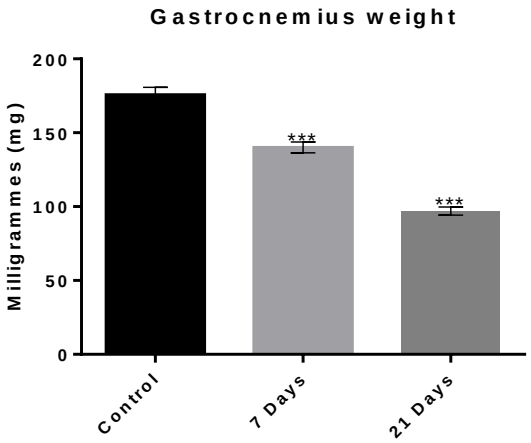

Figure 5.2. *Gastrocnemius muscle weights from control mice (non-denervated) and mice at 7 and 21 days post-denervation.*
Histograms represent the mean and the standard error of the mean for each experimental group (n=4).
**** p<0.001 compared with the control group.*

5.3.2 NMR Metabolomics

Analysis of the spectra obtained during the NMR analysis (presented in *Figure 5.3*), showed that denervation induces a series of very dramatic modifications in skeletal muscle. Differences between groups were highlighted by the Principal Component Analysis presented in *Figure 5.4* with Principal Component 1 and 2 able to explain over 70% of variability within the samples.

Over 100 annotated peaks were significantly altered in response to denervation (*Table 5.1* for complete list). From the significant peaks we were able to identify 27 different metabolites. The heatmap presented in *Figure 5.5* offers a better overview of the significant changes induced by denervation. In addition, to the heatmap, in *Figures 5.6-5.13* are presented the results of the *post-hoc* analysis of specific metabolites of interest in the context of this work. A MSEA analysis was also performed but failed to identify significant pathways altered in response to denervation ($p>0.05$); however the ranking, presented in *Table 5.2*, suggests that denervation may have induced insulin resistance, inhibition of glycolysis and increased activity of the purine metabolism.

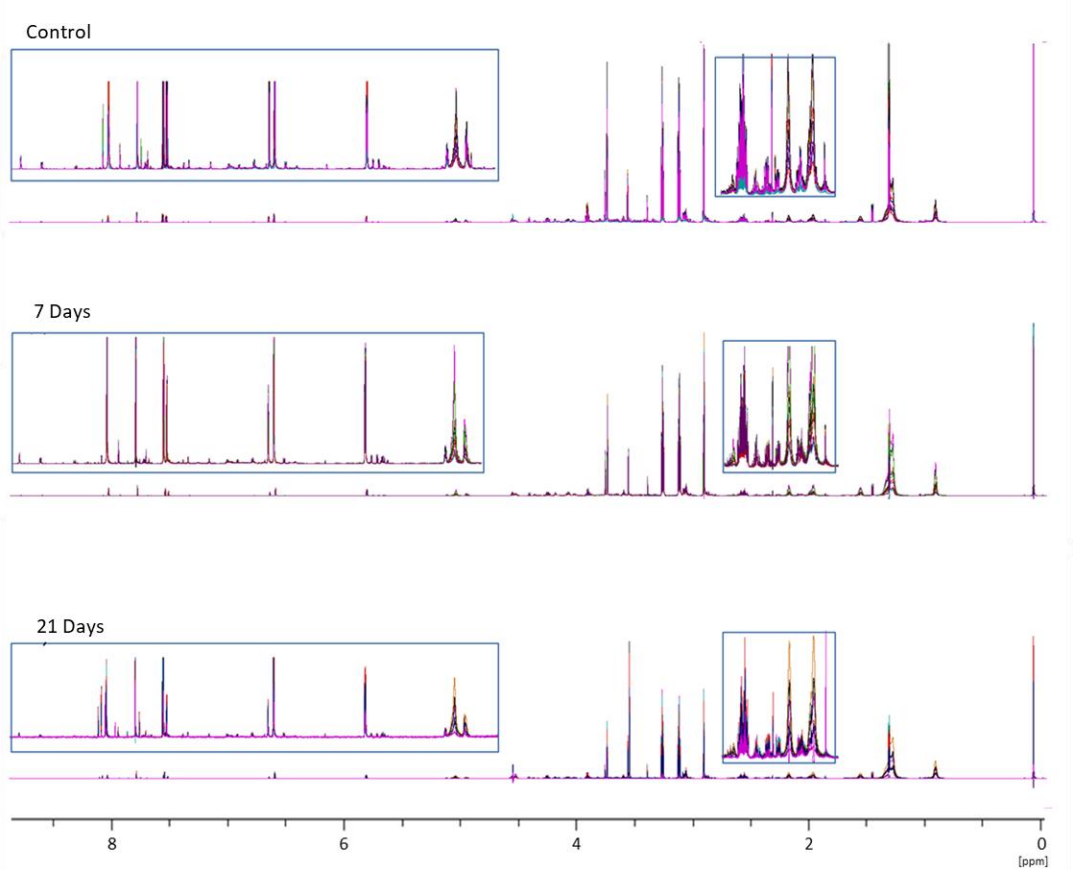

Figure 5.3. *^{1}H 1D NMR spectra (700MHz) of murine gastrocnemius muscle tissue extract for Control (non-denervated), 7 day and 21 days post-denervation groups (n=4). Inset spectra (Blue squares) represent 4x magnification of specific spectral regions: 10-7ppm (aromatic including NAD+ and ATP) and 2.8-3.8ppm polar amino acids (glutamine and glutamate).*

A

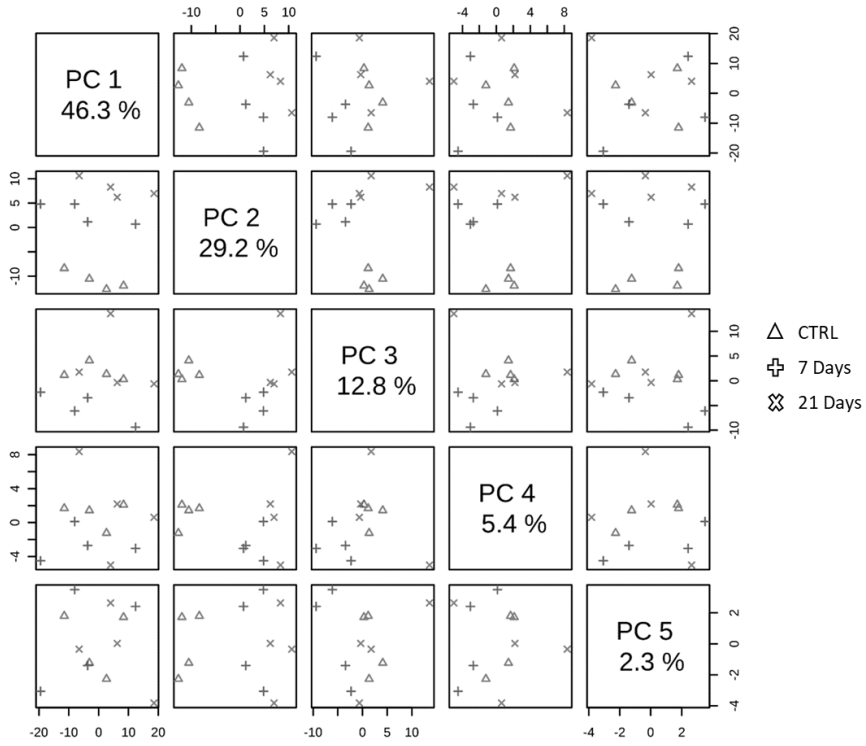

B

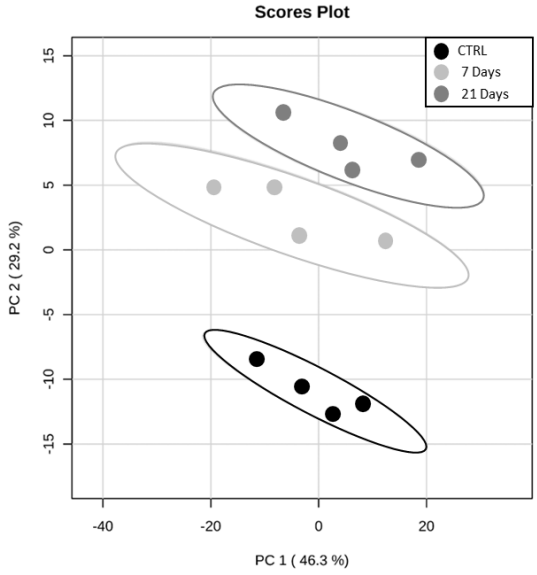

Figure 5.4. A) *Results of the principal component analysis. Figure shows the first 5 components able to explain more than 95% of the variance seen between the Control (Δ - non-denervated), 7 days post-denervation (+) and 21 days post-denervation (X) groups.* ***B)*** *Results of the Principal Component Analysis of the first 2 Principal Components able to explain 75.5% of the variance seen between the control (Black - non-denervated, n=4), 7 days post-denervation (light grey, n=4) and 21 days post-denervation (dark grey, n=4) groups. X and Y axis present the raw component score values derived from the formation of the principal components. These are arbitraty units explaining the differences between the groups.*

Table 5.1. *List of significant peaks identified using NMR Metabolomics. In the table are reported the metabolite(s) identified for a specific bin, the bin number, the statistical F value, with the original and adjusted p value.*

Metabolite (Bin Number)	F Statistic	p value	Adjusted p value
NAD+ (3)	10.7343	0.00414	0.005585686
NAD+ (15)	9.98037	0.0052	0.006772816
Adenine/NAD+ (25)	13.0918	0.00217	0.003402914
GTP (26)	7.81434	0.01078	0.012555179
Unknown (29)	67.5358	3.81E-06	5.38E-05
Xanthine (31)	92.113	1.02E-06	4.79E-05
Uridine (32)	15.8099	0.00113	0.002005478
Uknown (33)	31.7745	8.34E-05	0.000275274
Phenylalanine/3.Phenylpropionate/Thymine/5-hydroxyindoleacetate (39)	28.3505	0.00013	0.000379468
Phenylalanine/3.Phenylpropionate/Thymine (40)	14.1676	0.00166	0.00278187
Phenylalanine/3.Phenylpropionate/Imidazole (41)	22.4784	0.00032	0.000680396
Phenylalanine (42)	24.2867	0.00024	0.000569614
Histamine (45)	25.4151	0.0002	0.000504102
Anserine (46)	11.3987	0.00341	0.005020024
Uknown (48)	10.9754	0.00386	0.00533784
Uknown (49)	71.2376	3.04E-06	5.13E-05
3.4.Dihydroxymandelate (51)	26.9057	0.00016	0.000426922
Unknown (63)	10.9517	0.00388	0.00533784
UMP (64)	41.8095	2.78E-05	0.00013579
Unknown (65)	9.73188	0.00562	0.006955386
Unknown (66)	33.2664	6.96E-05	0.000240091
Unknown (67)	7.6476	0.01146	0.013194286
GTP (68)	8.49331	0.00847	0.010098919
Unknown (71)	9.73899	0.00561	0.006955386
Unknown (72)	10.7038	0.00418	0.005585686
Unknown (78)	16.278	0.00102	0.001842953
Glucose/Unknown (82)	79.2354	1.93E-06	4.79E-05
Inosine/NAD+ (93)	14.5684	0.00151	0.002571868
Inosine/UMP (94)	6.42893	0.01844	0.019847445
UMP (100)	11.3642	0.00345	0.005020024
Unknown (101)	11.0963	0.00372	0.00533784
Unknown (102)	9.93678	0.00527	0.006776163
Unknown (103)	8.98733	0.00716	0.008641927
Unknown (104)	3.43234	0.07801	0.078010149
Unknown (108)	4.3683	0.04723	0.048198893
Threonine/ATP/NAD+/ (110)	27.1325	0.00015	0.000424801
NAD+ (114)	11.4653	0.00335	0.005020024
Lactate (118)	22.9291	0.00029	0.000660214
Lactate (119)	20.2396	0.00047	0.000912085
Choline (122)	3.62857	0.06989	0.070599339
Choline/Creatinine (123)	4.73616	0.03933	0.040560959
Unknown (124)	6.56469	0.01745	0.019192132
IMP/UMP (125)	13.2986	0.00205	0.003291314
IMP/Phenylalanine/UMP (128)	33.1765	7.03E-05	0.000240091
T.Methylhistidine/Galactarate/Tyrosine/UMP/TT.Methylhistidine (130)	39.6254	3.45E-05	0.000142489
Creatine/Phosphate/Glycolate (131)	29.7554	0.00011	0.000323814
Methionine (136)	33.4385	6.82E-05	0.000240091
Methionine/O.Acetylcarnitine (137)	47.3292	1.67E-05	0.000117324
Methionine/O.Acetylcarnitine/Inosine/Glucose (138)	12.1759	0.00275	0.004260958
O.Acethylcholine (153)	45.242	2.01E-05	0.000117324

Metabolite (Bin Number)	F Statistic	p value	Adjuste
O.Phosphocholine/Threonine/O.Acetylcarnitine/Glycoproline (163)	24.1383	0.00024	0.000
Glycoproline (164)	20.542	0.00044	0.000
Glycine/Glycoproline (165)	30.3746	9.96E-05	0.000
Glucose.6.phosphate/Uknown (169)	40.4688	3.17E-05	0.00
Glycoproline/Glucose (170)	70.8518	3.11E-06	5.1
Glycoproline/Glucose (171)	12.0627	0.00284	0.004
Glucose.6.phosphate/Uknown (172)	81.6249	1.70E-06	4.7
Unknown (185)	35.9094	5.13E-05	0.00
Unknown (187)	43.4469	2.38E-05	0.000
Unknown (189)	46.498	1.80E-05	0.000
Unknown (191)	20.2044	0.00047	0.000
T.Methylhistidine/Tyrosine/Carnosine/Anserine (203)	51.6192	1.17E-05	9.6
T.Methylhistidine/Carnosine (207)	20.0321	0.00048	0.000
T.Methylhistidine/Carnosine (208)	19.7679	0.00051	0.000
Uknown (216)	28.0805	0.00014	0.000
3.Phenylpropionate (228)	15.4484	0.00123	0.002
Unknown (229)	41.6768	2.82E-05	0.00
Unknown (230)	13.6257	0.00189	0.003
Sarcosine/Anserine (233)	53.1347	1.04E-05	9.3
Anserine/Uknown (238)	57.4152	7.52E-06	7.4
Methionine/O/Acetylcarnitine/Carnosine/Anserine (242)	45.2582	2.01E-05	0.000
Methionine/O.Acetylcarnitine/Methylsuccinate/Carnosine/Anserine (243)	60.2328	6.16E-06	6.7
O.Acetylcarnitine/Methylsuccinate/Anserine (244)	62.6521	5.22E-06	6.4
Glutathione/Isocitrate (247)	26.1054	0.00018	0.000
Unknown (248)	41.4434	2.88E-05	0.00
Glutathione/Isocitrate/Citrate (249)	21.9513	0.00035	0.000
Glutathione/O.Acetylcarnitine/Isocitrate/Citrate (250)	19.1827	0.00057	0.001
Glutathione/O.Acetylcarnitine/3.Phenylpropionate/Isocitrate (251)	13.2858	0.00206	0.003
O.Acetylcarnitine/3.Phenylpropionate/Methylsuccinate/Isocitrate (252)	10.9689	0.00386	0.00
Glutamine/O.Acetylcarnitine/3.Phenylpropionate/Isocitrate (253)	24.5256	0.00023	0.000
Unknown (256)	127.532	2.49E-07	2.4
Pyruvate (258)	7.12191	0.01399	0.015
Glutamate (261)	22.5703	0.00031	0.000
Glutamate/Glycoproline (262)	30.3636	9.97E-05	0.000
Glutamate/Glycoproline (263)	6.51264	0.01782	0.019
Glutathione (265)	9.76454	0.00556	0.006
Glutathione (266)	23.462	0.00027	0.000
Glutamate/Glutathione/Glutamine (267)	37.4757	4.32E-05	0.000
Glutamate/Glutathione/Glutamine/Glycoproline (268)	47.9743	1.58E-05	0.000
Methionine/Glutamate/Glutamine/Methylsuccinate/Glycoproline (271)	21.4455	0.00038	0.00
Methionine/Glutamate/Glutamine (272)	9.98405	0.00519	0.006
Valine/Uknown (299)	7.45266	0.01233	0.014
Isoleucine (300)	9.66417	0.00574	0.007
Isoleucine (301)	7.98531	0.01013	0.011
Valine/Lipid (302)	5.73739	0.02475	0.026
Isoleucine (303)	5.8505	0.02356	0.025
Leucine/Lipid (305)	5.3677	0.02921	0.030
Isoleucine/Leucine (306)	6.97676	0.0148	0.016

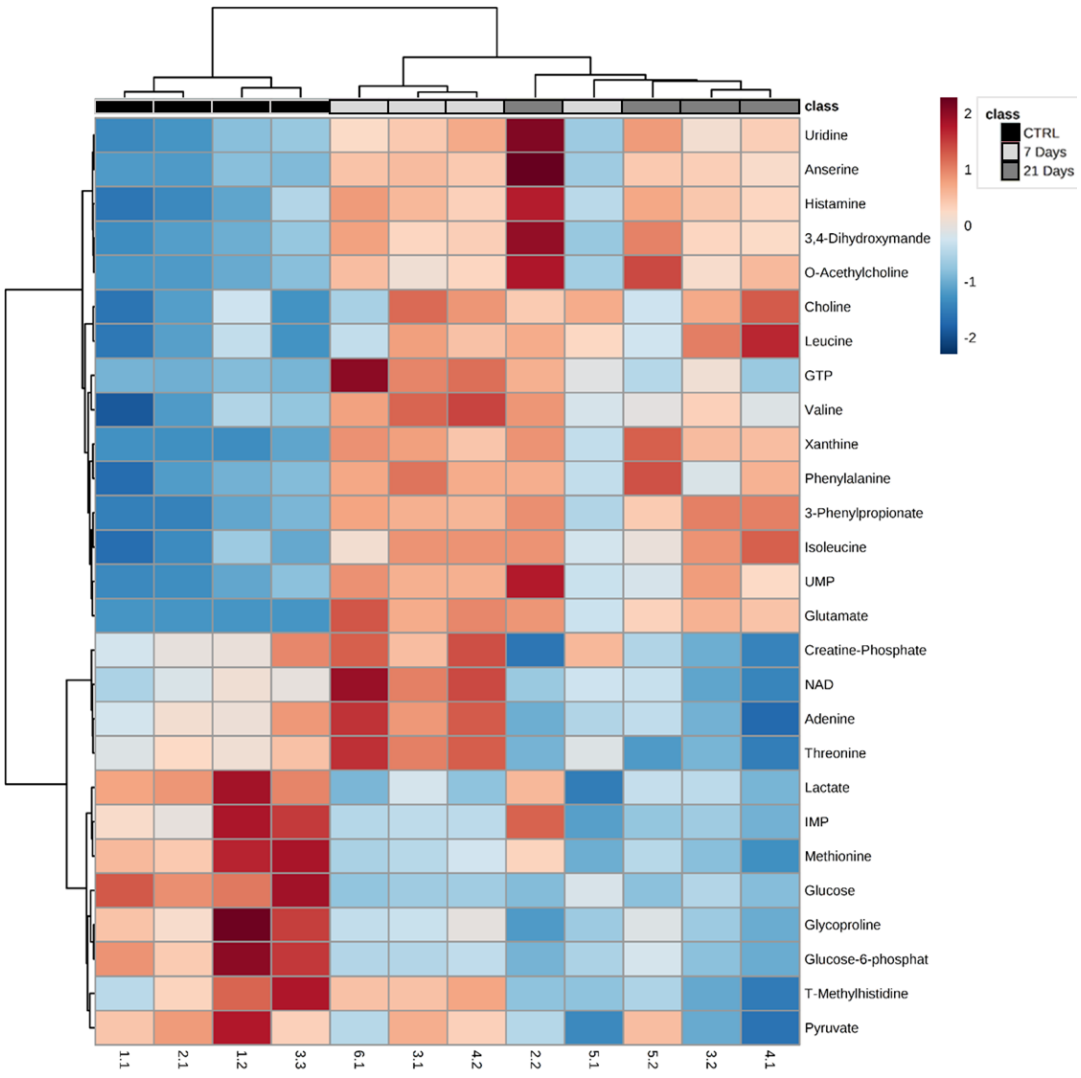

Figure 5.5. *Heatmap representing the results of the statistically significant metabolites ($p<0.05$) identified from NMR metabolomics (shown on the right of the figure). Groups are indicated at the top of the figure in black (Control), light grey (7 days post-denervation) and dark grey (21 days post denervation). Individual samples IDs are indicated at the bottom of the figure while a reference to understand the fold changes of each sample compared to each peak $\sqrt{SD}$ is presented in the top right corner of the image.*

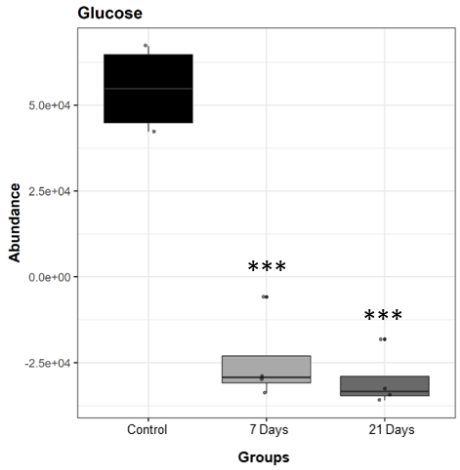

Figure 5.6. *Box plot presenting the mean-centered relative abundance of Glucose in control (non-denervated), 7 days and 21 days post-denervation groups. Dots represent individual samples (n=4 per group) while asterisks show the statistical differences between 7 and 21 days post-denervation groups and the control group (non-denervated) as follows: *** p<0.001. Note: The mean-centred relative abundance is expressed in arbitrary units and is directly proportional to the metabolite concentration.*

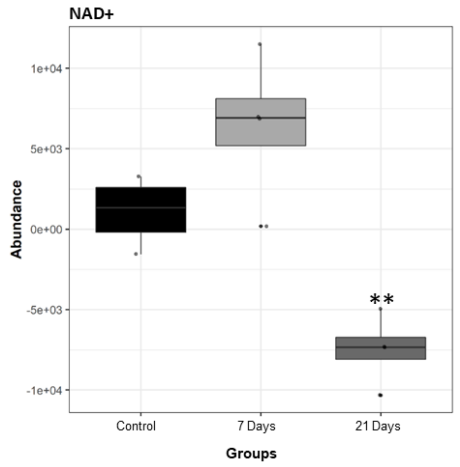

Figure 5.7. *Box plot presenting the mean-centred relative abundance of NAD+ in control (non-denervated), 7 days and 21 days post-denervation groups. Dots represent individual samples (n=4 per group) while asterisks show the statistical differences between 7 and 21 days post-denervation groups and the control group (non-denervated) as follows: ** p<0.01. Note: The mean-centred relative abundance is expressed in arbitrary units and is directly proportional to the metabolite concentration.*

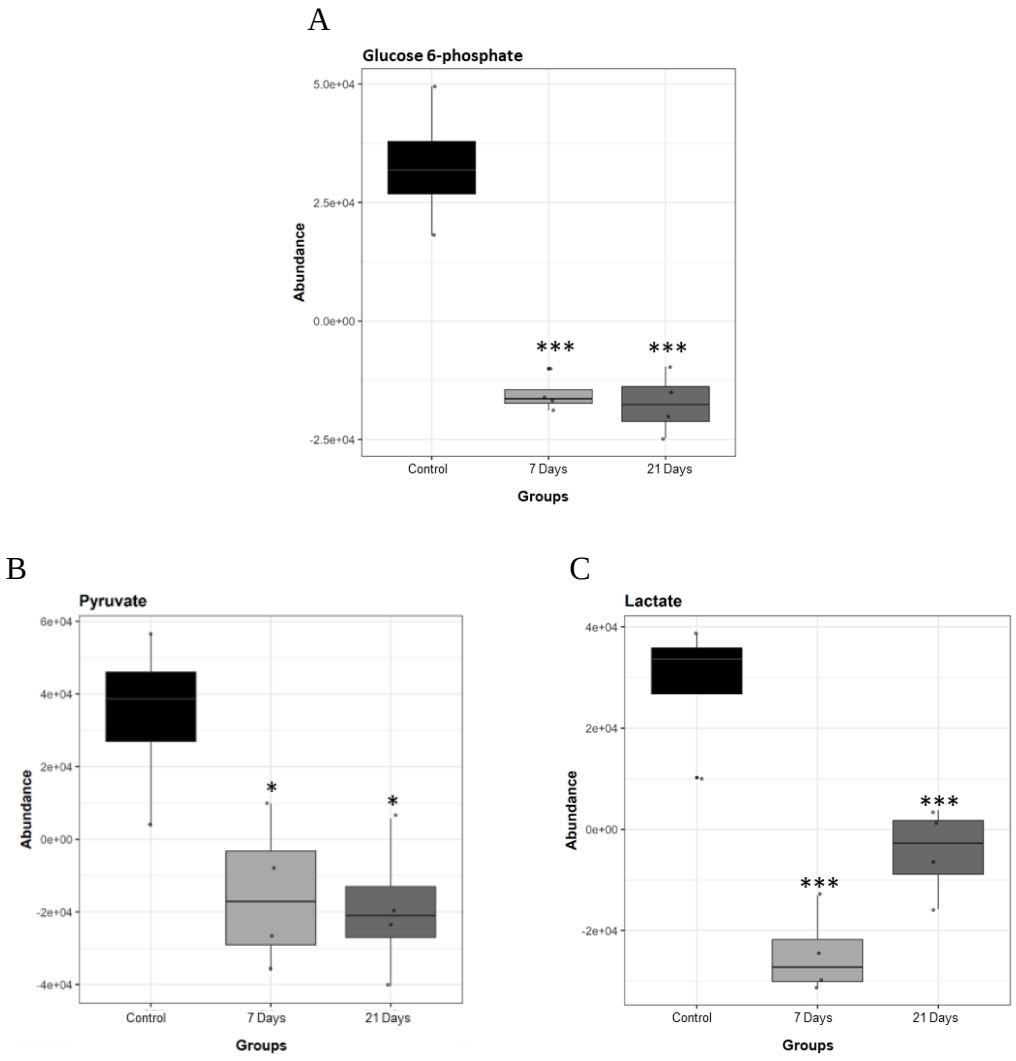

Figure 5.8. *Box plot presenting the mean-centred relative abundance of* ***A)*** *Glucose 6 phosphate,* ***B)*** *Pyruvate and* ***C)*** *Lactate in control (non-denervated), 7 days and 21 days post-denervation groups. Dots represent individual samples (n=4 per group) while asterisks show the statistical differences between 7 and 21 days post-denervation groups and the control group (non-denervated) as follows: * p<0.05 - *** p<0.001. Note: The mean-centred relative abundance is expressed in arbitrary units and is directly proportional to the metabolite concentration.*

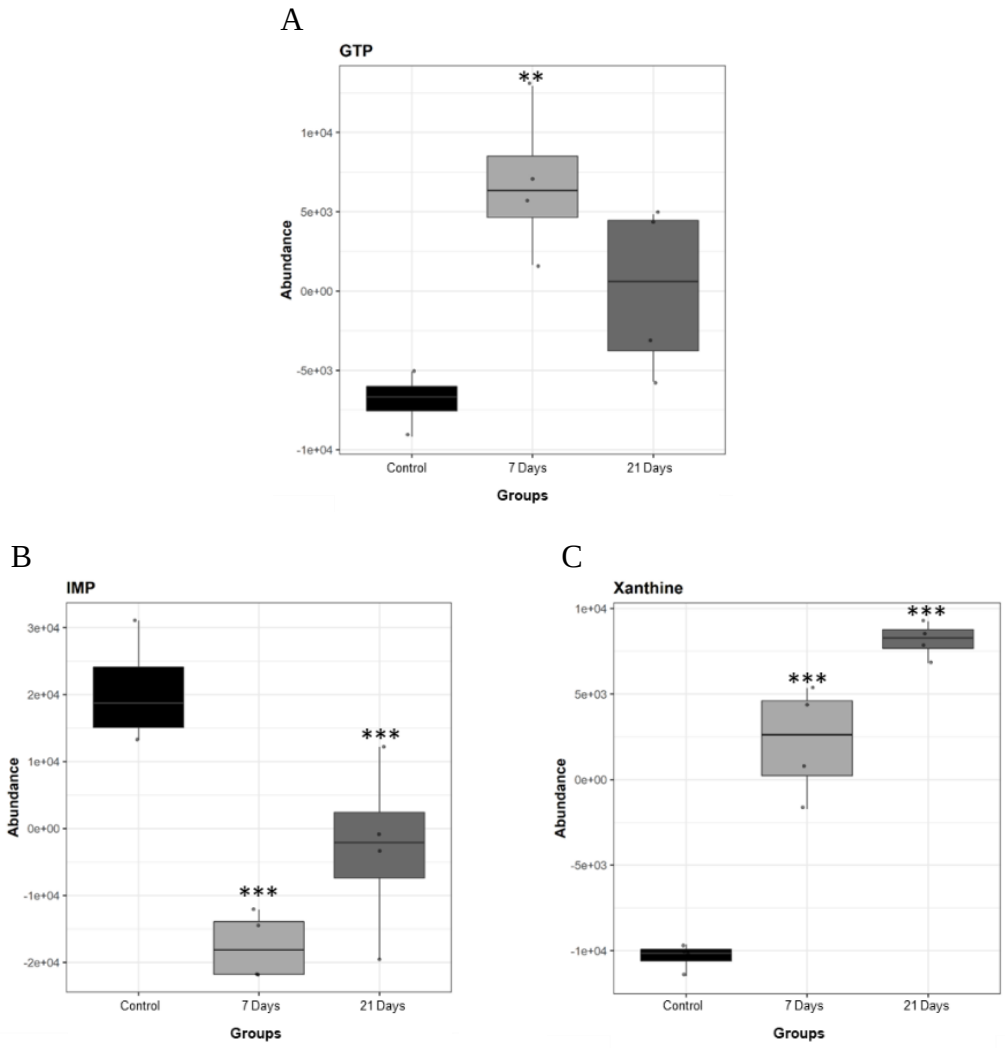

Figure 5.9. *Box plot presenting the mean-centred relative abundance of* ***A)*** *GTP,* ***B)*** *IMP and* ***C)*** *Xanthine in control (non-denervated), 7 days and 21 days post-denervation groups. Dots represent individual samples (n=4 per group) while asterisks show the statistical differences between 7 and 21 days post-denervation groups and the control group (non-denervated) as follows: ** p<0.01 - *** p<0.001. Note: The mean-centred relative abundance is expressed in arbitrary units and is directly proportional to the metabolite concentration.*

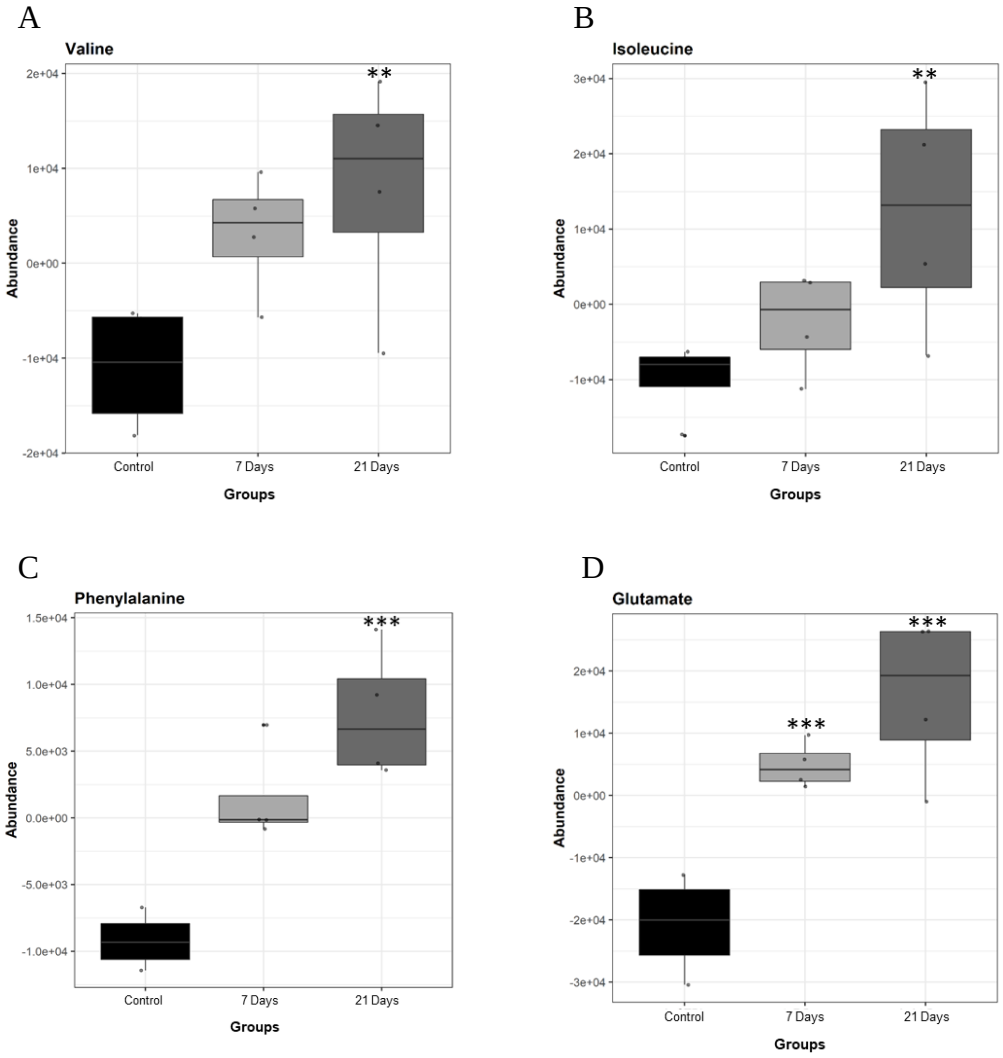

Figure 5.10. *Box plot presenting the mean-centred relative abundance of* ***A)*** *Valine,* ***B)*** *Isoleucine and* ***C)*** *Phenylalanine and* ***D)*** *Glutamate in control (non-denervated), 7 days and 21 days post-denervation groups. Dots represent individual samples (n=4 per group) while asterisks show the statistical differences between 7 and 21 days post-denervation groups and the control group (non-denervated) as follows: ** p<0.01 - *** p<0.001. Note: The mean-centred relative abundance is expressed in arbitrary units and is directly proportional to the metabolite concentration.*

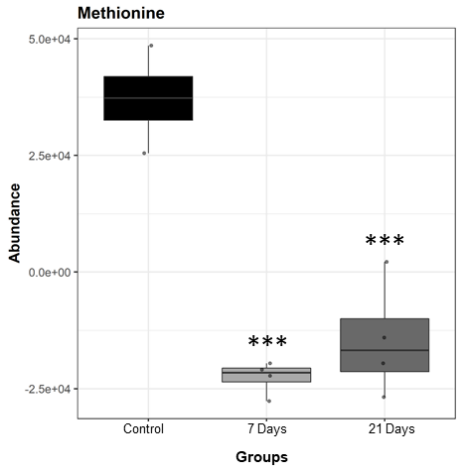

Figure 5.11. *Box plot presenting the mean-centred relative abundance of Methionine in control (non-denervated), 7 days and 21 days post-denervation groups. Dots represent individual samples (n=4 per group) while asterisks show the statistical differences between 7 and 21 days post-denervation groups and the control group (non-denervated) as follows: *** p<0.001. Note: The mean-centred relative abundance is expressed in arbitrary units and is directly proportional to the metabolite concentration.*

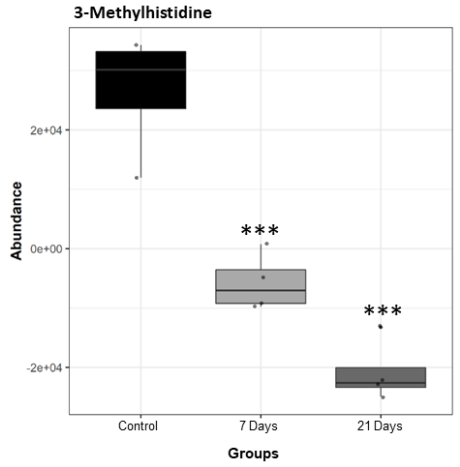

Figure 5.12. *Box plot presenting the mean-centred relative abundance of 3-Methylhistidine in control (non-denervated), 7 days and 21 days post-denervation groups. Dots represent individual samples (n=4 per group) while asterisks show the statistical differences between 7 and 21 days post-denervation groups and the control group (non-denervated) as follows: *** p<0.001. Note: The mean-centred relative abundance is expressed in arbitrary units and is directly proportional to the metabolite concentration.*

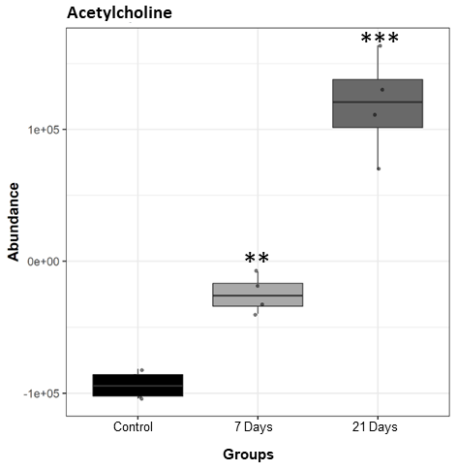

Figure 5.13. *Box plot presenting the mean-centred relative abundance of Acetylcholine in control (non-denervated), 7 days and 21 days post-denervation groups. Dots represent individual samples (n=4 per group) while asterisks show the statistical differences between 7 and 21 days post-denervation groups and the control group (non-denervated) as follows: ** p<0.01 - *** p<0.001. Note: The mean-centred relative abundance is expressed in arbitrary units and is directly proportional to the metabolite concentration.*

Table 5.2. *List of the pathways identified using MSEA in order from the most mapped to the least mapped. The table shows the pathways, the pathways size, the number of metabolites mapped together with the raw p value, the adjusted p value and the confidence interval.*

Pathway	Pathway Size	Metabolites Mapped To Pathway	Mapping Percentage	Raw p value	CI 95	Adjusted p value
Insulin Resistance	19	4	21.053	0.417253795	(0.3292,Inf)	1
Glucagon Signalling	26	4	15.385	0.612359179	(0.241,Inf)	1
ETC	16	2	12.5	0.586637357	(0.1687,Inf)	1
Purine Metabolism	95	10	10.526	0.818278514	(0.3555,Inf)	1
Citrate cycle	20	2	10	0.909839266	(0.0197,Inf)	1
Glycolysis	31	3	9.677	0.887100592	(0.0868,Inf)	1
Arginine	23	2	8.696	0.936734813	(0.0171,Inf)	1
Pentose phosphate	35	2	5.714	0.985085462	(0.011,Inf)	1
Fructose and Mannose	54	1	1.852	1	(0,Inf)	1

5.4 Discussion

The initial aim of the work described in this chapter was to perform NMR Metabolomics directly on mitochondria extracted from muscle. To do so, the isolation of mitochondria for NMR metabolomics required significant optimisation as the gold standard protocol for mitochondria isolation uses a sucrose gradient for isolation. Sucrose is a disaccharide (chemical structure shown in *Figure A1.3* - Appendix 1) that, when analysed with NMR metabolomics, presents a very high "*clarity x dynamic range*" (the range of concentration that allows the visualisation of a metabolite) preventing the visualisation of several metabolites with a lower clarity x dynamic range (e.g. NAD+). An alternative buffer suggested in literature for mitochondria isolation (Corcelli et al, 2010) contains EDTA and MOPS (chemical structure shown in *Figure A1.4* and *Figure A1.5* - Appendix 1) that also have the potential to obscure the signal of other metabolites in a similar way (*Figure A1.6* - Appendix 1). Despite the mitochondrial isolation being successful (*Figure A1.1* and *Figure A1.2* - Appendix 1), the traces of buffers retained did not allow an accurate analysis and therefore it was decided to perform the analysis on the entire denervated skeletal muscle. By performing NMR metabolomics of the entire denervated muscle, we were able to obtain information regarding the metabolic changes induced by denervation in skeletal muscle.

MSEA analysis (*Table 5.2*) indicates that denervated muscle shows insulin resistance, alteration of the glycolysis pathway and of purine metabolism with analysis of the single metabolites supporting this hypothesis. In the previous chapter it was reported that, in response to denervation, there was a significant increase in the content of NOX2 subunits. It was speculated that the increase in content of these subunits corresponds to an increase of NOX2 activity and production of H_2O_2 able to drive different responses in skeletal muscle including mechanical contraction, activation of apoptotic pathways

(Kadoguchi et al, 2018) and insulin resistance (Ferreira and Laitano, 2016). Interfering with the Angiotensin II system (Sukumar et al, 2013) NOX2 induces the phosphorylation of insulin receptor substrate-1 (IRS1) and the activation of both Protein Kinase B (Akt) and NF-κB preventing the translocation of GLUT-4 to the fibre membrane (Wei et al, 2008). The significant decrease in glucose abundance observed (*Figure 5.6*) suggests that the H_2O_2 production by NOX2 at later stages following denervation may trigger a series of responses that prevent glucose uptake by the skeletal muscle. This significant decrease in glucose availability in the denervated muscle fibres would result in reduced glycolysis with lower concentrations of intermediate products such as glucose 6-phosphate (*Figure 5.8a*) and of the final products pyruvate (*Figure 5.8b*) and lactate (*Figure 5.8c*).

NMR metabolomics also revealed a significant decrease of NAD+ abundance at 21 days following denervation (*Figure 5.7*). NAD is a coenzyme that can be found in two different forms: oxidised (NAD+) and reduced (NADH). NAD+ is a common product of Complex I of the ETC which uses NADH (normally produced during the citric acid cycle) as substrate. The reduction of NAD+ seen post-denervation suggests a possible reduction in NADH availability that may result in the substantial reduction of the ETC activity and ATP synthesis by ATP synthase.

The MSEA analysis also highlighted possible denervation-induced changes in the purine metabolism pathway. Purine metabolism is responsible for the production and degradation of the purine nucleotides adenine and guanine producing different intermediates of the citric acid cycle as well as ATP and Guanosine Triphosphate (GTP) (Yin et al, 2018). The central component of this pathway is inosine-5'-Monophosphate (IMP) that, once synthetised from a ribose-phosphate, can be utilised for the production of ATP and GTP (Yin et al, 2018). IMP can directly be converted onto Adenosine Monophosphate (AMP) in a two-step

reaction that involves the enzymes adenylosuccinate synthase and adenylosuccinate lyase using the energy released from the hydrolysis of GTP (Armenta-Medina et al, 2014). Once formed, AMP can quickly be converted onto ADP and then converted onto ATP through oxidative phosphorylation (Schultheisz et al, 2008). IMP can also be converted into Xanthosine monophosphate (XMP) by IMP dehydrogenase that uses NAD+ as electron donor for this reaction (Sigel et al, 2009). The production of XMP is a necessary step for the generation of GTP which, in addition to serving as substrate for the generation of AMP, is also responsible of the activation of guanine nucleotide-binding proteins (G Proteins) (Yanamadala et al, 2009). G proteins are a family of proteins responsible for the signal transduction involved in different processes including apoptosis (Yanamadala et al, 2009). Several studies have shown that G proteins can stimulate apoptosis regulating numerous downstream effectors including the Bcl-2 family (Yanamadala et al, 2009). Furthermore, as previously mentioned (section 1.5.4.3), GTP is needed to activate Rac proteins therefore promoting the activation of NOX2 enzyme and the subsequent H_2O_2 production observed in denervated muscles. Our data show an increase in GTP at 7 days post-denervation (*Figure 5.19a*) accompanied by a simultaneous significant reduction in IMP content (*Figure 5.9b*). The decrease in IMP and increase in GTP contents (together with the changes that we observed in NAD+ abundance) suggest that the activation of this pathway may result in the activation of G proteins and stimulation of apoptosis through the Bcl-2 family (which is in line with the findings presented in the previous chapter - section 4.3.3). A significant increase in xanthine was also seen (*Figure 5.9c*). This is an intermediate product resulting from the activity of xanthine oxidase. Xanthine oxidase is an enzyme involved in the production of uric acid and H_2O_2 from hypoxanthine (Cao et al, 2010), a natural derivate of purine metabolism resulting from the spontaneous deamination of adenine (Lee et al, 2009).

Independent studies demonstrated that xanthine oxidase plays a fundamental role in muscle atrophy in immobilised limb (Childs et al, 2003; Di Giovanni et al, 2004; Cao et al, 2010). The results of previous studies found that, following limb immobilisation, there is a 128% increase in p38 activation associated with a 38% decrease in muscle mass.

Administration of allopurinol, an inhibitor of xanthine oxidase, was able to partially prevent muscle atrophy in rats (Cao et al, 2010). It is therefore possible that the increase in xanthine seen in our model is related to the activation of the atrophy pathways as described above.

Increased proteolysis in skeletal muscle has been described also following fasting or prolonged exercise (Evans et al, 2017). During these conditions the body experiences significantly low levels of glucose availability that can induce an increase in protein catabolism in the muscle aimed to produce certain glucogenic amino acids. Glucogenic amino acids (such as valine or isoleucine) can be used by the muscle as intermediate substrates of the citric cycle or converted onto alanine that, once released onto the bloodstream, is used by the liver and converted into glucose that can be made available to the different tissues (Rui, 2014). Following denervation, we also observed a significant increase in valine (*Figure 5.10a*) and isoleucine (*Figure 5.10b*) that previous studies have reported to accumulate in muscles of diabetic patients (Lynch and Adams, 2014; Vendelbo et al, 2014) but also of phenylalanine (*Figure 5.10c*) and glutamate (*Figure 5.10d*). These latter two amino acids can be used to generate fumarate or α-ketoglutarate, two substrates that can be used by the citric acid cycle to generate NADH for the ETC. We speculated that the progressive accumulation of these amino acids in denervated skeletal muscles is the result of increased proteolysis but also due to a significant reduction of mitochondria number and functionality.

Another relevant change in the analysis is the significant reduction in methionine (*Figure 5.11*), an essential amino acid that plays a central role in protein biosynthesis and in oxidative resistance (Campbell et al, 2016). Methionine exerts its functions during oxidative resistance by inducing activation of enzymes such as methionine sulfoxide reductase A and biosynthesis of glutathione (Dos Santos et al, 2018). A previous study performed by Bianchi and colleagues (2000) showed that in plasma, the production of glutathione was directly proportional to the methionine load. To our knowledge this link between glutathione and methionine levels has not been investigated in skeletal muscle. Nevertheless, the low levels of methionine in denervated skeletal muscle may fit with the lack of response in glutathione previously reported (section 3.3.3). Another interesting change observed is the significant reduction of 3-Methylhistidine. 3-Methylhistidine is a metabolic product of actin and myosin methylation (Terman and Kashina, 2013). In a ground breaking study in 1973, Young and colleagues highlighted a negative correlation between 3-Methylhistidine and muscle protein catabolism. Our results show that following denervation, the concentration of this metabolite drops significantly (*Figure 5.12*) suggesting that the muscle fibre contractile proteins actin and myosin may remain unaffected and may still be functional.

Following denervation there is also a significant increase in ACh levels in muscle fibres (*Figure 5.13*). This increase appears to be in line with the progressive breakdown of the post-synaptic receptors discussed earlier (section 3.3.1) and with a previous study from Stanley and Drachman (1981). Another interesting study from An and colleagues (2010) showed that the accumulation of ACh in embryonic muscle prevents the formation of NMJ limiting axonal branching and synapse formation. To our knowledge, no other studies have investigated the ACh localisation following denervation. Future studies using genetically encoded fluorescent indicators such as the one recently developed by

Borden and colleagues (2020) called iAChSnFR may help determine ACh localisation following denervation. Gathering information regarding ACh localisation following recpetors breakdown in denervated muscle fibres may help to understand if the Ach accumulation measured in this study using NMR metabolomics can prevent the formation of neuromuscular junctions as seen at embryonic level by An and colleagues (2010).

NMR Metabolomics is an interesting and fast developing technique that, to our knowledge, has not been previously performed on denervated skeletal muscle. This technique provides a snapshot of the metabolic changes occurring in a tissue, shows high reproducibility and allows a fast and reliable analysis. However, compared to other techniques such as Liquid Chromatography – Mass Spectrometry, it has lower sensitivity (Edison et al, 2016; Viant et al, 2017). In addition, due to the limited availability of metabolite libraries, we were unable to annotate several peaks that may contain important information. This is reflected in the MSEA analysis which, based on the Fisher's exact test, highlighted only few pathways that were altered following denervation. Nevertheless, by analysing specific metabolites it was speculated that denervation is able to induce insulin resistance in denervated muscle fibres with inhibition of glycolysis, possibly limiting the ETC activity and activating several proteolytic and apoptotic pathways.

Chapter 6. Age-related skeletal muscle denervation and its effect on muscle structure

6.1 Introduction

In normal physiology the neuromuscular system goes through continuous modifications and adaptations (Hepple and Rice, 2016). Among these series of adaptations, of particular relevance is the denervation-reinnervation cycle (Aare et al, 2016). The efficiency of this cycle is reduced with the advancing age with a major impact on muscle health and function (Jang and Van Remmen, 2011). In a study aimed to analyse the stability of NMJs in C57BL6 mice, Balice-Gordon and colleagues (1997) found that the stability of the NMJs tends to decrease around 12-18 months of age with a significant loss of motor terminal branches and a reduction of post-synaptic receptors in the muscles. These changes induce several physiological adaptive responses in the motor units affected by the lack of NMJ stability. For example, in order to compensate for the loss of synaptic contact, motor axons respond with nerve sprouting to create new junctions. However, this compensatory response is far from being efficient given that newly formed junctions are unstable, vulnerable and can be quickly lost, explaining the decrease in motor units seen during ageing (Balice-Gordon et al, 1997; Jang and Van Remmen, 2011). This decrease is also accompanied by a shift in protein metabolism from protein synthesis to protein degradation with loss of muscle mass and an increased proportion of connective tissue within the muscle (Park, 2015). These changes have a severe impact on health and quality of life of older people. Therefore, to consider the neuromuscular system in its entirety becomes mandatory for scientists wishing to understand the process that leads to sarcopenia (Vellas et al, 2018).

The first aim of the present study was to evaluate the age-related changes in nerve-muscle interactions at different time points during adulthood and ageing in mice, this in order to understand whether the age-related loss in the stability of the NMJs precedes skeletal muscle loss or *vice versa*. In the present study we also aimed to investigate whether

the redox-related changes observed in our denervation model also occur during skeletal muscle ageing since muscle denervation appears to be a key characteristic of sarcopenia.

6.2 Materials and Methods

6.2.1 Mice strain

In the present study 28 B6.Cg-Tg(Thy1-YFP)16Jrs/J$^{(+/-)}$ both male and female were bred within the Biomedical Service Unit at the University of Liverpool. Mice were divided in groups of 4 (2 males and 2 females) and sacrified at: 6, 12, 15, 18, 21, 24, 27 months of age. Experiments were performed in accordance with United Kingdom Home Office guidelines under the United Kingdom Animals (Scientific Procedures) Act 1986 as presented in section 2.1.

6.2.2 Samples preparation for immunohistochemical analysis

For immunohistochemical analysis, samples were prepared as described in section 2.3.4.

6.2.3 WGA Staining

Wheat germ agglutinin (Vector Lab, Burlingame, CA, USA) was used to stain the slides for cross sectional area analysis. The samples were treated as explained in section 2.10 and examined using a Zeiss LSM 800 confocal microscope (Zeiss, Oberkochen, Germany).

6.2.4 Myosin Heavy Chain immunostaining

Following defrosting (30 minutes at room temperature), sections were rehydrated in PBS for 10 minutes (2x5 minutes) and blocked in PBS containing M.O.M blocking (Vector Lab, Burlingame, CA,USA) with 5% goat serum for 1 hour at room temperature. Sections were then incubated with MyHC-IIa primary antibody (1:250, Developmental Studies Hybridoma Bank, Iowa, USA) overnight at 4ºC. The following day, sections were washed with PBS-T20 3 times for 5 minutes each. Goat Anti-Mouse IgG1 secondary antibody conjugated with Alexa Fluor 647 (1:500 in PBS with 12% Goat Serum - Invitrogen, Paisley, United Kingdom) was added to each slide for 60 minutes

at room temperature. Sections were washed with PBS-T20 3 times for 5 minutes each and were then incubated overnight with MyHC-I antibody (Abcam, Cambridge, United Kingdom) conjugated with Alexa Fluor 408 using the Bio-Rad kit (Bio-Rad, Hercules, CA, USA). The following day, sections were washed with PBS-T20 as described before and the antibody for MyHC-IIb (1:250, Developmental Studies Hybridoma Bank, Iowa, USA) was added overnight. Following overnight incubation and washing, samples were incubated with the goat Anti-Mouse IgM secondary antibody conjugated with Alexa Fluor 488 (1:500 in PBS with 12% Goat Serum - Invitrogen, Paisley, United Kingdom) for 1 hour at room temperature. At this point, sections were stained with Rhodamine WGA (1:1000 Vector Lab, Burlingame, CA, USA) following the protocol previously described (Section 2.11). Sections were visualised using confocal microscopy at 10x magnification and analysed using ImageJ software.

6.2.5 SDS-PAGE and western blot analysis

Thirty micrograms of total protein from the TA muscle were added to 4μL of Blu-mercaptoethanol (4x) and ddH_2O to reach a final volume of 16μL. SDS-PAGE and western blot analysis was performed as previously described (section 2.5). Ponceau red (Sigma-Aldrich, St. Louis, MI, USA) was used to verify the effectiveness of the transfer procedure and to normalise the results as described in Appendix 1. Densitometry analysis was performed using the ImageJ software following the protocol described by McLean (2011).

6.2.6 Assessments of Neuromuscular junctions

B6.Cg-Tg(Thy1-YFP)16Jrs/$J^{(+/-)}$ mice express a yellow fluorescent protein in their nervous system that allows detection and analysis via confocal fluorescent microscopy with excitation at 488nm. To fully examine the NMJ, the acetylcholine receptors were also stained with α-bungarotoxin conjugated with Alexa-642 as explained in section

2.11. Samples were analysed using a Nikon intravital confocal microscope (Nikon A1, Kingston, United Kingdom).

6.2.7 Neuromuscular junction analysis with ImageJ

Fifty to 100 NMJs from each group were analysed to determine different structural parameters that change with ageing including: area of synaptic contact, complexity, fragmentation, overlap of post-synaptic terminals. This analysis was performed on ImageJ using the BinaryConnectivity plugin developed by Landini (available at https://blog.bham.ac.uk) and following the protocol described by Jones and colleagues (2016) and summarised in *Figure 6.1*. Full and partial innervation cut points were determined as follow: Fully innervated (100-80% overlap), partially innervated (80-15% overlap) and denervated (<15%). Denervated post-synaptic receptors were analysed manually using ImageJ software to determine number and max Feret's diameter.

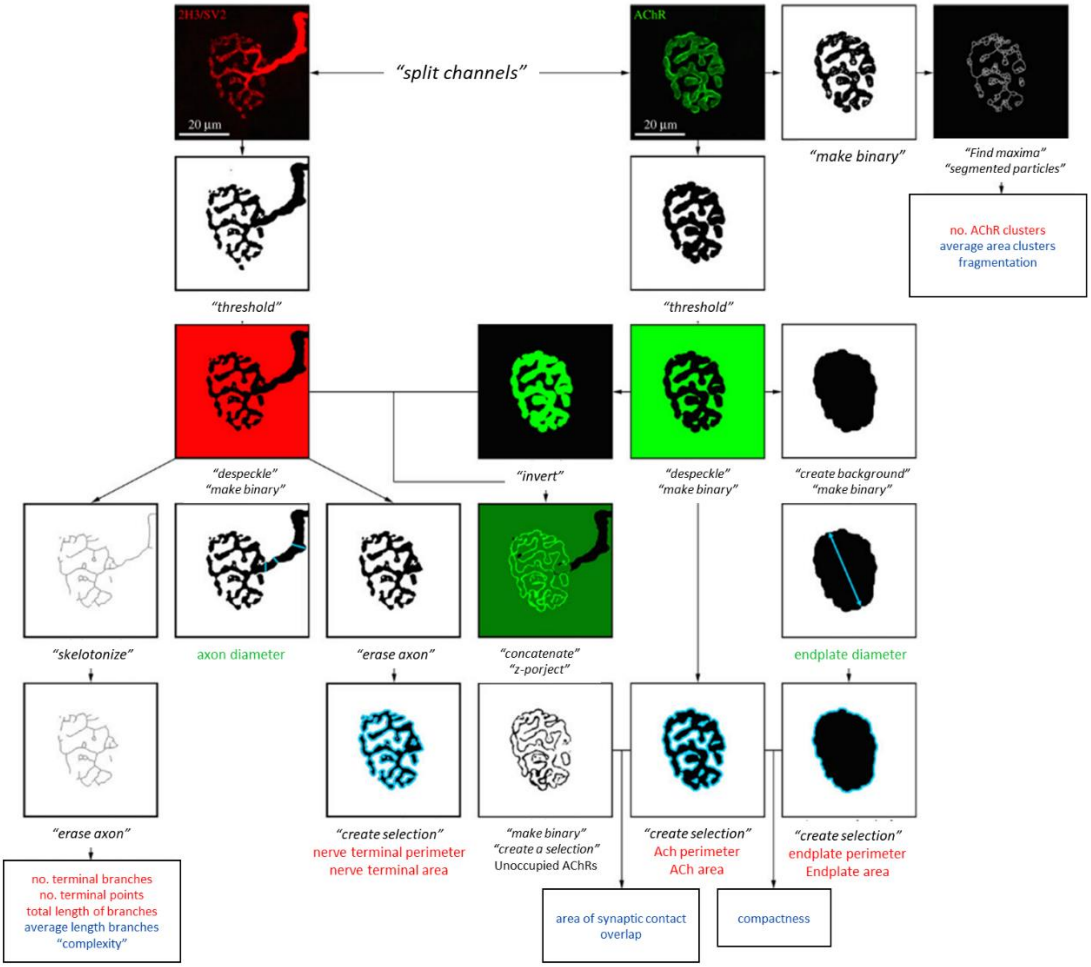

Figure 6.1. *Schematic representation of the steps necessary to analyse the NMJ structure using the ImageJ extension Binary connectivity. (Image adapted from Jones et al, 2016).*

6.3 Results

6.3.1 Anthropometric measurements

No statistically significant changes in the body weight were observed with ageing (*Figure 6.2a*). We observed a slight tendency to a decrease in the TA muscle mass starting at 18 months that did not reach statistical significance (*Figure 6.2b*). Similarly, analysis of the EDL muscle weight, showed a tendency to a progressive decrease in the mean muscle mass starting around 18 months which did not reach statistical significance (*Figure 6.2c)*. The analysis of the TA muscle fibre minimum Feret's diameter showed a trend with a decrease in large muscle fibres (50-60.1 and 60+ thresholds) in favour of medium size fibres (40.1-50.1 threshold). However, these changes were not statistically significant $F(30, 62) = 0.747$, $p > 0.05$; Wilk's $\Lambda = 0.291$, partial $\eta 2 = 0.219$ (*Figure 6.2d*).

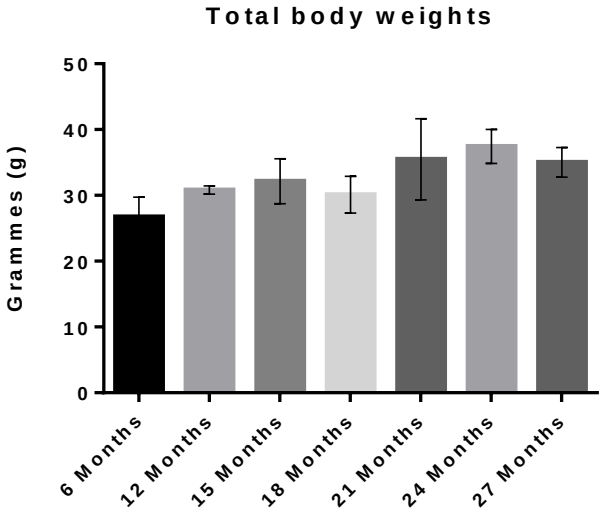

Figure 6.2a. *Total body weights from mice sacrified at different ages: 6, 12, 15, 18, 21, 24 and 27 months. Histograms represent the mean and the standard error of the mean for each experimental group (n=4).*

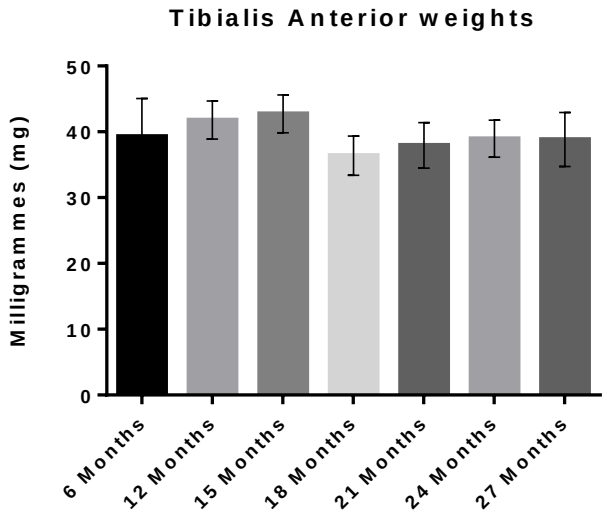

Figure 6.2b. *Tibialis Anterior muscle weights from mice sacrified at different ages: 6, 12, 15, 18, 21, 24 and 27 months. Histograms represent the mean and the standard error of the mean for each experimental group (n=4).*

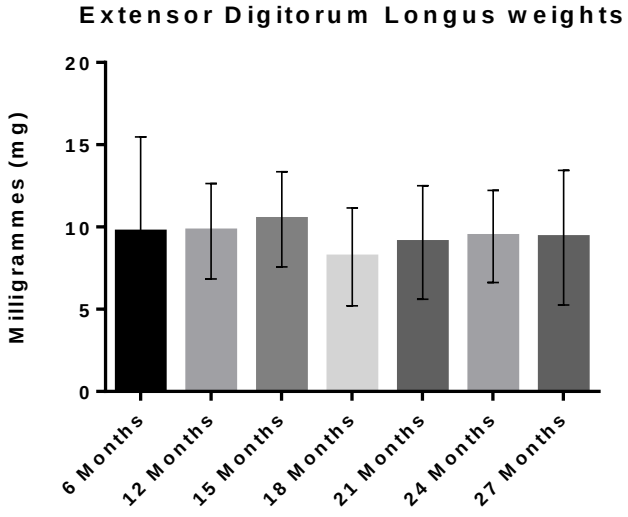

Figure 6.2c. *Extensor Digitorum Longus muscle weights from mice sacrified at different ages: 6, 12, 15, 18, 21, 24 and 27 months. Histograms represent the mean and the standard error of the mean for each experimental group (n=4).*

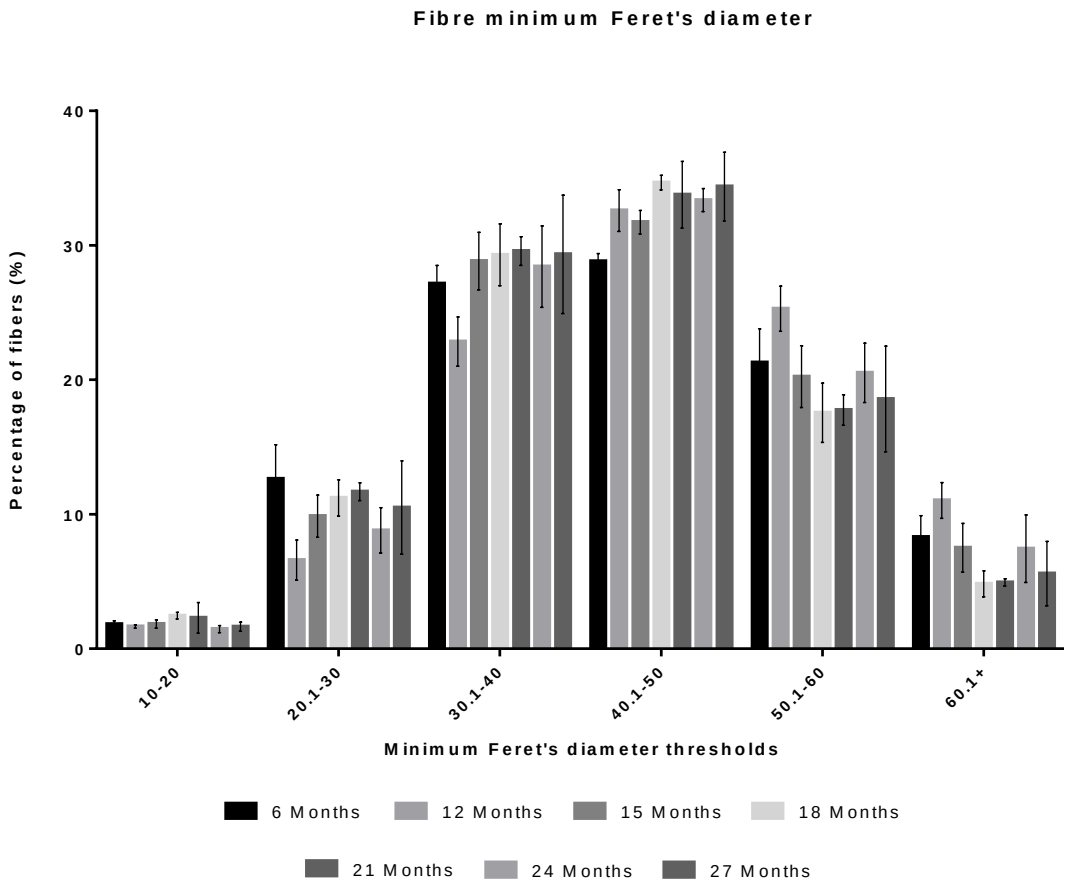

Figure 6.2d. *Muscle fibre minimum Feret's diameter. Histograms represent the mean and standard error of the mean of the percentage of fibres counted in each threshold (10-20, 20.1-30, 30.1-40, 40.1-50, 50.1-60, 60.1+) for each experimental group: 6, 12, 15, 18, 21, 24 and 27 months.*

6.3.2 Age-related changes of the neuromuscular junction

Although high variability was seen, significant changes occurred at the NMJ level. The BinaryConnectivity plugin allowed the analysis of several parameters related to the NMJ morphology. Analysis of the numbers of fully innervated, partially innervated and denervated post-synaptic terminals shows a progressive reduction in fully innervated post-synaptic terminals that was statistically significant at 24 and 27 months of age with a significant increase in denervated acetylcholine receptors at 27 months of age $F(18,99) = 3.999$, $p > 0.05$; Wilk's $\Lambda = 0.214$, partial $\eta^2 = 0.401$ (*Figure 6.3a*).

Significant changes were also seen in average overlap between the pre- and post-synaptic terminals of the NMJ $F(6,285)=5.393$ $p<0.05$ (*Figure 6.3b*), area of synaptic contact $F(6,285)=3.081$ $p<0.05$ (*Figure 6.3c*), post-synaptic receptors area $F(6,297)=5.401$ $p<0.05$ (*Figure 6.3d*) and diameter $F(6,297)=10.376$ $p<0.05$ (*Figure 6.3e*). With ageing there was also a progressive increase in nerve sprouting and "*blebbing*" and an example is presented in F*igure 6.4.*

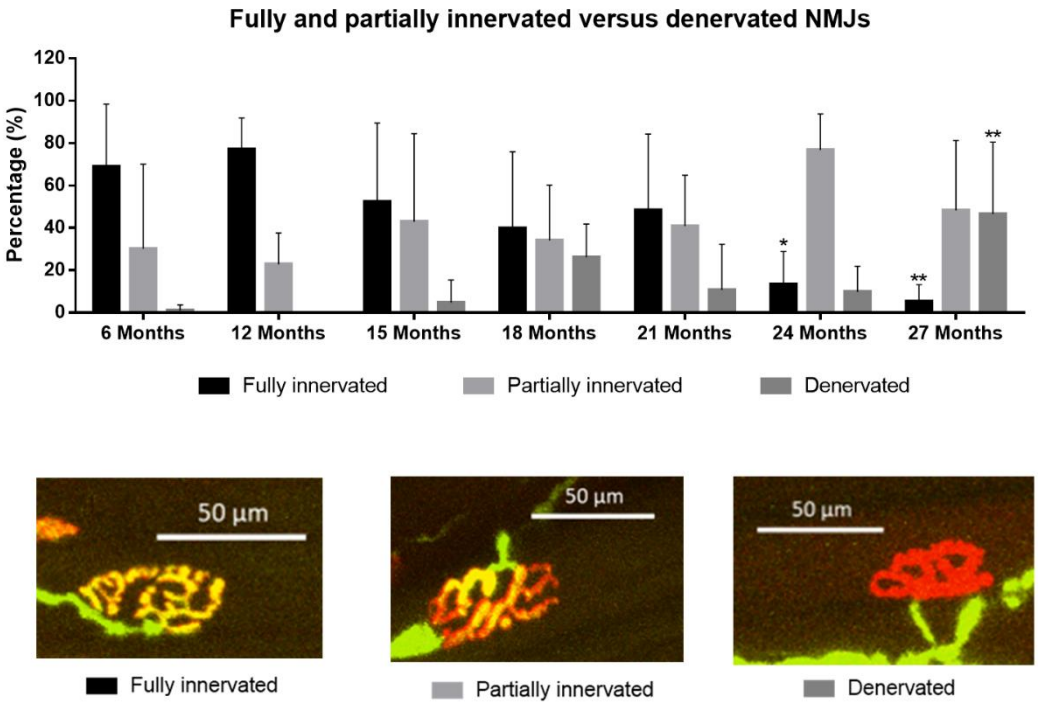

Figure 6.3a. *Percentage of fully innervated (Black - 100-80% overlap), partially innervated (Light grey - 79-15% overlap) and denervated (Dark grey - <15% overlap) acetylcholine receptors together with representative NMJs. Histogram represent the percentage of overlap of the NMJs for each experimental group: 6, 12, 15, 18, 21, 24 and 27 months.*
** $p<0.05$ - ** $p<0.01$ compared with the 6 months group.*

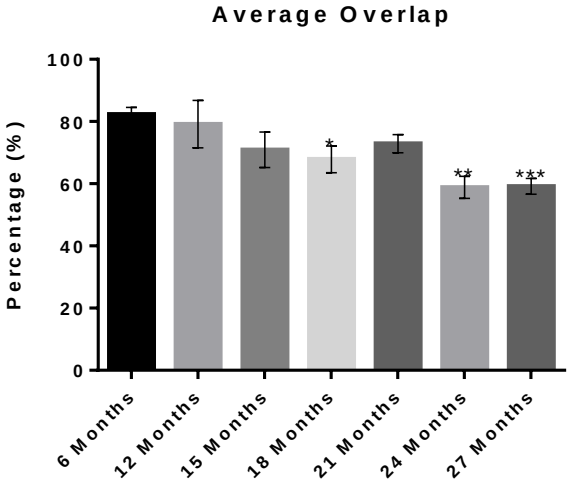

Figure 6.3b. *Average overlap between the motor neuron and the post-synaptic receptors from mice sacrified at different ages: 6, 12, 15, 18, 21, 24 and 27 months. Histograms represent the mean and the standard error of the mean for each experimental group (n=4).*
** p<0.05 - ** p<0.01 - *** p<0.001 compared with the 6 months group.*

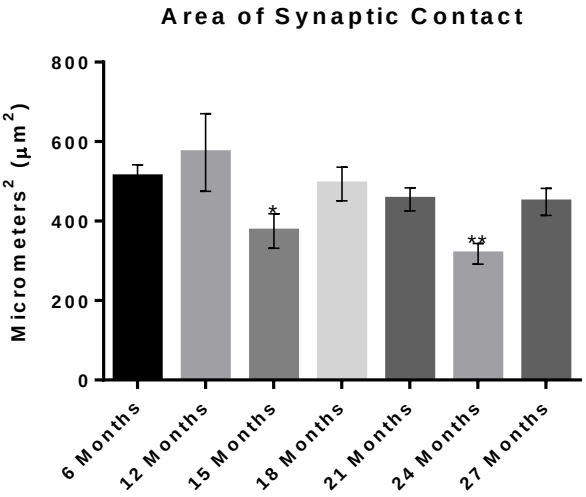

Figure 6.3c. *Analysis of the Area of synaptic contact between motor neurons and post-synaptic receptors from mice sacrified at different ages: 6, 12, 15, 18, 21, 24 and 27 months. Histograms represent the mean and the standard error of the mean for each experimental group (n=4).*
** p<0.05 - ** p<0.01 compared with the 6 months group.*

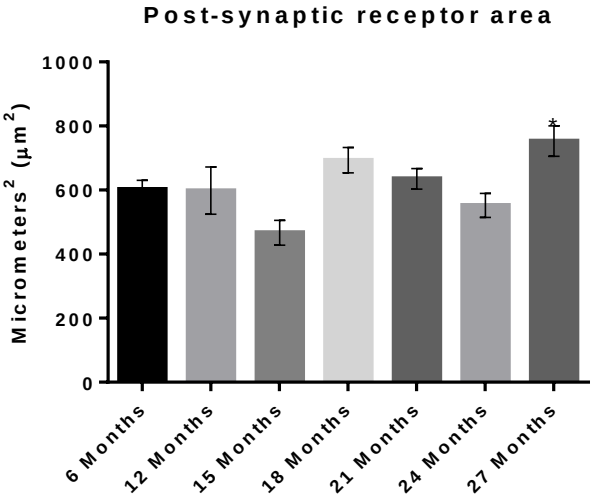

Figure 6.3d. *Analysis of the post-synaptic receptors area from mice sacrified at different ages: 6, 12, 15, 18, 21, 24 and 27 months. Histograms represent the mean and the standard error of the mean for each experimental group (n=4).*
** p<0.05 compared with the 6 months group.*

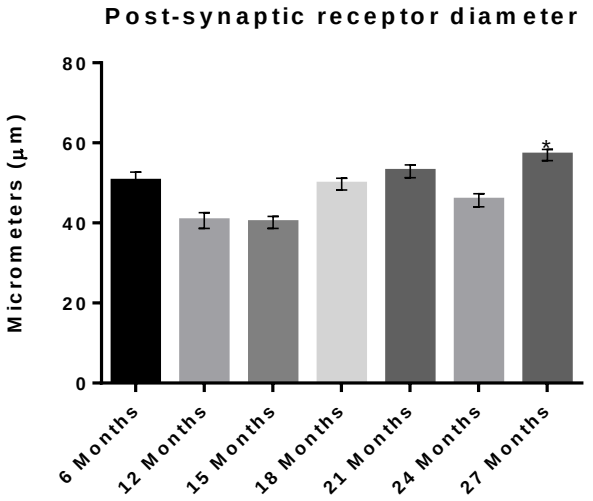

Figure 6.3e. *Analysis of the post-synaptic receptors diameter of acetylcholine receptors from mice sacrified at different ages: 6, 12, 15, 18, 21, 24 and 27 months. Histograms represent the mean and the standard error of the mean for each experimental group (n=4).*
** p<0.05 compared with the 6 months group.*

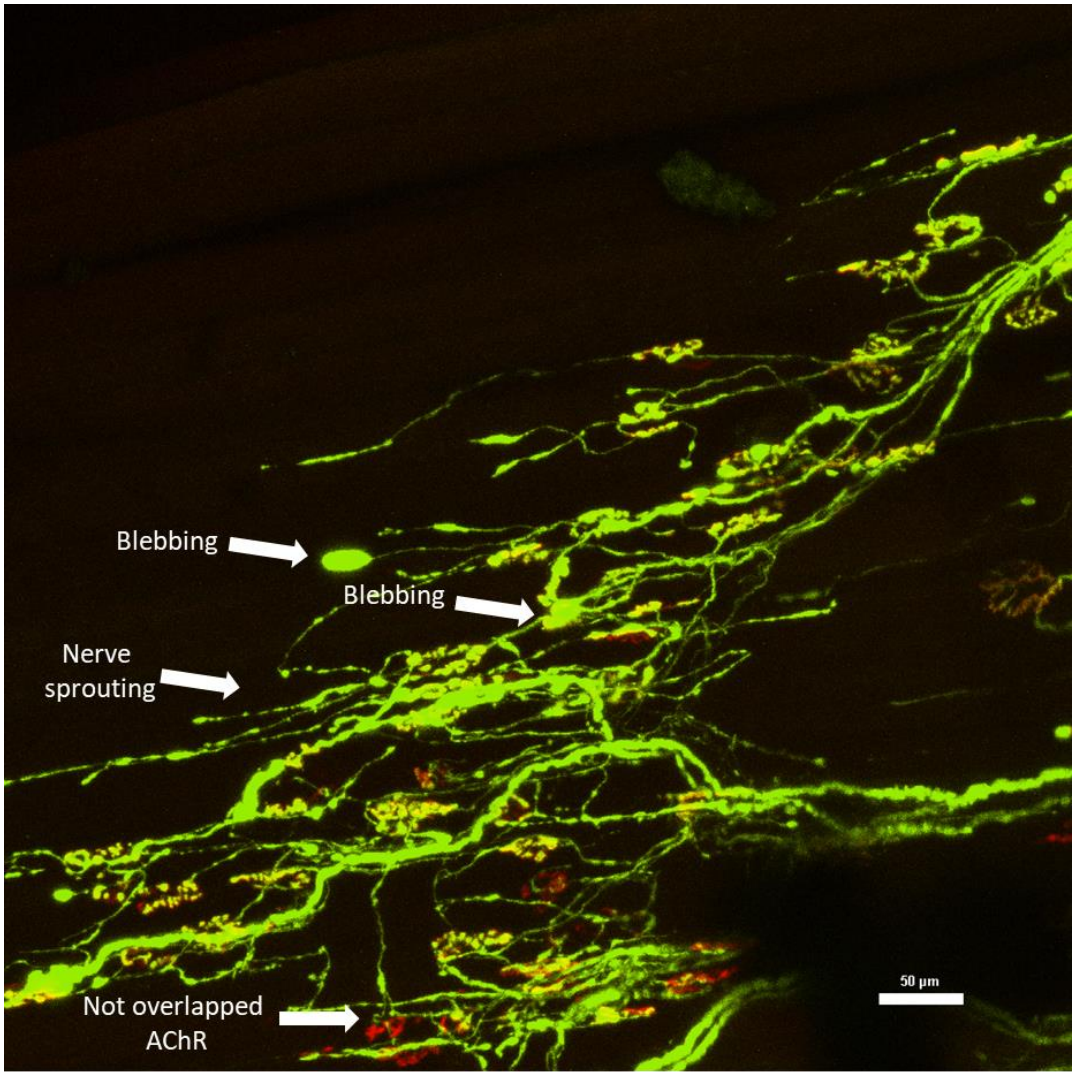

Figure 6.4. *Representative image of muscle innervation obtained from a 27 months old mouse. Axon branches (green), acetylcholine receptors (red) and NMJs (yellow) formed by the overlap between the pre-synaptic terminal and the acetylcholine receptors.*

6.3.3 Analysis of changes of muscle structure and composition

Analysis of the MyHC isoforms present in the TA muscle showed significant changes associated with ageing $F(18,43) = 2.564$, $p < 0.05$; Wilk's $\Lambda = 0.127$, partial $\eta^2 = 0.498$ (*Figure 6.5*). With the exception of few sporadic fibres, no fibres expressing the MyHC-I isoform in the TA muscle were seen. With ageing there was a significant reduction in the number of fibres expressing MyHC-IIa with advancing age (*Figure 6.5*). In contrast MyHC-IIb fibres showed a statistically significantly increase at 27 months of age. MyHC-IIx fibres showed a significant decrease at 27 months (*Figure 6.5*).

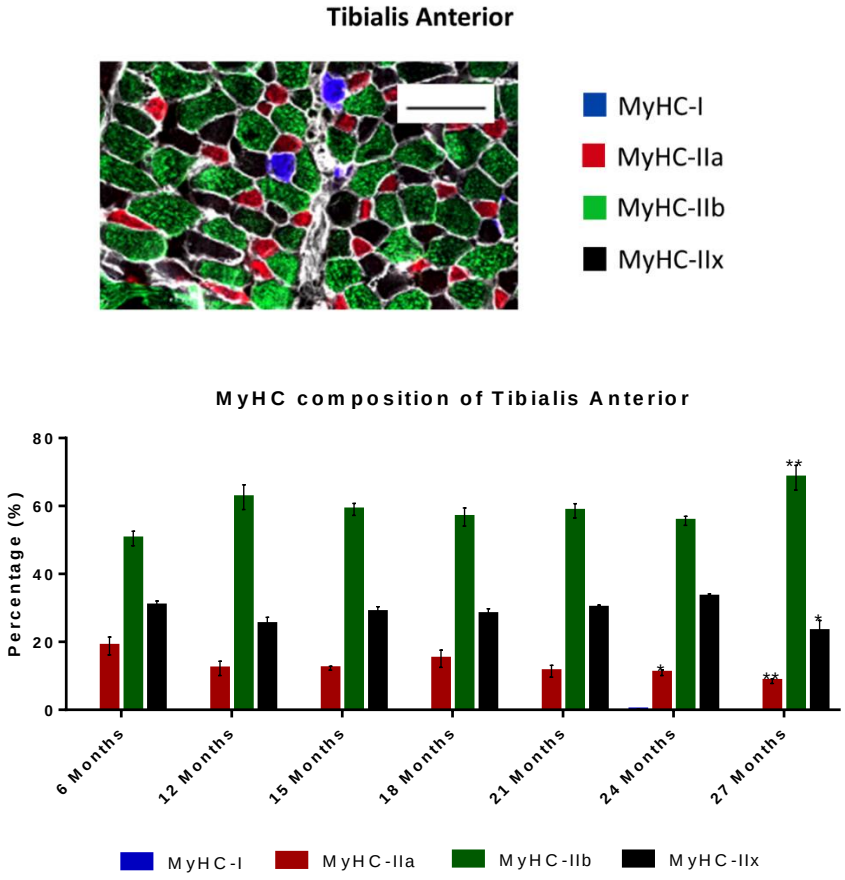

Figure 6.5. *Representative image of a TA muscle (scale bar 100μm) stained for the four myosin heavy chain isoforms present in murine muscle: MyHC-I (Blue), MyHC-IIa (Red), MyHC-IIb (Green) and MyHC-IIx (Black).*
Histograms represent the mean percentage of fibres expressing one of the 4 myosin heavy chain isoforms in tibialis anterior muscle and the standard error of the mean for each experimental group: 6, 12, 15, 18, 21, 24 and 27 months.
** $p<0.05$ - ** $p<0.01$ compared with the 6 months group.*

6.3.4 Age-related changes in neuromuscular junction markers

Analysis of the protein contents of Agrin (*Figure 6.6a*) and MuSK (*Figure 6.6b*) failed to show significant changes with ageing.

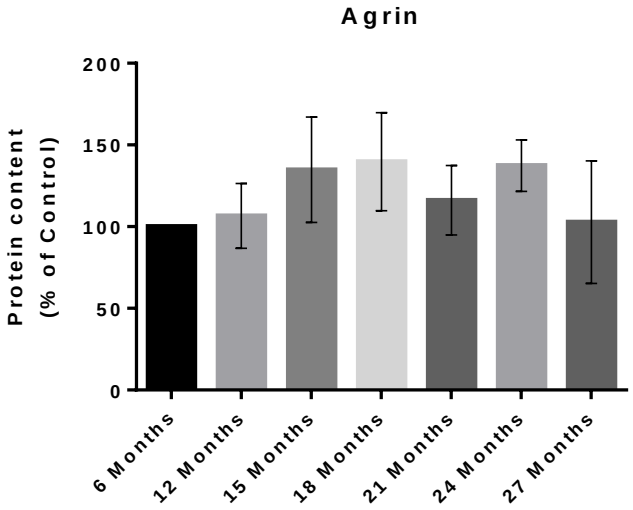

Figure 6.6a. *Agrin protein content of Tibialis Anterior muscle from mice sacrified at 6, 12, 15, 18, 21, 24 and 27 months. Histograms represent the mean and the standard error of the mean for each experimental group (n=4).*

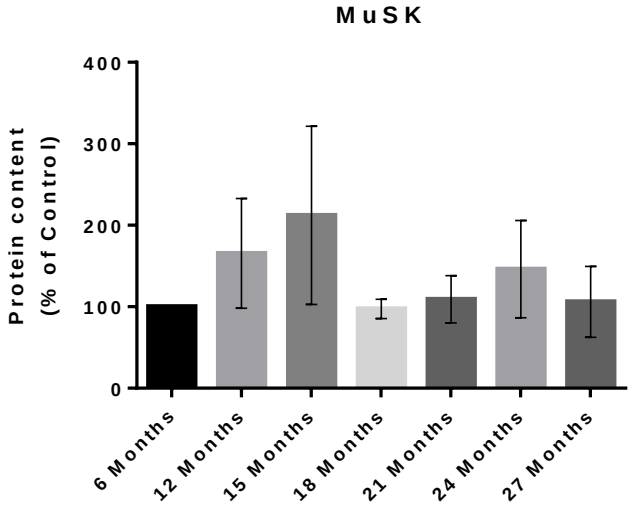

Figure 6.6b. *MuSK protein content of Tibialis Anterior muscle from mice sacrified at 6, 12, 15, 18, 21, 24 and 27 months. Histograms represent the mean and the standard error of the mean for each experimental group (n=4).*

6.3.5 Age-related changes in protein content of antioxidant enzymes

No changes in CuZnSOD (*Figure 6.7a*), MnSOD (*Figure 6.7b*), GPx1 (*Figure 6.7c*) and Catalase (*Figure 6.7d*) proteins content were observed during ageing.

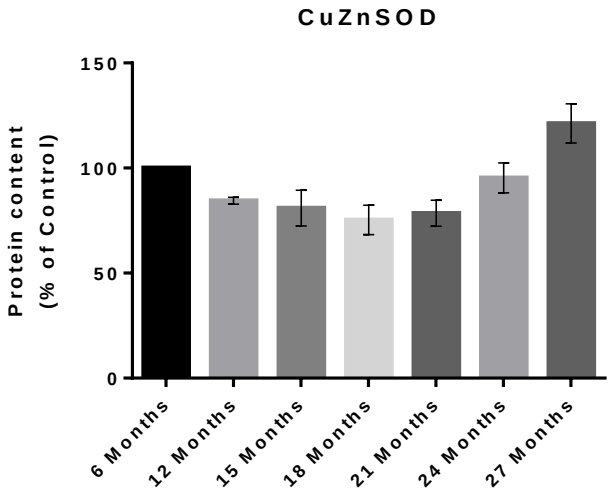

Figure 6.7a. *CuZnSOD protein content of Tibialis Anterior muscle from mice sacrified at 6, 12, 15, 18, 21, 24 and 27 months. Histograms represent the mean and the standard error of the mean for each experimental group (n=4).*

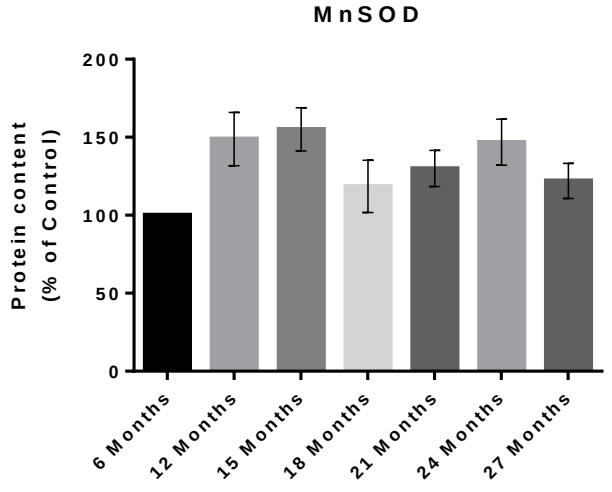

Figure 6.7b. *MnSOD protein content of Tibialis Anterior muscle from mice sacrified at 6, 12, 15, 18, 21, 24 and 27 months. Histograms represent the mean and the standard error of the mean for each experimental group (n=4).*

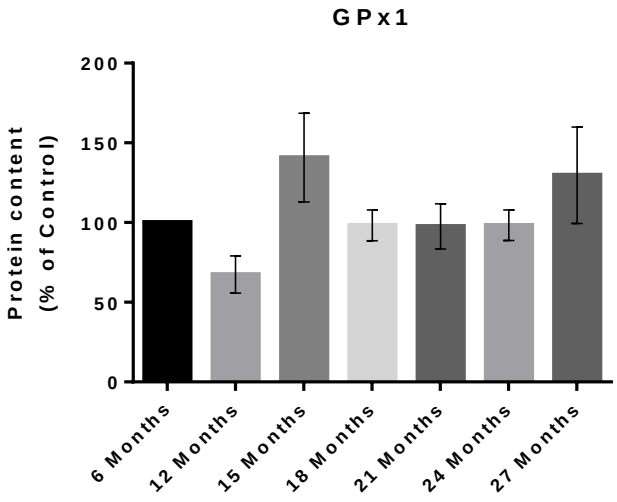

Figure 6.7c. *GPx1 protein content of Tibialis Anterior muscle from mice sacrified at 6, 12, 15, 18, 21, 24 and 27 months. Histograms represent the mean and the standard error of the mean for each experimental group (n=4).*

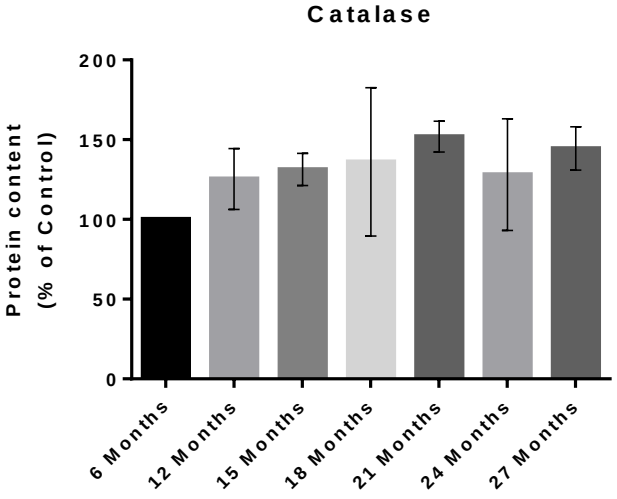

Figure 6.7d. *Catalase protein content of Tibialis Anterior muscle from mice sacrified at 6, 12, 15, 18, 21, 24 and 27 months. Histograms represent the mean and the standard error of the mean for each experimental group (n=4).*

6.3.6 Age-related changes in autophagy/mitophagy and apoptosis markers

Analysis of p62 (*Figure 6.8a*) and of the BAX/Bcl-2 ratio (*Figure 6.8b*) did not show any statistically significant changes with ageing.

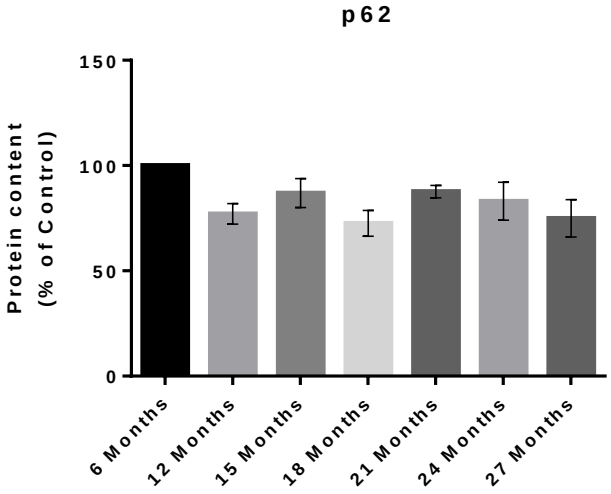

Figure 6.8a. *p62 protein content of Tibialis Anterior muscle from mice sacrified at 6, 12, 15, 18, 21, 24 and 27 months. Histograms represent the mean and the standard error of the mean for each experimental group (n=4).*

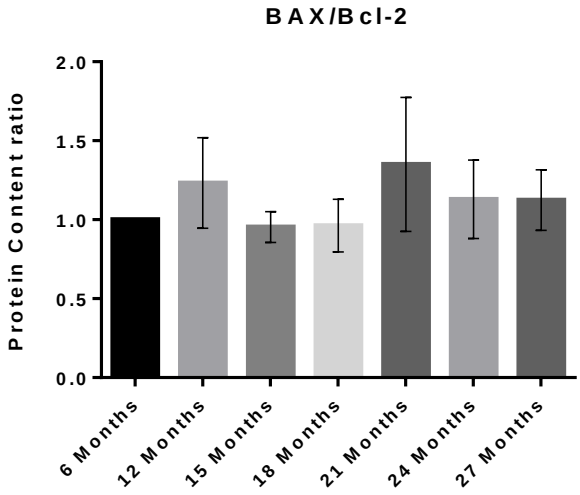

Figure 6.8b. *BAX/Bcl-2 ratio of Tibialis Anterior muscle from mice sacrified at 6, 12, 15, 18, 21, 24 and 27 months. Histograms represent the mean and the standard error of the mean for each experimental group (n=4).*

6.4 Discussion

Ageing is a multifactorial process that affects the majority of tissues in the body (Bulla and Shafwe, 2011). One of the tissues most affected by ageing is skeletal muscle that, in humans, after reaching a peak in muscle mass around the age of 24, experiences a progressive loss that from the age of 50 accelerates to up to 10% per decade (Lexell et al, 1988). Sarcopenia, the loss of muscle mass, strength and functionality has a tremendous impact on the health and quality of life of older adults (Baumann et al, 2016). To limit and prevent sarcopenia, a better understanding of this disease is essential but it is still unclear which factors play a primary role in inducing the loss of muscle mass and strength typically seen in sarcopenic patients.

Previous reports have suggested that muscle fibre denervation may be one of the main factors responsible for the significant loss of muscle mass and functionality observed with ageing (Jang and Van Remmen, 2011; Aare et al, 2016; Hepple and Rice, 2016). During ageing, changes occurring at the level of the NMJ are known to trigger a series of consequences that can have a direct effect on the skeletal muscles (Jang and Van Remmen, 2011; Hepple and Rice, 2016). The process of denervation-reinnervation is a normal process that involves the NMJs and gives the skeletal muscle the plasticity necessary to continuously adapt to external stimuli (Hepple and Rice, 2016). Previous studies have reported that with ageing the efficiency of this process tends to decrease inducing decreased pre- and post-synaptic overlap at the NMJ level, altered distribution of laminin, post-synaptic receptors disruption and nerve sprouting (Balice-Gordon, 1997; Jang and Van Remmen, 2010; Samuel et al, 2012).

In line with these previous studies the analyses presented here of the area of synaptic contact in young (6 months), adult (12-18 months) and old (21-27 months) mice showed a pattern that suggests an age-related impairment of the neuromuscular system with a

progressive reduction of the area of synaptic contact (*Figure 6.3c*) that was statistically significant at 24 months. Furthermore, there was also an age-related reduction in the average overlap between the pre- and post-synaptic terminals (*Figure 6.3b*). This progressive reduction of the average overlap suggests a progressive deterioration of the NMJ but may also lead to false conclusions. As suggested by Pennefather and Quastel (1981), only an overlap lower as 15% would significantly compromise the NMJ functionality preventing muscle fibre contraction. To provide a better understanding of the age-related changes occurring in the NMJs, data has been presented as percentages of post-synaptic terminals defined by the programme as fully innervated (100-80% overlap), partially innervated (79-15% overlap) and denervated (<15% overlap) (*Figure 6.3a*). The percentage of fully innervated post-synaptic terminals decreases with ageing and this is accompanied by an increase in denervated post-synaptic terminals that becomes significant at 27 months of age. Previous studies have also reported a progressive breakdown of post-synaptic receptors not appropriately connected with the nerve terminal (Hepple and Rice, 2016; Pollock et al, 2017). In the present study, the progressive reduction in the area of synaptic contact (*Figure 6.3c*) was accompanied by an age-related increase in both post-synaptic receptor area (*Figure 6.3d*) and diameter (*Figure 6.3e*) resulting from the progressive breakdown of denervated post-synaptic terminals.

The content of important bio-markers that play a role in maintaining the NMJ stability was examined. Agrin is a large proteoglycan located in the basal lamina of the muscle cells and is responsible for the clustering and localisation of post-synaptic receptors on the muscle fibre surface (Samuel et al, 2012). During development, a specific agrin isoform (z-agrin) is secreted by the nerve inducing phosphorylation and activation of MuSK a high-affinity cell surface receptor that plays a fundamental role in the formation and maintenance of the NMJ. Upon activation of MuSK by z-agrin through the activity

of casein kinase 2, Dok-7 and rapsyn (Cheusova et al, 2006; Okada et al, 2006) the clustering and formation of the post-synaptic receptors is stimulated (Samuel et al, 2012). A study focused on understanding the role of agrin in adult NMJs (Samuel et al, 2012) found that depletion of agrin induces several consequences such as:

- Loss of acetylcholine receptors aggregates;
- Depletion of important components of the post-synaptic membrane, rapsyn, and laminins α-4 and α-5;
- Remodelling of the nerve terminal and eventual loss of the connection between the motoneuron and the post-synaptic terminal.

These alterations resulted in a phenotype similar to the one seen in aged wild type mice supporting the speculation that agrin plays a fundamental role not only in the development of the NMJ but also in its maintenance. In the present study we observed no significant changes in agrin or MuSK protein contents despite the progressive disruption of the NMJ with ageing. Samuel and colleagues (2012) also failed to see such changes with ageing. These authors suggested that during ageing, it may be an alteration in the distribution of these proteins that potentially affects the stability of the NMJs rather than reduction of the protein contents and activities (Samuel et al, 2012).

Loss of stability of the NMJ can trigger responses that allows a neighbouring axon to re-innervate the denervated post-synaptic receptors (Kung et al, 2014; Greising et al, 2015). This phenomenon known as nerve sprouting (presented in *Figure 6.4*) is also accompanied by the appearance of NMJ "*blebbing*". The origin, role and function of these protuberances are still poorly understood. Formation of these structures (presented in *Figure 6.4*) appears symptomatic of nerve deterioration and ineffectiveness in stabilising the NMJ, even when these overlap with an ACh receptor. In the context of

this study nerve sprouting and "*blebbing*" were observed starting around 12 months of age with a progressive increase in frequency up to 27 months of age.

As suggested by Hepple and Rice (2016) and as briefly introduced earlier, nerve sprouting can be seen following the disruption of the NMJ as a nearby motoneuron attempts to restore the connection with an unoccupied post-synaptic terminal. However, even if this physiological attempt of restoring the NMJs succeeds in re-establishing a connection between the nerve and the muscle cell, these newly formed NMJs are very unstable and can be lost within few weeks from formation (Jang and Van Remmen, 2011; Hepple and Rice, 2016). When unstable NMJs are lost, some structural changes can also be observed at muscle fibre level. Denervated fibres quickly become more angular, atrophy and will eventually be lost over longer term (Hepple and Rice, 2016) reinforcing the hypothesis that impairments at the NMJs level may play a central role in sarcopenia (Kent-Braun et al, 2000; Lexell et al, 1988; Williams et al, 2002; Baumann et al, 2016). In the present study it was not possible to perform an accurate analysis of the muscle fibre number as some sections presented significant cryo-damage. Despite this limitation, we were able to analyse the muscle fibre Feret's diameter observing high variability in our groups. Our results showed a trend towards a loss of large muscle fibres (50.1-60 and 60+ thresholds - *Figure 6.2d*) commencing at 18 months of age, however this loss did not reach statistical significance.

When nerve sprouting is successful, it has the potential to restore the NMJ inducing alterations in the muscle fibre composition (fibre clustering) and changes in the muscle fibre contractile properties through the modification of the MyHC isoform of the reinnervated fibres (Maggs et al, 2008; Kung et al, 2014; Greising et al, 2015). Murine muscle fibre composition of specific muscles differs significantly from humans (Augusto et al, 2004). For instance, in the murine lower hind limb, the soleus muscle is the muscle

that presents a high percentage of MyHC-I fibres and, with around 40% percent of slow twitch muscle fibres (Augusto et al, 2004), is comparable to the human vastus lateralis (Staron et al, 2000). Tibialis Anterior in mice is composed of less than 1% of MyHC-I type fibres and in the present analysis this isoform was not detected in the majority of the samples. To guarantee that the lack of detection of MyHC-I fibres in our samples was due to the absence of this isoform rather than an issue with the staining protocol, alongside the TA a soleus muscle was also stained as a control (*result not shown in detail*).

With ageing we observed a decrease in fibres expressing MyHC-IIa at 24 and 27 months of age while the percentage of MyHC-IIx fibres remained stable until 27 months of age when a significant reduction was observed. The loss of MyHC-IIa and MyHC-IIx appeared to be in favour of MyHC-IIb which showed a statistically significant increase at 27 months of age. The mouse TA muscle mainly expresses the MyHC-IIb isoform with a high density of fast contracting motoneurons (Augusto et al, 2004) explaining the progressive switch from MyHC-IIa and MyHC-IIx fibres toward MyHC-IIb fibres. These modifications result in fibre clustering, a situation where two or more fibres of the same type present adjoining sarcolemma (Greising et al, 2015). Fibre clustering is a condition typical of ageing that, despite not having a direct impact on muscle functionality (Baumann et al, 2016) is symptomatic of sarcopenic muscles. This result reinforces the hypothesis that impairment at the NMJ level can have a direct effect on skeletal muscle structure and functionality.

During ageing, alongside the progressive impairment of the neuromuscular system, there is also a significant increase in H_2O_2 accumulation resulting in oxidative stress (Stefanatos and Sanz, 2017; Staunton et al, 2019). As mentioned earlier in this chapter, one of the aims of the present work was to determine whether the adaptive response to the

significant increase in peroxide release that we observed in our denervation model, also occurs during ageing. Our work in full denervation model has demonstrated that in the first days (between day 1 and day 7) post-denervation, the antioxidant system responded by increasing the content of the antioxidant enzyme GPx1 (section 3.3.8) while we did not observe any significant change in MnSOD content. Similarly, in our ageing model we did not observe any significant change in MnSOD content and these results are in line with what previously reported by Brown and colleagues (2007) showing that during ageing the levels of MnSOD remain stable. Previous studies from our group (Palomero et al, 2013) have reported a significant increase in GPx1 activity in skeletal muscle during ageing. GPx1 is an enzyme mainly located in the cytosol and mitochondria and is able to catalyse the reduction of H_2O_2 into water also catalysing the reduction of lipid peroxides into alcohols (Brigelius-Flohé and Maiorino, 2013). In the present study we failed to show a similar increase in GPx1 protein content; however, activity was not measured and the possibility that this is increased during ageing cannot be excluded.

The protein content of CuZnSOD and catalase, two proteins that have been proposed to play an important role during ageing were also examined. Previous studies showed that overexpression of CuZnSOD and catalase were capable of extending the lifespan of drosophila melanogaster (Orr and Sohal, 1994; Orr et al, 2003). However, these results were never replicated in mammalian models (Orr et al, 2003). Lack of CuZnSOD has been associated with an early and progressive modifications in muscle innervation including: fragmentation of the endplate, nerve sprouting and partial or no overlap between the motor neuron and the post-synaptic receptors in the NMJs (Sakellariou et al, 2014b; Park, 2015). Models overexpressing catalase have shown protection of mitochondria with reduced oxidative stress, increased genomic stability resulting in a significant

maintenance of skeletal muscle structures and functions (Schriner et al, 2005; Umanskaya et al, 2014). Previous studies from our group showed that during ageing there is a significant increase in CuZnSOD and catalase enzymes activities (Vasilaki et al, 2006b; Palomero et al, 2013), but in the present study no significant age-related alterations in CuZnSOD and catalase contents were seen compared to the 6 months old group. Nevertheless, we cannot exclude the possibility that, despite the lack of changes observed in protein content, there may be an alteration of these enzymes activities similar to those previously reported by our group.

In chapter 4 we described how mitochondria of denervated skeletal muscle fibres can play a fundamental role in driving muscle atrophy with an increase of the BAX/Bcl-2 ratio resulting in a significant increase in activity of executional caspases, including caspase-3. When activated, this protein is able to induce protein degradation enhancing the activity of the 26S proteasome through the cleavage of Rpt2 and Rpt6 (Wang et al, 2010). We previously speculated that the activation of this pathway is directly related to the significant increase in peroxide release from enzymes not involved in the ETC able to damage mitochondria and impair mitophagy. In contrast to the denervation models, we did not observe any accumulation of p62 suggesting that, in our ageing model, there may be correct recycle of damaged mitochondria and misfolded proteins with no activation of the 26S proteasome through the Bcl-2 family. This may be related to the lack of muscle atrophy observed in the present study as previous studies suggested that a close correlation exists between activation of apoptosis pathways and skeletal muscle atrophy (Dupont-Versteegden, 2006).

In summary, our results suggest that with ageing there is a progressive impairment of the NMJ that induces nerve sprouting and progressive loss of pre- and post-synaptic overlap. These changes result in an increase in the number of non-occupied post-synaptic

terminals that tend to increase in diameter and eventually start to breakdown. These changes, were not associated with statistically significant changes in muscle mass or fibre Feret's diameter that has been reported with ageing in previous studies (Palomero et al, 2013; Sakellariou et al, 2014b). Analysis of agrin and MuSK, two important proteins involved in the formation and stabilisation of the NMJ, also did not show significant age-related loss in protein content although we cannot exclude the possibility that changes in localisation of these proteins may be responsible of the progressive breakdown of the NMJ seen.

Chapter 7. General discussion

One of the major features of ageing is the loss of skeletal muscle mass and function known as sarcopenia with multiple factors contributing to its development and progression (Baumann et al, 2016). Several authors suggest that denervation of skeletal muscle fibres may play a prominent role in the age-related loss of muscle mass (Aare et al, 2006; Jang and Van Remmen, 2011; Hepple, 2014; Hepple and Rice, 2016; McDonagh et al, 2016; Spendiff et al, 2016; Pollock et al, 2017; Soniak et al, 2019). Furthermore, previous studies (Muller et al, 2007; Bhattacharya et al, 2009; Pollock et al, 2017) have also demonstrated a significant increase in mitochondrial peroxide release from denervated muscle fibres. Since the physiological roles of this peroxide release are still poorly understood, the aims of the present thesis were:

- Examine the effects of prolonged denervation on peroxide release and proteins that regulate redox homeostasis in skeletal muscle.
- Examine the effects of prolonged skeletal muscle denervation on mitochondria with a specific focus on: mitophagy, activation of apoptosis and mitochondrial number.
- Determine the metabolic changes induced by skeletal muscle denervation.
- Investigate whether the redox-related changes observed in our denervation model also occur during skeletal muscle ageing since muscle denervation appears to be a key characteristic of sarcopenia.
- Evaluate the age-related changes occurring in the nerve-muscle interactions and examine whether the age-related loss in the stability of the NMJs results in skeletal muscle loss or *vice versa*.

7.1 Discussion of the main findings

7.1.1 Mitochondrial peroxide release following denervation is driven by enzymes not involved in the ETC and induces activation of NOX2, PLA2 and Prx6 in the cytosolic environment

Following denervation a significant increase in mitochondrial peroxide release occurred becoming significant 7 days following denervation and was sustained up to 21 days. In line with previous studies (Bhattacharya et al, 2009; Pollock et al, 2017), our results suggest that this increase is induced by enzymes not involved in the ETC but by other enzymes present in the mitochondrion such as NOX, Monoamine Oxidase A, Monoamine Oxidase B and PLA2. The significant decrease in peroxide release following the addition of AACOCF3 (a PLA2 inhibitor added to the Amplex Red assay) suggests that PLA2 is active following denervation. This result indicates that, other than H_2O_2, mitochondria of denervated fibres also release other peroxides, including lipid peroxides.

The increase in peroxide generation from mitochondria appears to trigger responses also in the cytosolic environment. Fourteen days following denervation an increase in Prx6 content was seen. Prx6 is an enzyme that, when over-oxidised, can undergo conformational changes that allow the protein to acquire PLA2 activity. The significant increase in the NOX2 subunits between 7 and 14 days post-denervation suggests that an activation of this enzyme may have occurred. NOX2, using O_2 and NADPH as substrates, is able to produce superoxide that is usually released in the extracellular matrix and, once converted into H_2O_2, is able to translocate into the cell exploiting aquaporins (Sies, 2017; Tamma et al, 2018). Peroxide released by NOX2 can participate in different functions including: mechanical contraction stimulating E-C coupling, (Kadoguchi et al, 2018) promoting insulin resistance through the interaction with the angiotensin-II system (Sukumar et al, 2013; Ferreira and Laitano, 2016) and activating pro-apoptotic pathways upregulating

the activity of the 26S proteasome (Li et al, 2003; Bodine et al, 2014; Delafontaine and Yoshida, 2016). Thus overall, our data support the hypothesis that post-denervation, muscle mitochondria increase peroxide release leading to activation of NOX2 possibly through the Prx6-cPLA2 signalling pathways.

7.1.2 An initial adaptive response following denervation may be an attempt to protect mitochondria but is not sustained over long-term resulting in oxidative stress and possible activation of proteolytic pathways

In the present study, 3 major mitochondrial antioxidant enzymes were analysed: MnSOD, TRxR2 and GPx1. While MnSOD content did not change following denervation, TrxR2 and GPx1 contents were significantly increased between 3 and 7 days.

The initial increase in the content of these mitochondrial antioxidant enzymes may reflect an adaptive response triggered by the loss of innervation in an attempt to maintain redox homeostasis in the muscle. In prolonged denervation, an increase in the content of different Hsp proteins was observed and remained increased up to 21 days post-denervation. Activation of Hsc70, Hsp70 and Hsp25 may play a role in protein homeostasis and protection against H_2O_2-induced damage. Therefore, the data suggest that the increased peroxide release following denervation can stimulate adaptive responses against oxidative stress and repair mechanisms to protect the muscle from degeneration.

7.1.3 Mitophagy is significantly inhibited following denervation with an increase in fission, activation of pro-apoptotic pathways and reduction in mitochondria population

The effect of prolonged denervation on mitophagy and the mitochondria of denervated skeletal muscle fibres was examined. Mitophagy is a tightly regulated process that can be influenced and regulated by mitochondrial ROS (Forrester et al, 2018). It has been

previously demonstrated that oxidative stress is able to enhance Drp1 recruitment and activation (Giedt et al, 2012; Forrester et al, 2018). Results showed that 7 days following denervation, the significant increase in mitochondrial ROS production was associated with a significant activation of Drp1 resulting in fission of mitochondria. In contrast, the two different fusion markers analysed, OPA1 and Mfn-2, did not show any changes following denervation. Similar to fission, fusion activity can also be influenced by the production of mitochondrial ROS. For instance, as described by Forrester and colleagues (2018), an increase in mitochondrial ROS produced by NOX4, can prevent OPA1 and Mfn-2 accumulation and activity. Furthermore, a significant increase in p62 content, which is indicative of a significant impairment of mitophagy, was seen. The increase in fission and the impairment of mitophagy was also associated with a progressive reduction of mitochondria numbers post-denervation.

7.1.4 Activation of apoptosis in denervated skeletal muscle fibres

Alongside the inhibition of mitophagy, results showed that 7 days following denervation there was an increase in the BAX/Bcl-2 ratio. Elevated BAX/Bcl-2 ratio is indicative of an increase in susceptibility of skeletal muscle fibres to apoptosis. Apoptosis is characterised by the permeabilisation of the mitochondrial membrane, release of cytochrome C, formation of the apoptosome and activation of the executional caspases -3, -6 and -7 (Slee et al, 2001; Sandri et al, 2001). In the present study, together with the increase in BAX/Bcl-2 ratio, an increase in caspase-3 content and cleavage was seen. The activation of caspase-3 has been previously reported to induce protein degradation enhancing proteasomal activity through the cleavage of Rpt2 and Rpt6 two specific subunits of the 26S proteasome (Wang et al, 2010).

7.1.5 Denervation triggers significant metabolic changes in skeletal muscle

Following denervation several metabolic changes were seen by NMR metabolomics including insulin resistance accompanied by inhibition of glycolysis. In addition, increased activity of the purine metabolism was seen. The latter is an important source of GTP and an alternative source of ATP. GTP can induce activation of a family of proteins known as G Proteins able to function as signal transducers and involved in the activation of several pathways including apoptosis through the Bcl-2 family (Yanamadala et al, 2009). Furthermore, GTP is a fundamental substrate of Rac-1, a protein necessary for NOX2 activation. NMR metabolomics also suggested that post-denervation there is a significant increase in proteolysis with a progressive accumulation of amino acids such as valine, isoleucine, phenylalanine and glutamate. These amino acids are usually released from the breakdown of proteins during extreme conditions such as fasting or prolonged exercise where they can function as intermediate products of the citric acid cycle or to generate alanine (Lynch and Adams, 2014; Vandelbo et al, 2014). The accumulation of these amino acids resulting from an acceleration in proteolysis can also be associated with an impairment of mitochondria, unable to use these substrates to generate ATP.

7.1.6 During ageing there is a progressive instability of the NMJ, accompanied by nerve sprouting and post-synaptic receptor breakdown. These changes were accompanied by mild structural changes at muscular level

One of the focuses of the present thesis was to evaluate the age-related changes in nerve-muscle interaction at different time points during adulthood and ageing in order to better understand whether the age-related loss in the stability of the NMJs induces skeletal muscle loss or *vice versa*. Previous studies in humans and murine models showed that during ageing there are significant changes of the NMJs that compromise

its stability and functionality (Hepple and Rice, 2016). Instability of the NMJs triggers a cascade of events able to induce: nerve sprouting, fibre type grouping (Lexell and Taylor, 1991) and motor unit loss (McNeil et al, 2005) resulting in myofibre atrophy (Hepple and Rice, 2016). In the current study a progressive instability of the NMJ starting around 18 months of age was seen together with an increase in nerve sprouting and "*blebbing*" and other structural post-synaptic terminal changes resulting in a progressive increase in denervation.

Nerve sprouting is a physiological response to the loss of NMJs as adjacent motor neurons spread in an attempt to re-innervate denervated post-synaptic receptors (Pestronk et al, 1980; Jang and Van Remmen, 2011; Kung et al, 2014; Greising et al, 2015 Hepple and Rice, 2016). When successful, nerve sprouting has the potential to alter the activity of the genes regulating the MyHC fibre phenotype by imposing a different electrical activity to the fibre (Maggs et al, 2008). A switch from MyHC-IIa and MyHC-IIx fibres towards MyHC-IIb fibres was seen with ageing. This progressive switch reinforce the possibility that denervation plays a fundamental role in inducing age-related structural changes of the skeletal muscle. In the present work, a trend (not statistically significant) indicating a loss of large muscle fibres occurred in concomitance with the impairment of the NMJs.

Another focus of the present work was to investigate whether the redox-related changes observed in the full denervation model also occur during skeletal muscle ageing since muscle denervation appears to be a key characteristic of sarcopenia. Previous studies from our group (Vasilaki et al, 2006b; Palomero et al, 2013) have reported a significant increase in the activity of different antioxidant enzymes during ageing. Surprisingly, our analysis failed to show similar changes in catalase, CuZnSOD and GPx1 contents. The discrepancy between previous results from our group and the results presented in this work could be

due to the high variability observed in the present study. Furthermore, the current study investigated protein content and hence cannot exclude age-related changes in the activity of these antioxidant enzymes. The lack of changes in p62 content and BAX/Bcl-2 ratio with ageing also suggest correct functioning of the autophagy and mitophagy machineries without the apparent activation of pro-apoptotic pathways as seen in our denervation models.

7.2 Future perspectives

7.2.1 Alternative methods for ROS detection

Direct and quantitative measurement of ROS production continue to represent a challenge due to the reactive nature of ROS as well as methodological shortcomings (He et al, 2016). In addition to the the Amplex Red assay other methods such as Electron Paramagnetic Resonance (EPR) or fluorescent probes can be used for the detection of ROS production, their primary source and localisation. EPR is considered the gold standard for the analysis of oxygen centered free radicals such as superoxide, both in vivo and in vitro, using a "*spin trap*" such as DMPO (a nitrogen spin trap) (Griendling et al, 2016). Alternatively, probes similar to TMRM such as MitoSOX or the cell-permeant 2',7'-dichlorodihydrofluorescein diacetate allow researchers to determine the source and localisation of ROS both in cells and isolated muscle fibres.

7.2.2 Analysis of the H_2O_2/lipid peroxide ratio

The Amplex Red assay is unable to distinguish between lipid peroxides and H_2O_2 as both are able to induce oxidation of the Amplex Red reagent to the same extent. Future studies to determine the lipid peroxides produced during prolonged denervation will provide clearer information regarding the physiological impact of the peroxide released from denervated muscle fibres. Different methodologies are available to determine the extent

of lipid peroxidation including: measuring the losses of unsaturated fatty acids and measuring primary peroxidation products. The most widely used method to detect lipid peroxidation (although non-specific) is the thiobarbituric acid assay that analyses the formation of a pink chromogen that can be detected at 532nm wavelength and that is formed by the interaction of one molecule of malondialehyde and two molecules of thiobarbituric acid (Gutteridge and Halliwell, 1990).

7.2.3 Activity of the 26 proteasome in denervated muscle fibres

Following denervation a significant muscle fibre atrophy was seen. These results suggest activation of different pathways able to drive muscle fibre atrophy through apoptosis. In particular, the significant increase in content of NOX2 subunits and cleaved caspase-3 suggests the activation of the 26S proteasome system. Analysis of the activity of this molecular complex would allow to determine its actual role in denervated skeletal muscle fibres.

7.2.4 ATP production during oxidative phosphorylation in denervated skeletal muscle fibres

In the present work a progressive accumulation of amino acids that can function as intermediate substrates for the citric acid cycle was seen. This accumulation may be related to an impairment of the mitochondrial network with mitochondria unable to generate ATP. NMR was unable to identify changes in ATP abundance and changes may have been obscured by metabolites with higher *clarity x dynamic range*.

Analysing mitochondrial respiration in denervated muscle fibres would allow the determination of whether denervation significantly impairs mitochondria functions and ATP production via oxidative phosphorylation.

7.2.5 Muscle fibres contractility post-denervation

Despite the significant proteolysis and activation of pro-apoptotic pathways, NMR metabolomics showed a significant decrease in 3-methylhistidine abundance. As this metabolite is usually produced by the breakdown of actin and myosin, this result may indicate a preservation of the contractile structures of the muscle. In future studies, performing ex-vivo muscle contractions of denervated muscles will allow the determination of whether the contractile apparatus is still functional.

7.2.6 Redox proteomics

New developments in the field of mass spectrometry allow investigation of the reversible and irreversible post-translational modifications induced by the activity of ROS (McDonagh, 2017). In future studies, redox mass spectrometry may allow integration of the results obtained from NMR metabolomics analysis to obtain a more complete picture of the impact that prolonged denervation has on skeletal muscle fibres.

7.2.7 Alternative mitophagy markers

In the present study we used the accumulation of p62 as a marker of mitophagy impairment. An alternative method to verify an eventual impairment of mitophagy using immunoblotting is by measuring the rate of conversion of Microtubule associated protein light chain 3 (LC3) (Mizushima and Yoshimori, 2007). LC3 is ubiquitously expressed in mammalian tissues. During the formation of autophagosomal membranes, LC3-I (the cytosolic form of LC3) is conjugated to phosphatidylethanolamine to form LC3-phosphatidylethanolamine conjugate (LC3-II) and this is then recruited to autophagosomal membranes (Tanida et al, 2008). An increase of the LC3-II/LC3-I ratio is associated with an increase in autophagy and mitophagy.

In conclusion, sarcopenia is a serious threat to the health of older adults, increased understanding of this disease will significantly help in reducing its incidence and its consequences. Future studies to implement the findings of the present work will contribute to provide a better picture of the role that ROS and denervation play in the age-related loss of muscle mass.

Bibliography

A

Aare, S., Spendiff, S., Vuda, M., Elkrief, D., Perez, A., Wu, Q., Mayaki D., Hussain S., Hettwer S. and Hepple, R. T. (2016). Failed reinnervation in aging skeletal muscle. *Skeletal Muscle, 6*(1), 29.

Abruzzo, P. M., di Tullio, S., Marchionni, C., Belia, S., Fano, G., Zampieri, S., Carraro, U., Kern, H., Sgarbi, G., Lenaz, G., Marini, M. (2010). Oxidative stress in the denervated muscle. *Free Radical Research, 44*(5), 563-576.

Afgan, E., Baker, D., van den Beek, M., Blankenberg, D., Bouvier, D., Cech, M., Goecks, J. (2016). The Galaxy platform for accessible, reproducible and collaborative biomedical analyses: 2016 update. *Nucleic Acids Research*, 44(W1), W3–W10.

Agostini, F., Libera, L. D., Rittweger, J., Mazzucco, S., Jurdana, M., Mekjavic, I. B., Pišot, R., Gorza, L., Narici, M., & Biolo, G. (2010). Effects of inactivity on human muscle glutathione synthesis by a double-tracer and single-biopsy approach. *Journal of Physiology*, *588*(24), 5089–5104.

Alberts B, Johnson A, Lewis J, et al. (2002), Molecular Biology of the Cell. 4th edition. New York: Garland Science.

Alway, S. E., Mohamed, J. S., & Myers, M. J. (2017). Mitochondria Initiate and Regulate Sarcopenia. *Exercise and Sport Science Review, 45*(2), 58-69.

Andersen, J. K. (2004). Oxidative stress in neurodegeneration: cause or consequence? *Nature Medicine, 10,* S18-25.

Aon, M. A., Cortassa, S., & O'Rourke, B. (2010). Redox-optimized ROS balance: a unifying hypothesis. *Biochimica et Biophysica Acta*, *1797*(6-7), 865-877.

Armenta-Medina, D., Segovia, L., & Perez-Rueda, E. (2014). Comparative genomics of nucleotide metabolism: a tour to the past of the three cellular domains of life. *BMC Genomics*, 15, 800.

Augusto V, P. C. a. R. C. G. (2004). Skeletal Muscle Fiber Types in C57BL6J Mice. *Brazilian Journal of morphological Science, 21*(2), 89-94.

Ayala, A., Munoz, M. F., & Arguelles, S. (2014). Lipid peroxidation: production, metabolism, and signaling mechanisms of malondialdehyde and 4-hydroxy-2-nonenal. *Oxidative Medicine and Cell Longevity*, *2014*, 360438.

B

Baker, A., Cerniglia, G. J., & Zaman, A. (1990). Microtiter Plate Assay for the Measurement of Glutathione and Glutathione Disulfide in Large Numbers of Biological Samples. *Analytical Biochemistry*, 365(190), 360–365.

Baker, B. M., & Haynes, C. M. (2011). Mitochondrial protein quality control during biogenesis and aging. *Trends in Biochemistry, 36*(5), 254-261.

Balice-Gordon RJ (1997), Age-related changes in neuromuscular innervation. *Muscle Nerve*, Suppl. 1997;5:S83-7.

Baloh, R. H., Rakowicz, W., Gardner, R., & Pestronk, A. (2007). Frequent atrophic groups with mixed-type myofibers is distinctive to motor neuron syndromes. *Muscle Nerve, 36*(1), 107-110.

Balsinde, J., Winstead, M. V., & Dennis, E. A. (2002). Phospholipase A2 regulation of arachidonic acid mobilization. *FEBS Letters, 531*(1), 2-6.

Barbieri, E., & Sestili, P. (2012). Reactive oxygen species in skeletal muscle signaling. *Journal of Signal Transduction, 2012*, 982794.

Baumann, C. W., Kwak, D., Liu, H. M., & Thompson, L. V. (2016). Age-induced oxidative stress: how does it influence skeletal muscle quantity and quality? *Journal of Applied Physiology (1985), 121*(5), 1047-1052.

Beckman, J. S., & Koppenol, W. H. (1996). Nitric oxide, superoxide, and peroxynitrite: the good, the bad, and ugly. *American Journal of Physiology*, 271(5 Pt 1), C1424-37.

Becuwe, P., Ennen, M., Klotz, R., Barbieux, C., & Grandemange, S. (2014). Manganese superoxide dismutase in breast cancer: from molecular mechanisms of gene regulation to biological and clinical significance. *Free Radical Biology and Medicine, 77*, 139-151.

Bell, E. L., Klimova, T. A., Eisenbart, J., Moraes, C. T., Murphy, M. P., Budinger, G. R., & Chandel, N. S. (2007). The Qo site of the mitochondrial complex III is required for the transduction of hypoxic signaling via reactive oxygen species production. *Journal of Cell Biology, 177*(6), 1029-1036.

Bhattacharya, A., Muller, F. L., Liu, Y., Sabia, M., Liang, H., Song, W., Van Remmen, H. (2009). Denervation induces cytosolic phospholipase A2-mediated fatty acid hydroperoxide generation by muscle mitochondria. *Journal of Biology and Chemistry, 284*(1), 46-55.

Bianchi, G., Brizi, M., Rossi, B., Ronchi, M., Grossi, G., & Marchesini, G. (2000). Synthesis of glutathione in response to methionine load in control subjects and in patients with cirrhosis. *Metabolism*, 49(11), 1434–1439.

Bienert, G. P., Schjoerring, J. K., & Jahn, T. P. (2006). Membrane transport of H_2O_2. *Biochimica et Biophysica Acta, 1758*(8), 994-1003.

Billett, E. (2004). Monoamine Oxidase (MAO) in Human Peripheral Tissues. *NeuroToxicology, 25*(1-2), 139-148.

Bleier, L., & Drose, S. (2013). Superoxide generation by complex III: from mechanistic rationales to functional consequences. *Biochimica et Biophysica Acta, 1827*(11-12), 1320-1331.

Bodine, S. C., & Baehr, L. M. (2014). Skeletal muscle atrophy and the E3 ubiquitin ligases MuRF1 and MAFbx/atrogin-1. *American Journal of Physiology, 307*(6), E469-484.

Bonora, M., Patergnani, S., Rimessi, A., De Marchi, E., Suski, J. M., Bononi, A., Giorgi, C., Marchi, S., Missiroli, S., Poletti, F., Wieckowski, M. R., Pinton, P. (2012). ATP synthesis and storage. *Purinergic Signalling*, 8(3), 343–357.

Bouzid, M. A., Hammouda, O., Matran, R., Robin, S., & Fabre, C. (2014). Changes in oxidative stress markers and biological markers of muscle injury with aging at rest and in response to an exhaustive exercise. *PloS One*, 9(3), e90420.

Bozler, E. (1954). Interactions between magnesium, pyrophosphate, and the contractile elements. *The Journal of General Physiology*, 38(1), 53–58.

Bradford, M. M. (1976). A rapid and sensitive method for the quantitation of microgram quantities of protein utilizing the principle of protein-dye binding. *Analytical Biochemistry, 72*, 248-254.

Brand, M. D., & Nicholls, D. G. (2011). Assessing mitochondrial dysfunction in cells. *Biochemisty Journal*, 312(435), 297–312.

Brand, M. D., Orr, A. L., Perevoshchikova, I. V., & Quinlan, C. L. (2013). The role of mitochondrial function and cellular bioenergetics in ageing and disease. *British Journal of Dermatology, 169 Suppl 2*, 1-8.

Brandes, R. P., Weissmann, N., & Schroder, K. (2014). Nox family NADPH oxidases: Molecular mechanisms of activation. *Free Radical Biology and Medicine, 76*, 208-226.

Breitenbach, M., Rinnerthaler, M., Weber, M. *et al.* The defense and signaling role of

NADPH oxidases in eukaryotic cells. *Wien Med Wochenschr* **168,** 286–299 (2018).

Brigelius-Flohe, R., & Maiorino, M. (2013). Glutathione peroxidases. *Biochimica et Biophysica Acta, 1830*(5), 3289-3303.

Borden M., Zhang P., Shivange A.V., Marvin J.S., Cichon J., Dan C., Podgorski K., Figueiredo A., Novak O., Tanimoto M., Shigetomi E., Lobas M.A., Kim H., Zhu P., Zhang Y., Zheng S.W., Fan C., Wang F., Xiang B., Gan L., Zhang G., Guo K., Lin L., Cai Y., Yee A.G., Aggarwal A., Ford C., Rees D., Dietrich D., Khakh B., Dittman J., Gan W., Koyama M., Jayaraman V., Cheer J., Lester H, Zhu J., Looger L (2020). A fast genetically encoded fluorescent sensor for faithful in vivo acetylcholine detection in mice, fish, worms and flies. Biorxiv.

Brown, K. A., Didion, S. P., Andresen, J. J., & Faraci, F. M. (2007). Effect of aging, MnSOD deficiency, and genetic background on endothelial function: evidence for MnSOD haploinsufficiency. *Arteriosclerosis, Thrombosis, and Vascular Biology*, 27(9), 1941–1946.

Bulla, L., & Shafwe, S. (2011). Biology of aging. *National Institute of Aging*. Baltimore, Maryland, USA.

C

Cadenas, E., Boveris, A., Ragan, C. I., & Stoppani, A. O. M. (1977). Production of superoxide radicals and H_2O_2 by NADH-ubiquinone reductase and ubiquinol-cytochrome c reductase from beef-heart mitochondria. *Archives of Biochemistry and Biophysics, 180*(2), 248-257.

Cadenas, E., & Davies, K. J. A. (2000). Mitochondrial free radical generation, oxidative stress, and ageing (1920–1998), *Free Radical Biology and Medicine, 29*(3-4), 222-230.

Campbell, K., Vowinckel, J., Keller, M. A., & Ralser, M. (2016). Methionine Metabolism Alters Oxidative Stress Resistance via the Pentose Phosphate Pathway. *Antioxidant Redox Signalling, 24*(10), 543-547.

Cao, H., Pauff, J. M., & Hille, R. (2010). Substrate orientation and catalytic specificity in the action of xanthine oxidase: the sequential hydroxylation of hypoxanthine to uric acid. *Journal of Biological Chemistry, 285*(36), 28044-28053.

Casas, F., Pessemesse, L., Grandemange, S., Seyer, P., Gueguen, N., Baris, O.,

Lepourry, L., Cabello, G., & Wrutniak-Cabello, C. (2008). Overexpression of the mitochondrial T3 receptor p43 induces a shift in skeletal muscle fiber types. *PLoS ONE, 3*(6).

Chae, H. Z., Robison, K., Poole, L. B., Church, G., Storz, G., & Rhee, S. G. (1994). Cloning and sequencing of thiol-specific antioxidant from mammalian brain: alkyl hydroperoxide reductase and thiol-specific antioxidant define a large family of antioxidant enzymes. *PNAS, 91*(15), 7017-7021.

Chatterjee, S., Feinstein, S. I., Dodia, C., Sorokina, E., Lien, Y. C., Nguyen, S., Debolt, K., Speicher, D., Fisher, A. B. (2011). Peroxiredoxin 6 phosphorylation and subsequent phospholipase A2 activity are required for agonist-mediated activation of NADPH oxidase in mouse pulmonary microvascular endothelium and alveolar macrophages. *Journal of Biological Chemistry, 286*(13), 11696-11706.

Cheatham, S. (2013). Section 7: Muscular Strength, Endurance and Flexibility. *ACSM Guidelines*, 4, 94–107.

Chen, J. W., Dodia, C., Feinstein, S. I., Jain, M. K., & Fisher, A. B. (2000). 1-Cys peroxiredoxin, a bifunctional enzyme with glutathione peroxidase and phospholipase A2 activities. *Journal of Biological Chemistry, 275*(37), 28421-28427.

Cheng, Q., Antholine, W. E., Myers, J. M., Kalyanaraman, B., Arner, E. S., & Myers, C. R. (2010). The selenium-independent inherent pro-oxidant NADPH oxidase activity of mammalian thioredoxin reductase and its selenium-dependent direct peroxidase activities. *Journal of Biological Chemestry, 285*(28), 21708-21723.

Cheusova, T., Khan, M. A., Schubert, S. W., Gavin, A. C., Buchou, T., Jacob, G., Sticht, H., Allende, J., Boldyreff, B., Brenner, H. R., Hashemolhosseini, S. (2006). Casein kinase 2-dependent serine phosphorylation of MuSK regulates acetylcholine receptor aggregation at the neuromuscular junction. *Genes and Development, 20*(13), 1800-1816.

Childs, T. E., Spangenburg, E. E., Vyas, D. R., & Booth, F. W. (2003). Temporal alterations in protein signaling cascades during recovery from muscle atrophy. *American Journal of Physiology-Cell Physiology, 285*(2), C391-398.

Chong, J., & Xia, J. (2018). MetaboAnalystR: an R package for flexible and reproducible analysis of metabolomics data. *Bioinformatics, 34*(24), 4313-4314.

Connelly, D. M., Rice, C. L., Roos, M. R., & Vandervoort, A. A. (1999). Motor unit firing rates and contractile properties in tibialis anterior of young and old men. *Journal of Applied Physiology (1985), 87*(2), 843-852.

Corcelli, A., Sublimi, M., Zaccagnino, P., Lopalco, P., Mastrodonato, M., Liquori, G. E., & Lorusso, M. (2010). Biochimica et Biophysica Acta Mitochondria isolated in nearly isotonic KCl buffer : Focus on cardiolipin and organelle morphology. *Biochimica et Biophysica Acta*, 1798(3), 681–687.

Cruz-Jentoft, A. J., Bahat, G., Bauer, J., Boirie, Y., Bruyere, O., Cederholm, T., Cooper, C., Landi, F., Rolland, Y., Sayer, A. A., Schneider, S. M., Sieber, C., Topinkova, E., Vandewoude, M., Visser, M., Zamboni, M. (2019). Sarcopenia: revised European consensus on definition and diagnosis. *Age Ageing, 48*(1), 16-31.

Cuervo, A. M., & Wong, E. (2014). Chaperone-mediated autophagy: roles in disease and aging. *Cell Research, 24*(1), 92-104.

D

Delafontaine, P., & Yoshida, T. (2016). The Renin-Angiotensin System and the Biology of Skeletal Muscle: Mechanisms of Muscle Wasting in Chronic Disease States. *Transactions of the American Clinical and Climatological Association, 127*(127), 245-258.

Deschenes, M. R. (2004). Effects of aging on muscle fibre type and size. *Sports Medicine, 34*(12), 809-824.

Di Giovanni, S., Molon, A., Broccolini, A., Melcon, G., Mirabella, M., Hoffman, E. P., & Servidei, S. (2004). Constitutive activation of MAPK cascade in acute quadriplegic myopathy. *Annual Neurology, 55*(2), 195-206.

Dillin, A., Gottschling, D. E., & Nyström, T. (2014). The good and the bad of being connected: the integrons of aging. *Current Opinion in Cell Biology*, 26, 107–12.

Dimauro, I., Pearson, T., Caporossi, D., & Jackson, M. J. (2012). A simple protocol for the subcellular fractionation of skeletal muscle cells and tissue. *BMC Research Notes, 5*, 513.

Dona, A. C., Kyriakides, M., Scott, F., Shephard, E. A., Varshavi, D., Veselkov, K., & Everett, J. R. (2016). A guide to the identification of metabolites in NMR-based metabonomics/metabolomics experiments. *Computional Structural Biotechnology Journal, 14*, 135-153.

Dos Santos, S., Petropoulos, I., & Friguet, B. (2018). The Oxidized Protein Repair Enzymes Methionine Sulfoxide Reductases and Their Roles in Protecting against Oxidative Stress, in Ageing and in Regulating Protein Function. *Antioxidants (Basel)*, 7(12).

Duan, J., & Kasper, D. L. (2011). Oxidative depolymerization of polysaccharides by reactive oxygen/nitrogen species. *Glycobiology*, 21(4), 401–409.

Duicu, O. M., Lighezan, R., Sturza, A., Balica, R., Vaduva, A., Feier, H., Gaspar, M. Ionac, A., Noveanu, L., Borza, C., Muntean, D., M Mornos, C. (2016). Assessment of Mitochondrial Dysfunction and Monoamine Oxidase Contribution to Oxidative Stress in Human Diabetic Hearts. *Oxidative Medicine and Cell Longevity, 2016*, 8470394.

Dumitru, A., Radu, B. M., Radu, M., & Cretoiu, S. M. (2018). Muscle Changes During Atrophy. *Advanced Experimental Medical Biology*, 1088, 73–92.

Dupont-Versteegden, E. E. (2006). Apoptosis in skeletal muscle and its relevance to atrophy. *World Journal of Gastroenterology, 12*(46), 7463-7466.

E

Edison, A. S., Hall, R. D., Junot, C., Karp, P. D., Kurland, I. J., Mistrik, R., Viant, M. R. (2016). The Time Is Right to Focus on Model Organism Metabolomes. *Metabolites, 6*(1).

Edmondson, D. E. (2014). Hydrogen peroxide produced by mitochondrial monoamine oxidase catalysis: biological implications. *Current Pharmacology Design, 20*(2), 155-160.

Eisenberg BR (1983). Quantitative ultrastructure of mammalian skeletal muscle In Handbook of Physiology, section 10, Skeletal Muscle, ed. Peachey LD, editor. , pp. 73–112. *American Physiological Society*, Bethesda.

Eismann, T., Huber, N., Shin, T., Kuboki, S., Galloway, E., Wyder, M., Lentsch, A. B. (2009). Peroxiredoxin-6 protects against mitochondrial dysfunction and liver injury during ischemia-reperfusion in mice. *American Journal of Physiology Gastrointestinal Liver Physiology, 296*(2), G266-274.

Elgass, K., Pakay, J., Ryan, M. T., & Palmer, C. S. (2013). Recent advances into the understanding of mitochondrial fission. *Biochimica et Biophysica Acta, 1833*(1), 150-161.

Elguero, E., Gabriela, V., Arciuch, A., & Jose, J. (2012). Mitochondrial Regulation of Cell Cycle and Proliferation. *Antioxidants and Redox Signaling*, 16(10), 1150–1180.

Emwas, A. H., Roy, R., McKay, R. T., Tenori, L., Saccenti, E., Gowda, G. A. N., Wishart, D. S. (2019). NMR Spectroscopy for Metabolomics Research. *Metabolites, 9*(7).

Escobedo, J., Pucci, A. M., & Koh, T. J. (2004). HSP25 protects skeletal muscle cells against oxidative stress. *Free Radical Biology and Medicine, 37*(9), 1455-1462.

Espinosa-Diez, C., Miguel, V., Mennerich, D., Kietzmann, T., Sánchez-Pérez, P., Cadenas, S., & Lamas, S. (2015). Antioxidant responses and cellular adjustments to oxidative stress. *Redox Biology*, *6*, 183–197.

Evans, M., Cogan, K. E., & Egan, B. (2017). Metabolism of ketone bodies during exercise and training : physiological basis for exogenous supplementation. *Journal of Physiology*, 9(595.9), 2857–2871.

F

Ferreira, L. F., & Laitano, O. (2016). Regulation of NADPH oxidases in skeletal muscle. *Free Radical Biology and Medicine*, *98*, 18-28.

Fisher, A. B. (2011). Peroxiredoxin 6: a bifunctional enzyme with glutathione peroxidase and phospholipase A(2) activities. *Antioxidant Redox Signaling, 15*(3), 831-844.

Flohe, L., Toppo, S., Cozza, G., & Ursini, F. (2011). A comparison of thiol peroxidase mechanisms. *Antioxidant Redox Signalling*, *15*(3), 763-780.

Forrester, S. J., Kikuchi, D. S., Hernandes, M. S., Xu, Q., & Griendling, K. K. (2018). Reactive Oxygen Species in Metabolic and Inflammatory Signaling. *Circulation Research, 122*(6), 877-902.

Friedman, J. R., Lackner, L. L., West, M., DiBenedetto, J. R., Nunnari, J., & Voeltz, G. K. (2011). ER tubules mark sites of mitochondrial division. *Science, 334*(6054), 358-362.

Frontera, W. R., & Ochala, J. (2015). Skeletal muscle: a brief review of structure and function. *Calcified Tissue International, 96*(3), 183-195.

Fukai, T., & Ushio-Fukai, M. (2011). Superoxide dismutases: role in redox signaling, vascular function, and diseases. *Antioxidant Redox Signalling, 15*(6), 1583-1606.

Fulco, M., Schiltz, R. L., Iezzi, S., King, M. T., Zhao, P., Kashiwaya, Y., Sartorelli, V. (2005). Sir2 regulates skeletal muscle differentiation as a potential sensor of the redox state (Vol 12, pg 51, 2003). *Molecular Cell*, 20(3), 491.

G

Gaschler, M. M., & Stockwell, B. R. (2017). Lipid peroxidation in cell death. *Biochemical and Biophysical Research Communications, 482*(3), 419-425.

Giedt, R. J., Yang, C., Zweier, J. L., Matzavinos, A., & Alevriadou, B. R. (2012). Mitochondrial fission in endothelial cells after simulated ischemia/reperfusion: role of nitric oxide and reactive oxygen species. *Free Radical Biology and Medicine, 52*(2), 348-356.

Giniatullin, A. R., Darios, F., Shakirzyanova, A., Davletov, B., & Giniatullin, R. (2006). SNAP25 is a pre-synaptic target for the depressant action of reactive oxygen species on transmitter release. *Journal of Neurochemistry, 98*(6), 1789-1797.

Go, Y. M., Chandler, J. D., & Jones, D. P. (2015). The cysteine proteome. *Free Radical Biology and Medicine, 84*, 227-245.

Gomes, M. J., Martinez, P. F., Pagan, L. U., Damatto, R. L., Cezar, M. D. M., Lima, A. R. R., Okoshi, M. P. (2017). Skeletal muscle aging: influence of oxidative stress and physical exercise. *Oncotarget, 8*(12), 20428-20440.

Greising, S. M., Medina-Martinez, J. S., Vasdev, A. K., Sieck, G. C., & Mantilla, C. B. (2015). Analysis of muscle fiber clustering in the diaphragm muscle of sarcopenic mice. *Muscle Nerve, 52*(1), 76-82.

Griffith, O. W. (1980). Determination of glutathione and glutathione disulfide using glutathione reductase and 2-vinylpyridine. *Analytical Biochemistry, 106*(1), 207-212.

Griendling, K. K., Touyz, R. M., Zweier, J. L., Dikalov, S., Chilian, W., Chen, Y.-R., Harrison, D. G., & Bhatnagar, A. (2016). Measurement of Reactive Oxygen Species, Reactive Nitrogen Species, and Redox-Dependent Signaling in the Cardiovascular System. Circulation Research, 119(5), 139–148.

Groemping, Y., & Rittinger, K. (2005). Activation and assembly of the NADPH oxidase: a structural perspective. *Biochem J, 386*(Pt 3), 401-416.

Guo, R., Gu, J., Zong, S., Wu, M., & Yang, M. (2018). Structure and mechanism of mitochondrial electron transport chain. Biomed J, 41(1), 9–20.

Gutmann, E., & Hanzlikova, V. (1966). Motor unit in old age. *Nature, 209*(5026), 921-922.

Gutteridge, J. M. C., & Halliwell, B. (1990). The measurement and mechanism of lipid peroxidation in biological systems. *Trends in Biochemical Sciences, 15*(4), 129-135.

H

Halliwell, B. (1989). Free radicals, reactive oxygen species and human disease: a critical evaluation with special reference to atherosclerosis. *British Journal of Experimental Pathology, 70*(6), 737-757.

Han, D., Antunes, F., Canali, R., Rettori, D., & Cadenas, E. (2003). Voltage-dependent anion channels control the release of the superoxide anion from mitochondria to cytosol. *Journal of Biology and Chemestry*, 278(8), 5557–5563.

Harridge, S. D., Bottinelli, R., Canepari, M., Pellegrino, M. A., Reggiani, C., Esbjornsson, M., & Saltin, B. (1996). Whole-muscle and single-fibre contractile properties and myosin heavy chain isoforms in humans. *European Journal of Physiology, 432*(5), 913-920.

Heck, D. E., Shakarjian, M., Kim, H. D., Laskin, J. D., & Anna, M. (2010). Mechanisms of oxidant generation by catalase. *Annual New York Academy of Science*, 1203, 120–125.

Hepple, R. T. (2014). Mitochondrial involvement and impact in aging skeletal muscle. *Frontiers, 6*, 211.

Hepple, R. T., & Rice, C. L. (2016). Innervation and neuromuscular control in ageing skeletal muscle. *Journal of Physiology, 594*(8), 1965-1978.

Holmstrom, K. M., & Finkel, T. (2014). Cellular mechanisms and physiological consequences of redox-dependent signalling. *Nature Reviews Molecular Cell Biology, 15*(6), 411-421.

Hoppins, S., Lackner, L., & Nunnari, J. (2007). The machines that divide and fuse mitochondria. *Annual Review in Biochemestry, 76*, 751-780.

Hu, C., Huang, Y., & Li, L. (2017). Drp1-Dependent Mitochondrial Fission Plays Critical Roles in Physiological and Pathological Progresses in Mammals. *International Journal of Molecular Science, 18*(1).

I

Inoguchi, T., Sonta, T., Tsubouchi, H., Etoh, T., Kakimoto, M., Sonoda, N., Nawata, H. (2003). Protein kinase C-dependent increase in reactive oxygen species (ROS) production in vascular tissues of diabetes: role of vascular NAD(P)H oxidase. *Journal of the American Society of Nephrology, 14*(8 Suppl 3), S227-232.

Ishikawa, K., Takenaga, K., Akimoto, M., Koshikawa, N., Yamaguchi, A., Imanishi, H., Hayashi, J. (2008). ROS-generating mitochondrial DNA mutations can regulate tumor cell metastasis. *Science, 320*(5876), 661-664.

J

Jackson, M. J., Vasilaki, A., & McArdle, A. (2016). Cellular mechanisms underlying oxidative stress in human exercise. *Free Radical Biology and Medicine*, 98, 13-17.

Jackson, M. J., & McArdle, A. (2016). Role of reactive oxygen species in age-related neuromuscular deficits. *Journal of Physiology, 594*(8), 1979-1988.

Jacob, M. C., Favre, M., & Bensa, J. (1991). Membrane Cell Permeabilisation With Saponin and Multiparametric Analysis by Flow Cytometry. *Cytometry*, 12, 550–558.

Jang, Y. C., & Van Remmen, H. (2011). Age-associated alterations of the neuromuscular junction. *Experimental Gerontology, 46*(2-3), 193-198.

Janssen, I., Heymsfield, S. B., Wang, Z. M., & Ross, R. (2000). Skeletal muscle mass and distribution in 468 men and women aged 18-88 yr. *Journal of Applied Physiology (1985), 89*(1), 81-88.

Janssen-Heininger, Y. M., Mossman, B. T., Heintz, N. H., Forman, H. J., Kalyanaraman, B., Finkel, T., van der Vliet, A. (2008). Redox-based regulation of signal transduction: principles, pitfalls, and promises. *Free Radical Biology and Medicine, 45*(1), 1-17.

Jee, H. (2016). Size dependent classification of heat shock proteins: a mini-review. J *Exercise Rehabilitation*, 12(4), 255–259.

Jezek, J., Cooper, K. F., & Strich, R. (2018). Reactive Oxygen Species and Mitochondrial Dynamics: The Yin and Yang of Mitochondrial Dysfunction and Cancer Progression. *Antioxidants, 7*(1).

Jiao, Y., Wang, Y., Guo, S., & Wang, G. (2017). Glutathione peroxidases as oncotargets. *Oncotarget*, 8(45), 80093–80102.

Jones, R. A., Harrison, C., Eaton, S. L., Llavero Hurtado, M., Graham, L. C., Alkhammash, L., Gillingwater, T. H. (2017). Cellular and Molecular Anatomy of the Human Neuromuscular Junction. *Cell Reports, 21*(9), 2348-2356.

Jones, R. A., Reich, C. D., Dissanayake, K. N., Kristmundsdottir, F., Findlater, G. S., Ribchester, R. R., Gillingwater, T. H. (2016). NMJ-morph reveals principal components of synaptic morphology influencing structure-function relationships at the neuromuscular junction. *Open Biology, 6*(12).

Jones, S., Eisenberg, H. M., & Jia, X. (2016). Advances and Future Applications of Augmented Peripheral Nerve Regeneration. *International Journal of Molecular Science, 17*(9).

K

Kadoguchi, T., Takada, S., Yokota, T., Furihata, T., Matsumoto, J., Tsuda, M., Kinugawa, S. (2018). Deletion of NAD(P)H Oxidase 2 Prevents Angiotensin

II-Induced Skeletal Muscle Atrophy. *Biomedical Research International, 2018*, 3194917.

Kalyani, R., Corriere, M., & Ferrucci, L. (2014). Age-related and disease-related muscle loss: the effect of diabetes, obesity, and other diseases. *The Lancet*, 2(10), 819–829.

Karam, C., Yi, J., Xiao, Y., Dhakal, K., Zhang, L., Li, X., Zhou, J. (2017). Absence of physiological Ca(2+) transients is an initial trigger for mitochondrial dysfunction in skeletal muscle following denervation. *Skeletal Muscle, 7*(1), 6.

Kasai, S., Shimizu, S., Tatara, Y., Mimura, J., & Itoh, K. (2020). Regulation of Nrf2 by mitochondrial reactive oxygen species in physiology and pathology. *Biomolecules, 10*(2).

Kaushik, S., & Cuervo, A. M. (2015). Degradation of lipid droplet-associated proteins by chaperone-mediated autophagy facilitates lipolysis. *Nature Cell Biology, 17*(6), 759-770.

Kaushik, S., & Cuervo, A. M. (2015). Proteostasis and aging. *Nature Medicine, 21*(12), 1406-1415.

Keller, K., & Engelhardt, M. (2013). Strength and muscle mass loss with aging process. Age and strength loss. Muscles, *Ligaments and Tendons Journal*, 3(4), 346–350.

Kemp W. (1986), NMR in Chemestry, Macmillan Publishers Limited 1986, Palgrave, London

Kent-Braun, J. A., Ng, A. V., & Young, K. (2000). Skeletal muscle contractile and noncontractile components in young and older women and men. *Journal of Applied Physiology (1985), 88*(2), 662-668.

Kim, K. H., Lee, W., & Kim, E. E. (2016). Crystal structures of human peroxiredoxin 6 in different oxidation states. *Biochemical and Biophysical Research Communications, 477*(4), 717-722.

Koneczny, I., Cossins, J., & Vincent, A. (2014). The role of muscle-specific tyrosine kinase (MuSK) and mystery of MuSK myasthenia gravis. *Journal of Anatomy, 224*(1), 29-35.

Konior, A., Schramm, A., Czesnikiewicz-Guzik, M., & Guzik, T. J. (2014). NADPH oxidases in vascular pathology. *Antioxidant Redox Signalling, 20*(17), 2794-2814.

Kung, T. A., Cederna, P. S., van der Meulen, J. H., Urbanchek, M. G., Kuzon, W. M., Jr., & Faulkner, J. A. (2014). Motor unit changes seen with skeletal muscle sarcopenia in oldest old rats. *Journal of Gerontology, 69*(6), 657-665.

Kurutas, E. B. (2016). The importance of antioxidants which play the role in cellular response against oxidative / nitrosative stress : current state. *Nutrition Journal*, 1–22.

Kussmaul, L., & Hirst, J. (2006). The mechanism of superoxide production by NADH:ubiquinone oxidoreductase (complex I) from bovine heart mitochondria. *Proceedings of the National Academy of Sciences of the United States of America, 103*(20), 7607-7612.

Kuznetsov, A. V., Veksler, V., Gellerich, F. N., Saks, V., Margreiter, R., & Kunz, W. S. (2008). Analysis of mitochondrial function in situ in permeabilized muscle fibers, tissues and cells. *Nature Protocols, 3*(6), 965–976.

L

Lang, F., Aravamudhan, S., Nolte, H., Turk, C., Holper, S., Muller, S., Kruger, M. (2017). Dynamic changes in the mouse skeletal muscle proteome during denervation-induced atrophy. *Disease Models & Mechanisms, 10*(7), 881-896.

Larsson Forsell, P. K., Kennedy, B. P., & Claesson, H. E. (1999). The human calcium-independent phospholipase A2 gene multiple enzymes with distinct properties from a single gene. *European Journal of Biochemestry, 262*(2), 575-585.

Lee, C. Y., Delaney, J. C., Kartalou, M., Lingaraju, G. M., Maor-Shoshani, A., Essigmann, J. M., & Samson, L. D. (2009). Recognition and processing of a new repertoire of DNA substrates by human 3-methyladenine DNA glycosylase (AAG). *Biochemistry, 48*(9), 1850-1861.

Lennicke, C., Rahn, J., Lichtenfels, R., Wessjohann, L. A., & Seliger, B. (2015). Hydrogen peroxide - production, fate and role in redox signaling of tumor cells. *Cell Communication and Signaling*, 13, 39.

Lexell, J., & Taylor, C. C. (1991). Variability in Muscle-Fiber Areas in Whole Human Quadriceps Muscle - Effects of Increasing Age. *Journal of Anatomy, 174*, 239-249.

Lexell, J., Taylor, C. C., & Sjöström, M. (1988). What is the cause of the ageing atrophy? *Journal of the Neurological Sciences, 84*(2-3), 275-294.

Li, X., Fang, P., Mai, J., Choi, E. T., Wang, H., & Yang, X. F. (2013). Targeting mitochondrial reactive oxygen species as novel therapy for inflammatory diseases and cancers. *Journal of Oncology, 6*, 19.

Li, Y. P., Chen, Y., Li, A. S., & Reid, M. B. (2003). H2O2 stimulates ubiquitin-conjugating activity and expression of genes for specific E2 and E3 proteins in skeletal muscle myotubes. *American Journal of Physiology and Cell Physiology, 285*(4), C806-812.

Liu, H., Dai, C., Fan, Y., Guo, B., Ren, K., Sun, T., & Wang, W. (2017). From autophagy to mitophagy: the roles of P62 in neurodegenerative diseases. *Journal of Bioenergetic and Biomembranes, 49*(5), 413-422.

Lodish H, Berk A, Zipursky SL, et al. (2000) Molecular Cell Biology. 4th edition. New York: W. H. Freeman; Section 18.3, Myosin: The Actin Motor Protein.

Loureiro, A. C., do Rego-Monteiro, I. C., Louzada, R. A., Ortenzi, V. H., de Aguiar, A. P., de Abreu, E. S., Carvalho, D. P. (2016). Differential Expression of NADPH Oxidases Depends on Skeletal Muscle Fiber Type in Rats. *Oxidative Medicine and Cell Longevity, 2016*, 6738701.

Lubos, E., Loscalzo, J., & Handy, D. E. (2011). Glutathione peroxidase-1 in health and disease: from molecular mechanisms to therapeutic opportunities. *Antioxidant Redox Signalling, 15*(7), 1957-1997.

Lynch, C. J., & Adams, S. H. (2014). Branched-chain amino acids in metabolic signalling and insulin resistance. *Nature Reviews, 10*(12), 723-736.

Lyons, T. J., Jenkins, A. J., & Carolina, S. (1997). Glycation, oxidation, and lipoxidation in the development of the complications of diabetes: a carbonyl stress hypothesis. *Diabetes Reviews* (Alex), 5(4), 365–391.

M

Maggs, A. M., Huxley, C., & Hughes, S. M. (2008). Nerve-dependent changes in skeletal muscle myosin heavy chain after experimental denervation and cross-reinnervation and in a demyelinating mouse model of Charcot-Marie-Tooth disease type 1A. *Muscle Nerve, 38*(6), 1572-1584.

Manoli, I., Le, H., Alesci, S., McFann, K. K., Su, Y. A., Kino, T., Blackman, M. R. (2005). Monoamine oxidase-A is a major target gene for glucocorticoids in human skeletal muscle cells. *Faseb Journal, 19*(8), 1359.

Mattson, M. P., & Calabrese, E. J. (2010). *Hormesis*. New York: Humana Press - Springer Science and Business Media.

McBride, H. M., Neuspiel, M., & Wasiak, S. (2006). Mitochondria: more than just a powerhouse. *Current Biology, 16*(14), R551-560.

McCormick, R., & Vasilaki, A. (2018). Age-related changes in skeletal muscle: changes to life-style as a therapy. *Biogerontology*, 19(6), 519–536.

McDonagh, B. (2017). Detection of ROS Induced Proteomic Signatures by Mass Spectrometry. *Frontiers, 8*, 470.

McDonagh, B., Scullion, S. M., Vasilaki, A., Pollock, N., McArdle, A., & Jackson, M. J. (2016). Ageing-induced changes in the redox status of peripheral motor nerves imply an effect on redox signalling rather than oxidative damage. *Free Radical Biology and Medicine, 94*, 27-35.

McLean A, (2011). Densitometry Of Western Blots Using Image J Software.

McMahan, U. J. (1990). The agrin hypothesis. Cold Spring Harbor Symposia on Quantitative Biology, 55, 407–418.

McNeil, C. J., Doherty, T. J., Stashuk, D. W., & Rice, C. L. (2005). Motor unit number estimates in the tibialis anterior muscle of young, old, and very old men. *Muscle Nerve, 31*(4), 461-467.

Miki, H., & Funato, Y. (2012). Regulation of intracellular signalling through cysteine oxidation by reactive oxygen species. Journal of Biochemistry, 151(3), 255–261.

Mishra, P., & Chan, D. C. (2016). Metabolic regulation of mitochondrial dynamics. *Journal of Cell Biology, 212*(4), 379-387.

Mizushima, N., & Yoshimori, T. (2007). How to interpret LC3 immunoblotting. *Autophagy*, *3*(6), 542–545.

Moise, L., Piserchio, A., Basus, V. J., & Hawrot, E. (2002). NMR structural analysis of alpha-bungarotoxin and its complex with the principal alpha-neurotoxin-binding sequence on the alpha 7 subunit of a neuronal nicotinic acetylcholine receptor. *Journal of Biology and Chemistry, 277*(14), 12406-12417.

Mosoni, L., Breuillé, D., Buffière, C., Obled, C., & Mirand, P. P. (2004). Age-related changes in glutathione availability and skeletal muscle carbonyl content in healthy rats. *Experimental Gerontology*, *39*(2), 203–210.

Muller, F. L., Song, W., Jang, Y. C., Liu, Y., Sabia, M., Richardson, A., & Van Remmen, H. (2007). Denervation-induced skeletal muscle atrophy is associated with increased mitochondrial ROS production. *American Journal of Physiology*, 293(3), R1159-1168.

Muller, F. L., Lustgarten, M. S., Jang, Y., Richardson, A., & Van Remmen, H. (2007). Trends in oxidative aging theories. *Free Radical Biology and Medicine, 43*(4), 477-503.

Murphy, M. P. (2009). How mitochondria produce reactive oxygen species. *Biochemistry Journal, 417*(1), 1-13.

Murray, C. I., & Van Eyk, J. E. (2012). Chasing cysteine oxidative modifications: proteomic tools for characterizing cysteine redox status. *Circulation and Cardiovascular Genetics, 5*(5), 591.

N

Nabben, M., Shabalina, I. G., Moonen-Kornips, E., van Beurden, D., Cannon, B., Schrauwen, P., Hoeks, J. (2011). Uncoupled respiration, ROS production, acute lipotoxicity and oxidative damage in isolated skeletal muscle mitochondria from UCP3-ablated mice. *Biochimica et Biophysica Acta, 1807*(9), 1095-1105.

Nagy, P., & Winterbourn, C. C. (2010). Redox Chemistry of Biological Thiols. In Fishbein JC, editor. Advances in Molecular Toxicology. Elsevier, B.V. (pp. 183-222).

Nakada, K., Inoue, K., Ono, T., Isobe, K., Ogura, A., Goto, Y. I., Hayashi, J. I. (2001). Inter-mitochondrial complementation: Mitochondria-specific system preventing mice from expression of disease phenotypes by mutant mtDNA. *Nature Medicine, 7*(8), 934-940.

Neft, N., & Farley, T. M. (1972). Conditions influencing antimycin production by a Streptomyces species grown in chemically defined medium. *Antimicrobial Agents Chemotherapy, 1*(3), 274-276.

Nguyen, G. T., Green, E. R., & Mecsas, J. (2017). Neutrophils to the ROScue : Mechanisms of NADPH Oxidase Activation and Bacterial Resistance. *Frontiers in Cellular and Infection Microbiology*, 7(August).

Nicolas, J. P., Lin, Y., Lambeau, G., Ghomashchi, F., Lazdunski, M., & Gelb, M. H. (1997). Localization of structural elements of bee venom phospholipase A2 involved in N-type receptor binding and neurotoxicity. *Journal of Biology and Chemistry*, *272*(11), 7173-7181.

Nisimoto, Y., Diebold, B. A., Cosentino-Gomes, D., & Lambeth, J. D. (2014). Nox4: a hydrogen peroxide-generating oxygen sensor. *Biochemistry,* 53(31), 5111–5120.

Nordberg, J., & Arnér, E. S. J. (2001). Reactive oxygen species, antioxidants, and the mammalian thioredoxin system. Karolinska Institute, Stockholm, ISBN 91-631-1064-4. *Free Radical Biology and Medicine, 31*(11), 1287-1312.

O

Oda, K. (1984). Age changes of motor innervation and acetylcholine receptor distribution on human skeletal muscle fibres. *Journal of the Neurological Sciences*, *66*(2-3), 327-338.

Okada, K., Inoue, A., Okada, M., Murata, Y., Kakuta, S., Jigami, T., Yamanashi, Y. (2006). The muscle protein Dok-7 is essential for neuromuscular synaptogenesis. *Science, 312*(5781), 1802-1805.

Orr, W. C., Mockett, R. J., Benes, J. J., & Sohal, R. S. (2003). Effects of overexpression of copper-zinc and manganese superoxide dismutases, catalase, and thioredoxin reductase genes on longevity in Drosophila melanogaster. *Journal of Biology and Chemestry, 278*(29), 26418-26422.

Orr, W. C., & Sohal, R. S. (1994). Extension of life-span by overexpression of superoxide dismutase and catalase in Drosophila melanogaster. *Science, 263*(5150), 1128-1130.

Ortenblad, N., Nielsen, J., Boushel, R., Soderlund, K., Saltin, B., & Holmberg, H. C. (2018). The Muscle Fiber Profiles, Mitochondrial Content, and Enzyme Activities of the Exceptionally Well-Trained Arm and Leg Muscles of Elite Cross-Country Skiers. *Frontiers in Physiology*, 9, 1031.

P

Palikaras, K., Lionaki, E., & Tavernarakis, N. (2015). Balancing mitochondrial biogenesis and mitophagy to maintain energy metabolism homeostasis. *Cell Death Differantiation, 22*(9), 1399-1401.

Palomero, J., Vasilaki, A., Pye, D., McArdle, A., & Jackson, M. J. (2013). Aging increases the oxidation of dichlorohydrofluorescein in single isolated skeletal muscle fibers at rest, but not during contractions. *American Journal of Physiology Regulatory, Integrative and Comparative Physiology*, (September 2016).

Panday, A., Sahoo, M. K., Osorio, D., & Batra, S. (2015). NADPH oxidases: an overview from structure to innate immunity-associated pathologies. *Cell and Molecular Immunology, 12*(1), 5-23.

Paravicini, T. M., & Touyz, R. M. (2006). Redox signaling in hypertension. *Cardiovascular Research, 71*(2), 247-258.

Park, K. H. (2015). Mechanisms of Muscle Denervation in Aging: Insights from a Mouse Model of Amyotrophic Lateral Sclerosis. *Aging Disease, 6*(5), 380-389.

Patel, M. (2006) Principal Component Analysis (PCA): an Unsupervised learning. Rstudio publications-statistics

Patenaude, A., Ven Murthy, M. R., & Mirault, M. E. (2004). Mitochondrial thioredoxin system: effects of TrxR2 overexpression on redox balance, cell growth, and apoptosis. *Journal of Biology and Chemistry, 279*(26), 27302-27314.

Pennefather, P., & Quastel, D. M. (1981). Relation between subsynaptic receptor blockade and response to quantal transmitter at the mouse neuromuscular junction. *Journal of General Physiology, 78*(3), 313-344.

Perry, S. W., Norman, J. P., Barbieri, J., Brown, E. B., & Gelbard, H. A. (2011). Mitochondrial membrane potential probes and the proton gradient: a practical usage guide. *Biotechniques, 50*(2), 98-115.

Pestronk, A., Drachman, D. B., & Griffin, J. W. (1980). Effects of aging on nerve sprouting and regeneration. *Experimental Neurology, 70*(1), 65-82.

Pollock, N., Staunton, C. A., Vasilaki, A., McArdle, A., & Jackson, M. J. (2017). Denervated muscle fibers induce mitochondrial peroxide generation in

neighboring innervated fibers: Role in muscle aging. *Free Radical Biology and Medicine, 112*, 84-92.

Poole, L. B. (2015). The basics of thiols and cysteines in redox biology and chemistry. *Free Radical Biology and Medicine*, *80*(5), 148–157.

Porter, C., & Wall, B. T. (2012). Skeletal muscle mitochondrial function: is it quality or quantity that makes the difference in insulin resistance? *Journal of Physiology, 590*(23), 5935-5936.

Powers, G. A., Dalton, B. H., & Rice, C. L. (2013). Human neuromuscular structure and function in old age: A brief review. *Journal of Sport and Health Science, 2*(4), 215-226.

Powers S.K. and Howley E.T. (1994). Skeletal muscle: Structure and Function. In Exercise Physiology: Theory and application to Fitness and Performance, Second Edition. Brown and Benchmark, Dubuque, 145-170

Powers, S. K., & Jackson, M. J. (2008). Exercise-induced oxidative stress: cellular mechanisms and impact on muscle force production. *Physiology Reviews, 88*(4), 1243-1276.

Powers, S. K., Ji, L. L., Kavazis, A. N., & Jackson, M. J. (2011). Reactive oxygen species: impact on skeletal muscle. *Comprehensive Physiology, 1*(2), 941-969.

R

Raghunath, A., Sundarraj, K., Nagarajan, R., Arfuso, F., Bian, J., Kumar, A. P., Sethi, G., & Perumal, E. (2018). Antioxidant response elements: Discovery, classes, regulation and potential applications. *Redox Biology*, *17*(May), 297–314.

Rahal, A., Kumar, A., Singh, V., Yadav, B., Tiwari, R., Chakraborty, S., & Dhama, K. (2014). Oxidative stress, pro-oxidants, and antioxidants: the interplay. Biomedical Research International, 2014, 761264.

Ray, P. D., Huang, B. W., & Tsuji, Y. (2012). Reactive oxygen species (ROS) homeostasis and redox regulation in cellular signaling. *Cell Signalling, 24*(5), 981-990.

Ramakrishnan, N. A., Drescher, M. J., & Drescher, D. G. (2012). The SNARE complex in neuronal and sensory cells. Mol Cell Neurosci, 50(1), 58–69.

Rhee, S., Zoon, H., & Kim, K. (2005). Peroxiredoxins : A historical overview and speculative preview of novel mechanisms and emerging concepts in cell signaling. *Free Radical Biology and Medicine*, 38(2005), 1543–1552.

Rogers, R. S., Tungtur, S., Tanaka, T., Nadeau, L. L., Badawi, Y., Wang, H., Nishimune, H. (2017). Impaired Mitophagy Plays a Role in Denervation of Neuromuscular Junctions in ALS Mice. *Frontiers in Neuroscience, 11*, 473.

Romanello, V., Guadagnin, E., Gomes, L., Roder, I., Sandri, C., Petersen, Y., Sandri, M. (2010). Mitochondrial fission and remodelling contributes to muscle atrophy. *EMBO, 29*(10), 1774-1785.

Romero-Calvo, I., Ocon, B., Martinez-Moya, P., Suarez, M. D., Zarzuelo, A., Martinez-Augustin, O., & de Medina, F. S. (2010). Reversible Ponceau staining as a loading control alternative to actin in Western blots. *Analytical Biochemistry, 401*(2), 318-320.

Rubinstein, J. L., Walker, J. E., & Henderson, R. (2003). Structure of the mitochondrial ATP synthase by electron cryomicroscopy. *EMBO, 22*(23), 6182-6192.

Rui, L. (2014). Energy metabolism in the liver. *Comprehensive Physiology*, 4(1), 177–197.

Rygiel, K. A., Picard, M., & Turnbull, D. M. (2016). The ageing neuromuscular system and sarcopenia: a mitochondrial perspective. *Journal of Physiology, 594*(16), 4499-4512.

S

Sadi, G., & Sadi, Ö. (2010). Antioxidants and Regulation of Antioxidant Enzymes by Cellular Redox Status. *Turkish Journal of Scientific Reviews, 3*(2), 95–107.

Sakellariou, G. K., Jackson, M. J., & Vasilaki, A. (2014). Redefining the major contributors to superoxide production in contracting skeletal muscle. The role of NAD(P)H oxidases. *Free Radical Research*, 48(1), 12-29.

Sakellariou, G. K., Davis, C. S., Shi, Y., Ivannikov, M. V., Zhang, Y., Vasilaki, A., Brooks, S. V. (2014). Neuron-specific expression of CuZnSOD prevents the loss of muscle mass and function that occurs in homozygous CuZnSOD-knockout mice. *FASEB, 28*(4), 1666-1681.

Sakellariou, G. K., Pearson, T., Lightfoot, A. P., Nye, G. A., Wells, N., Giakoumaki, I. I., Jackson, M. J. (2016). Mitochondrial ROS regulate oxidative damage and mitophagy but not age-related muscle fiber atrophy. *PLoS One*, (March), 1–15.

Saladin, Kenneth (2012). Anatomy and Physiology: The Unity of Form and Function. New York: McGraw Hill.

Salway J.G (2013), Metabolism at a glance 3rd edition, Blackwell publishing ltd, Hoboken, New Jersey, USA

Samuel, M. A., Valdez, G., Tapia, J. C., Lichtman, J. W., & Sanes, J. R. (2012). Agrin and synaptic laminin are required to maintain adult neuromuscular junctions. *PLoS One*, *7*(10), e46663.

Sandri, M., El Meslemani, A. H., Sandri, C., Schjerling, P., Vissing, K., Andersen, J. L., Angelini, C. (2001). Caspase 3 expression correlates with skeletal muscle apoptosis in Duchenne and facioscapulo human muscular dystrophy. A potential target for pharmacological treatment? *Journal of Neuropathology and Experimental Neurology, 60*(3), 302-312.

Sawano, S., Komiya, Y., Ichitsubo, R., Ohkawa, Y., Nakamura, M., Tatsumi, R., Mizunoya, W. (2016). A One-Step Immunostaining Method to Visualize Rodent Muscle Fiber Type within a Single Specimen. *PLoS One, 11*(11), e0166080.

Schemidt RA, Q. J., Williams JA, and Brusilow WSA. (1998). Effects of Carbon Source on Expression of Fo Genes and on the Stoichiometry of the c Subunit in the F1Fo ATPase of Escherichia coli. *Journal of Bacteriology, Jun: 180(12): 3205-3208*.

Schriner, S. E., Linford, N. J., Martin, G. M., Treuting, P., Ogburn, C. E., Emond, M., Rabinovitch, P. S. (2005). Extension of murine life span by overexpression of catalase targeted to mitochondria. *Science*, *308*(5730), 1909-1911.

Schultheisz, H. L., Szymczyna, B. R., Scott, L. G., & Williamson, J. R. (2008). Pathway engineered enzymatic de novo purine nucleotide synthesis. *ACS Chemical Biology*, 3(8), 499–511.

Scott, W., Stevens, J., & Binder-Macleod, S. A. (2001). Human skeletal muscle fiber type classifications. *Physical Therapy, 81*(11), 1810-1816.

Seo, D. Y., Lee, S. R., Kim, N., Ko, K. S., Rhee, B. D., & Han, J. (2016). Age-related changes in skeletal muscle mitochondria: the role of exercise. *Integrated Medicine Research*, *5*(3), 182-186.

Shiber, A., Breuer, W., Brandeis, M., & Ravid, T. (2013). Ubiquitin conjugation triggers misfolded protein sequestration into quality control foci when Hsp70 chaperone levels are limiting. *Molecular Biology Cell, 24*(13), 2076-2087.

Shigeoka, S., & Maruta, T. (2014). Cellular redox regulation, signaling, and stress response in plants. *Bioscience, Biotechnology, and Biochemistry, 78*(9), 1457-1470.

Schröder, K. (2019). NADPH oxidase-derived reactive oxygen species: Dosis facit venenum. *Experimental Physiology*, *104*(4), 447–452.

Shukla, V., Mishra, S. K., & Pant, H. C. (2011). Oxidative stress in neurodegeneration. *Advanced Pharmacological Science, 2011*, 572634.

Sigel, H., Operschall, B. P., & Griesser, R. (2009). Xanthosine 5'-monophosphate (XMP). Acid-base and metal ion-binding properties of a chameleon-like nucleotide. *Chemical Society Reviews*, 38(8), 2465–2494.

Sies, H. (2017). H2O2 as a central redox signaling molecule in physiological oxidative stress: Oxidative eustress. *Redox Biology, 11*, 613-619.

Siu, P. M., & Alway, S. E. (2005). Mitochondria-associated apoptotic signalling in denervated rat skeletal muscle. *Journal of Physiology, 565*(Pt 1), 309-323.

Slee, E. A., Adrain, C., & Martin, S. J. (2001). Executioner caspase-3, -6, and -7 perform distinct, non-redundant roles during the demolition phase of apoptosis. *Journal of Biology and Chemestry*, *276*(10), 7320-7326.

Smith, P. K., Krohn, R. I., Hermanson, G. T., Mallia, A. K., Gartner, F. H., Provenzano, M. D., Klenk, D. C. (1985). Measurement of protein using bicinchoninic acid. *Analytical Biochemistry, 150*(1), 76-85.

Soininen, P., Kangas, A. J., Wurtz, P., Tukiainen, T., Tynkkynen, T., Laatikainen, R., Ala-Korpela, M. (2009). High-throughput serum NMR metabonomics for cost-effective holistic studies on systemic metabolism. *Analyst, 134*(9), 1781-1785.

Son, Y., & Thompson, W. J. (1995). Nerve sprouting in muscle is induced and guided by processes extended by schwann cells. *Neuron*, 14, 133–141.

Sonjak, V., Jacob, K. J., Spendiff, S., Vuda, M., Perez, A., Miguez, K., Hepple, R. T. (2019). Reduced mitochondrial content, elevated ROS, and modulation by denervation in skeletal muscle of pre-frail/frail elderly women. *Journal of Gerontology*.

Sparling, ML. (1990). Analysis of mixed lipid extracts using 1H NMR spectra. *Cabios, 6* (1), 29-42.

Spendiff, S., Vuda, M., Gouspillou, G., Aare, S., Perez, A., Morais, J. A., Hepple, R. T. (2016). Denervation drives mitochondrial dysfunction in skeletal muscle of octogenarians. *Journal of Physiology, 594*(24), 7361-7379.

Stanley, E. F., & Drachman, D. B. (1981). Denervation accelerates the degradation of junctional acetylcholine receptors. *Experimental Neurology, 73*(2), 390-396.

Staron, R. S., Hagerman, F. C., Hikida, R. S., Murray, T. F., Hostler, D. P., Crill, M. T., Toma, K. (2000). Fiber type composition of the vastus lateralis muscle of young men and women. *Journal of Histochemestry and Cytochemestry, 48*(5), 623-629.

Staunton, C. A., Owen, E. D., Pollock, N., Vasilaki, A., Barrett-Jolley, R., McArdle, A., & Jackson, M. J. (2019). HyPer2 imaging reveals temporal and heterogeneous hydrogen peroxide changes in denervated and aged skeletal muscle fibers in vivo. *Scientific Reports*, 9(1), 14461.

Steinbacher, P., & Eckl, P. (2015). Impact of Oxidative Stress on Exercising Skeletal Muscle. *Biomolecules*, 5(2), 356–377.

Stefanatos, R., & Sanz, A. (2018). The role of mitochondrial ROS in the aging brain. *FEBS Letters*, 592(5), 743–758.

Stotland, A., & Gottlieb, R. A. (2015). Mitochondrial quality control: Easy come, easy go. *Biochimica et Biophysica Acta, 1853*(10 Pt B), 2802-2811.

Stowe, D. F., & Camara, A. K. (2009). Mitochondrial reactive oxygen species production in excitable cells: modulators of mitochondrial and cell function. *Antioxidant Redox Signalling, 11*(6), 1373-1414.

Sugiura, Y., & Lin, W. (2011). Neuron-glia interactions: the roles of Schwann cells in neuromuscular synapse formation and function. *Bioscience Reports*, 31(5), 295–302.

Sukumar, P., Viswambharan, H., Imrie, H., Cubbon, R. M., Yuldasheva, N., Gage, M., Kearney, M. T. (2013). Nox2 NADPH oxidase has a critical role in insulin resistance-related endothelial cell dysfunction. *Diabetes, 62*(6), 2130-2134.

Sun, G. Y., Shelat, P. B., Jensen, M. B., He, Y., Sun, A. Y., & Simonyi, A. (2010). Phospholipases A2 and inflammatory responses in the central nervous system. *Neuromolecular Medicine, 12*(2), 133-148.

Sun, H., Liu, J., Ding, F., Wang, X., Liu, M., & Gu, X. (2006). Investigation of differentially expressed proteins in rat gastrocnemius muscle during denervation-reinnervation. *J Muscle Res Cell Motil, 27*(3-4), 241-250.

Sun, N., Youle, R. J., & Finkel, T. (2016). The Mitochondrial Basis of Aging. *Mol Cell, 61*(5), 654-666.

Szentesi, P., Csernoch, L., Dux, L., & Keller-Pinter, A. (2019). Changes in Redox Signaling in the Skeletal Muscle with Aging. *Oxidative Medicine and Cell Longevity, 2019*, 4617801.

Szeto, H. H. (2008). Mitochondria-targeted cytoprotective peptides for ischemia-reperfusion injury. *Antioxidant Redox Signalling, 10*(3), 601-619.

T

Tamma, G., Valenti, G., Grossini, E., Donnini, S., Marino, A., Marinelli, R. A., & Calamita, G. (2018). Aquaporin Membrane Channels in Oxidative Stress, Cell Signaling, and Aging: Recent Advances and Research Trends. *Oxidative Medicine and Cell Longevity, 2018*, 1501847.

Tanaka, K. (2009). The proteasome: overview of structure and functions. *Proceedings of the Japan Academy, Ser. B, Physical and Biological Sciences, 85*(1), 12-36.

Tanida I., Ueno T., Kominami E., (2008) Autophagosome and Phagosome, Humana Press, NJ, USA

Terman, J. R., & Kashina, A. (2013). Post-translational modification and regulation of actin. *Current Opinion in Cell Biology*, 25(1), 30–38.

Thacker, J. S., Yeung, D. H., Staines, W. R., & Mielke, J. G. (2016). Total protein or high-abundance protein: Which offers the best loading control for Western blotting? *Analytical Biochemistry, 496*, 76-78.

Tintignac, L. A., Brenner, H. R., & Ruegg, M. A. (2015). Mechanisms Regulating Neuromuscular Junction Development and Function and Causes of Muscle Wasting. *Physiology Reviews, 95*(3), 809-852.

Tognarelli, J. M., Dawood, M., Shariff, M. I. F., Grover, V. P. B., Crossey, M. M. E., Cox, I. J., McPhail, M. J. W. (2015). Magnetic Resonance Spectroscopy: Principles and Techniques: Lessons for Clinicians. *Journal of Clinical and Experimental Hepatology, 5*(4), 320-328.

Trachootham, D., Alexandre, J., & Huang, P. (2009). Targeting cancer cells by ROS-mediated mechanisms: a radical therapeutic approach? *Nature Review Drug Discovery, 8*(7), 579-591.

Trivedi MV, L. J., Siahaan TJ. (2009). The role of thiols and disulfides in protein chemical and physical stability. *Current Protein and Peptide Science* (10).

Tsen, G., Halfter, W., Kroger, S., & Cole, G. J. (1995). Agrin is a heparan sulfate proteoglycan. *Journal of Biology and Chemistry, 270*(7), 3392-3399.

Tsunoda, M., Sakaue, T., Naito, S., Sunami, T., Abe, N., Ueno, Y., Takenaka, A. (2010). Insights into the structures of DNA damaged by hydroxyl radical: crystal structures of DNA duplexes containing 5-formyluracil. *Journal of Nucleic Acids, 2010*, 107289.

U

Umanskaya, A., Santulli, G., Xie, W., Andersson, D. C., Reiken, S. R., & Marks, A. R. (2014). Genetically enhancing mitochondrial antioxidant activity improves muscle function in aging. *Proceedings of the National Academy of Sciences of the United States of America, 111*(42), 15250-15255.

Ursini, F., Maiorino, M., & Forman, H. J. (2016). Redox homeostasis: The Golden Mean of healthy living. *Redox Biology, 8*, 205-215.

Uttara, B., Singh, A. V., Zamboni, P., & Mahajan, R. T. (2009). Oxidative stress and neurodegenerative diseases: a review of upstream and downstream antioxidant therapeutic options. *Current Neuropharmacology, 7*(1), 65-74.

V

Vainshtein, A., Desjardins, E. M., Armani, A., Sandri, M., & Hood, D. A. (2015). PGC-1alpha modulates denervation-induced mitophagy in skeletal muscle. *Skeletal Muscle, 5*, 9.

van den Berg, R. A., Hoefsloot, H. C. J., Westerhuis, J. A., Smilde, A. K., & van der Werf, M. J. (2006). Centering, scaling, and transformations: Improving the biological information content of metabolomics data. *BMC Genomics*, *7*, 1–15.

Vasilaki, A., Mansouri, A., Van Remmen, H., van der Meulen, J. H., Larkin, L., Richardson, A. G., Jackson, M. J. (2006). Free radical generation by skeletal muscle of adult and old mice: effect of contractile activity. *Aging Cell*, 5(2), 109-117.

Vasilaki, A., Csete, M., Pye, D., Lee, S., Palomero, J., McArdle, F., Jackson, M. J. (2006). Genetic modification of the manganese superoxide dismutase/glutathione peroxidase 1 pathway influences intracellular ROS

generation in quiescent, but not contracting, skeletal muscle cells. *Free Radical Biology and Medicine, 41*(11), 1719-1725.

Vatansever, F., de Melo, W. C., Avci, P., Vecchio, D., Sadasivam, M., Gupta, A., Hamblin, M. R. (2013). Antimicrobial strategies centered around reactive oxygen species--bactericidal antibiotics, photodynamic therapy, and beyond. *FEMS Microbiology Review, 37*(6), 955-989.

Vellas, B., Fielding, R. A., Bens, C., Bernabei, R., Cawthon, P. M., Cederholm, T., Cesari, M. (2018). Implications of ICD-10 for Sarcopenia Clinical Practice and Clinical Trials: Report by the International Conference on Frailty and Sarcopenia Research Task Force. *Journal of Frailty and Aging, 7*(1), 2-9.

Vendelbo, M. H., Moller, A. B., Christensen, B., Nellemann, B., Clasen, B. F., Nair, K. S., Moller, N. (2014). Fasting increases human skeletal muscle net phenylalanine release and this is associated with decreased mTOR signaling. *PLoS One, 9*(7), e102031.

Viant, M. R., Kurland, I. J., Jones, M. R., & Dunn, W. B. (2017). How close are we to complete annotation of metabolomes? *Current Opinions in Chemistry and Biology, 36*, 64-69.

Voet, Donald; Judith G. Voet; Charlotte W. Pratt (2006). Fundamentals of Biochemistry, 2nd Edition. John Wiley and Sons, Inc. pp. 547, 556.

W

Wagner A. (2014). Arrival of the Fittest (I ed.). New York: Penguin Group. p. 100.

Wan, F., & Lenardo, M. J. (2010). The nuclear signaling of NF-κB: current knowledge, new insights, and future perspectives. *Cell Research, 20*(1), 24–33.

Wang, X. H., Zhang, L., Mitch, W. E., LeDoux, J. M., Hu, J., & Du, J. (2010). Caspase-3 cleaves specific 19 S proteasome subunits in skeletal muscle stimulating proteasome activity. *Journal of Biology and Chemestry, 285*(28), 21249-21257.

Wang, Y., & Pessin, J. E. (2013). Mechanisms for fiber-type specificity of skeletal muscle atrophy. *Current Opinion in Clinical Nutrition*, 16(3), 243–250.

Ward, C. W., Prosser, B. L., & Lederer, W. J. (2014). Mechanical stretch-induced activation of ROS/RNS signaling in striated muscle. *Antioxidant Redox Signalling, 20*(6), 929-936.

Wei, Y., Sowers, J. R., Clark, S. E., Li, W., Ferrario, C. M., & Stump, C. S. (2008). Angiotensin II-induced skeletal muscle insulin resistance mediated by NF-kappaB activation via NADPH oxidase. *Am Journal of Physiology Endocrinol Metab, 294*(2), E345-351.

Williams, G. N., Higgins, M. J., & Lewek, M. D. (2002). Aging skeletal muscle: physiologic changes and the effects of training. *Physical Therapy, 82*(1), 62-68.

Winterbourn, C. C., & Hampton, M. B. (2008). Thiol chemistry and specificity in redox signaling. *Free Radical Biology and Medicine, 45*(5), 549-561.

Wollman EE, d'Auriol L, Rimsky L, Shaw A, Jacquot JP, Wingfield P, Graber P, Dessarps F, Robin P, Galibert F (October 1988). Cloning and expression of a cDNA for human thioredoxin. *The Journal of Biological Chemistry*. 263 (30): 15506–12

Wood, S. T., Long, D. L., Reisz, J. A., Yammani, R. R., Burke, E. A., Klomsiri, C., Poole, L. B., Furdui, C. M., & Loeser, R. F. (2016). Cysteine-Mediated Redox Regulation of Cell Signaling in Chondrocytes Stimulated With Fibronectin Fragments. *Arthritis & Rheumatology*, *68*(1), 117–126.

Wood, Z. A., Poole, L. B., & Karplus, P. A. (2003). Peroxiredoxin evolution and the regulation of H2O2 signaling. *Science, 300*(5619), 650-653.

Wu, Y., Feinstein, S. I., Manevich, Y., Chowdhury, I., Pak, J. H., Kazi, A., Fisher, A. B. (2009). Mitogen-activated protein kinase-mediated phosphorylation of peroxiredoxin 6 regulates its phospholipase A(2) activity. *Biochemistry Journal, 419*(3), 669-679.

X

Xia, J., & Wishart, D. S. (2010). MSEA: a web-based tool to identify biologically meaningful patterns in quantitative metabolomic data. *Nucleic Acids Research*, 38, W71-7.

Xilouri, M., & Stefanis, L. (2016). Chaperone mediated autophagy in aging: Starve to prosper. *Ageing Research, 32*, 13-21.

Y

Yanamadala, V., Negoro, H., Denker, B.M. (2009) Heterotrimeric G proteins and apoptosis: intersecting signaling pathways leading to context dependent phenotypes. *Current Molecular Medicine*, 9(5), 527-545.

Yin, J., Ren, W., Huang, X., Deng, J., Li, T., & Yin, Y. (2018). Potential Mechanisms Connecting Purine Metabolism and Cancer Therapy. *Frontiers in Immunology, 9*, 1697.

Youle, R. J., & van der Bliek, A. M. (2012). Mitochondrial fission, fusion, and stress. *Science, 337*(6098), 1062-1065.

Z

Zamocky, M., Furtmüller, P.G., and Obinger, C. (2008). Evolution of catalases from bacteria to humans. *Antioxidant Redox Signalling* 10, 1527–1548.

Zhang, Y., Marcillat, O., Giulivi, C., Ernster, L., & Davies, K. J. (1990). The oxidative inactivation of mitochondrial ETC components and ATPase. *Journal of Biology and Chemistry, 265*(27), 16330-16336.

Zhao, X., Bey, E. A., Wientjes, F. B., & Cathcart, M. K. (2002). Cytosolic phospholipase A2 (cPLA2) regulation of human monocyte NADPH oxidase activity. cPLA2 affects translocation but not phosphorylation of p67(phox) and p47(phox). *Journal of Biology and Chemistry, 277*(28), 25385-25392.

Zhao RZ, Jiang S, Zhang L, Yu ZB. Mitochondrial electron transport chain, ROS generation and uncoupling (Review). Int J Mol Med. 2019;44(1):3–15.

Zhou, J., Chong, S. Y., Lim, A., Singh, B. K., Sinha, R. A., Salmon, A. B., & Yen, P. M. (2017). Changes in macroautophagy, chaperone-mediated autophagy, and mitochondrial metabolism in murine skeletal and cardiac muscle during aging. *Aging (Albany NY), 9*(2), 583-599.

Zorzano, A., Hernandez-Alvarez, M. I., Sebastian, D., & Munoz, J. P. (2015). Mitofusin 2 as a driver that controls energy metabolism and insulin signaling. *Antioxidant Redox Signalling, 22*(12), 1020-1031.

Websites

https://blog.bham.ac.uk

https://bruker.com

https://courses.lumenlearning.com

https://galaxy.liv.ac.uk

https://jax.org

https://metaboanalyst.ca

https://pearson.co.uk

Appendix 1. Western blot analysis and Ponceau normalisation

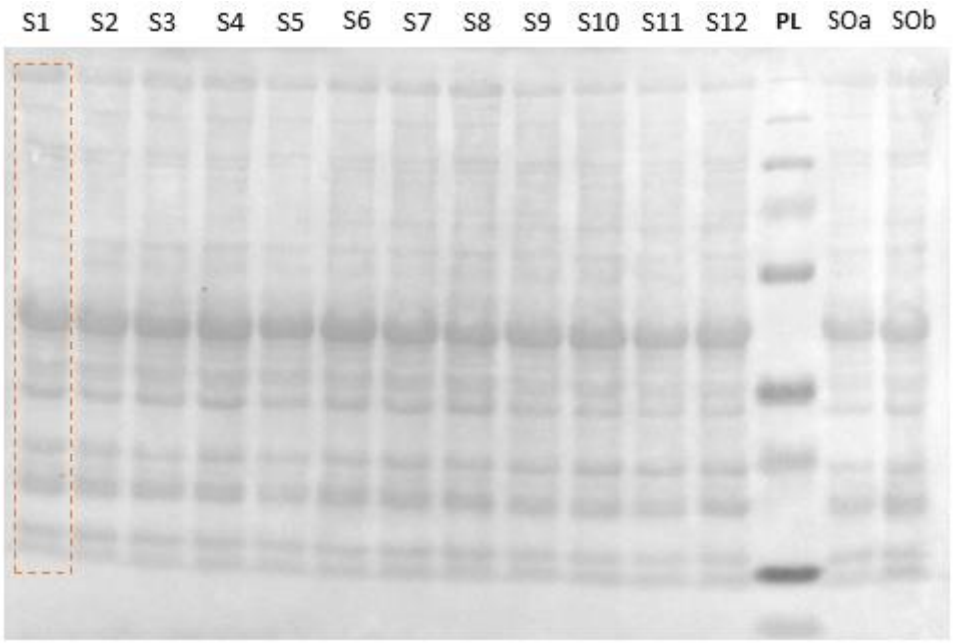

Figure A1.1. *Representative membrane stained with Ponceau. Each lane represents a different sample (S1-12) together with a protein ladder (PL) used as molecular weight reference and 2 extra samples (SOa-b) used to verify the specificity of the secondary antibody. The representative orange box shows the area used for the densitometry analysis of each lane.*

Table A1.1. *In the table are presented the raw values obtained from the ImageJ analysis of the ponceau staining as shown in Figure A1.1 and the ratio obtained dividing the raw values by the blot reference (S1).*

	Raw value	Ratio of S1 (Sn/S1)
S1	72843.98	1
S2	70902.03	0.973
S3	69555.65	0.955
S4	84312.44	1.157
S5	53233.74	0.731
S6	71079.96	0.976
S7	67629.03	0.928
S8	70318.84	0.965
S9	72541.84	0.996
S10	77135.62	1.059
S11	51215.67	0.703
S12	73842.25	1.014

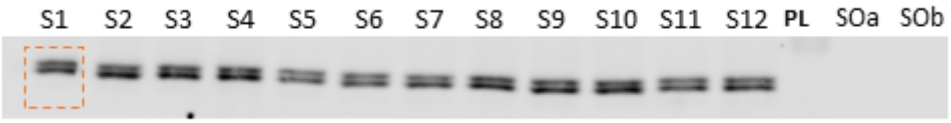

Figure A1.2. *Representative membrane blotted for Mfn2. Each lane represents a sample (S1-12), together with a protein ladder (PL) and 2 extra samples (SOa-b) used to verify the specificity of the secondary antibody. The representative orange box shows the area used for the densitometry analysis of each lane. The lack of signal coming from SOa and SOb suggests the specificity of the secondary antibody for its primary.*

Table A1.2. *In the table are presented the raw values obtained from the densitometry analysis of the Mfn2 bands shown in Figure A1.2 (DRV) and the normalised valued obtained dividing DRV by the S1 ratio of the corresponding lane obtained analysing the ponceau S (Table A1.1). The normalised results are expressed in arbitrary units and were used for statistical analysis.*

	Raw value (DRV)	Normalised (DRV/Ratio of S1)
S1	20318.87	20318.87
S2	25151.99	25840.88
S3	25160.25	26349.73
S4	25907.42	22383.41
S5	17227.23	23573.40
S6	19479.52	19962.95
S7	19921.04	21457.17
S8	25031.52	25930.40
S9	26413.54	26523.56
S10	27008.76	25506.06
S11	21057.71	29950.36
S12	24498.71	24167.52

Appendix 2. Carbonyls blot analysis

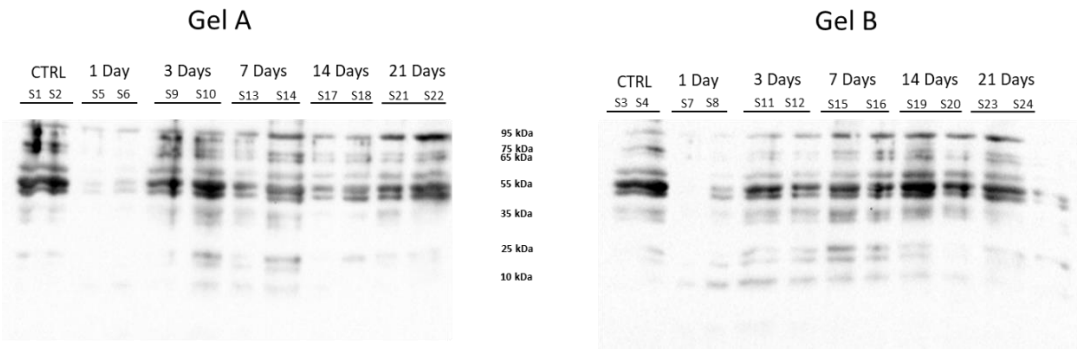

Figure A2.1 *Original oxyblots analysed to generate the data presented in section 3.3.5. The nature of the protocol did not allow the use of any normalisation method (i.e. Ponceau S, GADPH or β-Actin) therefore it was impossible to normalise the results and verify the effectiveness of the transfer.*

Appendix 3. Mitochondria isolation and NMR metabolomics of isolated mitochondria

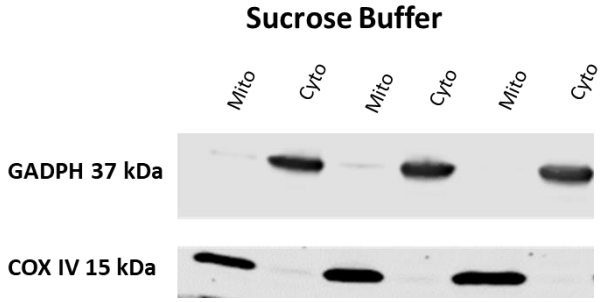

Figure A3.1. *Representative blots of GADPH and COXIV in mitochondrial (Mito) and cytosolic (Cyto) extracts obtained using the Sucrose Buffer as in by Dimauro and Pearson et al, 2012.*

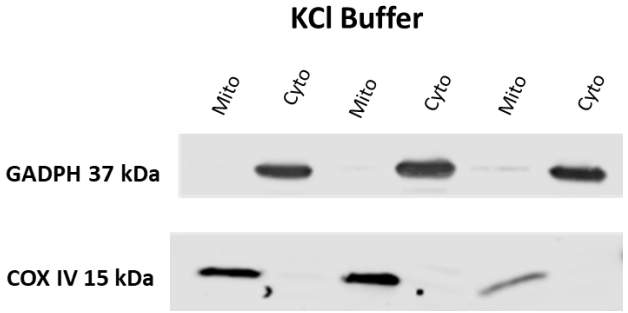

Figure A3.2. *Representative blots of GADPH and COXIV in mitochondrial (Mito) and cytosolic (Cyto) extracts obtained using the KCl Buffer as in Corcelli et al, 2010.*

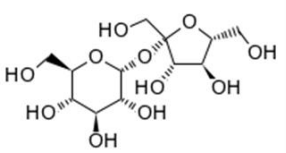

Sucrose

Figure A3.3. *Chemical structure of Sucrose. The presence of two aromatic rings generate a series of peaks in the NMR metabolomics spectra with the potential to obscure the signal of other metabolites.*

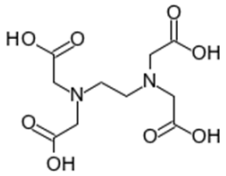

EDTA

Figure A3.4. *Chemical structure of EDTA. Although not presenting an aromatic ring in its structure this chemical, similar to Sucrose, generates a series of peaks in the NMR metabolomics spectra with the potential to obscure the signal of other metabolites.*

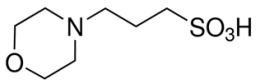

MOPS

Figure A3.5. *Chemical structure of MOPS. This N-substituted amino sulfonic acid, similarly to Sucrose, generates a series of peaks in the NMR metabolomics spectra with the potential to obscure the signal of other metabolites.*

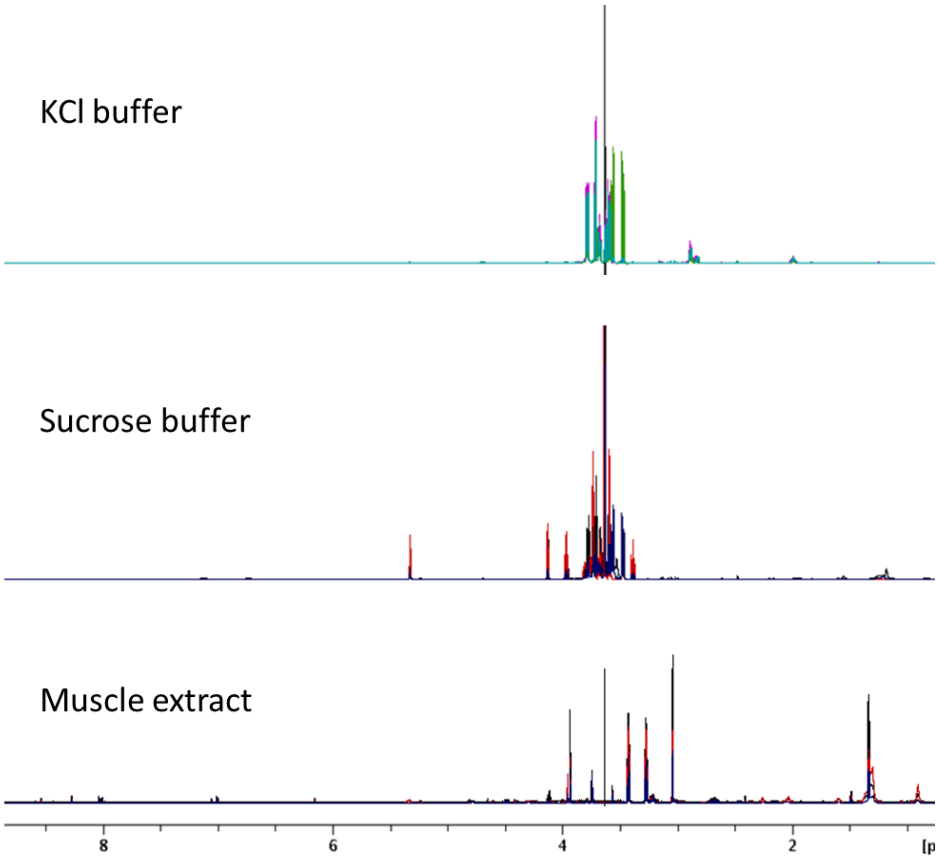

Figure A3.6. *^{1}H ^{1}D NMR spectra (700MHz) of mitochondria extracted from mouse gastrocnemius using KCl or Sucrose buffers and of the extract from C2C12 cells using a standard extraction buffer for NMR metabolomics containing 50% HPLC grade acetonitrile and 50 % ultra-pure water.*

Appendix 4. Publications

Redox Biology 26 (2019) 101294

Contents lists available at ScienceDirect

Redox Biology

journal homepage: www.elsevier.com/locate/redox

Research Paper

Redox responses in skeletal muscle following denervation

Mattia Scalabrin[a,1], Natalie Pollock[a,1], Caroline A. Staunton[a], Susan V. Brooks[b], Anne McArdle[a], Malcolm J. Jackson[a], Aphrodite Vasilaki[a,*]

[a] MRC-Arthritis Research UK Centre for Integrated Research Into Musculoskeletal Ageing (CIMA), Department of Musculoskeletal Biology, Institute of Ageing and Chronic Disease, University of Liverpool, UK

[b] Department of Molecular and Integrative Physiology, University of Michigan, Ann Arbor, MI, USA

ARTICLE INFO

Keywords:
Reactive oxygen species
Denervation
Skeletal muscle
Peroxide release
Hydrogen peroxide

ABSTRACT

Previous studies have shown a significant increase in the mitochondrial generation of hydrogen peroxide (H_2O_2) and other peroxides in recently denervated muscle fibers. The mechanisms for generation of these peroxides and how the muscle responds to these peroxides are not fully established. The aim of this work was to determine the effect of denervation on the muscle content of proteins that may contribute to mitochondrial peroxide release and the muscle responses to this generation. Denervation of the tibialis anterior (TA) and extensor digitorum longus (EDL) muscles in mice was achieved by surgical removal of a small section of the peroneal nerve prior to its entry into the muscle. An increase in mitochondrial peroxide generation has been observed from 7 days and sustained up to 21 days following denervation in the TA muscle fibers. This increased peroxide generation was reduced by incubation of skinned fibers with inhibitors of monoamine oxidases, NADPH oxidases or phospholipase A2 enzymes and the muscle content of these enzymes together with peroxiredoxin 6 were increased following denervation. Denervated muscle also showed significant adaptations in the content of several enzymes involved in the protection of cells against oxidative damage. Morphological analyses indicated a progressive significant loss of muscle mass in the TA muscle from 7 days up to 21 days following denervation due to fiber atrophy but without fiber loss. These results support the possibility that, at least initially, the increase in peroxide production may stimulate adaptations in an attempt to protect the muscle fibers, but that these processes are insufficient and the increased peroxide generation over the longer term may activate degenerative and atrophic processes in the denervated muscle fibers.

1. Introduction

Loss of muscle mass occurs during aging and is known as sarcopenia. This has a significant impact on health and is caused by several factors, among which impairment of the neuromuscular system appears to play a primary role. The neuromuscular system shows great plasticity and muscle fibers undergo a process of denervation and re-innervation repeatedly throughout life. With advancing age, the efficiency of this cycle appears to decline with a characteristic loss of neuromuscular junction (NMJ) structure (the synapse between a motor neuron and muscle fiber), motor units (the unit consisting of a single motor neuron and the muscle fibers it innervates), muscle mass (due to both the loss of motor units and individual muscle fiber atrophy) and together with an increase in neuronal axon sprouting with preferential re-innervation of slow-twitch muscle fibers [1–4]. Denervated fibers atrophy and, on average, they are 35–50% smaller in comparison with innervated fibers in muscles of old rats [1]. However, the reasons for the age-related changes in muscle fiber denervation and disrupted NMJ innervation and function are not currently known.

A characteristic of aging is an increase of reactive oxygen species (ROS) activities that, if not adequately counteracted, can result in oxidative stress with decreased mitochondrial efficiency and cellular damage. Although numerous studies have highlighted the degenerative roles played by chronic increases in ROS [5], others have highlighted

Abbreviations: Extensor digitorum longus, EDL; Glutathione, GSH; Glutathione peroxidase 1, GPx1; Hydrogen peroxide, H_2O_2; Heat Shock Proteins, HSPs; Manganese superoxide dismutase, MnSOD; Monoamine Oxidase A, MAO-A; NADPH oxidase 2, Nox2; NADPH oxidase 4, Nox4; Neuromuscular junction, NMJ; Oxidized glutathione, GSSG; Peroxiredoxin 6, Prx6; Phospholipase A2, PLA2; Phospholipase A2 (cytosolic isoform), cPLA2; Reactive oxygen species, ROS; Thioredoxin reductase 2, TrxR2; Tibialis anterior, TA; Wild type, WT

* Corresponding author.
E-mail address: vasilaki@liverpool.ac.uk (A. Vasilaki).

[1] These authors contributed equally to this publication.

https://doi.org/10.1016/j.redox.2019.101294
Received 21 June 2019; Received in revised form 1 August 2019; Accepted 7 August 2019
Available online 08 August 2019

the signalling role played by ROS in response to alterations in redox homeostasis [2]. Thus, oxidants can activate and inactivate transcription factors, membrane channels and metabolic enzymes in addition to modulating calcium-dependent and phosphorylation signalling pathways [6].

Nerve transection models have been extensively used to investigate the mechanisms leading to rapid decline in muscle mass and function following the loss of innervation. Studies using this denervation model in rodents also point to a role of mitochondrial oxidative stress in the mechanisms of denervation-induced muscle atrophy [7]; Bhattacharya et al., 2008, [10].

Hydrogen peroxide (H_2O_2) plays a key role in cell signalling and is usually formed within the mitochondria by dismutation of superoxide generated from the electron transport chain. Beside the mitochondrial electron transport chain, up to 31 other enzymes have been implicated in the generation of H_2O_2 in skeletal muscle [9]. Studies performed by Muller et al. [7] indicated that H_2O_2 and other peroxides are produced in high amounts by muscle mitochondria [10] following short-term denervation and recent data published by our group show that this increased H_2O_2 may be generated by sources other than the electron transport chain within mitochondria [8].

The aim of the present study was to determine the effect of prolonged denervation on peroxide release and proteins that regulate redox homeostasis in muscle fibers.

2. Materials and methods

2.1. Mice

8–10 month old male C57BL/6 WT and B6. Cg-Tg (Thy1-YFP) mice were used for this study, with 4 mice used per time point (unless otherwise stated). The C57BL/6 WT mice were used for biochemical analyses whereas the B6. Cg-Tg (Thy1-YFP) mice were used for histological analyses and NMJ visualization as previously described [8]. Mice were fed ad libitum on a standard laboratory diet, subjected to a 12-h light/dark cycle and maintained under SPF conditions. All experiments were performed in accordance with UK Home Office guidelines under the UK Animals (Scientific Procedures) Act 1986 and received ethical approval from the University of Liverpool Animal Welfare Ethical Review Body (AWERB).

2.2. Surgical denervation of the tibialis anterior (TA) and extensor digitorum longus (EDL) muscles

Mice underwent surgical denervation of the tibialis anterior (TA) and extensor digitorum longus (EDL) muscles as described by Pollock et al. [8]. Briefly, mice were anesthetized with Isoflurane 0.2% (ISO) while Buprenorphine (analgesic; 1 mg/kg, SC 0.1 ml) was administered before surgery. To induce denervation of the TA and EDL muscles, a small section of the peroneal nerve was removed. The external wound was sutured and mice were maintained under close observation until recovery from anesthetic. Mice were then sacrificed at different time points after denervation (1, 3, 7, 14, 21 days) through cervical dislocation and TA and EDL muscles were immediately removed.

2.3. Assessment of morphological changes in muscle and nerve

TA muscles were mounted directly on a cork disk, surrounded with O·C.T. mounting medium (Thermo Fisher Scientific, Waltham, MA, USA), frozen rapidly in isopentane cooled in liquid nitrogen and sectioned (12 μm) using a cryostat (Leica CM1850, Leica, Wetzlar, Germany) as described by Vasilaki et al., [11]. To assess fiber cross-sectional area (CSA) transverse sections were fixed onto slides in ice-cold methanol and stained with Alexa Fluor 488 nm conjugated wheat germ agglutinin (WGA-488) (5 μM) (Vectorlabs, Burlingame, CA, USA). Multiple images were collected by confocal microscopy (Nikon, Kingston, UK) using ×20 objective to capture the section in its entirety. The images were collated into a montage and analyzed using ImageJ software (U.S. National Institutes of Health, USA). Separate transverse sections of TA muscle were stained with hematoxylin and eosin (H&E) using a standard protocol [12]. Each slide was examined using a Nikon Ci microscope (Nikon Kingston, UK) equipped with ×4 and ×20 objectives.

In order to assess the loss of innervation at different time points the EDL muscle from Thy1-YFP mice was pinned onto sylgard plates (Fernell, Preston, UK) and fixed in 10% neutral buffered formalin. Whole EDL muscles were incubated (30 min) with bungarotoxin conjugated with Alexa Fluor-532nm (10 μg/ml) and Dapi (1:500) (Invitrogen, Paisley, United Kingdom). Nerves were visible due to the expression of YFP. Muscles were imaged via confocal microscopy (Nikon A1, Kingston, UK) using a water immersion lens.

2.4. Analysis of mitochondrial peroxide generation

Analysis of the mitochondrial release of H_2O_2 (and other peroxides) from the TA muscle was performed by following the oxidation of amplex red as described by Pollock et al. [8]. Small bundles of muscle fibers were placed into 200 μM saponin (Sigma Aldrich, UK) in relax solution (containing 4.5 mM MgATP, 1 mM Free Mg, 10 mM Imidazole, 2 mM EGTA and 100 mM KCl, pH 7.0) to permeabilize the fibers. Saponin was washed from the tissue through 3 cycles of fresh relax solution with gentle agitation prior to placing the bundles into amplex red solution (containing 37.5U/ml SOD, 19.44 mM Amplex red, 5U/ml Horse radish Peroxidase (HRP) in ROS buffer (125 mM KCL, 10 mM Hepes, 5 mM $MgCl_2$, 2 mM K_2HPO_4) in black 96 well plates (Corning, Wiesbaden, Germany). Bundles were then incubated at 37 °C with amplex red solution without added substrates to assess state 1 peroxide production, or in the presence of specific enzyme inhibitors: (20 μM AACOCF3 - phospholipase A2 inhibitor; 0.5 mM apocynin – a non specific NADPH oxidase inhibitor; 100 μM chlorgyline - monoamine oxidase A inhibitor; 100 μM pargyline - monoamine oxidase B inhibitor) as described in Pollock et al. [8]. The fluorescent signal was recorded at 590 nm using a fluorimeter (Fluorstar, BMG Labteck, Germany).

2.5. Muscle content of total and oxidized glutathione

TA muscles were ground under liquid nitrogen and the resulting powder was added to 1% sulfosalicylic acid. Following homogenization, samples were centrifuged for 10 min at 14,000g and the supernatant was collected for total and oxidized glutathione analyses as described by Vasilaki et al. [13]; whilst the pellet was re-suspended in 0.5 M Tris/HCl buffer (pH 7.6) for total protein content determination [14]. The automated glutathione recycling method described by Anderson [15] was used to assess the total glutathione content using a 96-well plate reader (SPECTROstar Nano, BMG labtech, Ortenberg, Germany). To determine the oxidized glutathione content, samples were firstly derivatized with 2-Vinylpyridine and analyzed as above.

2.6. SDS-PAGE and immunoblotting

Denervated and control TA muscles were ground in liquid nitrogen. The resulting powder was added to 1% SDS (Sigma-Aldrich Ltd, Gillingham, Dorset, United Kingdom) containing protease inhibitors (Thermo Fisher Scientific, Waltham, MA, USA) and homogenized for 30–60 s. Samples were centrifuged for 10 min at 13,000g, the supernatant collected and protein content analyzed using a BCA assay kit (Thermo Fisher Scientific, Waltham, MA, USA). Thirty micrograms of total protein was applied to a 12% polyacrylamide gel with a 4% stacking gel. The separated proteins were transferred onto nitrocellulose membranes by western blotting as previously described by Sakellariou et al. [16]. Ponceau red (Sigma-Aldrich, St. Louis, MI, USA) was used to verify the effectiveness of transfer procedure and to

Table 1
List of the antibodies utilized for SDS-PAGE Western blot analysis.

Target	Company	Code	Clonal	Host species	Dilution
GPx1	Abcam	ab22604	Polyclonal	Rabbit	1:1000
Hsp25	ENZO	801d	Polyclonal	Rabbit	1:1000
Hsp70	Abcam	ab31010	Polyclonal	Rabbit	1:1000
Hsc70	Stress Gen	SPA815	Monoclonal	Rat	1:750
MAO-A	Abcam	ab126751	Monoclonal	Rabbit	1:1000
Nox4	Abcam	ab133303	Monoclonal	Rabbit	1:1000
Nox2/gp91phox	Abcam	ab43801	Polyclonal	Mouse	1:500
P22 phox	SCBT	sc271968	Monoclonal	Mouse	1:500
P40 phox	SCBT	sc48388	Monoclonal	Mouse	1:500
P47 phox	SCBT	sc17845	Monoclonal	Mouse	1:500
P67 phox	BD Bioscience	610913	Monoclonal	Mouse	1:500
cPLA2	CST	2832S	Polyclonal	Rabbit	1:1000
Prx6	Abcam	ab133348	Monoclonal	Rabbit	1:1000
Rac-1	Abcam	ab33186	Monoclonal	Mouse	1:500
MnSOD	CST	13194S	Monoclonal	Rabbit	1:1000
TRxR2	CST	12029S	Monoclonal	Mouse	1:1000

Table 2
List of the secondary antibodies utilized for SDS-PAGE Western Blot analysis.

Secondary Antibody	Company	Code	Dilution
Anti-mouse IgG, HRP-linked	CST	7076S	1:5000
Anti-rabbit IgG, HRP-linked	CST	7074S	1:5000
Anti-rat IgG, HRP-linked	CST	7077S	1:5000

normalize the results as described by Romero-Calvo et al. [17]. The membranes were analyzed using antibodies against; Nox2/gp91 phosphorylated (Nox2/gp91^{phox}), Nox4, p22 phosphorylated (p22^{phox}), p40 phosphorylated (p40^{phox}), p47 phosphorylated (p47^{phox}) and p67 phosphorylated (p67^{phox}), Ras-related C3 botulinum toxin substrate 1 (Rac-1), peroxiredoxin 6 (Prx6), cytosolic phospholipase A2 isoform (cPLA2), monoamine oxidase A (MAO-A), thioredoxin reductase 2 (TrxR2), glutathione peroxidase 1 (GPx1), manganese superoxide dismutase (MnSOD; SOD2) and Heat Shock Proteins (HSPs) Hsp25, Hsc70 and Hsp70 (Tables 1 and 2). Chemiluminescence was detected using the ChemiDocTM imaging system (Bio-Rad, Hercules, CA, USA) following addition of ECL (Bio-Rad, Hercules, CA, USA). Densitometry analysis was performed using ImageJ software according to the protocol described by McLean [18].

2.7. Analysis of protein carbonylation

Denervated and control TA muscles from C57/Bl6 mice were homogenized in Hepes buffer and analyzed using the *OxyBlot* protein oxidation detection kit (Merk, Darmstadt, Germany). Samples were separated on 12% polyacrylamide gels, transferred on a PVDF membrane (GE Healthcare Bio-Sciences, Pittsburgh, USA) and analyzed as specified. Densitometry analysis of the bands at different molecular weights was performed using ImageJ software.

2.8. Statistical analysis

Statistical analysis was performed using IBM SPSS statistic version 22 software (IBM analytics, New York, USA). All tests have been carried out with a 95% confidence interval and the level of significance was set at 0.05. Normal distribution was verified using the Shapiro-Wilk test and the data were expressed as the mean ± standard error mean. One-way ANOVA was performed using Bonferroni's correction to identify significant differences between the control group and the other time points. For those variables where the assumption of normal distribution was violated, differences within and between groups were determined by Kruskal-Wallis test followed by Mann-Whitney *U* test for post hoc analysis applying Bonferroni's correction.

3. Results

3.1. Morphological and structural changes following denervation

No significant difference in body weights of mice were observed between the control and the denervated groups (Fig. 1A). Analyses indicated a progressive and significant loss of mass in the TA muscle from 7 days up to 21 days following denervation ($F(5,19) = 33.204$ $p < 0.01$) (Fig. 1B) which was not associated with any loss of fiber number ($F(5,10) = 0.316$ $p > 0.05$) (Fig. 1C) but appeared entirely due to fiber atrophy (Fig. 1D). Analysis of the distribution of fiber CSA indicated that denervation induced a decrease in the number of larger fibers at 7, 14 and 21 days post-nerve transection with an increase in the number of smaller fibers compared with control muscle (Fig. 1D).

While the decline in fiber size reported in Fig. 1 was clearly evident, histological examination revealed no structural abnormalities within muscles (i.e. presence of necrotic or regenerating fibers; Fig. 2A). No significant infiltration of the muscle by immune or other mononuclear cells was apparent following denervation with hematoxylin and eosin staining (Fig. 2A). Since this was not within the scope of the study, specific staining for potential invading cells was not performed and therefore, it is not possible to entirely rule out the possibility that increased numbers of immune cells were present at some time points.

Examination of the EDL muscles confirmed that neuronal input to the NMJs was lost by 3 days post-nerve transection [8]. There was no evidence of re-innervation at 14 or 21 days and acetylcholine receptors (stained using α-bungarotoxin) remained present in characteristic clusters. Further bungarotoxin-staining distant from NMJs was also apparent along the length of the muscle fibers by 21 days post-denervation (Fig. 2B).

3.2. Peroxide production by mitochondria in bundles of TA muscle fibers in state 1

A statistically significant increase in the rate of oxidation of amplex red was observed from bundles of permeabilized TA fibers following denervation ($F(4,11) = 44.354$ $p < 0.001$) (Fig. 3A). Peak mitochondrial peroxide production in state 1 was seen at 7 days following denervation although levels remained elevated up to 21 days after denervation (Fig. 3A).

3.3. Total and oxidized glutathione content of muscle

The total glutathione (GSH) and oxidized glutathione (GSSG) contents of denervated TA muscles are shown in Fig. 3B. Data show no significant differences in total GSH ($F(5,16) = 1.473$ $p > 0.05$) or GSSG ($F(5,15) = 1.291$ $p > 0.05$) content following denervation.

3.4. Protein oxidation in TA muscles following denervation

Analysis of protein carbonylation has been widely used as a measure of oxidative damage to proteins. The *OxyBlot* approach is relatively non-specific and semi-quantitative but potentially provides insight into the molecular mass of oxidized protein targets. Soluble proteins from denervated and control TA muscles were separated by SDS-PAGE and were analyzed for carbonyl content following western blotting. An illustrative blot of the pattern of bands is shown in Fig. 3C. Six major bands of approximate molecular weight 95, 75, 65, 55, 35, and 25 kDa were quantified by band densitometry (Fig. 3D). Densitometry analysis revealed no major differences in the carbonyl content between control and denervated muscles except from the band seen at approximately ~25 KDa, which showed increased intensity at 7 days following denervation ($F(5,17) = 3.616$ $p < 0.05$) (Fig. 3D) when the significant increase in mitochondrial peroxide generation from the denervated

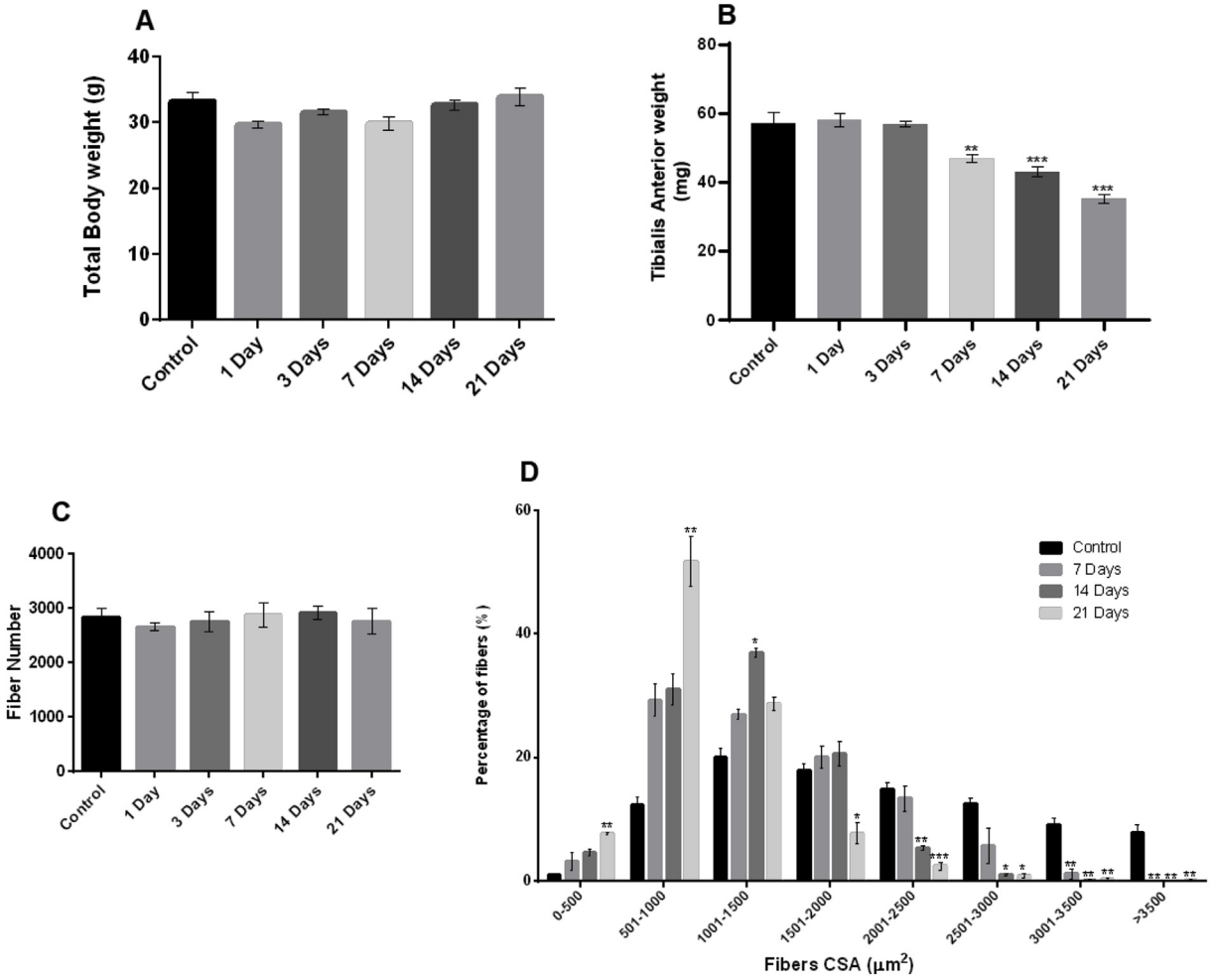

Fig. 1. (A) Total body weights (B) TA muscle weights (C) fiber number and (D) fiber CSA from control mice (non-denervated) and mice at 1, 3, 7, 14 and 21 days post-denervation. Histograms represent the mean and the standard error of the mean for each experimental group (n = 4). *p < 0.05 - **p < 0.01 - ***p < 0.001 compared with the control group.

muscle fibers was also evident (Fig. 3A).

3.5. Potential sources of H_2O_2 in TA muscle following denervation

In order to determine potential sources of H_2O_2 production in TA muscles in state 1 following denervation, permeabilized muscle fiber bundles were incubated with specific enzyme inhibitors during analysis of peroxide generation as previously described [8]. All inhibitors reduced peroxide release to variable extents at the different time points examined (7, 14 and 21 days post-denervation) (Fig. 4A).

Functionally active NADPH oxidase 2 (Nox2) is a multimeric enzyme composed of various subunits: Nox2/gp91^{phox} and p22^{phox} comprise the membrane-bounded part of the enzyme whereas, p47^{phox}, p67^{phox}, p40^{phox}, and Rac-1 subunits organize and assemble the functional complex and regulate its activity [19–21]. The muscle content of all of the Nox2 subunits examined increased after denervation, although the relative increases differed between subunits in terms of timing and magnitude of change. While most of the subunits showed changes that could be quantified by densitometry within the dynamic range of western blots, some of the regulatory subunits were undetectable, or barely detectable in the baseline (non-denervated) samples and in these cases only example blots are shown in the supplementary data to provide examples of the changes observed. Nox2/gp91^{phox} content ($F(5,14) = 10.309$, $p < 0.01$, Fig. 4B) increased with time to an apparent peak at 14 days post-denervation and p67^{phox} protein content showed a significant increase compared to control at 14 days after denervation which increased further at 21 days post denervation ($F(5,17) = 15.595$, $p < 0.01$).

Example blots showing the increased p40^{phox} content are presented in Supplementary data 1A. The p22^{phox} content was significantly increased at 7, 14 and 21 days post-denervation whereas p47^{phox} protein content was significantly increased at 3 days following denervation ($F(5,15) = 7.390$, $p < 0.01$; Supplementary data 1B). Rac-1 is reported to trigger activation of the NADPH oxidase complex and Rac-1 content showed a statistically significant increase at 7 days ($F(5,16) = 3.829$, $p < 0.01$) post-denervation (Supplementary data 1B).

The muscle content of NADPH oxidase 4 (Nox4) showed little change up to 14 days post-denervation compared with control and although a trend towards an increase was seen at 21 days, this did not reach statistical significance when compared with the control group (Fig. 4B).

The protein levels of three other proteins that might potentially be involved in generation of fatty acid peroxides or H_2O_2 were examined. The muscle content of cPLA2 increased post-denervation and was significantly higher than control at 14 and 21 days ($F(5, 16) = 98.569$, $p < 0.01$) (Fig. 4C). Monoamine oxidase A protein content was significantly increased at 1 day following denervation and remained increased up to 14 days following denervation ($F(5, 16) = 10.986$, $p < 0.01$) (Fig. 4C). Prx6 is a peroxiredoxin that may also have PLA2 activity under some conditions and although this protein was undetectable in control muscle samples, a clear increase was seen in muscle up to 21 days post-denervation (Supplementary data 2A).

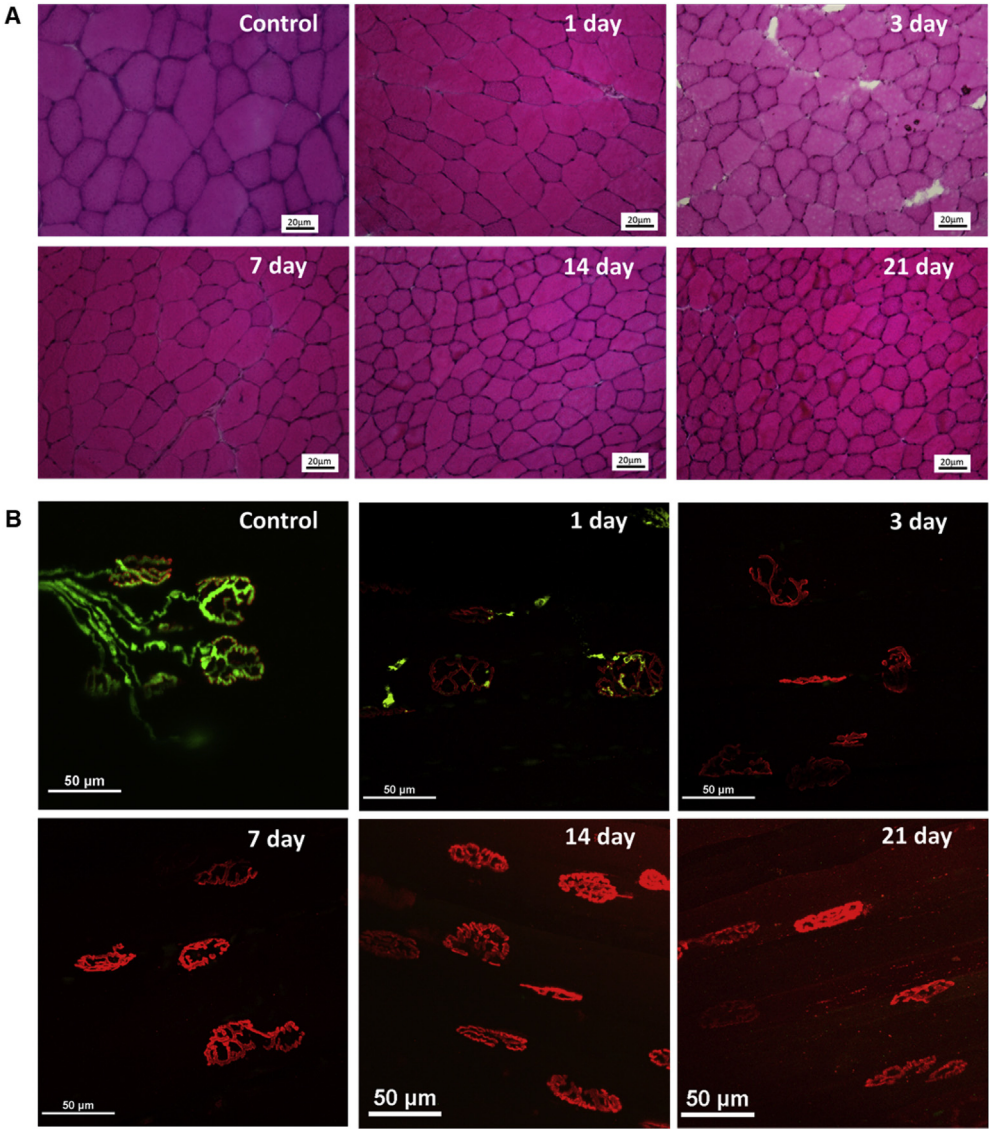

Fig. 2. (A) Cross-sections of TA muscles visualized by H&E staining and (B) NMJs observed in whole mount EDL muscles from control mice (non-denervated) and mice at 1, 3, 7, 14 and 21 days post-denervation. Images show the peripheral nerves (green) and acetylcholine receptors (red). (For interpretation of the references to colour in this figure legend, the reader is referred to the Web version of this article.)

3.6. Muscle content of mitochondria-localized regulatory enzymes following denervation

The content of three major mitochondrial enzymes involved in redox regulation were analyzed: The MnSOD content in muscle did not change significantly following denervation (Fig. 5A), but TrxR2 was significantly increased at 3 and 7 days post denervation and then declined over the following time points ($F(5,15) = 10.899$ $p < 0.01$), while the GPx1 content was significantly increased at 3, 7 and 21 days following denervation (Fig. 5A).

3.7. HSP content of TA muscles following denervation

Data in Fig. 5B show that skeletal muscles from adult mice also responded to denervation by an increase in the content of some HSPs. Hsp25 was significantly increased at 3 days and continued to increase at 7, 14 and 21 days following denervation ($F(5, 16) = 147.142$, $p < 0.01$). The Hsc70 content of denervated TA muscles was significantly increased at 14 and 21 days post-denervation ($F(5, 15) = 16.073$, $p < 0.01$). Hsp70 was undetectable in some control muscle samples but appeared to increase at 14 and 21 days post-denervation (Supplementary data 2B).

4. Discussion

It is now well established that during aging a number of muscle fibers lose functional innervation, leading to significant fiber degeneration and atrophy [1,3] and studies using nerve transection models in rodents have indicated a role for mitochondrial oxidative stress in the mechanism of denervation-induced muscle atrophy [7,8,10]. Specifically, previous work from our group and others has shown that denervation of muscle leads to a large increase in the release of H_2O_2 and lipid peroxides from muscle mitochondria over a short time course [7,8,10]. In this study, we extended the time course of denervation in order to examine the longer-term effect of muscle denervation on peroxide release and proteins that regulate redox homeostasis in muscle fibers.

Full denervation of the TA muscle was achieved by surgically removing a small section of the peroneal nerve prior to entry into the muscle. Morphological analyses of the TA muscle indicated a

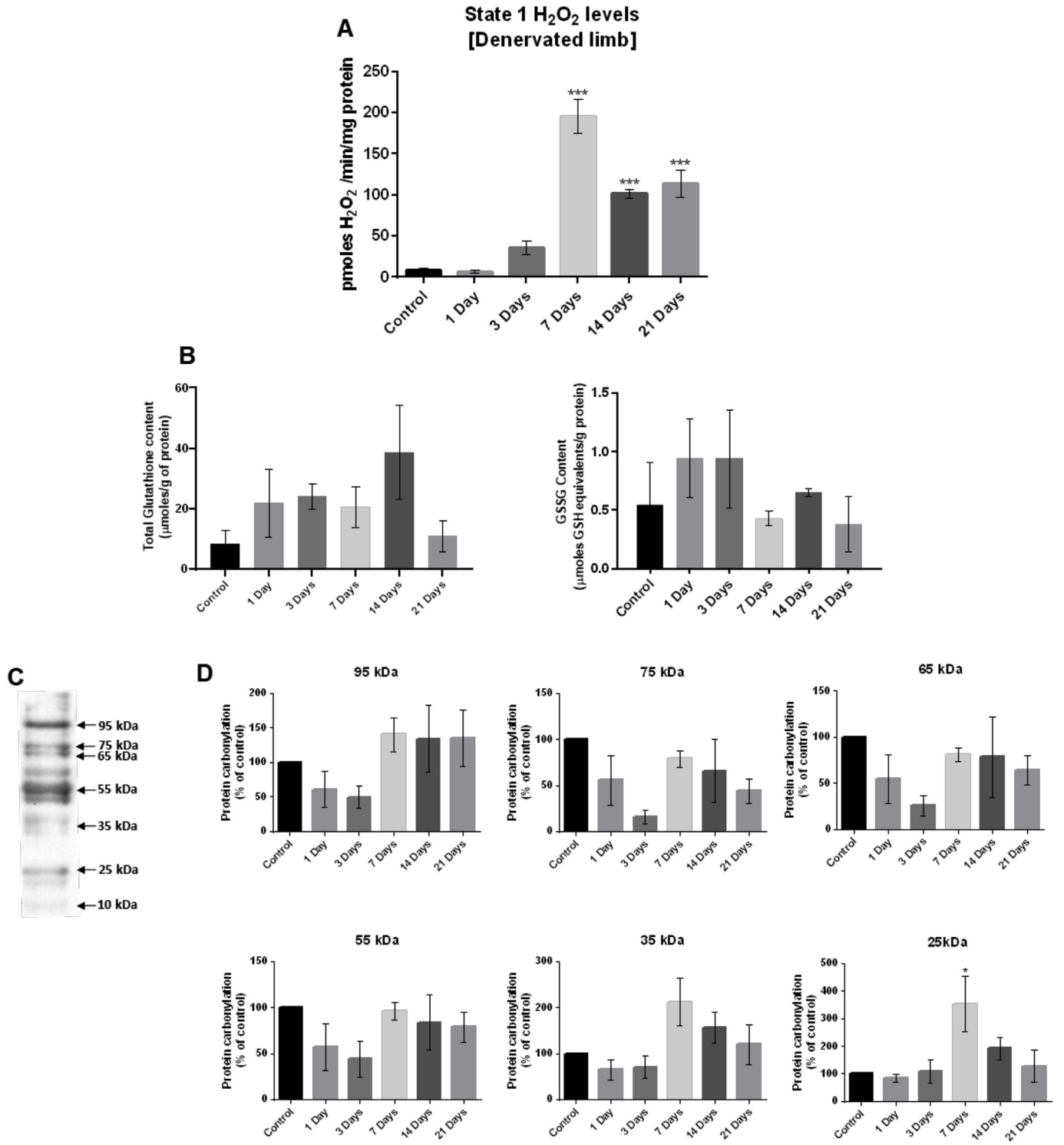

Fig. 3. (A) State 1 H_2O_2 production in mitochondria from permeabilized fibers from the TA muscles determined by oxidation of amplex red. (B) Total glutathione (GSH) and oxidized glutathione (GSSG) contents in TA muscles from control (non-denervated) mice and mice at 1, 3, 7, 14 and 21 days post-denervation. (C) A representative lane of an *OxyBlot* for control muscle showing the bands detected with approximate molecular weights (MW) indicated. (D) Quantification of protein carbonyls by densitometric analysis of the protein bands at different molecular weights. Histograms represent the mean and standard error of the mean for each experimental group (n = 4). *p < 0.05 - **p < 0.01 - ***p < 0.001 compared with the control group.

progressive significant loss of muscle mass from 7 days up to 21 days post-denervation. This occurred without loss of fibers (Fig. 1C) and hence was due to fiber atrophy (Fig. 1D). Our previous published data have demonstrated that by 7 days following denervation there was complete loss of pre-synaptic axonal input at the NMJs [8] and our current data confirm this (Fig. 2B) and demonstrate the longer-term effects on muscle fiber atrophy (Fig. 1).

The extended time course of mitochondrial peroxide generation reported here showed a significant increase in H_2O_2 generation from fiber bundles by 7 days post-denervation, which was sustained up to 21 days (Fig. 3A). Pollock et al. [8] previously demonstrated by addition of substrates and inhibitors of the electron transport chain that the

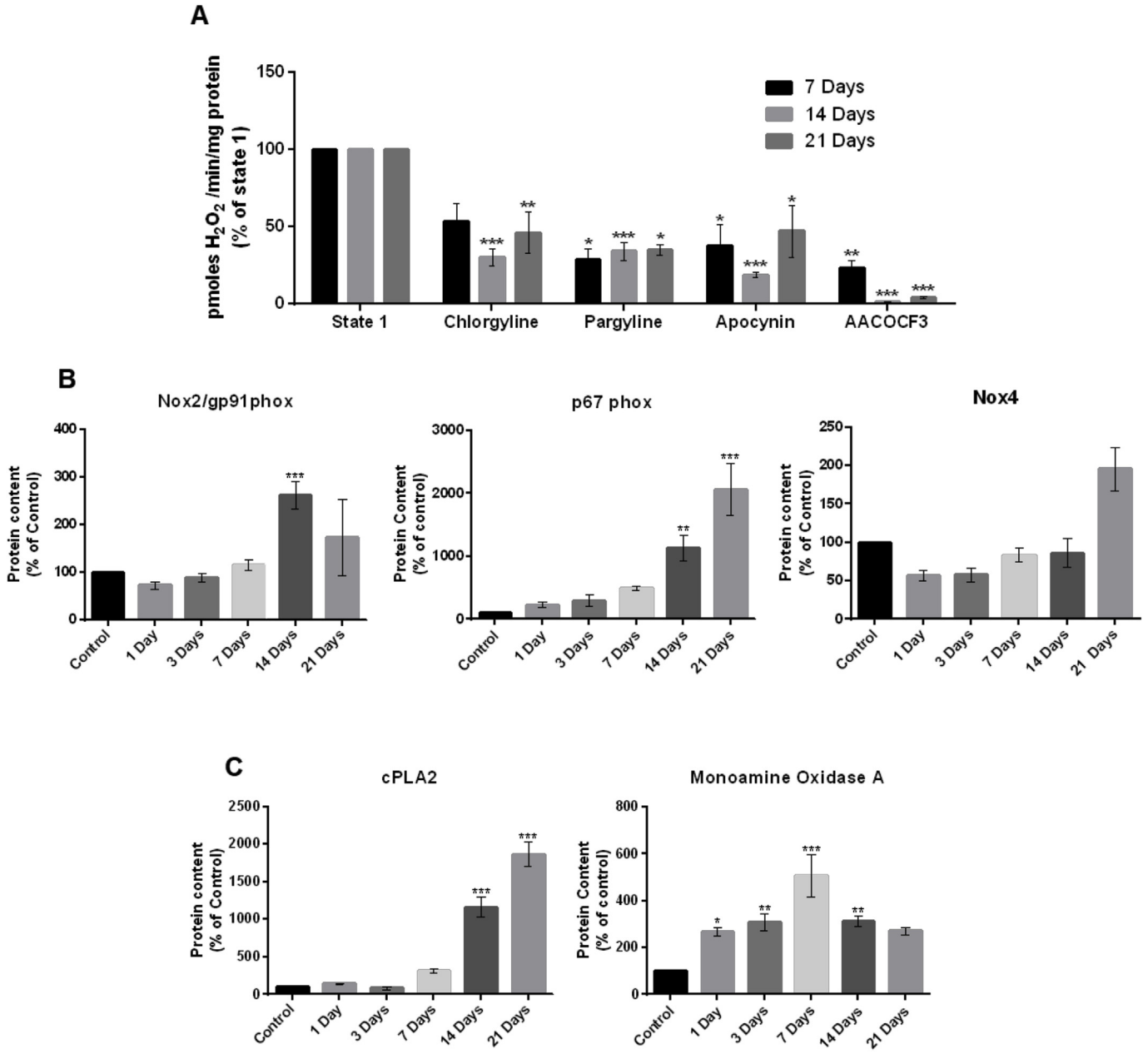

Fig. 4. (A) State 1 mitochondrial H_2O_2 generation from permeabilized fibers of the TA muscle in the presence of different enzyme inhibitors. Addition of each inhibitor (chlorgyline (monoamine oxidase A), parglyline (monoamine oxidase B), apocynin (NADPH oxidase), AACOCF3 (PLA2) resulted in significantly reduced H_2O_2 generation compared to untreated fiber bundles at 14 and 21 days post-denervation. Histograms represent the mean and standard error of the mean for each experimental group (n = 4). *p < 0.05 - **p < 0.01 - ***p < 0.001 compared with its state 1. (B) Quantification of western blots of NADPH oxidase 2 subunits (Nox2/gp91^{phox} and p67^{phox}) and NADPH oxidase 4 (mitochondrial isoform) and (C) of cPLA2 and monoamine oxidase A content in TA muscle from control mice (non-denervated) and mice at 1, 3, 7, 14 and 21 days post-denervation. Histograms represent the mean protein content and standard error of the mean for each experimental group (n = 4). *p < 0.05 - **p < 0.01 - ***p < 0.001 compared with the control group.

increased peroxide generation by muscle mitochondria post-denervation did not derive from the electron transport chain but indicated that alternative sources of peroxides were likely to be involved. Skeletal muscle mitochondria contain several other potential sources of ROS including monoamine oxidases [22]), NADPH oxidase [16] and phospholipases [23] and inhibitor studies have suggested that all of these proteins may be involved in the denervation-induced increase in mitochondrial ROS ([8] and Fig. 4A).

Monoamine oxidases are flavoenzymes that are present in the mitochondrial outer membrane [24] and exist in two isoforms, monoamine oxidase A and B that share approximately 70% of sequence identities but are distinguished by different substrate specificity [25]. Both monoamine oxidase A and B play a primary function in regulating neurotransmitter levels and the degradation of amines [24]. Skeletal muscle has been reported to contain both monoamine oxidase A [26] and B [27] and addition of chlorgyline (monoamine oxidase A) and pargyline (monoamine oxidase B) inhibitors reduced the oxidation of amplex red by permeabilized muscle fibers. Monoamine oxidase A protein content was also found to be increased prior to the increase in mitochondrial peroxide release (Fig. 4C) whereas monoamine oxidase B protein content was unchanged (data not shown).

Previous studies have shown that, following denervation, lipid peroxides are also released from mitochondria and can oxidize amplex red [8,10]. Our current inhibitor data supports this possibility since

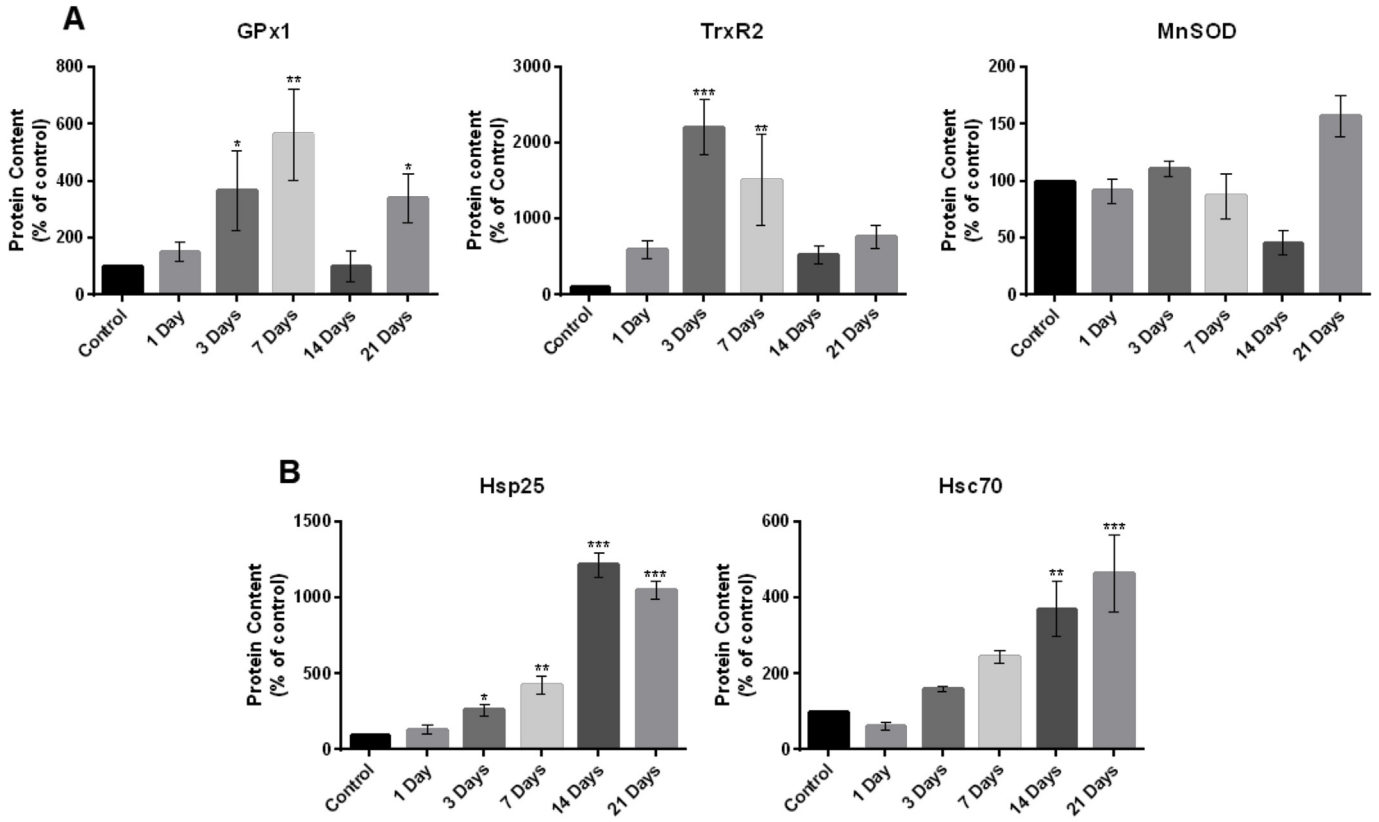

Fig. 5. (A) Quantification of western blots for mitochondrial antioxidant enzymes (GPx1, TRxR2, MnSOD) and (B) HSP (Hsp25, Hsc70) content in TA muscle from control mice (non-denervated) and mice at 1, 3, 7, 14 and 21 days post-denervation. Histograms represent the mean protein content and standard error of the mean for each experimental group (n = 4). *p < 0.05 - **p < 0.01 - ***p < 0.001 compared with the control group.

addition of the cPLA2 inhibitor, AACOCF3, reduced mitochondrial peroxide production (Fig. 4A) and muscle levels of cPLA2 were also increased post-denervation (Fig. 4C and [8]).

Other studies have demonstrated that skeletal muscles contain different isoforms of NADPH oxidase [16,28]. Addition of apocynin (a non-specific NADPH oxidase inhibitor) significantly reduced the denervation-induced mitochondrial amplex red oxidation at all time points following denervation (Fig. 4A), but the cPLA2 inhibitor AACOCF3 and the monoamine oxidase inhibitors also caused a marked reduction of peroxide release. These apparently conflicting pieces of data may potentially be explained by a lack of specificity of the inhibitors used or by involvement of complex interacting pathways, such as for instance, a potential direct role for PLA2 in the production of peroxide together with a role for PLA2 in activation of NADPH oxidase [29,30].

In the present study, we examined two NADPH oxidase isoforms that are reported to be present in skeletal muscle, Nox4, present within mitochondria, and Nox2 which is found mainly in the cytosolic environment [28]. Due to the reported sub-cellular location of the two isoforms, only Nox4 could likely contribute to the post-denervation increase in mitochondrial peroxide generation, but the muscle content of Nox4 showed no significant changes throughout the time course (Fig. 4B). However, our study focused on measuring protein content and not activity, therefore we cannot rule out altered activity of Nox4.

In contrast, significant post-denervation increases in muscle were seen in the content of components of the Nox2 complex. All Nox2-related subunits were seen to increase to some extent after denervation (Fig. 4B and Supplementary data 1). The interaction of Nox2/gp91^{phox} with p22^{phox} is a necessary step for the assembly of the Nox2 complex and the content data presented suggest that this would be maximal from 14 days following denervation. The protein content of p47^{phox} and Rac-1 were significantly increased between 3 and 7 days post-denervation (Supplementary data 1). Phosphorylation of p47^{phox} and Rac-1 activation have previously been reported in skeletal muscle and these post-translational events lead to translocation and binding of cytosolic subunits to the cell membrane and Nox2 and p22^{phox} to form a functionally active complex [21]. The content of p67^{phox} and p40^{phox} subunits was also increased at 14 days post-denervation. These are reported to be mainly cytosolic and translocate to the cell membrane upon Nox2 activation [21].

NADPH oxidases can be activated by different stimuli and different pathways can induce their assembly. It has previously been shown that PLA2 activity can activate NADPH oxidases [29] and can promote ROS generation in muscle mitochondria [31] and cytosol [32]. PLA2 is mainly involved in the hydrolysis of sn-2 fatty acyl chains of phospholipids generating fatty acids such as arachidonic acid which are important substrates for cyclooxygenases (COX) and lipoxygenases (LOX) and involved in the activation of NADPH oxidase and generation of ROS [33]. In the present study, an increase in cPLA2 content was seen at 14 days following denervation which would be compatible with a potential role for this enzyme in Nox2 activation. Previously published data has shown that cPLA2 is a negative regulator of growth, specifically of striated muscle and deletion of cPLA2 promotes striated muscle growth [34]. Our data demonstrated that the cPLA2 content was significantly increased in muscle at 14 days post-denervation and remained increased thereafter (Fig. 4C) when muscle fiber atrophy was evident.

Prx6 protein content was also increased in muscle at 3 days post-denervation (Supplementary data 2A). This protein is an atypical peroxiredoxin, which has potential PLA2 activity [35]. It is a 1-Cys peroxiredoxin with unique bi-functional characteristics and can translocate into the mitochondria during stress conditions where it plays a primary role in binding and reducing phospholipid hydroperoxides [36]). This protein also acquires PLA2 activity if it is over-oxidized [37]. This

suggests the possibility that the increased peroxide release from mitochondria may induce the translocation of Prx6 into mitochondria where it becomes over-oxidized and undergoes conformational changes acquiring PLA2 properties. These conformational changes allow Prx6 to produce fatty acids, including arachidonic acid that have been reported to induce the phosphorylation of $p40^{phox}$, $p47^{phox}$ and $p67^{phox}$ and their subsequent translocation to the plasma membrane allowing the assembly of Nox2 [38].

Thus, overall, the data obtained are compatible with the hypothesis that, following denervation, muscle mitochondria increase peroxide release and this leads to an adaptive increase in Nox2 content and that this enzyme may be activated via Prx6-PLA2-mediated signalling pathways. It is important to note that the increases in muscle content of Nox2 protein and its regulatory sub-units are unlikely to have contributed to the observed increase in mitochondrial peroxide generation post-denervation. Previous studies have not identified Nox2 in muscle mitochondria [16]. Rather these changes are likely to reflect an additional adaptation of the muscle to denervation. We have previously speculated that a key role of the increased mitochondrial peroxide generation following denervation may be to stimulate axonal sprouting and regrowth [8] and the increase in Nox2 may also reflect a similar adaptive response. Nox2 has been shown to play a role in axonal growth cone dynamics and modulation of cytoskeletal proteins [39] and since this enzyme predominantly generates superoxide to the external face of the plasma or T-tubule membrane it is tempting to speculate that may play a role in muscle-nerve communication to modulate axonal regrowth or guidance [39].

To examine the effect of denervation on the antioxidant system response in skeletal muscle mitochondria, the contents of 3 major mitochondrial antioxidant enzymes, MnSOD, TRxR2 and GPx1 were analyzed. The MnSOD content in muscle did not change following denervation but our study focused on measuring protein content and not activity, therefore we cannot rule out altered activity. In contrast, both TrxR2 and GPx1 contents were significantly increased at 3 and 7 days post-denervation (Fig. 5A). The rapid increase in the content of these mitochondrial antioxidant enzymes may therefore also reflect an adaptive response following loss of innervation in an attempt to maintain redox homeostasis in the muscle.

We also hypothesized that the increased peroxide production following denervation would stimulate adaptive responses against oxidative damage and repair processes in an attempt to protect the muscle from degeneration. We observed that the Hsp70 content was increased following denervation and remained increased up to 21 days post-denervation (Supplementary data 2B) which is compatible with the possibility that the increased Hsp70 may play a role in protein homeostasis in the denervated muscle. Prolonged denervation of muscle also resulted in the increase content of Hsc70 (Fig. 5B).

Finally, we observed that the muscle Hsp25 content was also significantly increased from 3 days following denervation and remained increased until 21 days post-denervation (Fig. 5B). It has previously been shown that overexpression of Hsp25 in skeletal muscle cells produced dose-dependent protection against H_2O_2-induced damage that was associated with increased glutathione levels and GPx1 activity [40]. We did not observe any significant differences with time post-denervation in glutathione levels (Fig. 3B) but found a significant increase in the content of GPx1 which was maintained up to 21 days post denervation. Thus, the data are in accord with the possibility that the increased Hsp25 together with the changes in GPx1 are important in enhancing resistance to H_2O_2 damage in skeletal muscle fibers following denervation.

In summary, data indicate that following denervation, increased mitochondrial peroxide generation is evident at 7 days post-denervation and maintained up to 21 days post-denervation and that this increase is associated with a significant increase in the muscle content of various proteins involved in the potential generation of peroxides including Prx6 and cPLA2 which may be involved in the activation of NADPH oxidase. A significant increase was also seen in the content of several antioxidant enzymes and HSPs involved in the protection against oxidative damage, maintenance of redox homeostasis and proteostasis. These results support the possibility that, at least initially, the increase in peroxide production following denervation may stimulate adaptations to protect the muscle fibers; however sustained increased peroxide generation over the longer-term is likely to activate degenerative processes that lead to degeneration and muscle atrophy.

Acknowledgements

This work was supported by the U.S. National Institutes of Health [grant number AG-051442] and UK Biotechnology and Biological Sciences Research Council (BBSRC, Grant reference BB/K003860/1). We also thank the Biomedical Services Unit at the University of Liverpool.

Appendix A. Supplementary data

Supplementary data to this article can be found online at https://doi.org/10.1016/j.redox.2019.101294.

References

[1] S. Aare, S. Spendiff, M. Vuda, D. Elkrief, A. Perez, Q. Wu, ... R.T. Hepple, Failed reinnervation in aging skeletal muscle, Skelet. Muscle 6 (1) (2016) 29 https://doi.org/10.1186/s13395-016-0101-y.
[2] B. McDonagh, S.M. Scullion, A. Vasilaki, N. Pollock, A. McArdle, M.J. Jackson, Ageing-induced changes in the redox status of peripheral motor nerves imply an effect on redox signalling rather than oxidative damage, Free Radic. Biol. Med. 94 (2016) 27–35 https://doi.org/10.1016/j.freeradbiomed.2016.02.008.
[3] Y.C. Jang, H. Van Remmen, Age-associated alterations of the neuromuscular junction, Exp. Gerontol. 46 (2–3) (2011) 193–198 https://doi.org/10.1016/j.exger.2010.08.029.
[4] K.H.J. Park, Mechanisms of muscle denervation in aging: insights from a mouse model of amyotrophic lateral sclerosis, Aging and Disease 6 (5) (2015) 380–389 https://doi.org/10.14336/AD.2015.0506.
[5] I. Liguori, G. Russo, F. Curcio, G. Bulli, L. Aran, D. Della-Morte, ... P. Abete, Oxidative stress, aging, and diseases, Clin. Interv. Aging 13 (2018) 757–772 https://doi.org/10.2147/CIA.S158513.
[6] C.C. Winterbourn, M.B. Hampton, Thiol chemistry and specificity in redox signaling, Free Radic. Biol. Med. 45 (5) (2008) 549–561 https://doi.org/10.1016/j.freeradbiomed.2008.05.004.
[7] F.L. Muller, W. Song, Y.C. Jang, Y. Liu, M. Sabia, A. Richardson, H. Van Remmen, Denervation-induced skeletal muscle atrophy is associated with increased mitochondrial ROS production, Am. J. Physiol. Regul. Integr. Comp. Physiol. 293 (3) (2007) R1159–R1168 https://doi.org/10.1152/ajpregu.00767.2006.
[8] N. Pollock, C.A. Staunton, A. Vasilaki, A. McArdle, M.J. Jackson, Denervated muscle fibers induce mitochondrial peroxide generation in neighboring innervated fibers: role in muscle aging, Free Radic. Biol. Med. 112 (July) (2017) 84–92 https://doi.org/10.1016/j.freeradbiomed.2017.07.017.
[9] Y. Go, J.D. Chandler, D.P. Jones, The cysteine proteome, Free Radic. Biol. Med. 84 (2016) 227–245 (The), https://doi.org/10.1016/j.freeradbiomed.2015.03.022.
[10] A. Bhattacharya, F.L. Muller, Y. Liu, M. Sabia, H. Liang, W. Song, ... H. Van Remmen, Denervation induces cytosolic phospholipase a 2-mediated fatty acid hydroperoxide generation by muscle mitochondria, J. Biol. Chem. 284 (1) (2009) 46–55 https://doi.org/10.1074/jbc.M806311200.
[11] A. Vasilaki, N. Pollock, I. Giakoumaki, K. Goljanek-Whysall, G.K. Sakellariou, T. Pearson, ... A. McArdle, The effect of lengthening contractions on neuromuscular junction structure in adult and old mice, Age (2016) 1–14 September https://doi.org/10.1007/s11357-016-9937-7.
[12] R.D. Cardiff, C.H. Miller, R.J. Munn, Manual hematoxylin and eosin staining of mouse tissue sections, Cold Spring Harb. Protoc. 6 (2014) 655–658 2014 https://doi.org/10.1101/pdb.prot073411.
[13] A. Vasilaki, A. Mansouri, H. Van Remmen, J.H. Van Der Meulen, L. Larkin, A.G. Richardson, A. Mcardle, J.A. Faulkner, M.J. Jackson, Free radical generation by skeletal muscle of adult and old mice: effect of contractile activity, Aging Cell 5 (2006) 109–117 https://doi.org/10.1111/j.1474-9726.2006.00198.x.
[14] O.H. Lowry, Ni J. Rosebrough, R.J. Randall, A. Lewis, Protein Measurement with the folin phenol reagent, J. Biol. Chem. 193 (1) (1951) 265–275 https://doi.org/10.1016/0304-3894(92)87011-4.
[15] M.E. Anderson, Measurement of antioxidants: glutathione, Free Radicals, A Practical Approach (NA Punchard, FJ Kelly, IRL Press, Oxford, 1996, pp. 213–226.
[16] G.K. Sakellariou, A. Vasilaki, J. Palomero, A. Kayani, L. Zibrik, A. McArdle, M.J. Jackson, Studies of mitochondrial and nonmitochondrial sources implicate nicotinamide adenine dinucleotide phosphate oxidase(s) in the increased skeletal muscle superoxide generation that occurs during contractile activity, Antioxidants Redox Signal. 18 (6) (2013) 603–621 https://doi.org/10.1089/ars.2012.4623.

[17] I. Romero-Calvo, B. Ocón, P. Martínez-Moya, M.D. Suárez, A. Zarzuelo, O. Martínez-Augustin, F.S. de Medina, Reversible Ponceau staining as a loading control alternative to actin in Western blots, Anal. Biochem. 401 (2) (2010) 318–320 https://doi.org/10.1016/j.ab.2010.02.036.
[18] A. McLean, Densitometry of Western Blots Using Image J Software. *Bennett Lab (NRL)*, 9, (2011) Retrieved from http://rsb.info.nih.gov/ij/docs/index.html.
[19] Y. Groemping, K. Rittinger, Activation and assembly of the NADPH oxidase: a structural perspective, Biochem. J. 386 (3) (2005) 401–416 https://doi.org/10.1042/BJ20041835.
[20] A. Panday, M.K. Sahoo, D. Osorio, S. Batra, NADPH oxidases: an overview from structure to innate immunity-associated pathologies, Cell. Mol. Immunol. 12 (1) (2015) 5–23 https://doi.org/10.1038/cmi.2014.89.
[21] L.F. Ferreira, O. Laitano, Regulation of NADPH oxidases in skeletal muscle, Free Radic. Biol. Med. 98 (4) (2016) 18–28 https://doi.org/10.1016/j.freeradbiomed.2016.05.011.
[22] J. Himms-Hagen, C. Irwin, Monoamine oxidase in outer membrane of skeletal muscle mitochondria, Biochim. Biophys. Acta 437 (1976) 498–504 1976.
[23] K.S. Cheah, M. Cheah, Mitochondria and sarcoplasmic reticulum in porcine malignant hyperthermia, Biochim. Biophys. Acta 638 (1981) 40–49 1981.
[24] E. Cadenas, K.J.a. Davies, Mitochondrial free radical generation, oxidative stress, and aging, Free Radic. Biol. Med. 29 (3–4) (2000) 222–230.
[25] O.M. Duicu, R. Lighezan, A. Sturza, R. Balica, A. Vaduva, H. Feier, ... C. Mornos, Assessment of mitochondrial dysfunction and monoamine oxidase contribution to oxidative stress in human diabetic hearts, Oxidative Medicine and Cellular Longevity (2016) 12 2016(Dm) https://doi.org/10.1155/2016/8470394.
[26] E.E. Billett, Monoamine oxidase (MAO) in human peripheral tissues, NeuroToxicology 25 (1–2) (2004) 139–148 https://doi.org/10.1016/S0161-813X(03)00094-9.
[27] I. Manoli, H. Le, S. Alesci, K.K. McFann, Y.A. Su, T. Kino, ... M.R. Blackman, Monoamine oxidase-A is a major target gene for glucocorticoids in human skeletal muscle cells, FASEB J. 19 (10) (2005) 1359–1361 https://doi.org/10.1096/fj.04-3660fje.
[28] G.K. Sakellariou, M.J. Jackson, A. Vasilaki, Redefining the major contributors to superoxide production in contracting skeletal muscle. The role of NAD(P)H oxidases, Free Radic. Res. 48 (1) (2014) 12–29 https://doi.org/10.3109/10715762.2013.830718.
[29] X. Zhao, E.A. Bey, F.B. Wientjes, M.K. Cathcart, Cytosolic phospholipase A2 (cPLA2) regulation of human monocyte NADPH oxidase activity: cPLA2 affects translocation but not phosphorylation of p67phox and p47phox, J. Biol. Chem. 277 (28) (2002) 25385–25392 https://doi.org/10.1074/jbc.M203630200.
[30] J.T. Colston, S.D. De La Rosa, J.R. Strader, M.A. Anderson, G.L. Freeman, H2O2activates Nox4 through PLA2-dependent arachidonic acid production in adult cardiac fibroblasts, FEBS (Fed. Eur. Biochem. Soc.) Lett. 579 (11) (2005) 2533–2540 https://doi.org/10.1016/j.febslet.2005.03.057.
[31] D. Nethery, L.A. Callahan, D. Stofan, R. Mattera, A. DiMarco, G. Supinski, PLA $_2$ dependence of diaphragm mitochondrial formation of reactive oxygen species, J. Appl. Physiol. 89 (1) (2000) 72–80 https://doi.org/10.1152/jappl.2000.89.1.72.
[32] M.C. Gong, S. Arbogast, Z. Guo, J. Mathenia, W. Su, M.B. Reid, Calcium-independent phospholipase A 2 modulates cytosolic oxidant activity and contractile function in murine skeletal muscle cells, J. Appl. Physiol. 100 (2006) 399–405 https://doi.org/10.1152/japplphysiol.00873.2005.
[33] K. Cho, J. Seo, J. Kim, Bioactive lipoxygenase metabolites stimulation of NADPH oxidases and reactive oxygen species, Mol. Cells 32 (2011) 1–5 https://doi.org/10.1007/s10059-011-1021-7.
[34] S. Haq, H. Kilter, A. Michael, J. Tao, E. O'Leary, X.M. Sun, ... T. Force, Deletion of cytosolic phospholipase A2 promotes striated muscle growth, Nat. Med. 9 (7) (2003) 944–951 https://doi.org/10.1038/nm891.
[35] R.P. Brandes, N. Weissmann, K. Schröder, Nox family NADPH oxidases: molecular mechanisms of activation, Free Radic. Biol. Med. 76 (2014) 208–226 https://doi.org/10.1016/j.freeradbiomed.2014.07.046.
[36] T. Eismann, N. Huber, T. Shin, S. Kuboki, E. Galloway, M. Wyder, ... L. Ab, Peroxiredoxin-6 Protects against Mitochondrial Dysfunction and Liver Injury during Ischemia-Reperfusion in Mice, (2018), pp. 266–274 https://doi.org/10.1152/ajpgi.90583.2008.
[37] A.B. Fisher, Peroxiredoxin 6: a bifunctional enzyme with glutathione peroxidase and phospholipase a $_2$ activities, Antioxidants Redox Signal. 15 (3) (2011) 831–844 https://doi.org/10.1089/ars.2010.3412.
[38] S. Chatterjee, S.I. Feinstein, C. Dodia, E. Sorokina, Y.C. Lien, S. Nguyen, ... A.B. Fisher, Peroxiredoxin 6 phosphorylation and subsequent phospholipase A2 activity are required for agonist-mediated activation of NADPH oxidase in mouse pulmonary microvascular endothelium and alveolar macrophages, J. Biol. Chem. 286 (13) (2011) 11696–11706 https://doi.org/10.1074/jbc.M110.206623.
[39] M.C.W. Oswald, N. Garnham, S.T. Sweeney, M. Landgraf, Regulation of neuronal development and function by ROS, FEBS (Fed. Eur. Biochem. Soc.) Lett. 592 (5) (2018) 679–691 https://doi.org/10.1002/1873-3468.12972.
[40] J. Escobedo, A.M. Pucci, T.J. Koh, HSP25 protects skeletal muscle cells against oxidative stress, Free Radic. Biol. Med. 37 (9) (2004) 1455–1462 https://doi.org/10.1016/j.freeradbiomed.2004.07.024.